Circuit Complexity of Mixed States

by

Shan-Ming Ruan

A thesis

presented to the University of Waterloo

in fulfillment of the

thesis requirement for the degree of

Doctor of Philosophy

in

Physics

Waterloo, Ontario, Canada, 2021

Examining Committee Membership

The following served on the Examining Committee for this thesis. The decision of the Examining Committee is by majority vote.

External Examiner:	Simon Ross Professor, Durham University
Supervisor(s):	Robert Myers Professor, Perimeter Institute for Theoretical Physics
Internal Member:	Robert Mann Professor, University of Waterloo
Internal-External Member:	Eduardo Martin-Martinez Associate Professor, University of Waterloo
Committee Member:	Alex Buchel Professor, University of Western Ontario

Author's Declaration

This thesis consists of material all of which I authored or co-authored: see Statement of Contributions included in the thesis. This is a true copy of the thesis, including any required final revisions, as accepted by my examiners.

I understand that my thesis may be made electronically available to the public.

Statement of Contributions

This thesis is based on the following published articles.

- Chapter 2 is based on:
  - M. Guo, J. Hernandez, R. C. Myers and S.-M. Ruan, *Circuit Complexity for Coherent States*, *JHEP* **10** (2018) 011 [1807.07677]

    This research was conducted at Perimeter Institute under the supervision of Prof. Robert Myers. I mainly contributed to part of analytical calculations in sections 2-5.
  - E. Caceres, S. Chapman, J. D. Couch, J. P. Hernandez, R. C. Myers and S.-M. Ruan, *Complexity of Mixed States in QFT and Holography*, *JHEP* **03** (2020) 012 [1909.10557]

    This research was conducted at Perimeter Institute under the supervision of Prof. Robert Myers. I mainly contributed to part of the analytical calculations and numerical work in sections 2-5.
- Chapters 3 and 4 is based on:
  - E. Caceres, S. Chapman, J. D. Couch, J. P. Hernandez, R. C. Myers and S.-M. Ruan, *Complexity of Mixed States in QFT and Holography*, *JHEP* **03** (2020) 012 [1909.10557]
- Chapter 5 is based on:
  - S.-M. Ruan, *Purification Complexity without Purifications*, *JHEP* **01** (2021) 092 [2006.01088]
- Work produced while a Ph.D. student at the University Waterloo but not included in the thesis:
  - A. Bernamonti, F. Galli, J. Hernandez, R. C. Myers, S.-M. Ruan and J. Simon, *First Law of Holographic Complexity*, *Phys. Rev. Lett.* **123** (2019) 081601 [1903.04511]
  - H. Z. Chen, Z. Fisher, J. Hernandez, R. C. Myers and S.-M. Ruan, *Information Flow in Black Hole Evaporation*, *JHEP* **03** (2020) 152 [1911.03402]

– A. Bernamonti, F. Galli, J. Hernandez, R. C. Myers, S.-M. Ruan and J. Simon, *Aspects of the first law of complexity*, *J. Phys. A: Math. Theor.* **53** (2020) 294002 [2002.05779]

– H. Z. Chen, Z. Fisher, J. Hernandez, R. C. Myers and S.-M. Ruan, *Evaporating Black Holes Coupled to a Thermal Bath*, *JHEP* **01** (2021) 065 [2007.11658]

– J. Hernandez, R. C. Myers and S.-M. Ruan, *Quantum extremal islands made easy. Part III. Complexity on the brane*, *JHEP* **02** (2021) 173 [2010.16398]

Abstract

Quantum information has produced fresh insights into foundational questions about the AdS/CFT correspondence. One fascinating concept, which has captured increasing attention, is quantum circuit complexity. As a natural generalization for the complexity of pure states, we investigate the circuit complexity of mixed states in this thesis.

First of all, we explore the so-called purification complexity which is defined as the lowest value of the circuit complexity, optimized over all possible purifications of a given mixed state. We focus on studying the complexity of Gaussian mixed states in a free scalar field theory using the 'purification complexity'. We argue that the optimal purifications only contain the essential number of ancillary degrees of freedom necessary in order to purify the mixed state. We also introduce the concept of 'mode-by-mode purifications' where each mode in the mixed state is purified separately and examine the extent to which such purifications are optimal. In order to compare with the results from using the various holographic proposals for the complexity of subregions, we explore the purification complexity for thermal states of a free scalar QFT, and for subregions of the vacuum state in two dimensions. We find a number of qualitative similarities between the two in terms of the structure of divergences and the presence of a volume law. We also examine the 'mutual complexity' in the various cases studied in this thesis.

In addition, we propose to generalize the Fubini-Study method for pure-state complexity to generic quantum states including mixed states by taking Bures metric or quantum Fisher information metric on the space of density matrices as the complexity measure. Due to Uhlmann's theorem, we show that the mixed-state complexity exactly equals the purification complexity measured by the Fubini-Study metric for purified states but without explicitly applying any purifications. We also find that the purification complexity is non-increasing under any trace-preserving quantum operations. As an illustration, we study the mixed Gaussian states as an example to explicitly show our conclusions for purification complexity.

Acknowledgements

When I moved to the last part of my thesis, countless memories of the past four years flooded my heart. I would like to express my appreciation to all of you for helping me during my Ph.D study.

My wholehearted appreciation is first to my distinguished supervisor Prof. Rob Myers. Without your numerous valuable comments, great patience and careful instruction during the whole process of my writing, the accomplishment of this thesis wouldn't have been possible. Your conscientious academic spirit, research enthusiasm, and open-minded personality deeply influenced me on my academic journey in the past, present and future. You have not only instructed me on how to do research but also set a good example to emulate. This is one of my fortunes in my life to be your student at Perimeter Institute.

I would also like to acknowledge many smart collaborators during our projects in my P.h.D program. Many thanks to Juan Hernandez, Minyong Guo, Alice Bernamonti, Federico Galli, Joan Simón, Elena Caceres, Shira Chapman, Josiah D. Couch, Hong Zhe Chen, Zachary Fisher, Antony Speranza, Alexandre Belin, and Gabor Sarosi for our wonderful collaborations, and for all the illuminating discussions. I would like to acknowledge my dissertation committee members, Simon Ross, Eduardo Martin-Martinez, Alex Buchel, and Robert Mann, for their time, extreme patience, and numerous illuminating comments and suggestions on my thesis. In particular, I am also deeply indebted to Prof. Rong-Gen Cai and Prof. Joán Simon for their strong support during my postdocs applications.

My sincere thanks also goes to Eugene Adjei, Yilber Fabian Bautista, Alfredo Guevara, Debbie Guenther, Qi Hu, Yanyan Li, Hugo Marrochio, Faroogh Moosavian, Ruocheng Ma, Dominik Neuenfeld, Bruno Umbert, Weicheng Ye, Keyou Zeng, Yehao Zhou, Yijian Zhou, and many other friends around Perimeter Institute. And thank you my flatmate JingXiang Dashen for encouraging me to get up from my bed every day to do research as well as for his encouragement during our postdocs applications. Without so many friends, my life in Canada would not be possible to be so wonderful.

Then I would like to extend my genuine thanks to Perimeter Institute, the best institute for theoretical physics on this planet. Prior to coming here, I never knew there is such a wonderful academic institute like Perimeter Institute in the world. It is my luck to spend four years on my Ph.D at Perimeter Institute. And thanks Black Hole Bistro for feeding me with a lot of delicious food and waking me up with great (and free) coffee every day.

At the last press on the keyboard, it is time to finish my thesis and say goodbye to my student life. I would like to leave the last word to future me,

愿你出走半生，归来仍是少年。

Dedication

This is dedicated to my parents.
For their endless love and support.

Table of Contents

List of Figures xii

List of Tables xvii

1 Introduction 1

1.1 A Short Introduction of AdS/CFT . . . 3

1.1.1 The Birth of the AdS/CFT Correspondence . . . 3

1.1.2 Holographic Dictionary . . . 8

1.1.3 Geometries and States . . . 12

1.2 Holography Meets Quantum Information . . . 16

1.2.1 Quantum States and Entanglement . . . 17

1.2.2 Holographic Entanglement Entropy . . . 22

1.3 Organization of the Thesis . . . 25

2 Complexity of Pure States 27

2.1 Circuit Complexity Proposals . . . 27

2.1.1 Nielsen's Geometric Approach . . . 27

2.1.2 Fubini-Study Metric Approach . . . 34

2.1.3 Path Integral Complexity . . . 39

2.2 Holographic Complexity Proposals . . . 43

2.2.1 Complexity=Volume . . . 44

2.2.2 Complexity=Action . . . 47

3 Circuit Complexity of Mixed States **51**
3.1 Optimal Purification and Purification Complexity 51
3.2 Warm-Up: Purification Complexity of a Single Harmonic Oscillator 54
3.2.1 Gaussian Purifications of One-Mode Mixed States 54
3.2.2 Alternative Description of the Purifications 55
3.2.3 Purification Complexity in the Diagonal Basis 59
3.2.4 Purification Complexity in the Physical Basis 62
3.3 Optimal Purification of Mixed Gaussian States 69
3.3.1 Purifying General Gaussian States 71
3.4 Circuit Complexity of Thermal States 74
3.4.1 Exercise: One-mode Thermal States 75
3.4.2 Discretization of the Free Scalar 77
3.4.3 Purification Complexity in the Diagonal Basis 78
3.4.4 Purification Complexity in the Physical Basis 81
3.4.5 Mutual Complexity of TFD States 84
3.5 Circuit Complexity of Vacuum Subregions 93
3.5.1 Purification Complexity in the Diagonal Basis 94
3.5.2 Purification Complexity in the Physical Basis 100

4 Holographic Complexity of Mixed States **107**
4.1 Review of the Holographic Proposals 108
4.2 Holographic Complexity of Thermal States 111
4.3 Holographic Complexity of Vacuum Subregions 114
4.3.1 Holographic Complexity in the Poincaré Patch 114
4.3.2 Holographic Complexity of Vacuum Subregions 118

5 Purification Complexity without Purification **123**
5.1 Uhlmann's fidelity and Quantum Fisher Information Metric 125
5.2 Properties of Purification Complexity 130
5.2.1 Purification Complexity without Purifications 130
5.2.2 The Non-increase of Purification Complexity 133
5.2.3 More on Purification Complexity of Mixed States 137
5.3 Application: Gaussian Mixed States 141
5.3.1 Geodesic and Complexity 142
5.3.2 Optimal Purifications and Purification Complexity 146
5.3.3 Purified States with Uhlmann's fidelity 148

6 Discussion **151**
6.1 Other Proposals for Mixed-State Complexity 152
6.2 Mutual Complexity in QFT 155
6.3 Holographic Complexity 158
6.4 Open Questions and Future Directions 164

References **171**

APPENDICES **191**

A Complexity Basis Dependence **192**
A.1 Example: Four Coupled Harmonic Oscillators 193

B Superadditivity of $\mathcal{C}_A(|\mathbf{TFD}\rangle)$ at general times **198**

C Background Materials on Quantum Information **200**
C.1 Gaussian State and Covariance Matrix 200
C.2 Quantum Operation (Quantum Channel) 202
C.3 Bures Metric and Quantum Fisher Information Metric 205
C.3.1 Bures Distance and Bures Metric 205
C.3.2 Quantum Fisher Information Metric 207

List of Figures

1.1 The illustration of the $\mathrm{AdS}_{d+1}/\mathrm{CFT}_d$ correspondence or gauge/gravity duality. The holographic direction is labeled by bulk coordinate z and the asymptotic boundary on which the dual QFT lives locates at $z = 0$. 8

1.2 The duality between quantum states of boundary field theory and bulk geometries in the $\mathrm{AdS}_{d+1}/\mathrm{CFT}_d$ correspondence. 14

1.3 Left: The Penrose diagram of the maximally extended AdS-Schwarzschild black hole. The light grey regions denote the interior regions behind the horizon. And the spacetime has two asymptotic boundaries where the left CFT and right CFT live, respectively. Right: The time slice at $t = 0$. The horizon located at the middle is the minimal area surface separating the left space and right space. 23

1.4 Illustration of the RT formula. The time direction has been suppressed. The red region $\mathcal{A}$ denotes the boundary subregion of a Cauchy slice in CFT_d. The vertical direction represents the radial direction in the bulk. 24

2.1 A general quantum circuit where $|\psi_{\mathrm{T}}\rangle$ is prepared beginning with $|\psi_{\mathrm{R}}\rangle$ and applying a sequence of elementary unitaries g_i. 28

2.2 The Penrose diagram for the eternal black hole in asymptotically AdS spacetime. The yellow curves connecting the two boundaries anchored at times t_{L} and t_{R} indicate the spacelike hypersurface with maximal volume. 45

2.3 The Penrose diagram for the eternal black hole in asymptotically AdS spacetime. The pink region bounder by four null surfaces is referred to as the Wheeler-DeWitt patch. The left/right plot corresponds to the WdW patch before/after the critical time t_c. 47

3.1 Circuit with the ancillary degrees of freedom. The mixed state $\hat{\rho}_{\mathcal{A}}$ that we want to prepare is obtained at the final step after tracing out the ancillae. 52

3.2 Possible values for the pure state complexity $\mathcal{C}_1^{\text{phys}}(|\psi_{12}\rangle)$ in the physical basis as a function of θ, for all possible sign combinations according to eq. (3.47) for fixed values of $\bar{r}$ and α. The complexity of the mixed state purified by $|\psi_{12}\rangle$ is obtained by minimizing over the uppermost envelope of each of these plots. 67

3.3 The difference between the complexity obtained for θ_c at the intersection of cases (a) and (c) and the exact purification complexity of one-mode Gaussian states in the physical basis $\mathcal{C}_{1,c}^{\text{phys}}(\hat{\rho}_1) - \mathcal{C}_1^{\text{phys}}(\hat{\rho}_1)$ as a function of $\bar{r}$ for some fixed values of α. We see that the complexity obtained at the intersection between cases (a) and (c) with $\mathcal{C}_{1,c}^{\text{phys}}(\hat{\rho}_1)$ in eq. (3.54) ceases to be optimal for some region of the parameter $\bar{r}$ for large enough values of α. 68

3.4 Purification complexity of one-mode Gaussian states in the physical basis $\mathcal{C}_1^{\text{phys}}(\hat{\rho}_1)$ as a function of α for some fixed values of $\bar{r}$. The fact that the curves with $\bar{r} = -6$ and $\bar{r} = -10$ coincide after a certain value of α is due to the fact that this minimization is obtained at the minimum of case (c) which is $\bar{r}$ independent. 68

3.5 Illustration of the different ways to purify a multi-mode Gaussian state $\hat{\rho}_A$. We refer to the purifications of the form $\Psi_{11^c} \otimes \Psi_{22^c} \otimes \cdots \otimes \Psi_{NN^c}$ as mode-by-mode purifications. 70

3.6 Different regimes of eq. (3.75): values of $\beta\mu$ above the blue curve, *i.e.,* $\beta\omega \coth(\beta\omega/4)$, correspond to the first regime in this equation; below the red curve *i.e.,* $\beta\omega \tanh(\beta\omega/4)$, correspond to the third regime; while between the blue and red curves correspond to the second regime. We observe that when $\beta\mu \gg 1$, there is a very narrow range of frequencies $\beta\omega$ between the blue and red lines (since both curves converge towards $\beta\omega$) for which the intermediate regime applies. 76

3.7 Illustration of the optimal purification of two mixed states in two complementary subsystems $\mathcal{A}$ and $\mathcal{B}$ of an original pure state $|\Psi\rangle_{\mathcal{AB}}$. The state in the subsystem $\mathcal{A}$ is purified by a state $|\Psi\rangle_{\mathcal{AA}^c}$ and the one in the subsystem $\mathcal{B}$ is purified by $|\Psi\rangle_{\mathcal{BB}^c}$. Even though the direct product of the purifying systems $|\Psi\rangle_{\mathcal{AA}^c} \otimes |\Psi\rangle_{\mathcal{BB}^c}$ generally has a larger number of degrees of freedom than the original state $|\Psi\rangle_{\mathcal{AB}}$, the mutual complexity eq. (3.105) can have either sign. 85

3.8 The integrated mutual complexity in the diagonal basis, *i.e.*, $\Delta\mathcal{C}_1^{\text{diag}}(|\text{TFD}\rangle)$ defined in eq. (3.111) for a massless field theory in different dimensions. . . 88

3.9 The mutual complexity $\Delta\mathcal{C}_1^{\text{phys}}(|\text{TFD}\rangle_{12})$ as defined in eq. (3.121) with fixed $\bar{r} = \frac{1}{2}\ln\frac{\omega}{\mu} < 0$ as a function of α. We find that the quantity $\Delta\mathcal{C}_1^{\text{phys}}$ can be either positive or negative. The right plot is the region with $\bar{r}$ near the transition point $\bar{r} = -2.177$. 92

3.10 The integrated mutual complexity in the physical basis $\Delta\mathcal{C}_1^{\text{phys}}(|\text{TFD}\rangle)$ in eq. (3.124) for a massless free scalar field theory in $d = 2$ as a function of $\beta\mu$. The two plots show different regimes of the parameter $\beta\mu$. The integrated mutual complexity is negative when $\beta\mu$ is very small or very large. 94

3.11 Purification complexity in the diagonal basis for subregions of the vacuum as a function of the subregion size. The cutoff was set to $N = L/\delta = 1000$ and the mass to $mL = 0.01$. The purification complexity for the subregion with $\ell \to L$ agrees with the complexity of the ground state in diagonal basis. 98

3.12 Purification complexity in the diagonal basis for subregions of the vacuum as a function of the lattice cutoff. The mass was set to $mL = 0.01$. The different plots correspond to different subregion sizes $\ell/L = 0.05$, 0.1, 0.9 and 0.95 as indicated and each plot contains five different reference frequencies of $\mu L = 100$, 200, 300, 400 and 500 respectively. 99

3.13 Subregion size dependence of the mutual complexity in the diagonal basis $\Delta\mathcal{C}_1^{\text{diag}}$ for different reference frequencies $\mu L = 100$, 200 and 300. The cutoff was set to $\delta/L = 1/N = 1/1000$ and the mass to $mL = 0.01$. 101

3.14 Cutoff dependence of the mutual complexity in the diagonal basis $\Delta\mathcal{C}_1^{\text{diag}}$ for different reference frequencies $\mu L = 100$, 200, 300, 400 and 500. The subregion sizes were fixed to $\ell/L = 0.1$ and 0.05 and the mass to $mL = 0.01$. 101

3.15 Left panel: subregion complexity as a function of the subregion size in physical basis for reference frequencies $\mu L = 0.1$, 1, 10, 100, 1000. Right panel: comparison of the subregion complexity to the complexity of the ground state in the physical basis for $\mu L = 100$. In both plots, the cutoff was set to to $L/\delta = N = 100$ and the mass to $mL = 0.01$. 103

3.16 Subregion complexity in the physical basis as a function of the cutoff $N = L/\delta$ for $\ell/L = 0.05$, 0.1, 0.9 and 0.95. The mass was set to $mL = 0.01$. . . 104

3.17 The two definitions of mutual complexity in the physical basis $\Delta\mathcal{C}_1^{\text{phys}}$ and $\Delta\tilde{\mathcal{C}}_1^{\text{phys}}$ as a function of the cutoff for various reference frequencies $\mu L = 100$, 200, 300, 400 and 500. The mass was set to $mL = 0.01$. 106

4.1 The intersection of the entanglement wedge and the WDW patch defines the region $\widetilde{\mathcal{W}}$ that is relevant for the evaluation of $\mathcal{C}_{\text{A}}(B)$. 115

5.1 The connections between pure-state complexity from the Fubini-Study metric and purification complexity derived from the Bures metric (or quantum Fisher information metric). The Hilbert space consisting of quantum states $\hat{\rho}_{\mathcal{A}}$ that we are interested in is denoted by $\mathcal{H}_{\mathcal{A}}$ and the extended Hilbert space with introducing auxiliary system is represented by $\mathcal{H}_{\mathcal{A}} \otimes \mathcal{H}_{\mathcal{A}^c}$. . . . 124

5.2 A lift of evolution $\hat{\rho}_{\mathcal{A}}(\sigma)$ to the extended Hilbert space: A general circuit connecting purified state $\hat{\sigma}_{\mathcal{A}\mathcal{A}^c}$ to $\hat{\rho}_{\mathcal{A}\mathcal{A}^c}$ with different ancillae after every step because we do not count the cost of introducing ancilla and tracing out the auxiliary system. More importantly, it is based on the fact that any trace-preserving quantum operation is equivalently described by the unitary evolution with ancilla. 132

5.3 Left side is the Hilbert space $\mathcal{H}_{\mathcal{A}\mathcal{A}^c}$ of purified state $|\Psi_{\mathcal{A}\mathcal{A}^c}\rangle$, which is equipped with the Fubini-study metric g_{FS} as the complexity measure. The black line is referred to as the geodesic γ_{FS} in this space. The right side represents the Hilbert space $\mathcal{H}_{\mathcal{A}}$ for density matrices $\hat{\rho}_{\mathcal{A}}$ with the quantum Fisher information metric g_{IM} defined in (5.20) as the complexity measure. The corresponding geodesic γ_{IM} is indicated by the blue line. By tracing out the ancillary part $\mathcal{A}^c$, we can find the projection-map from γ_{FS} to a path in the space of $\hat{\rho}_{\mathcal{A}}$ which is shown as the black curve. According to Uhlmann's theorem, we can also construct a lift-map from $\mathcal{H}_{\mathcal{A}}$ to $\mathcal{H}_{\mathcal{A}\mathcal{A}^c}$ with the fidelity bound is always saturating. 134

5.4 Circuit Complexity $\mathcal{C}_{\text{IM}}(\hat{\rho}_1)$ from the quantum Fisher information metric for one-mode Gaussian mixed state $\hat{\rho}_1(r(\sigma=1), \alpha(\sigma=1))$ with different boundary value $\bar{r}(\sigma=1)$. 143

5.5 Mutual Complexity $\Delta\mathcal{C}_{\text{IM}}(|\text{TFD}_{12}\rangle) = \Delta\mathcal{C}_{\text{FS}}(|\text{TFD}_{12}\rangle)$ for TFD state is always subadditive. 145

6.1 Fits (solid curves) and data (points) of the size dependence of the mutual complexity in the diagonal basis $\Delta\mathcal{C}_1^{\text{diag}}$ for different reference frequencies $\mu L = 100$, 200 and 300. The cutoff was set to $\delta/L = 1/N = 1/1000$. The solid lines correspond to the fit in eq. (6.9). 163

6.2 Left panel: the path-integral representation for a reduced density matrix $\hat{\rho}_{\mathcal{A}}$ in CFT_2. Right panel: The manifold after the optimization is given by two patches $\Sigma_{\pm}$ whose boundary is $\Sigma_{\pm} \cup \Gamma_{\mathcal{A}}$. 165

6.3 The optimal purified state with the smallest complexity corresponds to the holographic spacetime geometry shown in the shadowed region whose boundary is taken as the boundary subregion and its RT surface as shown by the red curves. The dashed black lines represent various cut-off surfaces and correspondingly define different purified states for a fixed boundary subregion. Left: A generic mixed state $\hat{\rho}_{\mathcal{A}}$ corresponding to a boundary subregion $\mathcal{A}$. Right: A bipartite mixed state $\hat{\rho}_{\mathcal{AB}}$. 170

List of Tables

1.1 The holographic dictionary for the AdS/CFT correspondence 11

6.1 Comparison of the mutual complexity in field theory and in holography for the various cases studied in this paper. Above, μ is the characteristic frequency of the reference state while β is the inverse temperature. $^{\diamond}$ there are two possible definitions for mutual complexity in the physical basis for subregions of the vacuum, see discussion around eq. (3.144) for more details; § the inequality is saturated (*i.e.,* $\Delta\mathcal{C}_{\rm V} = 0$) when evaluated for $t_{\rm L} = 0 = t_{\rm R}$ for the TFD state and for $t = 0$ for the vacuum state, as was done in the preceding QFT calculations; † in both cases, $\Delta\mathcal{C}$ was proportional to the entropy of the thermal state; ‡ in both cases, the leading contribution to $\Delta\mathcal{C}$ had the same form as the leading divergence in the entanglement entropy of the subregions. 158

Chapter 1

Introduction

General relativity (GR) and quantum mechanics (QM), which were both developed at the beginning of the 20th century, have since stood as the two pillars of theoretical physics and they comprise the framework of describing fundamental interactions in nature, *i.e.,* strong interaction, weak interaction, electromagnetic interaction, and gravity. By combining the first three interactions with gauge theories, the Standard model became the most successful theory in describing the fundamental structure of microscopic matter. It has been substantially tested and has demonstrated huge success in providing experimental predictions. On the other hand, general relativity as the geometric theory of gravitation and spacetime formulates the current understanding of our universe on a large scale. Built on GR, modern cosmology has developed along tandem tracks of theory and observation, and also gives detailed predictions that are in excellent agreement with various observations at remarkable accuracy.

However, the two fundamental theories are mutually incompatible as they stand. Superficially, GR is still a classical theory without including quantum effects such as quantized gravitons. In QM or quantum field theory (QFT), spacetime serves as background while it is dynamical in GR. Different from weakly gravitating systems, quantum effects can not be ignored in strongly gravitating systems such as the vicinity of black holes. In particular, a quantum theory of gravity is expected to shed new light on many intriguing and fundamental questions in theoretical physics, such as the black hole information paradox, singularities of cosmology, and the origin of our universe. It is natural and fascinating to seek a quantum gravity that can incorporate both the basic principles of general relativity and quantum theory. Constructing a quantum gravity theory that is expected to provide a satisfactory description of the microstructure of spacetime at the Planck scale has been one of the biggest challenges at the heart of modern theoretical physics.

So we have string theory. It offers a basic framework wherein one can find an elegant unification of gravity with all other fundamental interactions. It was first studied in the late 1960s in attempts to understand the dynamics of strongly interacting hadrons. Since 1974, when string theorists identified the massless spin-two particle in the string's spectrum as the graviton, string theory became the fascinating theory in high-energy physics because it manifestly obeys the principles of quantum mechanics and also includes gravitational interactions. In particular, string theory has experienced two major revolutions. During the first superstring revolution which took place in 1984-85, five distinct and consistent string theories, namely the type IIA, type IIB, type I superstring theories and SO(32), $E_8 \times E_8$ heterotic string theories, were discovered. Each of them requires a ten-dimensional spacetime and $\mathcal{N} = 1$ or $\mathcal{N} = 2$ supersymmetry. Then the second superstring revolution that happened in the mid-1990s unified these five string theories via nonperturbative T-duality and S-duality. Most importantly, all of these correspondences implied that there is a completely unique quantum theory in 11 dimensions, the so-called M-theory. With developments in subsequent decades, string theory has now become the most promising candidate for a consistent theory of quantum gravity.

More happily, Maldacena's exciting discovery of the AdS/CFT correspondence in 1997 [9] opened a new golden door. As the most brilliant discovery after the second superstring revolution, he conjectured that the type IIB superstring theory in the asymptotically Anti-de Sitter (AdS) spacetime, more precisely, $\mathrm{AdS}_5 \times S^5$, is dual to the $\mathcal{N} = 4$ supersymmetric Yang-Mills gauge theory in 3+1 dimensions, which is a conformal field theory (CFT). The CFT can be understood as the theory living on the boundary of the AdS bulk spacetime. As a result, it became the most prominent example of the *holographic principle*, which was proposed by 't Hooft and Susskind [10, 11]. With rapid developments building on Maldacena's profound discovery, his original conjecture was extended to a more general conjecture, namely the AdS/CFT correspondence or gauge/gravity duality or holographic duality. The most intriguing appeal of holographic duality stems from its strong-weak coupling duality, which makes hard calculations in one description easy in the other. Further, the AdS/CFT correspondence may provide some fresh insights to long-standing questions in quantum gravity (*e.g.,* the black hole information paradox) because quantum field theories have been well-studied from many perspectives. The AdS/CFT correspondence has been an active research field in the past twenty years and has developed as a real computational and powerful framework that can unify the theories of physics, *e.g.,* string theory, black hole physics, condensed matter physics, and also quantum information. See [12–19] for more pedagogical and comprehensive introductions to the AdS/CFT correspondence and its applications.

The main subject explored in this thesis is the circuit complexity of mixed states and the

conjectured holographic proposals for complexity in AdS/CFT. This concept, complexity, originates from the quantum information/computation field. It was brought to studies of high energy theory by Susskind's conjecture on its holographic dual in asymptotically AdS spacetime. As an introductory chapter for the background relevant to this thesis, we provide a rudimentary review of the basics of AdS/CFT in section 1.1. Next, we briefly introduce some basic concepts about quantum information in section 1.2. In particular, we will focus on entanglement entropy and introduce its holographic description, *i.e.,* the Ryu-Takayanagi formula, which initializes the exploration of the connections between holography and quantum information.

1.1 A Short Introduction of AdS/CFT

1.1.1 The Birth of the AdS/CFT Correspondence

The $\mathrm{AdS}_{d+1}/\mathrm{CFT}_d$ correspondence [9] or gauge/gravity duality is the duality between a particular quantum gravity theory in $(d+1)$-dimensional asymptotically Anti-de Sitter (AdS) spacetime and a certain conformal field theory (CFT) living on the boundary of a d-dimensional spacetime. In particular AdS_{d+1}, as a maximally symmetric $(d+1)$-dimensional spacetime with constant negative scalar curvature, is the exact vacuum solution of Einstein's field equation with negative cosmological constant, and CFT_d, as a d-dimensional QFT invariant under conformal transformations,[1] has no dimensionful parameters. There have been several canonical examples of holographic duality developed in the last two decades. In the following, we briefly motivate the AdS/CFT correspondence with Maldacena's original prominent example, which states that the four-dimensional $\mathcal{N}=4$ super Yang–Mills (SYM) theory with gauge group $\mathrm{SU}(N)$ is fully equivalent to ten-dimensional type IIB superstring theory defined on the product spacetime $\mathrm{AdS}_5 \times S^5$. The gravity theory is referred to as 'AdS' because the five-dimensional gravitational theory obtained from Kaluza–Klein reduction of type IIB string theory on S^5 is thus living in AdS_5. Correspondingly, the 'CFT' side of this correspondence denotes the $\mathcal{N}=4$ SYM theory, which is a non-gravitational quantum field theory and also a four-dimensional conformal field theory.

The origin of Maldacena's idea is associated with the non-perturbative higher dimensional objects in superstring theory, which are called Dirichlet branes or D-branes for short.

[1] Conformal transformations include translations, dilations, special conformal transformations, and Lorentz transformations and the conformal group, is locally isomorphic to $\mathrm{SO}(d,2)$ in Lorentzian spacetime.

Dp-branes, the D-branes extending in p spatial dimensions, can be considered as a class of extended objects on which open strings can end with Dirichlet boundary conditions. For example, a D0 brane is a single point, a D1 brane is an extended string, a D2 brane is a membrane, and so on. By tuning the value of the string coupling constant g_s that controls the interaction strength between open and closed strings, the low energy excitations in the D-branes system can be viewed from two different perspectives, *viz.* the open string perspective and the closed string perspective. Maldacena examined N D3-branes (with N large and fixed) stacked on top of each other and described the dynamics of the same system via the low-energy excitations in two limits, which we will proceed to briefly review in the following. For more details of this derivation, refer to *e.g.,* [9, 14, 15, 19].

Open string perspective

Specifically, we start by considering type IIB superstring theory in $(9+1)$-dimensional spacetime with N coincident D3-branes. In the open string perspective, D3-branes are considered as the higher dimensional objects on which the open strings begin and end, and open strings are viewed as low-energy excitations of the 4-dimensional hyperplane. Of course, the N coincident D3-branes gravitate and there are also closed strings playing the role of excitations of the $(9+1)$-dimensional flat spacetime. The gravitational backreaction is thus determined by the number N of superimposed D3-branes and the dimensionless string coupling constant g_s. First, we begin in the following regime

$$\lambda \equiv 2\pi N g_s \ll 1 \,, \tag{1.1}$$

where the dimensionless parameter λ is called the 't Hooft coupling. In this limit, the strength of gravitational effects of these D3-branes is proportional to $g_s N$ (see eq. (1.7)), implying that we can effectively consider the D3-branes as objects living in $(9+1)$-dimensional Minkowski spacetime. Then, we begin by considering the N D3-branes in flat spacetime at low energies $El_s \ll 1$ where $l_s \equiv (\alpha')^{1/2}$. It means that we can ignore all massive stringy excitations and consider only massless excitations. Because these N D3-branes are coincident in space, the low-energy degrees of freedom in this set-up, *i.e.,* open strings connecting pairs of D3-branes, are all massless.

To be precise, we can decompose the complete effective action for all massless string modes as

$$S \approx S_{\text{closed}} + S_{\text{open}} + S_{\text{int}} \,, \tag{1.2}$$

where S_{closed} contains the closed string modes, S_{open} contains the open string modes and S_{int} is referred to as the interactions between open and closed string modes. As described before,

S_{closed} is given by the effective action of $(9+1)$-dimensional supergravity; however, with $El_s \ll 1$, these modes are all free fields. In the limit $El_s \to 0$, S_{int} is expected to vanish, indicating that open and closed strings decouple in this limit. All massless excitations actually propagate on the three spatial dimensions of the D3-branes, which should be described by a specific $(3+1)$-dimensional field theory. It is shown that all excitations are grouped into a four-dimensional $\mathcal{N}=4$ supermultiplet which consists of a gauge field A_μ and six real scalar fields ϕ, as well as four fermionic fields ψ as superpartners. More importantly, it is easy to notice that a single open string can carry two indices running from 1 to N because its endpoints can reside on any one of the N D3-branes. Correspondingly, all of these fields are represented by $N \times N$ matrices and can be described by a $U(N)$ gauge field theory in the adjoint representation. At the lowest energy scales limit $\alpha' \to 0$, S_{open} reduces to

$$S_{\text{open}} = \frac{1}{2\pi g_s} \int d^4x \, \text{tr} \left(F^2 + (\nabla\phi)^2 + i\bar{\psi}\not{D}\psi + i\bar{\psi}[\phi,\psi] - [\phi,\phi]^2 \right) + \mathcal{O}(\alpha') \,, \tag{1.3}$$

The complete leading action in S_{open} is actually known as $\mathcal{N}=4$ super Yang-Mills theory by identifying its coupling g_{YM} as follows,

$$2\pi g_s = g_{\text{YM}}^2 \,. \tag{1.4}$$

Finally, after the low energy limit we consider the limit where the 't Hooft coupling grows large, *i.e.,* $\lambda = 2\pi g_s N \gg 1$. Then one arrives at the $\mathcal{N}=4$ super Yang-Mills theory at strong coupling. As a summary, we can conclude that the open string perspective with the low-energy limit reduces the effective theory of N D3-branes in type IIB superstring theory to a free type IIB supergravity in 10-dimensional Minkowski spacetime plus $\mathcal{N}=4$ super Yang-Mills theory with gauge group SU(N) [2] in four-dimensional flat spacetime, which we have taken to strong coupling.

Closed string perspective

In the closed string perspective, we consider the same limits but in the opposite order. Hence first, we leave the weak coupling regime (1.1) and consider the limit where

$$\lambda \equiv 2\pi N g_s \gg 1 \,. \tag{1.5}$$

[2]Note that the gauge group is SU(N) rather than U(N) since the U(1) degrees of freedom correspond to singleton fields located at the boundary and cannot propagate into the bulk AdS_5.

Here the gravitational effect of N D3-branes can not be neglected. In other words, we should view D3-branes as massive sources of the gravitational field that curves the $(9+1)$-dimensional spacetime. These coincident N branes form a black brane, *i.e.,* a solitonic solution of the supergravity theory. The supergravity solution of N D3-branes preserving $\mathrm{SO}(3,1) \times \mathrm{SO}(6)$ isometries of 10-dimensional Minkowski spacetime is written as

$$ds^2 = H(r)^{-1/2}\eta_{ab}dx^a dx^b + H(r)^{1/2}\delta_{ij}dx^i dx^j\,, \quad \text{with} \quad H(r) = 1 + \frac{L^4}{r^4} \tag{1.6}$$

where $a, b = 0, 1, 2, 3$, $i, j = 4 \cdots 9$ and L denotes the characteristic length scale that is related to stringy coupling by

$$L^4 = 4\pi g_s N \alpha'^2\,. \tag{1.7}$$

It is obvious that this geometry reduces to a 10-dimensional Minkowski spacetime in the region $r \gg L$. Hence beginning with the limit, we arrive at a theory of closed strings propagating in this curved spacetime background.

It is noted that the strong 't Hooft limit (1.5) and large N limit make the radius of curvature much larger than not only the stringy length scale l_s but also the Planck length scale l_{P}, *viz.*

$$\left(\frac{L}{l_s}\right)^4 = 4\pi g_s N = 2\lambda \gg 1\,, \qquad \left(\frac{L}{l_p}\right)^4 = 4\pi N \gg 1\,. \tag{1.8}$$

As a consequence, it guarantees the validity of the supergravity approximation and we can ignore quantum gravity corrections at order $\mathcal{O}(l_{\mathrm{p}})$ as well as highly excited string states at order $\mathcal{O}(l_{\mathrm{s}})$.

Next, we consider the low energy limit where excitations only have energies $El_s \ll 1$. Thanks to the gravitational redshift, the low-energy excitations only occur in the region close to the horizon (the throat region), *i.e.,* $H(r) \approx \frac{L^4}{r^4}$.[3] Hence the 10-dimensional spacetime (1.6) reduces to the near horizon geometry, namely

$$\begin{aligned} \mathrm{d}s^2 &= \frac{r^2}{L^2}\eta_{ab}\mathrm{d}x^a\mathrm{d}x^b + \frac{L^2}{r^2}\delta_{ij}\ \mathrm{d}x^i\ \mathrm{d}x^j \\ &= \frac{L^2}{z^2}\left(\eta_{ab}\mathrm{d}x^a\mathrm{d}x^b + \mathrm{d}z^2\right) + L^2\ \mathrm{d}\Omega^2_{\mathrm{S}^5} \end{aligned} \tag{1.9}$$

where the new radial coordinate is defined by $z = L^2/r$. The first part on the second line above is nothing but the AdS_5 geometry in Poincaré coordinates, and the second part

[3] We note that this near-horizon limit $L/r \gg 1$ is also accomplished by carefully implementing the so-called Maldacena limit, *i.e.,* $\alpha' \to 0$ with $\Delta r/\alpha'$ fixed and Δr as the distance between branes [9].

represents a five-dimensional sphere with radius L. This $(9+1)$-dimensional spacetime is known as $\mathrm{AdS}_5 \times S^5$.

In conclusion, the closed string perspective shows that the effective theory in the low-energy limit of large N coincident D3-branes is also described by two decoupled theories. In the asymptotically flat region, the dynamics of the closed strings is controlled by the free type IIB supergravity in 10-dimensional flat spacetime. The low-energy excitations in the near horizon region are described by type IIB superstring theory in $\mathrm{AdS}_5 \times S^5$.

Now it is time to derive the $\mathrm{AdS}_5/\mathrm{CFT}_4$ correspondence. Obviously, the open string perspective and closed string perspective are equivalent pictures of the same physics. We produced both of these pictures with the same limits, only applied in the opposite order. Counting the same type IIB supergravity in 10-dimensional flat spacetime presented in both perspectives, we are left with two decoupled theories, *i.e.,* $\mathcal{N}=4$ SYM theory and type IIB superstring theory. This is Maldacena's conjecture, *i.e.,* the first example of the AdS/CFT correspondence:

$$\begin{array}{c} \mathcal{N}=4 \text{ Super Yang-Mills theory on 4-dimensional flat spacetime} \\ \| \\ \text{Type IIB supergravity theory in } \mathrm{AdS}_5 \times S^5 \ . \end{array}$$

With such a correspondence between the gravity theory and (non-gravitational) quantum field theory, the coupling parameters on two sides are related by

$$g_{\mathrm{YM}}^2 = 2\pi g_{\mathrm{s}} \quad \text{and} \quad 2g_{\mathrm{YM}}^2 N = L^4/\alpha'^2 \,. \tag{1.10}$$

In particular, we stress that the gravity side in the the low-energy limit is a weakly-coupled classical gravitational theory, while the dual super Yang-Mills theory is strongly coupled (*i.e.,* $g_{\mathrm{YM}}^2 N \gg 1$). It is a crucial and alluring feature that the AdS/CFT correspondence is also a strong/weak coupling duality. Consequently, the AdS/CFT correspondence has been developed as a computational device because we can map a hard question in strongly coupled field theories to weakly coupled gravitating systems where the question is easier to be solved, or vise versa. For example, the applications of the AdS/CFT correspondence to condensed matter theory (CMT), especially strongly coupled systems, are generally referred to as the AdS/CMT correspondence.

To be more precise, AdS/CFT is still a conjecture without a strict mathematical 'proof'. However, there is no doubt that it is true since it has passed an enormous number of strong tests on various aspects. In particular, there are some non-perturbative quantities whose answers from both sides have been shown to agree with each other via the calculations in 'top-down' constructions. See the nice review paper [20] or recent textbooks [12, 14–16, 19] for more strong evidence and a variety of applications.

1.1.2 Holographic Dictionary

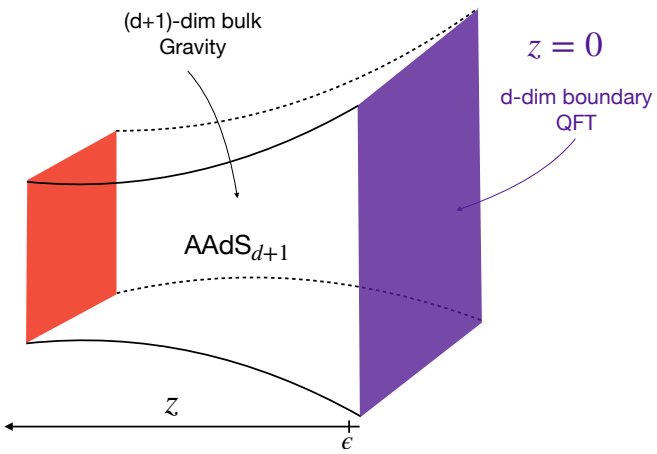

Figure 1.1: The illustration of the AdS$_{d+1}$/CFT$_d$ correspondence or gauge/gravity duality. The holographic direction is labeled by bulk coordinate z and the asymptotic boundary on which the dual QFT lives locates at $z = 0$.

With more curiosity and courage, the AdS/CFT correspondence is also expected to extend from CFTs to less symmetric QFTs with some or all supersymmetries and/or the conformal symmetry broken. Correspondingly, the bulk spacetime need not be AdS but only asymptotically AdS (AAdS). Such generalizations of AdS/CFT sometimes are specifically referred to as gauge/gravity dualities. See figure 1.1 for a simple illustration. In the rest of this thesis, we will adopt this strongest conjecture but with using the term AdS/CFT for all cases.

In particular, we should expect to match the symmetries of the field theory and gravity theory by virtue of the AdS/CFT correspondence. For example, we consider the previous duality as an illustration. As a four-dimensional conformal field theory with a vanishing β function, $\mathcal{N} = 4$ SYM's conformal symmetry group is given by SO$(4, 2)$. In addition, $\mathcal{N} = 4$ SYM also has a symmetry group SU$(4) \cong$ SO(6) associated with its R-symmetry. Correspondingly, it is clear that the geometric symmetry of the superstring theory in AdS$_5 \times S^5$ is its isometry group SO$(4, 2) \times$ SO(6), which matches the global symmetries of $\mathcal{N} = 4$ SYM. Furthermore, after counting the supersymmetry, one can show that all the symmetries of $\mathcal{N} = 4$ SYM form the supergroup PSU$(2|2, 4)$, which is also preserved by the type IIB string theory in AdS$_5 \times S^5$. Consequently, the symmetries from both sides of the AdS/CFT correspondence coincide as expected. More generally, the AdS/CFT dictionary

states that the gauge symmetries of the bulk gravitational theory are mapped to global symmetries of the boundary field theory.

As a realization of the holographic principle, the AdS/CFT correspondence obviously involves theories with different spacetime dimensions, and the CFT can be thought to live on the boundary of the AdS spacetime. To explicitly illustrate the meaning of the emergent direction we consider AdS_{d+1} in Poincaré coordinates, namely

$$ds^2 = \frac{L^2}{z^2}\left(\eta_{ab}\mathrm{d}x^a\mathrm{d}x^b + \mathrm{d}z^2\right) , \tag{1.11}$$

where z denotes the holographic radial direction, L is the AdS curvature scale as before and asymptotic boundary is located at $z = 0$. Of course, the AdS_{d+1} spacetime can be derived as the vacuum solution of Einstein gravity with the bulk action given by

$$I_{\mathrm{bulk}} = \frac{1}{16\pi G_{\mathrm{N}}}\int d^{d+1}y\sqrt{|g|}\left(\mathcal{R} + \frac{d(d-1)}{L^2}\right) , \tag{1.12}$$

which is the Einstein-Hilbert term with a negative cosmological constant $\Lambda = -\frac{d(d-1)}{2L^2}$. By virtue of the AdS/CFT dictionary, the field theory metric up to a conformal transformation is given by the induced metric at asymptotic infinity, which is parametrized by the d-dimensional coordinates x^a. It is noted that the field theory is invariant under scale transformations $x^a \to \alpha x^a$ that also rescale the energy according to $E \to E/\alpha$. From the viewpoint of the bulk spacetime, this transformation is mapped to the diffeomorphism $x^a \to \alpha x^a, z \to \alpha z$. In order to understand the emergent direction z emerging in the bulk, it is attractive to identify the holographic direction with the inverse of the energy scale in the boundary QFT, *i.e.,* $z \sim 1/E$. As a result, the evolution along the z direction corresponds to the renormalization group (RG) flow from UV to IR. Hence the scale/radius identification gives rise to the UV/IR duality. It means that high energy scale or equivalently short length scale on the QFT side maps to large radius in the bulk (*i.e.,* closer to the asymptotic boundary), and vice versa.

The AdS/CFT correspondence means that the two sides of the duality should describe the same physics. In other words, in addition to the symmetries, degrees of freedom and observables of the two distinct theories should also have a one-to-one correspondence, *i.e.,* there exists a 'holographic dictionary'. The first step towards a precise holographic dictionary between physical properties of the boundary field theory and the dual bulk gravity theory were made with the Gubser-Klebanov-Polyakov-Witten (GKPW) formula [21, 22], which we will introduce explicitly in what follows.

Focusing on the field theory side, the basic ingredients characterizing the observables in QFT are the n-point correlation functions of operators $\mathcal{O}_i(x)$, *i.e.,* $\langle\mathcal{O}_1(x_1)\cdots\mathcal{O}_n(x_n)\rangle$. It

is known that the n-point functions can be derived from the generating functional $W\left[J_i(x)\right]$ (in Lorentzian signature) that is defined by

$$Z_{\rm QFT}\left[\{J_i(x)\}\right] \equiv e^{iW[J_i]} = \left\langle \mathrm{e}^{i\sum_i \int \mathrm{d}^d x\, J_i(x)\mathcal{O}_i(x)} \right\rangle_{\rm QFT} , \tag{1.13}$$

where $J_i(x)$ denotes the source coupled to the operator $\mathcal{O}_i$. Any connected correlation function can be computed by varying the generating functional as follows

$$\langle \mathcal{O}_1(x_1)\cdots\mathcal{O}_n(x_n)\rangle_{\rm QFT,c} = (-i)^n \prod_{i=1}^{n} \frac{\delta}{\delta J_i\left(x_i\right)} \ln Z_{\rm QFT}\left[J_i(x)\right]\Big|_{J=0} . \tag{1.14}$$

Thus we should expect that the holographic dictionary is a recipe that rewrites the right hand side of eq. (1.14) in the language of the dual gravity theory in the bulk. However, it is subtle to characterize all observables in gravitational system because the spacetime itself is also dynamical. Roughly speaking, we can impose Dirichlet boundary conditions at $z=0$ and define the partition function of the gravity theory as a functional of the boundary values $\phi_i^{(0)}(x)$ of all the dynamical fields $\phi_i(z,x)$ propagating in the bulk spacetime, *viz.*

$$Z_{\rm Grav}\left[\phi_i^{(0)}(x)\right] \equiv \int^{\phi_i\to\phi_i^{(0)}(x)} \left(\prod_i \mathcal{D}\phi_i\right) \mathrm{e}^{iS_{\rm Grav}[\phi_i]} , \tag{1.15}$$

where $S_{\rm Grav}\left[\phi_i\right]$ is the action of gravity and the other bulk fields ϕ_i. As an essential step towards the AdS/CFT dictionary, Gubser, Klebanov, Polyakov, and Witten [21, 22] found that there is a one-to-one correspondence between single trace operators $\mathcal{O}_i$ in the boundary QFT and bulk dynamical fields $\phi_i(z,x)$ by relating the asymptotically AdS boundary value of the fields with the sources of boundary operators:

$$J_i(x) \longleftrightarrow \phi_i^{(0)}(x) , \tag{1.16}$$

where the asymptotic value $\phi_i^{(0)}(x)$ can be precisely determined, as we will see in the example discussed below. With this field/operator map, the GKPW formula identifies the partition function of a QFT in the presence of sources J_i with the partition function of a bulk gravity theory, namely

$$Z_{\rm QFT}\left[\phi_i^{(0)}(x)\right] = \left\langle \mathrm{e}^{i\sum_i \int \mathrm{d}^d x\, \phi_i^{(0)}\mathcal{O}_i} \right\rangle_{\rm QFT} = Z_{\rm Grav}\left[\phi_i^{(0)}(x)\right] , \tag{1.17}$$

which constructs an essential cornerstone of the holographic dictionary.

d-dim Boundary: Field Theory	$(d+1)$-dim Bulk: Gravity
Partition function Z_{QFT}	Partition Function Z_{Grav}
Scalar operator $\mathcal{O}$	Scalar field ϕ
Energy-momentum T^{ab}	Metric tensor $g_{\mu\nu}$
Fermionic operator $\mathcal{O}_\psi$	Dirac field ψ
Global current J^a	Maxwell field A_μ
Conformal dimension of operator	Mass of the corresponding field
Spin/charge of the operator	Spin/charge of the field
Global symmetries	Gauge(local) symmetries
Finite temperature	Hawking temperature T
Phase transition	Gravitational instability
Renormalization group flow	Evolution in the radial AdS direction
Free energy	On-shell value of the action
Entanglement entropy S_{EE} of a subregion $\mathcal{A}$	Area of the minimal surface

Table 1.1: The holographic dictionary for the AdS/CFT correspondence

As the simplest example, let us consider the free scalar field propagating in the Poincaré patch of AdS_{d+1} with action defined by

$$S_{\mathrm{matt}}[\phi] = -\int_{\mathrm{AdS}} \mathrm{d}z\mathrm{d}^d x\,\sqrt{-g}\left(\frac{1}{2}g^{\mu\nu}\nabla_\mu\phi\nabla_\nu\phi + \frac{m^2}{2}\phi^2\right) . \tag{1.18}$$

According to the AdS/CFT correspondence, it is dual to adding some particular scalar operator $\mathcal{O}$ in the dual CFT_d living on the asymptotic boundary. In the bulk theory, the dynamics of the scaler field is given by the massive Klein–Gordon equation $\nabla^2\phi = m^2\phi$. Since we are interested in the asymptotic boundary conditions, one can solve this equation in a series expansion as $z \to 0$ and obtain two linearly independent solutions as follows

$$\phi(z \to 0, x) = \phi^{(0)}(x)z^{\Delta_-} + \cdots + \phi^{(1)}(x)z^{\Delta_+} + \cdots . \tag{1.19}$$

with

$$\Delta_{\pm} = \frac{d}{2} \pm \sqrt{\frac{d^2}{4} + m^2 L^2}\,. \tag{1.20}$$

We call the two independent modes $\phi^{(0)}, \phi^{(1)}$ the non-normalizable mode and normalizable mode, respectively. By virtue of the AdS/CFT dictionary, the non-normalizable mode that gives rise to the boundary value of bulk scalar field $\phi(z,x)$ is equal to the source of the dual boundary operator $\mathcal{O}$, *i.e.,*

$$J(x) = \phi^{(0)}(x) \equiv \lim_{z\to 0} \phi(z,x) z^{-\Delta_-}\,. \tag{1.21}$$

Noting the non-normalizable mode is rescaled as $\phi^{(0)} \to \alpha^{-\Delta_-}\phi^{(0)}$ under the isometry $\{z, x^i\} \to \{\alpha z, \alpha x^i\}$, one can find that its dual operator $\mathcal{O}$ must rescale as

$$\mathcal{O}(x) \quad \longrightarrow \quad \alpha^{-\Delta_+}\mathcal{O}(\alpha x)\,, \tag{1.22}$$

indicating that the scalar operator inserted on the dual field theory has a conformal dimension Δ_+. Furthermore, we can find that the AdS/CFT dictionary also explains the meaning of the normalizable mode $\phi^{(1)}$ on the dual field theory. Evaluating the expectation value of the dual operator $\mathcal{O}$ by using the GKPW formula, one obtains

$$\langle \mathcal{O}(x) \rangle_{\text{QFT}} \propto \phi^{(1)}(x)\,. \tag{1.23}$$

In summary, we see that the holographic dictionary identifies the source with the leading contribution $\phi^{(0)}$ of the corresponding bulk field and also relates the vacuum expectation value to the subleading contribution $\phi^{(1)}$. We should note that it is also possible to reverse the relation between $\phi^{(1)}, \phi^{(0)}$ in the AdS/CFT dictionary if the scalar mass satisfies $-\frac{d^2}{4} < m^2L^2 \leq -\frac{d^2}{4} + 1$ and the conformal dimension of the dual operator is given by Δ_- [21, 22].

Although we only consider here the free scalar field for simplicity, one can also perform a similar analysis for other fields, *e.g.,* spin 2 field, fermionic field, Maxwell field and so on. To close this short review, we summarize some useful quantities appearing in the AdS/CFT dictionary in table 1.1.

1.1.3 Geometries and States

Recalling symmetry argument we mentioned before, the conformal symmetry group of CFT_d coincides with the isometry group $\text{SO}(2,d)$ of AdS_{d+1} spacetime. By virtue of the AdS/CFT correspondence, we can imagine that there is a certain 'holographic' CFT_d living

on the boundary of its dual AdS_{d+1} spacetime. An interesting question is which CFTs are holographic. However, it is not clear by now what are either the necessary or the sufficient conditions on a CFT for the existence of a semiclassical dual gravitational system. Roughly speaking, it is believed that a holographic CFT that is dual to Einstein gravity coupled with matter should have a large number of degrees of freedom (*e.g.,* large N) strong coupling, a large spectrum gap, and a sparse low energy spectrum [23–25]. We have seen that the AdS/CFT dictionary as shown in table 1.1 suffices to map the observables in CFT_d to those in AdS_{d+1}. On the other hand, it is worth pointing out that the AdS/CFT correspondence, as a duality between non-gravitational field theory and gravity theory, is about not only observables but also states. The holographic field theory can be in any of the states in its Hilbert space and the AdS/CFT correspondence also claims that each such state maps to an analogous state in the Hilbert space of its dual (quantum) gravity theory. From this point of view, the AdS/CFT correspondence is thus an isomorphism between the Hilbert spaces of the boundary field theory and the dual bulk gravity theory. Furthermore, we are more interested in a limited class of CFT states that can be described geometrically in terms of smooth bulk spacetimes. This subspace in the full CFT Hilbert space is referred to as the *code subspace*. For later use, we will explicitly discuss various quantum states of a CFT and the dual bulk spacetime geometry in this subsection.

First of all, it is easy to notice that the vacuum state of CFT_d should correspond to the vacuum AdS_{d+1} spacetime because the vacuum state of CFT_d preserves the $\text{SO}(2,d)$ conformal symmetry. Furthermore, excited states of the field theory are thus dual to non-trivial asymptotically AdS geometries. With the scalar example discussed in the last subsection, the excited states obtained by small perturbations of vacuum state with the scalar operator $\mathcal{O}$ can be understood as coherent states and the corresponding asymptotically AdS spacetimes are derived by solving the Einstein equation with the condensation of the scalar field ϕ propagating in the bulk spacetime. For high-energy excited states, the holographic spacetime may have significantly different geometry and even topology. In particular, we are interested in the thermal state of the CFT that is formally defined by the density matrix, namely

$$\hat{\rho}_{\text{th}} = \frac{e^{-\beta \hat{H}_{\text{CFT}}}}{\text{Tr}\left(e^{-\beta \hat{H}_{\text{CFT}}}\right)} = \frac{e^{-\beta \hat{H}_{\text{CFT}}}}{Z_{\text{CFT}}(\beta)}\,, \tag{1.24}$$

where $\hat{H}_{\text{CFT}}$ denotes the CFT Hamiltonian and $\beta = 1/T$ is the inverse temperature. Its holographic dual spacetime is nothing but a black hole geometry with the same temperature[4]. See the figure 1.2 for a graphical illustration. In the following, we list some widely

[4]For a thermal state with low temperature, its corresponding geometry may be only thermal AdS rather

discussed quantum states in CFT_d and the corresponding (asymptotically) AdS_{d+1} geometries in higher dimensions ($d > 2$).

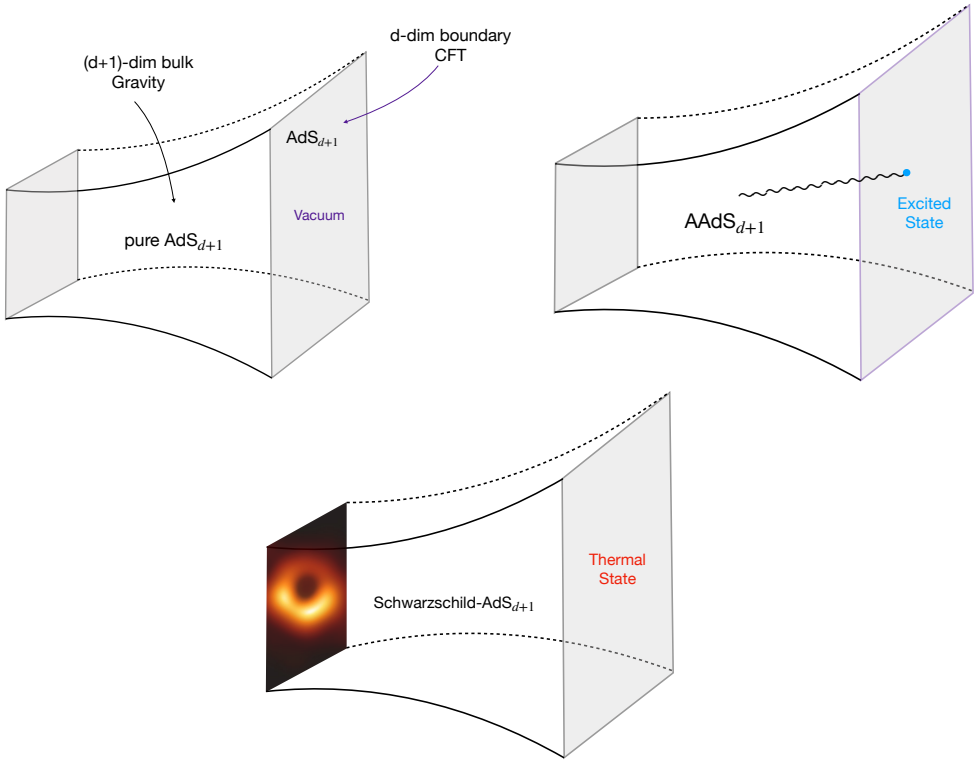

Figure 1.2: The duality between quantum states of boundary field theory and bulk geometries in the $\mathrm{AdS}_{d+1}/\mathrm{CFT}_d$ correspondence.

Vacuum State of CFT_d on $\mathbb{R}^{d-1,1}$

The bulk spacetime is the Poincaré patch of AdS_{d+1} (*i.e.*, eq. (1.11)) with metric

$$ds^2 = \frac{L^2}{z^2}\left(-dt^2 + d\mathbf{x}_{d-1}^2 + dz^2\right) , \tag{1.25}$$

where $\mathbf{x}_{d-1}$ indicates the $(d-1)$-dimensional spatial directions and the asymptotic boundary is obtained by the limit $z \to 0$.

than a black hole geometry. See the discussion below eq. (1.28).

Vacuum State of CFT$_d$ on $\mathbb{R} \times S^{d-1}$

The bulk spacetime is the global AdS$_{d+1}$ geometry with metric

$$\begin{aligned} ds^2 &= -f(r)dt^2 + \frac{dr^2}{f(r)} + r^2 d\Omega_{d-1}^2 \,, \\ \text{with} \qquad f(r) &= 1 + \frac{r^2}{L^2} \,, \end{aligned} \tag{1.26}$$

where the asymptotic boundary is obtained by the limit $r \to \infty$.

Thermal State of CFT$_d$ on $\mathbb{R}^{d-1,1}$

The bulk spacetime dual to the thermal state (with temperature T) of the CFT$_d$ living on Minkowski spacetime is given by the planar Schwarzschild-AdS$_{d+1}$ black hole with metric

$$\begin{aligned} ds^2 &= \frac{L^2}{z^2}\left(-f(z)dt^2 + d\mathbf{x}_{d-1}^2 + \frac{dz^2}{f(z)}\right) \,, \\ \text{with} \qquad f(z) &= 1 - \frac{z^d}{z_h^d} \,, \qquad T = \frac{d}{4\pi z_h} \,, \end{aligned} \tag{1.27}$$

where the planar horizon of the black hole is located at $z = z_h$.

Thermal State of CFT$_d$ on $\mathbb{R} \times S^{d-1}$

The bulk spacetime dual to the thermal density matrix at high temperature T of the CFT$_d$ on on $\mathbb{R} \times S^{d-1}$ is the global Schwarzschild-AdS black hole spacetime

$$\begin{aligned} ds^2 &= -f(r)dt^2 + \frac{dr^2}{f(r)} + r^2 d\Omega_{d-1}^2 \,, \\ \text{with} \qquad f(r) &= 1 + \frac{r^2}{L^2} - \frac{r_h^{d-2}}{r^{d-2}}\left(1 + \frac{r_h^2}{L^2}\right) \,, \\ T &= \frac{1}{4\pi r_h}\left(d\frac{r_h^2}{L^2} + (d-2)\right) \,, \end{aligned} \tag{1.28}$$

where the position of the black hole horizon is $r = r_h$. We also note that the global black hole geometry is the solution only for large black holes with $r_h \geq L$ or equivalently $T \geq \frac{d-1}{2\pi L}$ whereas the dual geometry at low temperature is thermal AdS$_{d+1}$. The transition between the two solutions happens at the critical temperature $T_c = \frac{d-1}{2\pi L}$, the so-called Hawking-Page transition.

Thermal State of CFT$_d$ on $\mathbb{R} \times \mathbb{H}^{d-1}$

The dual black hole geometry with a hyperbolic horizon is defined by the metric

$$\begin{aligned} ds^2 &= -f(r)dt^2 + \frac{dr^2}{f(r)} + r^2\left(du^2 + \sinh^2 u\, d\Omega_{d-2}^2\right) , \\ \text{with} \qquad f(r) &= \frac{r^2}{L^2} - 1 - \frac{r_h^{d-2}}{r^{d-2}}\left(\frac{r_h^2}{L^2} - 1\right) , \\ T &= \frac{1}{4\pi r_h}\left(d\frac{r_h^2}{L^2} - (d-2)\right) , \end{aligned} \tag{1.29}$$

where the hyperbolic horizon of the black hole is located at $r = r_h$.

Finally, let us point out that the black hole geometry associated with the thermal density matrix $\hat{\rho}_{\text{th}}$ denotes the one side of the full black hole spacetime, *i.e.,* the region observable from one asymptotic boundary. In the next section, we will show that the full two-sided black hole geometries are dual to particular pure states entangling two copies of the boundary CFT.

1.2 Holography Meets Quantum Information

After introducing the very basic ideas and concepts of the AdS/CFT correspondence in the last section, we will move to the interface between quantum information theory and holography (or quantum gravity). Recent research on this direction, *e.g.,* [26–38] has suggested that quantum information perspectives can produce fascinating new insights into fundamental questions about the AdS/CFT correspondence, as well as quantum gravity. Especially, it is found that the entanglement structure of the underlying quantum mechanical degrees of freedom plays a crucial role in understanding the emergent spacetime geometry and its dynamics. See *e.g.,* [17, 18, 29, 39, 40] for recent reviews about various aspects along this direction.

The connection between quantum information concepts and gravity has appeared in the early 1970s even before the birth of the AdS/CFT correspondence. Inspired by the similarities between the second law of thermodynamics and the non-decreasing property of the horizon area, Bekenstein conjectured that a black hole should have an entropy proportional to its horizon area. With the celebrated discovery from Hawking that a black hole also emits thermal radiation, it was confirmed that a black hole has a temperature

$T = \frac{\kappa}{2\pi}$ determined by its surface gravity κ. Furthermore, the precise relation between the black hole entropy and the area of its horizon, *i.e.,*

$$S_{\rm BH} = \frac{\text{Area(horizon)}}{4G_{\rm N}}\,, \tag{1.30}$$

is referred to as the Bekenstein–Hawking formula. It is worthwhile mentioning that this formula was a key inspiration for the holographic principle. In light of the statistical mechanics interpretation of entropy, the black hole entropy formula naturally suggests that a black hole should contain a large number of microstates as the statistical origin of its large entropy. The first realization of black hole microstate counting was achieved in string theory by Strominger and Vafa [41]. It is still a tantalizing and profound question and believed to be an extraordinary window from classical gravitational physics into the nature of quantum gravity at the Planck scale.

On the other hand, the AdS/CFT correspondence also brought fresh insights into understanding black hole entropy. From the geometry and state duality, the Schwarzschild-AdS black hole (*e.g.,* eq. (1.28)) is dual to the thermal state of a boundary CFT. From the view of the boundary field theory, the black hole entropy is thus equivalent to the entropy of its dual thermal state $\hat{\rho}_{\rm th}$, *i.e.,*

$$S_{\rm BH} = S_{\rm th}(\hat{\rho}_{\rm th})\,. \tag{1.31}$$

Particularly, this formula connects the entropy of the boundary field theory to a geometric quantity in the bulk spacetime, *i.e.,* the area of the horizon. Inspired by this area law as well as the AdS/CFT duality, Ryu and Takayanagi in 2006 [26] proposed that the entropy of a subsystem of the holographic CFT is geometrically described by the area of a certain minimal surface in the dual (asymptotically) AdS spacetime. In this section, we will introduce this wonderful discovery, *i.e.,* holographic entanglement entropy, in more detail. As preparation, we will first introduce some basic concepts about quantum states of subsystems and entanglement measures. An interested reader can refer to standard textbooks, *e.g.,* [42–44] for more introduction of associated concepts in quantum information science.

1.2.1 Quantum States and Entanglement

First of all, a quantum state of a system in quantum mechanics can be understood as an operator $\hat{\rho}$ acting on its Hilbert space $\mathcal{H}$ with the following properties:

$$\hat{\rho}^\dagger = \hat{\rho}\,, \qquad \hat{\rho} \geq 0\,, \qquad {\rm Tr}\hat{\rho} = 1\,. \tag{1.32}$$

To wit, a quantum state $\hat{\rho}$ known as the density operator is a non-negative hermitian operator with unit trace. By choosing some basis, the density operator is parametrized by a matrix and the components are also called the density matrix. In this thesis, we will not distinguish these two terminologies. It is convenient to choose a special basis denoted by a set of normalized vectors $\{|\psi_i\rangle\}$ and then diagonalize the density matrix as

$$\hat{\rho} = \sum_i p_i \, |\psi_i\rangle \, \langle\psi_i| \ , \tag{1.33}$$

where the eigenvalues $\{p_i\}$ form a probability distribution. The expectation value of any operator $\mathcal{O}$ with respect to the density matrix $\hat{\rho}$ is given by a trace, *viz.*

$$\langle\mathcal{O}\rangle_{\hat{\rho}} = \mathrm{Tr}\,(\hat{\rho}\,\mathcal{O}) = \sum_i p_i \, \langle\psi_i| \, \mathcal{O} \, |\psi_i\rangle \ . \tag{1.34}$$

In particular, a quantum state is called pure state if and only if it can be written as an outer product

$$\hat{\rho} = |\psi\rangle \, \langle\psi| \ . \tag{1.35}$$

Any other states are referred to as mixed states. For a given quantum state or density operator $\hat{\rho}$, it is not always easy to judge whether it is pure or mixed. A useful measure for this question is the von Neumann entropy S_{vN} that is defined by

$$S_{\text{vN}}\,(\hat{\rho}) \equiv -\mathrm{Tr}\,(\hat{\rho}\ln\hat{\rho}) = \langle -\ln\hat{\rho}\rangle_{\hat{\rho}}\,. \tag{1.36}$$

It is obvious that the von Neumann entropy of any pure state is always zero and that of any mixed state is non-zero. This is why the von Neumann entropy S_{vN} is a useful diagnostic of the mixedness of a quantum state. In addition, the von Neumann entropy has numerous remarkable properties. For example, the von Neumann entropy in a finite Hilbert space $\mathcal{H}$ is bounded from above, *viz.*

$$S_{\text{vN}}\,(\hat{\rho}) \leq \ln d\,, \tag{1.37}$$

where the number d is the dimension of $\mathcal{H}$ and the inequality is saturated if only if $\hat{\rho}$ is maximally mixed (*i.e.,* a state proportional to the identity operator, denoted by $\mathbb{I}$). From the definition and the simple relation $\ln\left(U\,\hat{\rho}\,U^\dagger\right) = U\ln\left(\hat{\rho}\right)U^\dagger$ [5], it also straightforward to show that the von Neumann entropy is invariant under any unitary transformation:

$$S_{\text{vN}}\,(\hat{\rho}) = S_{\text{vN}}\left(U\,\hat{\rho}\,U^\dagger\right) \ . \tag{1.39}$$

[5]This is derived by using the definition of the logarithm of an operator $\hat{\rho}$

$$\log\hat{\rho} \equiv \sum_n (-1)^{n+1}\frac{(\hat{\rho}-\mathbb{I})^n}{n}\,, \tag{1.38}$$

and also the relation $(U\,\hat{\rho}\,U^\dagger)^n = U\,\hat{\rho}^n\,U^\dagger$ for any unitary operator U.

For the purpose of showing the connection to information science, one can rewrite the von Neumann entropy of the density matrix (1.33) as

$$S_{\text{vN}}\left(\hat{\rho}\right) = -\sum_i p_i \ln p_i \,, \tag{1.40}$$

which is nothing but the Shannon entropy of the distribution $\{p_i\}$.

Now, we move to the discussion of entanglement between two subsystems. First of all, let us consider a total system that is partitioned into two subsystems $\mathcal{A}, \mathcal{B}$. In terms of Hilbert space, we define the total Hilbert space of the bipartite system $\mathcal{H}$ as the direct product of two factors,

$$\mathcal{H} = \mathcal{H}_{\mathcal{A}} \otimes \mathcal{H}_{\mathcal{B}} \,. \tag{1.41}$$

Focusing on the quantum states associated with one subsystem, say $\mathcal{A}$, we can construct an operator $\hat{\rho}_{\mathcal{A}}$ that only acts on $\mathcal{H}_{\mathcal{A}}$ by taking a partial trace over the subsystem $\mathcal{B}$,

$$\hat{\rho}_{\mathcal{A}} \equiv \text{Tr}_{\mathcal{B}}\left(\hat{\rho}\right) = \sum_j \left\langle \psi_j^{\mathcal{B}} \right| \hat{\rho} \left| \psi_j^{\mathcal{B}} \right\rangle \,, \tag{1.42}$$

with $\{\left|\psi_j^{\mathcal{B}}\right\rangle\}$ to be an orthonormal basis for $\mathcal{H}_{\mathcal{B}}$. This is often called a marginal state or a reduced density matrix. It is noted that the above definition does not depend on the choice of the basis $\{\left|\psi_j^{\mathcal{B}}\right\rangle\}$. An alternative definition of the reduced density matrix is the following condition

$$\text{Tr}\left(\hat{\rho}\,\mathcal{O}\right) = \text{Tr}_{\mathcal{A}}\left(\hat{\rho}_{\mathcal{A}}\,\mathcal{O}_{\mathcal{A}}\right) \,, \tag{1.43}$$

which should hold for any operator $\mathcal{O}$ of the form $\mathcal{O} = \mathcal{O}_{\mathcal{A}} \otimes \mathbb{I}_{\mathcal{B}}$.

Specifically, it is interesting to start from a pure state $\hat{\rho} = \left|\Psi\right\rangle\left\langle\Psi\right|$ in the total system $\mathcal{AB}$. We can choose the vector sets $\{\left|\psi_i^{\mathcal{A}}\right\rangle\}, \{\left|\phi_j^{\mathcal{B}}\right\rangle\}$ to be the orthonormal bases for $\mathcal{H}_{\mathcal{A}}$ and $\mathcal{H}_{\mathcal{B}}$, respectively, and define the bipartite pure state in the form of

$$\left|\Psi\right\rangle = \sum_{i,j} p_{ij} \left|\psi_i^{\mathcal{A}}\right\rangle \otimes \left|\phi_j^{\mathcal{B}}\right\rangle \,. \tag{1.44}$$

In this case, the rest of the subsystem $\mathcal{B}$ is complementary to the subsystem $\mathcal{A}$ and thus is often denoted by $\mathcal{A}^c$ for simplicity. When the coefficient factorizes, *i.e.,* $p_{ij} = p_i^{\mathcal{A}} p_j^{\mathcal{B}}$, the state $\left|\Psi\right\rangle$ is a product state such that

$$\left|\Psi\right\rangle = \left|\Psi_{\mathcal{A}}\right\rangle \otimes \left|\Phi_{\mathcal{B}}\right\rangle \,. \tag{1.45}$$

This is also called a *separable state*. This is the case where both reduced density matrices become pure states,

$$\hat{\rho}_{\mathcal{A}} = \left|\Psi_{\mathcal{A}}\right\rangle\left\langle\Psi_{\mathcal{A}}\right| \,, \qquad \hat{\rho}_{\mathcal{A}^c} = \left|\Phi_{\mathcal{A}^c}\right\rangle\left\langle\Phi_{\mathcal{A}^c}\right| \,, \tag{1.46}$$

which means that the subsystems $\mathcal{A}$ and $\mathcal{A}^c$ are not entangled. If the pure state $|\Psi\rangle$ is not separable, it is then called entangled (or inseparable). Roughly speaking, we can think that the quantum entanglement measures how much a given pure state differs from a separable state (*i.e.,* eq. (1.45)). Instead, from the perspective of subsystems, one can claim that the presence of quantum entanglement results in mixed states $\hat{\rho}_{\mathcal{A}}, \hat{\rho}_{\mathcal{A}^c}$ as the reduced density matrices of the respective subsystem $\mathcal{A}, \mathcal{A}^c$. As advertised before, we are interested in quantifying the amount of quantum entanglement between the subsystems. It turns out that the simplest entanglement measure is given by the von Neumann entropy of the reduced density matrix, *i.e.,*

$$S_{\text{EE}}\left(\hat{\rho}_{\mathcal{A}}\right) \equiv -\text{Tr}_{\mathcal{A}}\left(\hat{\rho}_{\mathcal{A}} \ln \hat{\rho}_{\mathcal{A}}\right) = S_{\text{vN}}\left(\hat{\rho}_{\mathcal{A}}\right) , \tag{1.47}$$

which is specifically referred to as the *entanglement entropy* [6].

Although we begin with a bipartite system to introduce the entanglement entropy, there is no reason to stop us considering the entanglement entropy in multipartite systems. Furthermore, the entanglement entropy obeys some interesting inequalities in bipartite and multipartite systems. As a summary, we list several useful properties of entanglement entropy without proof below.

- The entanglement entropy of the subsystem $\mathcal{A}$ and its complement $\mathcal{A}^c$ in a bipartite pure state are equivalent:
$$S_{\text{EE}}\left(\hat{\rho}_{\mathcal{A}}\right) = S_{\text{EE}}\left(\hat{\rho}_{\mathcal{A}^c}\right) . \tag{1.48}$$
- The entanglement entropies satisfy the subadditivity
$$S_{\text{EE}}\left(\hat{\rho}_{\mathcal{A}}\right) + S_{\text{EE}}\left(\hat{\rho}_{\mathcal{B}}\right) \geq S_{\text{EE}}\left(\hat{\rho}_{\mathcal{A}\mathcal{B}}\right) , \tag{1.49}$$
and also the triangle inequality
$$\left|S_{\text{EE}}\left(\hat{\rho}_{\mathcal{A}}\right) - S_{\text{EE}}\left(\hat{\rho}_{\mathcal{B}}\right)\right| \leq S_{\text{EE}}\left(\hat{\rho}_{\mathcal{A}\mathcal{B}}\right) , \tag{1.50}$$
which is known as the Araki-Lieb inequality [45].

[6] To be more precise, the entanglement entropy, as a measure of entanglement between subsystems, is only defined for a reduced density matrix for any of the subsystems while the von Neumann entropy can be defined for any given density matrix. However, some literature in high energy physics does not distinguish the entanglement entropy from the von Neumann entropy. There are also many other entanglement measures, which are different from the von Neumann entropy.

- The entanglement entropies satisfy the strong subadditivity, namely

$$\begin{aligned} S_{\text{EE}}\left(\hat{\rho}_{\mathcal{AB}}\right) + S_{\text{EE}}\left(\hat{\rho}_{\mathcal{BC}}\right) &\geq S_{\text{EE}}\left(\hat{\rho}_{\mathcal{A}}\right) + S_{\text{EE}}\left(\hat{\rho}_{\mathcal{C}}\right) \ , \\ S_{\text{EE}}\left(\hat{\rho}_{\mathcal{AB}}\right) + S_{\text{EE}}\left(\hat{\rho}_{\mathcal{BC}}\right) &\geq S_{\text{EE}}\left(\hat{\rho}_{\mathcal{ABC}}\right) + S_{\text{EE}}\left(\hat{\rho}_{\mathcal{B}}\right) \ , \end{aligned} \tag{1.51}$$

  in any tripartite system.

In particular, the subadditivity of entanglement entropy implies that we can define a non-negative quantity by

$$I(\mathcal{A}:\mathcal{B}) = S_{\text{EE}}\left(\hat{\rho}_{\mathcal{A}}\right) + S_{\text{EE}}\left(\hat{\rho}_{\mathcal{B}}\right) - S_{\text{EE}}\left(\hat{\rho}_{\mathcal{AB}}\right) \geq 0 \tag{1.52}$$

which is known as the mutual information. Later in the thesis, we will discuss a similar quantity defined for complexity.

In addition to the entanglement entropy, another set of measures that can characterize quantum entanglement is

$$S_n\left(\hat{\rho}_{\mathcal{A}}\right) \equiv \frac{1}{1-n}\ln\left(\text{Tr}_{\mathcal{A}}\left(\hat{\rho}_{\mathcal{A}}^n\right)\right) = \frac{1}{1-n}\ln\left(\sum_i p_i^n\right) \ , \tag{1.53}$$

which are known as the Rényi entropies. Although the canonical definition only takes $n \in \mathbb{Z}_+$, it is useful to generalize the definition by analytically extending the parameter regime to $n \in \mathbb{R}_+$. As a consequence, the Rényi entropies reduce to the entanglement entropy in the limit $n \to 1$. In calculations of entanglement entropy in QFT, this limit will be very useful in the path integral formalism and often referred to as the *replica trick*.

To close this subsection, we pay our attention on a particular entangled state that will be discussed in later of the thesis. By choosing $\mathcal{H}_{\mathcal{B}}$ to be a copy of $\mathcal{H}_{\mathcal{A}}$, the so-called *thermofield double state* (TFD state) [7] is constructed by

$$|\text{TFD}\rangle \equiv \frac{1}{Z(\beta)}\sum_{i=0} e^{-\frac{1}{2}\beta E_i}\left|E_i^{\mathcal{A}}\right\rangle \otimes \left|E_i^{\mathcal{B}}\right\rangle \ , \tag{1.54}$$

where $|E_i\rangle$ denotes the energy eigenstates and the partition function $Z(\beta) = \sum_i e^{-\beta E_i}$ normalizes the state. In the literature of high energy physics, this state is also referred to as the Hartle-Hawking state. The meaning of 'double' in TFD state becomes clear after

[7] This nomenclature, *i.e.,* thermofield double state, is common in the high energy theory literature, but the same state is often called a *squeezed state* in quantum information literature, *e.g.,* see [46–48]. For example, see the two-mode squeezed state defined in eq. (3.18).

tracing out either the system $\mathcal{A}$ or the system $\mathcal{B}$. For example, the reduced density matrix of the subsystem $\mathcal{A}$ is given by

$$\begin{aligned}\hat{\rho}_{\mathcal{A}}(\beta) &= \mathrm{Tr}_{\mathcal{B}}\left(|\mathrm{TFD}\rangle\langle\mathrm{TFD}|\right) \\ &= \frac{1}{Z(\beta)}\sum_i e^{-\beta E_i}\left|E_i^{\mathcal{A}}\right\rangle\left\langle E_i^{\mathcal{A}}\right| \\ &= \frac{1}{Z(\beta)}e^{-\beta\hat{H}_{\mathcal{A}}}\end{aligned} \tag{1.55}$$

where we introduced a Hamiltonian $\hat{H}_{\mathcal{A}}$ of the subsystem in the last line such that $\hat{H}_{\mathcal{A}}\left|E_i^{\mathcal{A}}\right\rangle = E_i\left|E_i^{\mathcal{A}}\right\rangle$. It is obvious that we can get the same state by tracing out the subsystem $\mathcal{A}$. The corresponding reduced density matrix is nothing but the thermal state with Hamiltonian $\mathcal{H}_{\mathcal{A}}$ and temperature $T = 1/\beta$. Furthermore, one can use the definition in (1.47) to evaluate the entanglement entropy of the thermal state $\hat{\rho}_{\mathcal{A}}$

$$\begin{aligned}S_{\mathrm{EE}}\left(\hat{\rho}_{\mathcal{A}}(\beta)\right) &= -\mathrm{Tr}_{\mathcal{A}}\left[\hat{\rho}_{\mathcal{A}}\left(-\beta\hat{H}_{\mathcal{A}} - \log Z\right)\right], \\ &= \frac{1}{T}(U - F) = S_{\mathrm{th}}\left(\hat{\rho}_{\mathcal{A}}(\beta)\right),\end{aligned} \tag{1.56}$$

where we defined the free energy $F \equiv -T\log Z$ and the average energy $U \equiv \langle\hat{H}_{\mathcal{A}}\rangle$ in the second line. Obviously, the entanglement entropy of the reduced density matrix derived from TFD state also equals the entropy $S_{\mathrm{th}}\left(\hat{\rho}_{\mathcal{A}}\right)$ of the thermal state. In the following, we will show that the TFD state and the entanglement entropy shown in eq. (1.56) both play notable roles in holography.

1.2.2 Holographic Entanglement Entropy

The key goal of the thesis is to study the connection between quantum information and the AdS/CFT correspondence. In many interesting cases, the dual of information-theoretic quantities are given by some geometric quantities in the AdS bulk spacetime. The most prominent example is the Ryu-Takayanagi formula that associates entanglement entropy in the boundary theory with the area of a specific surface in the AdS bulk. Before introducing the explicit example, let us motivate the RT formula by thinking of the Bekenstein-Hawking entropy again.

Recalling the duality between the Bekenstein-Hawking entropy and the thermal entropy of the thermal density matrix on boundary CFT, *i.e.,* eq. (1.31), as well as the equivalence

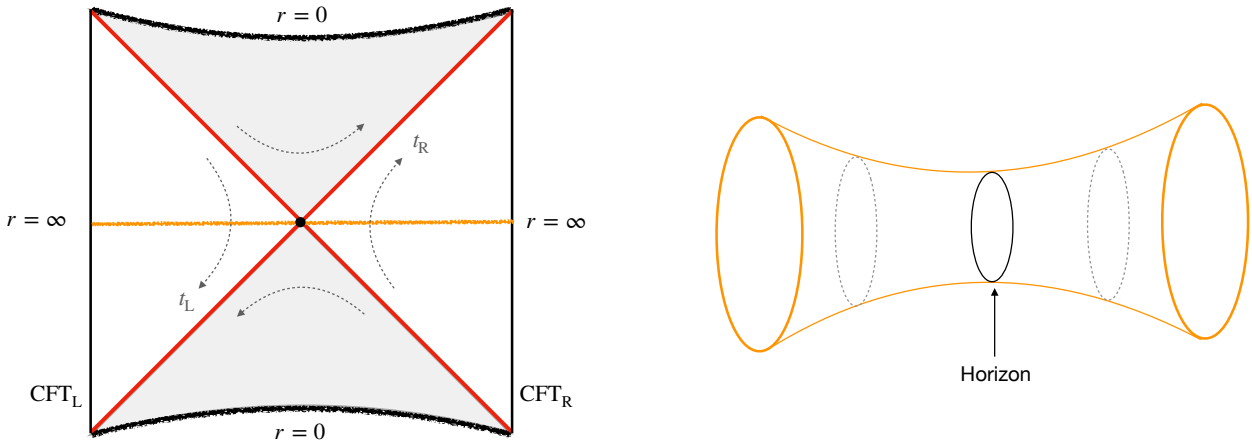

Figure 1.3: Left: The Penrose diagram of the maximally extended AdS-Schwarzschild black hole. The light grey regions denote the interior regions behind the horizon. And the spacetime has two asymptotic boundaries where the left CFT and right CFT live, respectively. Right: The time slice at $t = 0$. The horizon located at the middle is the minimal area surface separating the left space and right space.

$S_{\rm EE} = S_{\rm th}$ for thermal state, we can thus identify the Bekenstein-Hawking entropy with the entanglement entropy, *viz.*

$$S_{\rm EE}\left(\hat{\rho}_{\rm th}\right) = S_{\rm th}\left(\hat{\rho}_{\rm th}\right) = S_{\rm BH} = \frac{\text{Area(horizon)}}{4G_{\rm N}}\,, \tag{1.57}$$

by taking the reduced density matrix as the thermal density matrix $\hat{\rho}_{\rm th}$ of the boundary CFT and the right-hand side is a purely geometric quantity defined in the bulk black hole spacetime. Before we return to the generalization of the above formula, we should stress that this result is built on the AdS/CFT correspondence by which we explain the AdS black hole geometry as the dual of the thermal density matrix $\hat{\rho}_{\rm th}$. However, this state/geometry correspondence we argued before does not explain either which part of the black hole spacetime is dual to boundary thermal CFT or the meaning of 'entanglement'. In the case of the thermal density matrix (a mixed state), we can turn to the purification of thermal state, *i.e.,* TFD state, for help. Similarly, the gap in terms of the dual spacetime is bridged by the work of Maldacena in 2001 [49]. He argued that the pure TFD state is dual to the maximally extended black hole spacetime, *e.g.,* the two-sided (or eternal) AdS-Schwarzschild black hole as shown in the left plot in figure 1.3. Different from a one-sided black hole *e.g.,* formed by the collapsed a star, the eternal black hole geometry has two asymptotic regions that accommodate the left and right CFT, respectively. Noting that

the TFD state as a special purification of one thermal density matrix is associated with two separate copies of the boundary CFT (*i.e.,* the left CFT and right CFT in figure 1.3), this 'double copy' intuitively coincides with the fact the external black hole spacetime is also symmetric between two sides. Consequently, the two-sided geometry provides a perfect framework to understand the entanglement entropy $S_{\text{EE}}(\hat{\rho}_{\text{th}})$ and the black hole entropy, *i.e.,* the Bekenstein-Hawking entropy is the holographic entanglement entropy between the left CFT and right CFT, and also the thermal entropy of the thermal density matrix of a single CFT.

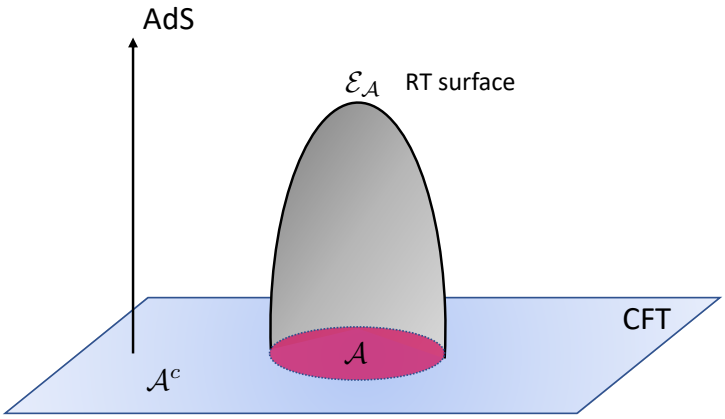

Figure 1.4: Illustration of the RT formula. The time direction has been suppressed. The red region $\mathcal{A}$ denotes the boundary subregion of a Cauchy slice in CFT_d. The vertical direction represents the radial direction in the bulk.

Note that two asymptotic regions on a fixed time slice (*e.g.,* $t_{\text{L}} = 0 = t_{\text{R}}$) are connected by a wormhole, *i.e.,* the Einstein-Rosen bridge, as shown in the right plot in figure 1.3, and the bifurcate horizon located at the middle is a codimension-2 surface that divides the bulk spacetime into two regions, one bounded by the subsystem CFT_{R} and the other by its complement CFT_{L}. One key property of the bifurcate horizon is that it is actually the minimal-area surface on its spacelike hypersurface.

In 2006, Ryu and Takayanagi generalized the above holographic formula (1.57) to any subsystems of the holographic CFT. The original RT proposal focuses on the static time-independent situation and the covariant version that includes arbitrary time dependent background was later derived by Hubeny, Rangamani, and Takayanagi (HRT) [28]. Their beautiful proposal for the holographic entanglement entropy, *i.e.,* the (H)RT formula, states that the entanglement entropy of any subregion $\mathcal{A}$ in a holographic CFT is geometrically

dual to the area of the codimension-2 extremal surface in the bulk spacetime anchored on $\partial\mathcal{A}$. To wit,

$$S_{\text{EE}}(\mathcal{A}) = \min_{\partial\tilde{\mathcal{E}}_{\mathcal{A}}=\partial\mathcal{A}} \frac{\text{Area}\left(\tilde{\mathcal{E}}_{\mathcal{A}}\right)}{4G_{\text{N}}} = \frac{\text{Area}\left(\mathcal{E}_{\mathcal{A}}\right)}{4G_{\text{N}}}, \tag{1.58}$$

where the minimization is performed over all codimention-2 spacelike surfaces $\tilde{\mathcal{E}}_{\mathcal{A}}$ that are homologous to $\mathcal{A}$ and anchored on the AdS boundary such that $\partial\mathcal{E}_{\mathcal{A}} = \partial\mathcal{A}$, and the surface $\mathcal{E}_{\mathcal{A}}$ with the minimal area is referred to as the (H)RT surface (see figure 1.4 for a graphic illustration of the RT surface.). The first derivation of the RT formula was provided by Casini, Huerta, and Myers (CHM) [50] by considering the spherically symmetric domains in the vacuum state of a CFT. Further, the RT formula was proved more generally by Lewkowycz and Maldacena in 2013 with using the AdS/CFT dictionary, *i.e.,* the GKPW formula shown in eq. (1.17), as well as the replica trick. Later, the proof of the covariant HRT proposal was provided by [51].

The celebrated (H)RT formula for holographic entanglement entropy has provided many new insights on the connection between geometry and entanglement in quantum gravity [52, 53]. However, from the quantum information perspective, entanglement entropy is simply one of a broad array of diagnostics with which to characterize quantum entanglement. On the one hand, it is interesting to explore other information-theoretic concepts and their geometric duals in the bulk. On the other hand, it is not surprising that the full understanding of quantum entanglement and spacetime geometry may require drawing on additional observables. For example, the holographic entanglement entropy does not capture the spacetime structure behind the horizon [54]. Motivated by the linear growth of the size of the wormhole, a new concept called 'complexity' and its conjectured holographic dual [55–58] were introduced in the field of high energy theoretical physics in recent years. In this thesis, we will explore the circuit complexity and the holographic complexity proposals for mixed states.

1.3 Organization of the Thesis

The rest of this thesis is organized as follows:

We start in chapter 2 by reviewing various proposals for circuit complexity of pure states, *i.e.,* Nielsen's geometric approach, Fubini-Study metric approach and also path-integral complexity. In addition, we also introduce holographic complexity proposals, *i.e.,* complexity=volume (CV) conjecture and complexity=action (CA) conjecture.

Next, we first evaluate the circuit complexity of mixed states by focusing on purification complexity in chapter 3. In section 3.2, we start by exploring the purification complexity for mixed states of a single harmonic oscillator, purified by the addition of a single extra ancillary degree of freedom. Especially, we consider the F_1 cost function and also stress the basis dependence by considering both the diagonal basis and the physical basis in our analysis. We proceed in section 3.3, by exploring the optimal purifications of multi-mode Gaussian states and further investigate the optimality of essential and mode-by-mode purifications. In sections 3.4 and 3.5, we examine the purification complexity for mixed states for two examples in a free scalar field theory: a thermal density matrix and the reduced density matrix for a subregion of the vacuum. In both cases, we study the purification complexity in both bases and also examine a quantity denoted as the mutual complexity.

In chapter 4, we move to holographic complexity and start with reviewing various holographic proposals for subregion complexity using volume and action. In sections 4.2 and 4.3, we then present the results for the holographic complexity of the thermal state associated with a single boundary of a two-sided black hole, as well as results for subregions of the vacuum in various dimensions and for various boundary geometries, which are relevant for the comparison to our QFT results in the previous chapter. Beyond the comparison of mixed-state complexity, we also investigate the mutual complexity with these holographic complexity proposals in detail and explore their additivity properties in various cases.

Next, we propose another definition for mixed-state complexity in chapter 5, which is motivated by the Fubini-Study metric approach for pure states. In particular, we explicitly use the quantum information metric as the complexity measure. Interestingly, we show in section 5.2 that this mixed state complexity is exactly the purification complexity using Fubini-Study complexity but without explicitly performing any purifications or minimization. Furthermore, we apply our proposal and study the complexity of mixed Gaussian states in section 5.3 to illustrate the conclusions for purification complexity.

Finally, we conclude with a brief review and discussion of our results in chapter 6. Specially, we discuss some other possible definitions for the complexity of mixed states in section 6.1. Next, we discuss the results about mutual complexity in detail. Further, we examine the similarities and differences between purification complexity in QFT and holographic subregion complexity. Finally, we provide some discussion of possible future directions.

Chapter 2

Complexity of Pure States

In this chapter, we review both circuit complexity and holographic complexity proposals for pure states. Parts of this chapter are based on the contents in published papers [1, 2].

2.1 Circuit Complexity Proposals

2.1.1 Nielsen's Geometric Approach

First of all, we briefly review the salient ideas required to apply Nielsen's geometric approach to circuit complexity [59–61] to evaluate the complexity of a pure state in a quantum field theory, as developed in [62]. In this setting, complexity is a measure of the difficulty or cost to prepare the particular target state $|\psi_{\rm T}\rangle$ starting with a certain simple reference state $|\psi_{\rm R}\rangle$. We are using a quantum circuit model where the preparation is accomplished by applying a series of elementary unitaries, chosen from a particular set of gates $\{g_1, \cdots, g_{\rm N}\}$. That is,[1]

$$|\psi_{\rm T}\rangle = U_{\rm TR}\ |\psi_{\rm R}\rangle = g_{i_{\rm n}} \cdots g_{i_2}\, g_{i_1}\, |\psi_{\rm R}\rangle\ , \tag{2.1}$$

whose circuit is shown in Figure 2.1. Now in general, we must expect that there are a large (*e.g.,* infinite) number of circuits or sequences of elementary gates which will accomplish the above transformation. The complexity of the target state $|\psi_{\rm T}\rangle$ is then defined as the

[1] When working with discrete gates as discussed here, we will typically only prepare $|\psi_{\rm T}\rangle$ within some tolerance ε, *e.g.,* $\| \, |\psi_{\rm T}\rangle - U_{\rm T}\, |\psi_{\rm R}\rangle \, \|^2 \leq \varepsilon$. However, with the continuous construction of unitaries introduced in eq. (2.2), we are always able to exactly prepare the target states with a finite cost, and so we will not need to introduce a tolerance.

minimum number of gates needed to construct a unitary $U_{\rm TR}$ satisfying eq. (2.1). We stress that this optimal number will depend on the choices for the reference state $|\psi_{\rm R}\rangle$ and for the gate set $\{g_1, \cdots, g_{\rm N}\}$, however, one can still obtain interesting physical insights by comparing the complexities for families of target states. Nonetheless, given a particular set of choices, the main challenge is to identify the optimal circuit from amongst the infinite range of possibilities to prepare a certain target state.

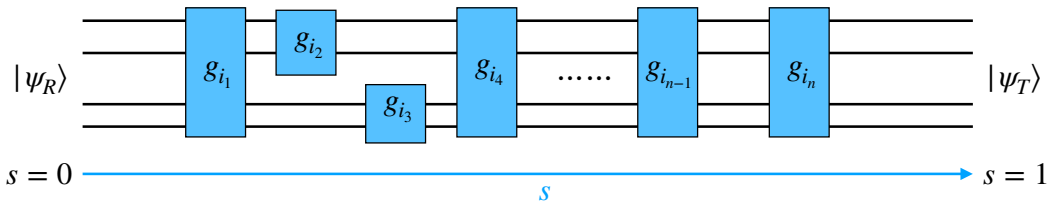

Figure 2.1: A general quantum circuit where $|\psi_{\rm T}\rangle$ is prepared beginning with $|\psi_{\rm R}\rangle$ and applying a sequence of elementary unitaries g_i.

To overcome this challenge, Nielsen and collaborators [59–61] developed a geometric method. Adapting this approach to evaluate the complexity of QFT states [62], one begins with a continuum construction of the unitary transformations acting on the states

$$U(\sigma) = \overleftarrow{\mathcal{P}} \exp\left[-i \int_0^\sigma ds\, \mathcal{H}(s)\right], \quad \text{where} \quad \mathcal{H}(s) = \sum_I Y^I(s)\, \mathcal{O}_I \tag{2.2}$$

where s parametrizes the circuit and $\overleftarrow{\mathcal{P}}$ indicates right-to-left path ordering. The (path-dependent) Hamiltonian $\mathcal{H}(s)$ is expanded in terms of a basis of Hermitian operators $\mathcal{O}_I$, which we think of as generators for elementary gates $g_I \sim \exp[-i\varepsilon\mathcal{O}_I]$ (where ε would be an infinitesimal parameter). The control functions $Y^I(s)$ then specify which gates (and how many times they) are applied at a particular point s in the circuit. Note that eq. (2.2) specifies not only the full transformation $U_{\rm TR}$ in eq. (2.1) but also a trajectory $U(\sigma)$ through the space of unitaries, or through the space of states with $|\psi(\sigma)\rangle = U(\sigma)\,|\psi_{\rm R}\rangle$, where $0 \leq \sigma \leq 1$. The circuits of interest are then the trajectories satisfying the boundary conditions

$$U(\sigma = 0) = \mathbb{1}\,, \qquad U(\sigma = 1) = U_{\rm TR}\,, \tag{2.3}$$

i.e., we start from the identity and end with the desired unitary $U_{\rm TR}$ producing the desired transformation in eq. (2.1). From this perspective, the $Y^I(s)$ can be understood as the tangent vectors to the trajectories with

$$Y^I(s)\, \mathcal{O}_I = i\, \partial_s U(s)\, U^{-1}(s)\,, \tag{2.4}$$

which will play a important role later.

Then Nielsen's approach for identifying the optimal circuit is to minimize the cost defined as [2]

$$\mathcal{D}(U(\sigma)) = \int_0^1 ds\ F\left(U(s), Y^I(s)\right), \tag{2.5}$$

where F is a local cost function depending on the position $U(s)$ and the tangent vector $Y^I(s)$. This question is then similar to the physical problem of identifying a particle trajectory by minimizing the action with Lagrangian $F(U(s), Y^I(s))$. While the precise form of the cost function F is not fixed, there are a number of desirable features for reasonable cost functions [61]: 1) Smoothness, 2) Positivity, 3) Triangle inequality and 4) Positive homogeneity – see also [62]. Some simple examples of cost functions that satisfy the above constraints are

$$F_1(U,Y) = \sum_I \left|Y^I\right| \ , \qquad\qquad F_2(U,Y) = \sqrt{\sum_I \left(Y^I\right)^2} \ . \tag{2.6}$$

Given the role of the $Y^I(s)$ as control functions, the F_1 measure comes the closest to the original concept of counting the number of gates. The F_2 measure can be recognized as the proper distance in a Riemannian geometry, and this choice reduces the problem of identifying the optimal circuit to finding the shortest geodesic connecting the reference and target states in this geometry.

Another class of cost functions introduced in [62] take the form

$$F_\kappa(U,Y) = \sum_I \left|Y^I\right|^\kappa \ . \tag{2.7}$$

These κ cost functions can be thought of as a generalization of the F_1 cost function. The corresponding vacuum complexity compares well with the results from holographic complexity but these cost functions do not satisfy the 'homogeneity' property above, *i.e.,* the cost (2.5) is not invariant under reparametrizations of s. We also note that the $\kappa = 2$ cost function will yield exactly the same extremal trajectories or optimal circuits as the F_2 cost function. An interesting suggestion in [65] was to construct a family of new cost functions using the Schatten norm (*e.g.,* see [44, 66, 67])

$$F_p(U,Y) = \|V\|_p = \left[\mathrm{Tr}\Big(\left(V^\dagger V\right)^{p/2}\Big)\right]^{1/p}, \tag{2.8}$$

[2] When this functional only depends on $Y^I(s)$ as in eq. (2.6), the cost (and the underlying geometry) is right invariant, *e.g.,* [63, 64].

where $V = Y^I(s)\mathcal{O}_I$ is the tangent vector defined as an operator that transforms the states. These cost functions satisfy all of the desired properties and further are independent of the particular choice of basis for the $\mathcal{O}_I$ – an issue for the F_1 measure and the general κ cost functions (for $\kappa \neq 2$) [62].

Before closing this short review, we must mention the group theoretic structure that naturally appears in applying this approach to evaluate the complexity of QFT states. For the problem to be tractable, one only considers a limited basis of operators $\mathcal{O}_I$ to constructing the unitaries (2.2). A practical restriction is that this basis should then form a closed algebra, and hence in many examples, the $\mathcal{O}_I$ provide a representation of a Lie algebra $\mathfrak{g}$, *i.e.*, $[\mathcal{O}_I, \mathcal{O}_J] = if_{IJ}{}^K\mathcal{O}_K$. For example, in examining the complexity of fermionic Gaussian states, an $\mathrm{O}(2N)$ group structure emerges [65]. In [62], a $\mathrm{GL}(N,\mathbb{R})$ algebra appeared in evaluating the complexity of the ground state of a free scalar field, and the latter was extended to an $\mathrm{Sp}(2N,\mathbb{R})$ algebra examining the corresponding thermofield double state in [68] – see also [65]. For excited states, an $\mathbb{R}^N \rtimes \mathrm{GL}(N,\mathbb{R})$ algebra plays a central role in evaluating the complexity of coherent states as shown in [1]. The utility of this group theoretic perspective is that the physical details of the basis operators $\mathcal{O}_I$ can be pushed to the background. Instead, the generators in eq. (2.2) are simply elements of the Lie algebra $\mathfrak{g}$, and we can choose the most convenient representation for the particular calculations of interest. In the following, we review some explicit results for circuit complexity of pure Gaussian states, which are also the necessary background for the studies of purification complexity of mixed Gaussian states in chapter 3.

2.1.1.1 Complexity of Pure Gaussian States

The first result on the complexity in QFT is developed in [62] by adopting Nielsen's geometric method to evaluate the complexity of Gaussian states in bosonic field theories. The idea was to discretize the field theory on a spatial lattice such that one obtains a chain of coupled harmonic oscillators with position operators $\hat{x}_a$ and momentum operators $\hat{p}_b$ satisfying usual commutation relations $[\hat{x}_a, \hat{p}_b] = i\delta_{ab}$, where $a, b = 1, \ldots, N$ indicate the positions on the lattice. The wavefunction of a pure Gaussian state with vanishing first moments (*i.e.*, $\langle \hat{x}_a \rangle = 0 = \langle \hat{p}_a \rangle$) that will serve as our target state takes the following form in the position-space representation

$$\langle x_a | \psi_{\mathrm{T}} \rangle \equiv \psi_{\mathrm{T}}(x_a) = \mathcal{N}_{\mathrm{T}} \exp\left[-\frac{1}{2} \sum_{a,b=1}^{N} M_{\mathrm{T}}^{ab}\, x_a\, x_b \right]. \tag{2.9}$$

The normalization constant is given by ${\mathcal{N}_{\mathrm{T}}}^4 = \det\left(\frac{M_T}{\pi}\right)$. For simplicity, we will focus on cases where the matrix M_{T}^{ab} is real (and of course, symmetric). The matrix M_{T}^{ab} can

be diagonalized by an orthogonal transformation in terms of a set of "normal mode" coordinates $\tilde{x}_k$ and characteristic frequencies ω_k[3]

$$\langle \tilde{x}_k | \psi_{\rm T} \rangle = \psi_{\rm T}(\tilde{x}_k) = \mathcal{N}_{\rm T} \exp\left[-\frac{1}{2} \sum_{k=1}^{N} \omega_k \, \tilde{x}_k^2 \right] . \tag{2.10}$$

The latter can be viewed as the Gaussian wavefunction

$$\psi_{\rm T}(\tilde{x}_k) = \mathcal{N}_{\rm T} \exp\left[-\frac{1}{2} \sum_{k,k'=1}^{N} \tilde{M}_{\rm T}^{kk'} \, \tilde{x}_k \, \tilde{x}_{k'} \right] \quad \text{with} \quad \tilde{M}_{\rm T} = O^T M_{\rm T} \, O = \text{diag}(\omega_1, \cdots, \omega_N) \, , \tag{2.11}$$

and where the orthogonal matrix O produces the change of basis $x_a = O_a{}^k \tilde{x}_k$ which diagonalizes the matrix $M_{\rm T}$. As an example, one might think of the ground state of a chain of coupled harmonic oscillators with normal mode frequencies ω_k, where the mass of the harmonic oscillators has been set to one. In fact, to be consistent with dimensional analysis, we have assumed that all the equations above also contain a characteristic mass which we will set to one from now on.

A natural reference state is the factorized Gaussian state

$$\langle x_a | \psi_{\rm R} \rangle \equiv \psi_{\rm R}(x_a) = \mathcal{N}_{\rm R} \exp\left[-\frac{1}{2} \sum_{a=1}^{N} \mu \, x_a^2 \right] , \tag{2.12}$$

where the normalization constant of the reference state is given by $\mathcal{N}_{\rm R}^4 = \det\left(\frac{M_{\rm R}}{\pi}\right) = \left(\frac{\mu}{\pi}\right)^N$. It is clear that the degrees of freedom in our reference state $|\psi_{\rm R}\rangle$ are completely disentangled in the position basis. Note that we are choosing the same reference frequency μ for each x_a so that the degrees of freedom are all on the same footing, *i.e.,*

$$M_{\rm R} = \mu \ \text{diag}(1, 1, \cdots, 1). \tag{2.13}$$

Hence for the example of a chain of oscillators, the reference state is translation invariant.[4] With this simple reference state, the change of basis introduced in eq. (2.11) yields

$$\langle \tilde{x}_k | \psi_{\rm R} \rangle = \psi_{\rm R}(\tilde{x}_k) = \mathcal{N}_{\rm R} \exp\left[-\frac{1}{2} \sum_{k=1}^{N} \mu \, \tilde{x}_k^2 \right] . \tag{2.14}$$

[3]In the following, we are taking the normal modes $\tilde{x}_k$ to be real linear combinations of the position basis modes x_a. Later we will find that for applications in QFT it is easier to consider complex normal modes x_k (see, *e.g.,* eqs. (3.80)). In this case we should replace $\tilde{x}_k^2 \to |x_k|^2$ in eq. (2.10).

[4]Similarly, the ground state of any translation invariant Hamiltonian will be translation invariant. This would be reflected in the entries of the parameter matrix $M_{\rm T}^{ab}$ in eq. (2.9) which will be a function of $a - b$.

That is, in the diagonal basis, the reference state remains a factorized Gaussian with $\tilde{M}_{\rm R} = M_{\rm R}$.

Now, the target state (2.10) can be produced by acting with a unitary transformation on this reference state (2.14), *i.e.,* $|\psi_{\rm T}\rangle = U_{\rm TR}\,|\psi_{\rm R}\rangle$ where $U_{\rm TR}$ is constructed as a string of fundamental gates,

$$g_{ab} = e^{i\frac{\varepsilon}{2}(\hat{x}_a\hat{p}_b+\hat{p}_b\hat{x}_a)}\,. \tag{2.15}$$

These gates produce a $GL(N,\mathbb{R})$ group of transformations. In the position-space representation, the action of these gates (denoted by Q_{ab}) on wavefunctional of states is illustrated with the following examples:

$$\begin{aligned} Q_{aa}\,\psi(x_a,x_b) &= e^{\varepsilon/2}\psi\left(e^{\varepsilon}x_a,x_b\right) \qquad \text{scale } x_a \to e^{\varepsilon}x_a\,,\\ Q_{ab}\,\psi(x_a,x_b) &= \psi(x_a+\varepsilon x_b,x_b) \qquad \text{shift } x_a \text{ by } \varepsilon x_b\,. \end{aligned} \tag{2.16}$$

Those with $a \neq b$ introduce entanglement between the different oscillators, while with $a = b$, the gates scale the coefficients of the corresponding coordinate – see [62] for further details.

Generally, there will be an infinite number of such "circuits," *i.e.,* sequences of fundamental gates, which will accomplish the desired transformation. The circuit complexity of pure Gaussian states (2.10) is then defined as the minimum number of gates needed to construct the desired target state (2.10) from the reference state (2.14). Based on a continuum representation of the unitary transformations (2.2), the "Hamiltonian" $\mathcal{H}(s)$ can be constructed from the (Hermitian) generators $\mathcal{O}_I$ of the fundamental gates, *i.e.,* $\mathcal{O}_{ab} = -\frac{1}{2}(\hat{x}_a\hat{p}_b+\hat{p}_b\hat{x}_a)$ in eq. (2.15). The coefficients $Y^I(s)$ are control functions specifying which gates (and how many times they) are applied at any particular point s in the circuit. Nielsen's approach identifies the optimal circuit by minimizing the cost function $D\left(U(\sigma)\right)$ defined by eq. (2.5).

With the F_2 measure, the cost (2.5) is simply the proper distance in a Riemannian geometry, and hence identifying the optimal circuit is equivalent to finding the shortest geodesic connecting the reference and target states in this geometry. Although the F_2 measure and its complexity denoted by $\mathcal{C}_2$ look like the most natural choice, it was found in [62, 69] that the $\mathcal{C}_2$ complexity does not reproduce the structure of the UV divergences shown in holographic complexity. However, this problem can be avoided by using the $F_{\kappa=2}$ measure whose circuit complexity is always given by $\mathcal{C}_{\kappa=2} = (\mathcal{C}_2)^2$. With the F_1 measure, the cost essentially counts the number of gates, and so this choice comes closest to the original concept of complexity. However, in contrast with the F_2 measure, a disadvantage of the F_1 cost function is that it is not "covariant", *i.e.,* the corresponding complexity

$\mathcal{C}_1$ depends on the choice of the basis for the generators $\mathcal{O}_I$.[5] However, the structure of the UV divergences for the $\mathcal{C}_1$ complexity was found to be similar to that for holographic complexity [62, 69]. Further, the basis dependence played an important role in [68], which studied the complexity of thermofield double (TFD) states for a free scalar. In particular, the complexity of formation was found to match that for holographic systems [71], *i.e.,* $\widetilde{\Delta\mathcal{C}}_{\text{formation}} \propto S_{\text{th}}$ in the massless limit,[6] when the gates were chosen to act on the physical degrees of freedom corresponding to the two separate copies of the field theory, *i.e.,* the Left-Right basis [68]. In contrast, if the basis of gates were chosen to act on the diagonal modes (with which the TFD state could be expressed as a simple product state), the $\mathcal{C}_1$ complexity produced $\widetilde{\Delta\mathcal{C}}_{\text{formation}} \simeq 0$ to leading order.

Obviously, the optimal circuit and circuit complexity depends on the choice of the cost functions. However, a simple result appears for a pure Gaussian state. For a broad variety of cost functions including those in eq. (2.6), the optimal circuit taking eq. (2.14) to eq. (2.10) is simply a straight-line path that only applies the scaling gates (2.15) (with $a = b$) to each of the corresponding normal modes $\tilde{x}_k$ [62]. In fact, [62] recasts the discussion of circuits in terms of a matrix representation. In particular, the trajectory through the space of states is described by

$$\tilde{M}(\sigma) = U(\sigma)\, \tilde{M}_{\text{R}}\, U^T(\sigma)\,, \tag{2.17}$$

where $\tilde{M}^{ab}$ and $\tilde{M}^{ab}_{\text{R}}$ define Gaussian wavefunctions in terms of the normal modes, as in eq. (2.11). For the case in hand, the optimal trajectory is simply

$$U(\sigma) = e^{\tilde{H}\sigma}, \qquad \text{with} \quad \tilde{H} = \frac{1}{2}\,\text{diag}(\ln(\omega_1/\mu), \cdots, \ln(\omega_N/\mu))\ . \tag{2.18}$$

For this linear trajectory, the complexity is given in terms of the elements of $\tilde{H}$, and in particular, the circuit complexity associated with various cost functions become

$$\begin{aligned} \mathcal{C}_1^{\text{diag}} &= \frac{1}{2}\sum_{k=1}^{N}\left|\ln\frac{\omega_k}{\mu}\right|\,, \\ \mathcal{C}_2 &= \frac{1}{2}\sqrt{\sum_{k=1}^{N}\left(\ln\frac{\omega_k}{\mu}\right)^2} = \sqrt{\mathcal{C}_{\kappa=2}}\,. \end{aligned} \tag{2.19}$$

[5] In [1, 70], a basis-independent alternative was proposed using the Schatten norm. For Gaussian states with vanishing first moments, *i.e.,* $\langle x_a\rangle = 0 = \langle p_a\rangle$, the complexity found using the $(p = 1)$ Schatten cost function is identical with $\mathcal{C}_1$, as shown in eq. (2.19). However, we note that this Schatten complexity does not yield the desired complexity of formation for the TFD states studied in [68].

[6] Here, S_{th} is the thermal entropy of the thermal mixed state living on either side of the TFD, or equivalently the entanglement entropy between the two copies of the field theory.

We make repeated use of this result in the following and so the interested reader is invited to see [62] for a detailed derivation. As we noted above, the $\mathcal{C}_1$ complexity is sensitive to the choice of basis for the gates (or generators), and the superscript 'diag' above is added to indicate that the complexity was evaluated using gates acting on the normal-mode coordinates $\tilde{x}_k$. As noted in the previous discussion, it is interesting to consider different choices of basis in certain cases. This is simply done by rotating the generator $\tilde{H}$ to the relevant basis and summing over (the absolute values of) its elements

$$H = O\,\tilde{H}\,O^T \qquad \text{and} \qquad \mathcal{C}_1 = \sum_{a,b=1}^{N} |H^{ab}|\,. \tag{2.20}$$

Implicitly, we have assumed here that the straight-line circuit (2.18) remains optimal in the new basis. However, in general (and for our examples below), it is difficult to prove that this simple trajectory is still optimal. Nevertheless, evaluating the cost of the trajectory (2.18) provides a bound on the $\mathcal{C}_1$ complexity for the new basis.

In addition to the Gaussian states shown in (2.9), we also note that Nielsen's geometric approach has been applied to calculate the circuit complexity of various pure states, *e.g.,* coherent states in [1, 72], TFD states in [68], fermionic Gaussian states in [65]. See *e.g.,* [4, 6, 73–79] for more exploration. The main goal of this thesis is exploring the circuit complexity of mixed states. As a generalization of Nielsen's geometric method to mixed states, a definition of mixed state complexity will be introduced in chapter 3. For explicit calculations and later comparisons with holographic complexity of subregions, we will focus on the mixed Gaussian states and F_1 measure. Besides the **diagonal basis**, we will also consider the **physical basis** that distinguishes between the two classes of oscillators in purifications of a mixed state, *i.e.,* the original physical oscillators and the auxiliary degrees of freedom. We will indicate when our calculations refer to this basis by using the superscript 'phys'. More details on different interesting bases and the distinction between them can be found in appendix A.

2.1.2 Fubini-Study Metric Approach

Distinct from Nielsen's geometric method, an alternative approach to the complexity of QFT states based on the Fubini-Study metric was developed in [69]. In this subsection, we turn our attention to a brief review of the Fubini-Study approach. In contrast to Nielsen's approach, which defines a geometric measure on the space of unitaries (2.2), this method makes use of the Fubini-Study metric to define a geometry on the space of states.

First, to introduce the basic definitions, let us imagine that the space of states of interest is covered by some convenient set of coordinates λ^μ. In the following, we focus on a family of pure states $|\psi(\lambda)\rangle$ and then we can consider the quantum fidelity as the inner product between two such states, *e.g.,* [42, 80],

$$F(\lambda, \lambda') = |\langle\psi(\lambda)|\psi(\lambda')\rangle| \,. \tag{2.21}$$

The quantum information metric then measures the distance between nearby states as

$$F(\lambda, \lambda + d\lambda) = 1 - \frac{1}{2} g^{\rm FS}_{\mu\nu}\, d\lambda^\mu\, d\lambda^\nu + \mathcal{O}(d\lambda^3) \tag{2.22}$$

with

$$g^{\rm FS}_{\mu\nu} = \frac{1}{2}\left(\langle\partial_\mu\psi|\partial_\nu\psi\rangle + \langle\partial_\nu\psi|\partial_\mu\psi\rangle\right) - \langle\partial_\mu\psi|\psi\rangle\langle\psi|\partial_\nu\psi\rangle \,. \tag{2.23}$$

The quantum information metric is also known as the fidelity susceptibility since it encodes the response of the fidelity to small changes in one of the states.[7] In the present case of pure states, eq. (2.23) also corresponds to the desired Fubini-Study metric. This metric may also be evaluated with the following expression

$$g^{\rm FS}_{\mu\nu} = -\left.\frac{\partial^2 F(\lambda, \lambda')}{\partial\lambda^\mu\, \partial\lambda^\nu}\right|_{\lambda'=\lambda} \,. \tag{2.24}$$

Then following [69], we consider curves $\lambda^\mu(\sigma)$ on the space of states parameterized by $\sigma \in [0, 1]$ which take us from the reference state to the desired target state, *i.e.,*

$$|\psi(\sigma = 0)\rangle = |\psi_{\rm R}\rangle \,, \qquad |\psi(\sigma = 1)\rangle = |\psi_{\rm T}\rangle \,. \tag{2.25}$$

We then assign a cost to each of these trajectories as the distance as measured by the Fubini-Study metric (2.23),

$$\mathcal{D}_{\rm FS} = \int_0^1 d\sigma\, \sqrt{g^{\rm FS}_{\mu\nu}\, \dot\lambda^\mu\, \dot\lambda^\nu} \,, \tag{2.26}$$

where $\dot\lambda^\mu(\sigma) = \frac{d\lambda^\mu(\sigma)}{d\sigma}$ specifies the tangent vector to the trajectory. The complexity assigned to the target state is then the minimal distance according to this measure, *i.e.,*

$$\mathcal{C}_{\rm FS} \equiv {\rm Min} \int_0^1 ds\, \sqrt{g^{\rm FS}_{\mu\nu}\, \dot\lambda^\mu\, \dot\lambda^\nu} \,, \tag{2.27}$$

[7] We might add that in the context of the AdS/CFT correspondence, the information metric or fidelity susceptibility for boundary states deformed by a marginal operator was proposed to be described by the volume of maximal time slice in AdS spacetime in [81]. Of course, the latter is also the conjectured dual of complexity according to the CV proposal [56, 82]. Different proposals for the holographic dual of information metric are also discussed in [83–86].

In a word, the FS complexity $\mathcal{C}_{\rm FS}$ is the length of the geodesic in the state space equipped with the Fubini-Study metric. Similar to the $\kappa = 2$ cost function used in the Nielsen's geometric method [1, 62], we can also use the Fubini-Study metric to define the energy of the geodesic as the complexity of pure states by

$$\mathcal{C}_{\rm FS}^{\kappa=2} = \int_0^1 d\sigma \; g^{\rm FS}_{\mu\nu} \, \dot{\lambda}^\mu \, \dot{\lambda}^\nu = \left(\mathcal{C}_{\rm FS}\right)^2 \,, \tag{2.28}$$

in order to match the divergence of holographic complexity for the vacuum state [62, 69]. Note the second equality $\mathcal{C}_{\rm FS}^{\kappa=2} = \left(\mathcal{C}_{\rm FS}\right)^2$ always holds since we have assumed that the integral is done with the on-shell solution and then the integrand is a constant with respect to an affine parameter σ along the geodesic. Due to the Riemannian structure, it is easy to find that the Euler-Lagrangian equation leads to the conclusion that $\frac{d}{d\sigma}\left(g^{\rm FS}_{\mu\nu} \, \dot{\lambda}^\mu \, \dot{\lambda}^\nu\right) = 0$.

Before proceeding with our calculation of the Fubini-Study complexity for coherent states, it is interesting to express this approach in a way that is closer to the circuit construction introduced in eq. (2.2). In particular, given a trajectory described by a particular choice of $\lambda^\mu(\sigma)$, we may express the corresponding states as

$$|\psi(\sigma)\rangle = \overleftarrow{\mathcal{P}} \exp\left[-i \int_0^\sigma ds \, \mathcal{H}(s)\right] |\psi_{\rm R}\rangle \qquad \text{where} \quad \mathcal{H}(s) = \sum_\mu \dot{\lambda}^\mu(s) \, \mathcal{O}_\mu(\lambda) \tag{2.29}$$

where $\mathcal{O}_\mu(\lambda)$ is the set of Hermitian operators that generate the evolution of state $|\psi(\lambda)\rangle$ in the λ^μ direction, *i.e.,*

$$i\partial_\mu \, |\psi(\lambda)\rangle = \mathcal{O}_\mu(\lambda) \; |\psi(\lambda)\rangle \; . \tag{2.30}$$

Note that we may think of the operators $\mathcal{O}_\mu(\lambda)$ as being linear combinations of the $\mathcal{O}_I$ appearing in eq. (2.2). We show a λ dependence to indicate that these linear combinations vary as we move through the space of states. However, this leaves the definition of the $\mathcal{O}_\mu(\lambda)$ ambiguous since, at any particular point, there will be degenerate operations that leave the state unchanged, *i.e.,* $\mathcal{O}_0(\lambda) \, |\psi(\lambda)\rangle = 0$. Therefore, in general, one finds that the space of states has a smaller dimension than the space of unitaries, as will be illustrated by the example discussed below. Given eq. (2.30), we can also rewrite the Fubini-Study metric as connected correlation functions of the operators $\mathcal{O}_\mu$,

$$\begin{aligned} g^{\rm FS}_{\mu\nu}(\lambda) &= \frac{1}{2} \, \langle\psi(\lambda)| \, \{\mathcal{O}_\mu \, , \mathcal{O}_\nu\} \, |\psi(\lambda)\rangle - \langle\psi(\lambda)| \, \mathcal{O}_\mu \, |\psi(\lambda)\rangle \, \langle\psi(\lambda)| \, \mathcal{O}_\nu \, |\psi(\lambda)\rangle \, , \\ &= \frac{1}{2} \langle \{\mathcal{O}_\mu - \langle\mathcal{O}_\mu\rangle_\lambda \, , \mathcal{O}_\nu - \langle\mathcal{O}_\nu\rangle_\lambda\}\rangle_\lambda \, . \end{aligned} \tag{2.31}$$

2.1.2.1 FS complexity of two harmonic oscillators

As an detailed illustration, we apply the Fubini-Study approach to examine the complexity of pure Gaussian states as (2.9). For simplicity, we focus on the two-mode Gaussian state (*e.g.,* a pair of coupled harmonic oscillators) as

$$\psi(x_+, x_-) = \frac{(\det M_2)^{1/4}}{\sqrt{\pi}} \exp\left[-\frac{1}{2} x_a \, [M_2]^{ab} x_b\right] , \tag{2.32}$$

where $a, b \in \{+, -\}$. Choosing the reference state as the factorized Gaussian state (2.12) (with only two modes), the Gaussian state $\psi(x_+, x_-)$ is fully parametrized by a 2×2 coefficient matrix

$$M_2 = U_2 \, M_{\rm R} \, U_2^T \qquad \text{where} \quad M_{\rm R} = \mu \, \mathbb{1}_2 \, . \tag{2.33}$$

and U_2 is chosen to be the $\mathrm{GL}(2, \mathbb{R})$ matrix. It will be convenient to parametrize a $\mathrm{GL}(2, \mathbb{R})$ matrix with the following polar decomposition

$$U_2 = e^y R(-x) \, S(\rho) \, R(z) = e^y \begin{pmatrix} \cos x & -\sin x \\ \sin x & \cos x \end{pmatrix} \begin{pmatrix} e^\rho & 0 \\ 0 & e^{-\rho} \end{pmatrix} \begin{pmatrix} \cos z & \sin z \\ -\sin z & \cos z \end{pmatrix} , \tag{2.34}$$

where R denotes a rotation matrix and S is a 'squeezing' matrix. Correspondingly, the explicit form of M_2 is given by

$$M_2 = \mu \begin{pmatrix} e^{2y}(\cosh(2\rho) + \cos(2x)\sinh(2\rho)) & e^{2y}\sin(2x)\sinh(2\rho) \\ e^{2y}\sin(2x)\sinh(2\rho) & e^{2y}(\cosh(2\rho) - \cos(2x)\sinh(2\rho)) \end{pmatrix} , \tag{2.35}$$

whose eigenvalues correspond to the characteristic frequencies of the normal modes, *i.e.,* $\omega_\pm = \mu e^{2(y\pm\rho)}$. And we note here that M_2 is independent of z, which is different from the $\mathrm{GL}(2, \mathbb{R})$ matrix U_2. Then our family (2.32) of states is described by only three dimensionless coordinates $\lambda^\mu = \{y, \, \rho, \, x\}$, and by construction, the origin of this coordinate system corresponds to the reference state.

Now by the methods introduced above, we can define the Fubini-Study metric for the space of states $|\psi(y, \rho, x)\rangle$. The metric can be constructed with eq. (2.23) by evaluating the integrals

$$g^{\rm FS}_{\mu\nu} = \frac{1}{2} \int dx_+ dx_- \left(\partial_\mu \bar\psi \, \partial_\nu \psi + \partial_\nu \bar\psi \, \partial_\mu \psi\right) - \int dx_+ dx_- \; \psi \, \partial_\mu \bar\psi \times \int dx_+ dx_- \; \bar\psi \, \partial_\nu \psi \, , \tag{2.36}$$

where the wave function $\psi(x_+, x_-; y, \rho, x)$ is defined in eq. (2.32). Alternatively, we can calculate the fidelity (2.21)

$$F(\lambda, \lambda') = \int dx_+ dx_- \, \bar\psi(x_+, x_-; y, \rho, x) \, \psi(x_+, x_-; y', \rho', x') \, , \tag{2.37}$$

and then evaluate the metric with eq. (2.24). Using either method, it is easy to find that the Fubini-Study metric reduces to

$$ds^2_{\rm FS} = dy^2 + d\rho^2 + \sinh^2(2\rho)\, dx^2 \,. \tag{2.38}$$

This three-dimensional subspace has the geometry $\mathbb{R} \times \mathbb{H}^2$. As noted above, the reference state corresponds to the origin, *i.e.,* $y = 0 = \rho$ (while the angle x is unspecified). Hence the geodesics are simply lines moving along the $\mathbb{R}$ and radially outward in the hyperbolic space, *i.e.,* $y = y_1\, s$, $\rho = \rho_1\, s$ and $x = x_1$ where $(y_1,\, \rho_1,\, x_1)$ is the position specifying the target state (an arbitrary two-mode Gaussian state). In terms of the frequencies in normal modes $\omega_\pm$, we easily obtain the length of the geodesic, *i.e.,* the FS complexity

$$\mathcal{C}_{\rm FS} = \sqrt{(y_1)^2 + (\rho_1)^2} = \frac{1}{2\sqrt{2}} \sqrt{\left(\ln \frac{\omega_k}{\mu}\right)^2 + \left(\ln \frac{\omega_-}{\mu}\right)^2} \,. \tag{2.39}$$

which is nothing but the circuit complexity $\mathcal{C}_2$ in (2.19), except for the overall constant factor. For comparison, we note that the geometry derived from Nielsen's geometric approach with F_2 cost function is still different. One can find that F_2 cost function specifies the metric on the space of $\mathrm{GL}(2, \mathbb{R})$ transformations as follows

$$ds^2 = \delta_{IJ} Y^I Y^J = 2dy^2 + 2d\rho^2 + 2dx^2 - 4\cosh(2\rho) dx dz + 2\cosh(4\rho) dz^2 \,. \tag{2.40}$$

Although we only take a two-mode Gaussian state as an example, it was shown in [62, 69] that the Fubini-Study approach for any N-mode Gaussian state with vanishing first moments produces precisely the same complexity as that from Nielsen's geometric method, taking F_2 cost function, *i.e.,* eq. (2.19).

Both the Nielsen and the Fubini-Study approaches identify the complexity of a state as the distance from a simple reference state in some geometry. Nielsen's method [59–61] is motivated by the definition of complexity as the number of elementary gates in the optimal circuit, and so in this case, a metric is defined on the space of quantum circuits or unitary transformations. Optimizing the trajectory in this space then has a direct interpretation as minimizing the number gates used in the circuit preparing the desired target state (or at least, optimizing this number according to some cost function). The Fubini-Study approach instead accounts for the complexity by keeping track of the changes of the state throughout the preparation of the target state. As its title indicates, this method makes use of the Fubini-Study metric (2.23), which defines a geometry directly on the space of states. An important difference is that the latter geometry assigns a variable cost to specific gates, *i.e.,* the cost depends on the details of the state on which they act, whereas the gates are assigned

fixed costs in the Nielsen approach. Further, at any point in the space of states, there will be degenerate operations that leave the state unchanged, *i.e.*, $|\psi\rangle = U_0 |\psi\rangle$. Therefore, in general, one finds that the space of unitaries has a larger dimension than the space of states, as illustrated by comparing the geometries in eqs. (2.38), (2.40).[8] Hence we see that the Fubini-Study and Nielsen approaches must define different complexities for the optimal circuit with the same target and reference state. However, we remind the reader that the ground state complexities, and in fact the optimal circuits, were found to agree with these two different approaches [62, 69]. In this case, the optimal circuits only involved $\mathrm{GL}(N, \mathbb{R})$ gates and so no additional scale was needed to define the corresponding generators. In fact, in this case, the Fubini-Study geometry can be embedded in the corresponding Nielsen geometry. On the contrary, in the case of coherent states, the Nielsen and Fubini-Study approaches produced different optimal circuits for a fixed pair of reference and target states and the corresponding complexities are also distinct in general [1].

To close this brief review, we remark that the Fubini-Study metric approach for circuit complexity only applies to pure states as the Nielsen's geometric method. As a natural generalization to mixed states, we propose a new measure for the complexity of mixed states in chapter 5 and show that it is also understood as the purification complexity based on Fubini-Study metric.

2.1.3 Path Integral Complexity

In the last two sections, we have reviewed Nielsen's geometric method and the Fubini-Study metric approach towards understanding complexity in field theories. It is obvious that both of them can be considered as geometric approaches that assign a distance measure or generally a cost function on the space, in which a path corresponds to the quantum circuit preparing a target state from a given reference state. At first glance, an apparent advantage in these two approaches is that the meaning of quantum circuit and the notion of complexity is clear. However, applying these geometric methods to quantum field theory may require more effort in finding the optimal circuit due to the fact that the dimension of state space (or alternatively, the space of unitaries) is infinite in this case. The interested reader is referred to [87–91] for recent progress focusing on defining the circuit complexity of CFT states. In a parallel vein, there exists an independent approach to complexity in quantum field theories, which is called path-integral complexity [92, 93]. For completeness,

[8] At a pragmatic level, this proves to be an advantage for the Fubini-Study approach since in many cases, one will find a single geodesic connecting the reference state and the target state. In contrast, the Nielsen approach yields a family of geodesics connecting these states and the complexity is determined by the length of the shortest geodesic in this family.

we will briefly review this approach in this section by using the vacuum state in a two dimensional CFT as an example.

2.1.3.1 Path-Integral Optimization

The idea of path-integral complexity originates from tensor networks and is closely related to the observation by Swingle [30] that MERA (multi-scale entanglement renormalization ansatz) tensor networks [94, 95] resemble a spatial slice of AdS spacetime. Hence, he conjectured that such quantum circuits may explain the emergent geometry and further the mechanism behind the AdS/CFT correspondence. This AdS/MERA correspondence naturally illustrates the holographic entanglement entropy formula by simply counting the number of entangling links in the networks. Beyond discretized lattice models, there also exist some improved constructions of tensor networks like cMERA (continuous MERA) [96] which may be able to describe the genuine conformal field theories.

In this approach to complexity, one starts from preparing a QFT state $|\Psi\rangle$ with a Euclidean path integral and considers an optimization procedure for the Euclidean path integral which produces the desired quantum wave functional. Indeed, an optimization procedure for tensor networks called tensor network renormalization (TNR), has been introduced in [94, 95]. This optimization procedure contracts tensors and removes unnecessary lattice sites. One then find that TNR optimizes the tensor network corresponding to a lattice version of the Euclidean path-integral computation of a ground state wave function with the MERA network. Instead, path-integral complexity is based on the so-called "path-integral optimization" procedure first proposed in [92, 93]. Path-integral optimization is achieved by minimizing a certain functional I_Ψ, which describes the number of path-integral operations in the discretized description, *i.e.,* a corresponding tensor network. The minimum of this functional I_Ψ is then interpreted as a candidate for complexity of a quantum state $|\Psi\rangle$ in QFTs and named as the "path-integral complexity" $\mathcal{C}_{\text{L}}(\Psi)$. Remarkably, it is argued that this functional I_Ψ can be identified as the well-known Liouville action in two dimensional CFTs.

More precisely, the optimization procedure is carried out as follows. First of all, we consider a Euclidean path integral representation of the ground state wave functional in a $d-$dimensional QFT on $R^d(z,x)$ as

$$\Psi_0\left[\tilde{\varphi}(x)\right] = \int \left(\prod_{x^i} \prod_{\epsilon \leq z < \infty} D\varphi(z,x) \right) e^{-S_{\text{QFT}}(\varphi)} \times \prod_x \delta(\varphi(\epsilon,x) - \tilde{\varphi}(x)) \,, \tag{2.41}$$

where z denotes the Euclidean time ($\tau \equiv -z$), x^i are the $(d-1)$ spatial coordinates on R^{d-1} and the UV cut-off is chosen to be ϵ. We can imagine that the Euclidean path-integral is discretized into a lattice description with ϵ as the lattice spacing. The path-integral optimization then is taken as the optimization procedure by changing the geometry of lattice regularization. In order to realize this, the authors in [92, 93] proposed introducing a metric on which the path integration is performed. As a result, the optimization can be performed by modifying the background metric for the path integrals.

Before the path-integral optimization, the original flat metric on the d-dimensional space (z, x) is chosen as

$$ds^2 = \frac{1}{\epsilon^2}\left(dz^2 + \sum_{i=1}^{d-1} dx^i dx^i\right) . \tag{2.42}$$

Correspondingly, the general background metric used in the optimization reads

$$ds^2 = g_{zz}(z,x)dz^2 + g_{ij}(z,x)dx^i dx^j + 2g_{zj}(z,x)dzdx^j \,, \tag{2.43}$$

with constraints as follows

$$g_{zz}(z=\epsilon,x) = \frac{1}{\epsilon^2}, \quad g_{ij}(z=\epsilon,x) = \frac{\delta_{ij}}{\epsilon^2}, \quad g_{iz}(z=\epsilon,x) = 0 \,, \tag{2.44}$$

which guarantees that the correct wave functional is reproduced at the end of the path integrals. In this metric formulation, the additional requirement is that the deformed wave functional in a non-trivial metric is still proportional to the state wave functional $\Psi_0\left[\tilde{\varphi}(x)\right]$ in a trivial metric as (2.42). This means that the optimization with respect to background metrics for the path integrals is finally realized by minimizing the overall normalization factor of the wave functional $\Psi\left[\tilde{\varphi}(x)\right]$ for the quantum state $|\Psi\rangle$.[9] More generally, we can assume that for each quantum state $|\Psi\rangle$, there exists a functional $I_\Psi\left[g_{ab}(z,x)\right]$ whose minimization with respect to the metric g_{ab} can implement the optimization procedure.

2.1.3.2 Path-Integral Complexity

In the discretized tensor network description, we can interpret the optimization as minimizing the number of tensors. Naturally, it is expected that the functional $I_\Psi\left[g_{ab}(z,x)\right]$ that is minimized in the path-integral optimization can estimate the amount of complexity for the network corresponding to the path-integral on the space with a specified metric $g_{ab}(z,x)$.

[9] The normalization factor only depends on the metric $g_{ab}(z,x)$ and couplings of the theory that we consider.

The path-integral complexity defined as the minimal value of the functional $I_\Psi\left[g_{ab}(z,x)\right]$, *i.e.*,

$$\mathcal{C}_{\rm L}\left(\Psi\right)=\min_{g_{ab}}\left[I_\Psi\left[g_{ab}(z,x)\right]\right]\,, \tag{2.45}$$

is then identified as the complexity of the quantum state $|\Psi\rangle$. For a generic QFT or holographic field theory, it is not clear how to derive the functional $I_\Psi\left[g_{ab}(z,x)\right]$ ever in principle. However, as we reviewed in the following, this functional is shown to be the Liouville action for two dimensional CFTs.

Due to the simplicity of the two-dimensional geometry, the general background metric g_{ab} is is fully characterized by a Weyl scaling function $\phi(z,x)$ and can thus be taken to have the form

$$ds^2=e^{2\phi}\left(dz^2+dx^2\right)\,, \tag{2.46}$$

with boundary condition $e^{2\phi(\epsilon,x)}=1/\epsilon^2$. In other words, various metrics are connected to each other by a Weyl transformation. Interestingly, the local Weyl rescaling also changes the measure of the path integral in two dimensional CFTs as follows

$$[D\varphi]_{g_{ab}=e^{2\phi}\delta_{ab}}=e^{S_{\rm L}[\phi]-S_{\rm L}[0]}\cdot[D\varphi]_{g_{ab}=\delta_{ab}}, \tag{2.47}$$

in which $S_{\rm L}[\phi]$ is derived as the Liouville action (see *e.g.,* [97])

$$S_{\rm L}[\phi]=\frac{c}{24\pi}\int_{-\infty}^{\infty}dx\int_{\epsilon}^{\infty}dz\left[\left(\partial_x\phi\right)^2+\left(\partial_z\phi\right)^2+\mu e^{2\phi}\right]\,. \tag{2.48}$$

As usual, the constant c appearing in the prefactor in front of $S_{\rm L}[\phi]$ is precisely the central charge of the CFT under consideration. Thanks to the universal transformation in eq. (2.47) for two-dimensional CFTs, we can find that the wave functionals appearing in the path-integral optimization is given by

$$\Psi_{g_{ab}=e^{2\phi}\delta_{ab}}(\tilde{\varphi}(x))=e^{S_{\rm L}[\phi]-S_{\rm L}[0]}\cdot\Psi_{g_{ab}=\delta_{ab}}(\tilde{\varphi}(x))\,. \tag{2.49}$$

Therefore, the optimization is explicitly performed by minimizing the normalization factor $e^{S_{\rm L}[\phi]}$ [92, 93]. Correspondingly, we can identify the complexity functional for the vacuum state of a two-dimensional CFT as

$$I_{\Psi_0}[\phi(z,x)]=S_{\rm L}[\phi(z,x)]\,. \tag{2.50}$$

At an intuitive level, it is argued in [98] that Liouville action appears to be the desired measure for complexity from the viewpoint of TNR because the potential term $\int e^{2\phi}$ and

the kinetic term $\int(\partial\phi)^2$ measure the number of unitary tensors and isometries in TNR, respectively.

For the sake of deriving the path-integral complexity $\mathcal{C}_{\text{L}}(\Psi)$ defined in eq. (2.45), we can minimize the Liouville action with respect to the Weyl scaling field $\phi(z,x)$ and obtain the solution

$$e^{2\phi} = \frac{1}{z^2}\,, \tag{2.51}$$

which leads to the hyperbolic plane metric $\mathbb{H}^2$

$$ds^2 = \frac{dz^2 + dx^2}{z^2}\,, \tag{2.52}$$

as the optimal metric for the Euclidean path integral of the vacuum state in 2D CFT. We note that this is nothing but a time slice of vacuum AdS_3, *i.e.,* the holographic dual spacetime for the vacuum state in two-dimensional (holographic) CFT. After this minimization, *i.e.,* path-integral optimization, we finally obtain the path-integral complexity of the vacuum state as

$$\mathcal{C}_{\text{L}}(\Psi_0) = \min_{\phi}\left[S_{\text{L}}[\phi]\right] = \frac{c\,l}{12\pi\epsilon}\,, \tag{2.53}$$

where $l \equiv \int dx$ is the length of the spatial direction. It then coincides with the result for holographic complexity at the leading order.

In addition to the vacuum states discussed in this section, one can also apply this path-integral optimization to excited states, finite temperature states [93], perturbed CFTs [99] and so on. Furthermore, a higher dimensional generalization of the path-integral complexity in CFTs has also been proposed in [93]. As discussed before, the connection between path-integral complexity and the standard notion of complexity is less apparent. Remarkably, the studies in [100] bridge the gap by explicitly recovering the Liouville action as the circuit complexity measure. It means that the path integral optimization for two-dimensional CFT can be also understood as a realization within the standard gate counting framework. For more recent developments on the path-integral optimization/complexity refer to *e.g.,* [101–108].

2.2 Holographic Complexity Proposals

Quantum information has produced surprising new insights into foundational questions about the AdS/CFT correspondence. In last section, we reviewed various methods towards

defining the complexity of quantum states in QFT. It is believed that the gravitational observables dual to complexity in the boundary theory can provide more information about the bulk spacetime than that coming from holographic entanglement entropy [54]. Under the heading of holographic complexity, a variety of proposals for the bulk description of the complexity of boundary states have been developed. The most studied of these are the complexity=volume (CV) [55,56] and the complexity=action (CA) [57,58] conjectures, which will be briefly reviewed in this section.

2.2.1 Complexity=Volume

A fascinating simple result about the eternal black hole geometry is the (almost) linear growth of the Einstein-Rosen (ER) bridge (or the size of the wormhole). Classically, the wormhole can keep increasing forever. However, this very late time dynamics and the bulk spacetime far behind the event horizon of black holes can not be appropriately probed by holographic entanglement entropy. Motivated by this fact, Susskind argued that the growth of the wormhole is an expected property of the complexity of quantum states living on the boundary. Furthermore, Susskind and Stanford proposed the so-called CV conjecture for the circuit complexity of quantum states on the holographic boundary theory.

The CV conjecture states that the complexity is dual to the volume of an extremal codimension-one bulk surface anchored at the time slice Σ in the asymptotic boundary on which the state is defined,

$$\mathcal{C}_{\rm V}(\Sigma) = \max_{\Sigma=\partial\mathcal{B}} \left[\frac{\mathcal{V}(\mathcal{B})}{G_N \, \ell_{\rm bulk}} \right] , \tag{2.54}$$

with $\mathcal{B}$ corresponding to the bulk hypersurface of interest and G_N denoting Newton's constant in the bulk gravitational theory. Further, $\ell_{\rm bulk}$ is some additional length scale associated with the bulk geometry, *e.g.,* see discussion in [57, 109]. For simplicity, most studies will set $\ell_{\rm bulk} = L$, *i.e.,* the curvature radius for the (asymptotic) AdS geometry. The above conjecture assumes that the quantum state of the boundary theory in question is a pure state defined on a global time slice, *i.e.,* the time slice Σ spans the entire asymptotic boundary.

As shown in figure 2.2, we consider eternal AdS black holes in $d+1$ dimensions as an example to discuss CV conjectures in more detail. The two-sided geometry is defined by

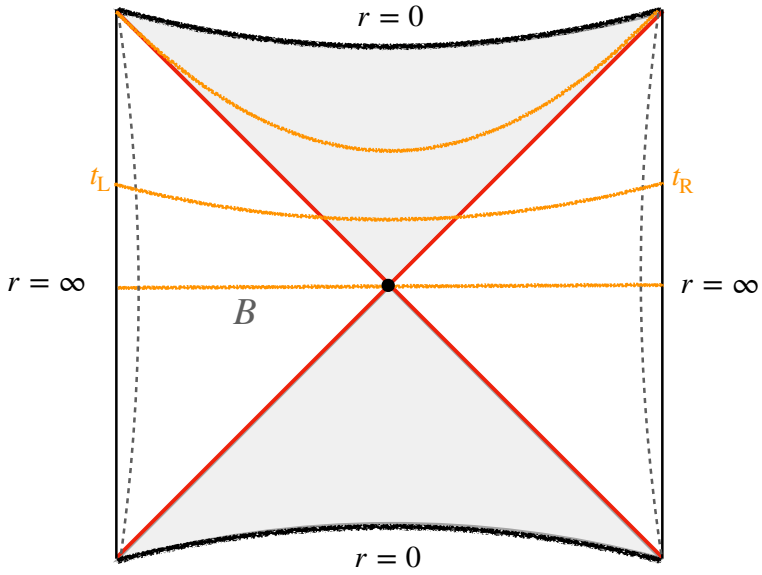

Figure 2.2: The Penrose diagram for the eternal black hole in asymptotically AdS spacetime. The yellow curves connecting the two boundaries anchored at times $t_{\rm L}$ and $t_{\rm R}$ indicate the spacelike hypersurface with maximal volume.

the metric as follows

$$\begin{aligned} ds^2 &= -f(r)dt^2 + \frac{dr^2}{f(r)} + r^2 d\Sigma_{k,d-1}^2 \,, \\ \text{with} \qquad f(r) &= k + \frac{r^2}{L^2} - \frac{\omega^{d-2}}{r^{d-2}} \,, \end{aligned} \tag{2.55}$$

where $k \in 0, \pm 1$ indicates the curvature of the $(d-1)$-dimensional line element $d\Sigma_{k,d-1}^2$ and the parameter ω is related to the position of the black hole horizon r_h

$$\omega^{d-2} = r_h^{d-2}\left(k + \frac{r_h^2}{L^2}\right) . \tag{2.56}$$

Correspondingly, the total energy is also determined by the parameter ω as

$$M = \frac{(d-1)\Omega_{k,d-1}}{16\pi G_{\rm N}}\omega^{d-2} \,, \tag{2.57}$$

in which $\Omega_{k,d-1}$ is referred to as the dimensionless volume of the $(d-1)$-dimensional spatial geometry.

The key ingredient in the CV conjecture is the hypersurface with a maximal volume whose position is determined by the boundary time $t_{\rm L}, t_{\rm R}$. By symmetry, it is easy to find that the maximal volume connecting the left/right boundaries at $t_{\rm L} = 0 = t_{\rm R}$ is given by the bulk $t = 0$ slice. The maximal volume reduces to

$$\mathcal{V} = 2\Omega_{k,d-1} \int_{r_h}^{r_{\rm max}} \frac{r^{d-1}}{\sqrt{f(r)}}\, dr\,, \tag{2.58}$$

where $r_{\rm max}$ indicates the position of the cut-off surface. Choosing a symmetric set-up with $t_{\rm L} = t_{\rm R}$, the volume of a spacelike hypersurface parametrized by $t(r)$ is given by

$$\mathcal{V}\left(\mathcal{B}\right) = 2\Omega_{k,d-1} \int_{r_{\rm min}}^{r_{\rm max}} r^{d-1} \sqrt{\frac{1}{f} - f\left(t'(r)\right)^2}\, dr\,, \tag{2.59}$$

with $t'(r) = \partial_r t(r)$. Here $r_{\rm min}$ denotes the minimum distance that the Einstein-Rosen bridge can reach inside the future horizon. Finding the extremal-volume surface then is similar to a classical mechanics problem. It is straightforward to find that the extremal surface is determined by a conserved quantity E as follows

$$E = \frac{r^{d-1} f t'}{\sqrt{\frac{1}{f} - f t'^2}}\,, \qquad \text{or} \qquad t'(r) = \pm \frac{E}{f\sqrt{f r^{2(d-1)} + E^2}}\,. \tag{2.60}$$

From a geometric viewpoint, the extremal-volume condition means that the extrinsic curvature of the hypersurface vanishes, *i.e.,* $K = 0$. Furthermore, the maximal volume can be written as

$$\max\left[\mathcal{V}\left(\mathcal{B}\right)\right] = 2\Omega_{k,d-1} \int_{r_{\rm min}}^{r_{\rm max}} \frac{r^{2(d-1)}}{\sqrt{f(r) r^{2(d-1)} + E^2}}\, dr\,, \tag{2.61}$$

where the minimal radius is obtain as the solution of $E^2 + f(r_{\rm min}) r_{\rm min}^{2(d-1)} = 0$. We are also interested in the full time-dependence of CV. Combining eq. (2.59) and eq. (2.61), one can easily obtain [110–112]

$$\frac{d\mathcal{C}_{\rm V}}{dt} = -\frac{\Omega_{k,d-1}}{G_N \ell_{\rm bulk}} E = \frac{\Omega_{k,d-1}}{G_N \ell_{\rm bulk}} \sqrt{-f\left(r_{\rm min}\right)} r_{\rm min}^{d-1}\,, \tag{2.62}$$

which is fully determined by the conserved energy E.

We note that the relations between conserved energy E and boundary times $t_{\rm L}, t_{\rm R}$ is more complicated. We refer readers to [110–112] for more details about the general time dependence of holographic complexity. In particular, we only highlight a universal property

that the growth rate approach a constant in the late time limit. For example, the growth of complexity for planar AdS black hole ($k = 0$) yields [56, 110]

$$\left.\frac{d\mathcal{C}_{\rm V}}{dt}\right|_{t\to\infty} = \frac{8\pi}{d-1}M\,, \tag{2.63}$$

which is considered as supporting the complexity=volume conjecture. Other evidence for CV is given by the switchback effect in shock wave geometries [56, 111, 112]. The CV conjecture has stimulated a wide variety of recent research efforts investigating the properties and applications of holographic complexity, see *e.g.,* [6, 109–129].

2.2.2 Complexity=Action

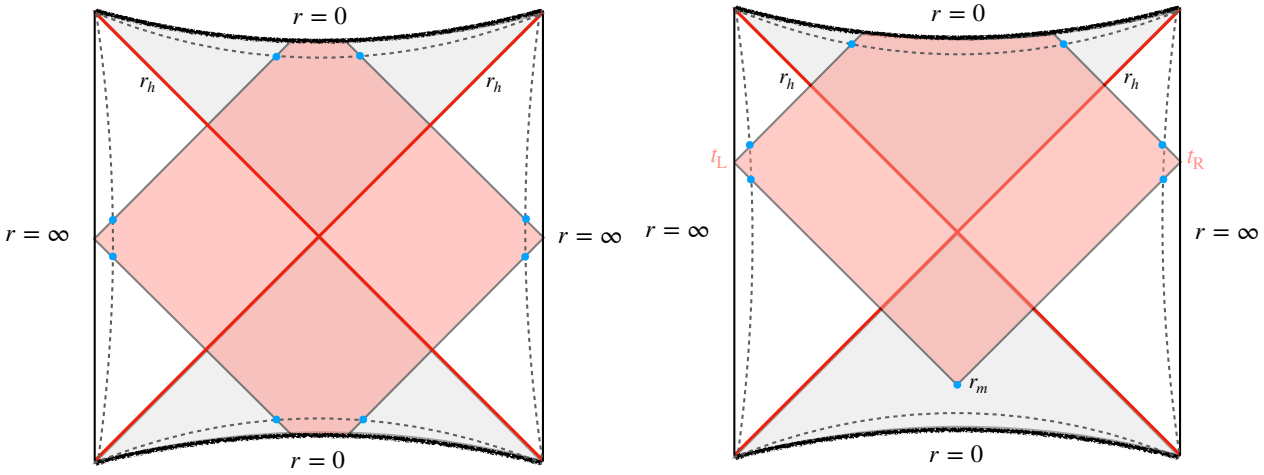

Figure 2.3: The Penrose diagram for the eternal black hole in asymptotically AdS spacetime. The pink region bounder by four null surfaces is referred to as the Wheeler-DeWitt patch. The left/right plot corresponds to the WdW patch before/after the critical time t_c.

As introduced in last section, the CV conjecture is motived by the growth of the wormhole. However, noticing the dimension of the volume $\mathcal{V}$ and Newton constant $G_{\rm N}$, it is obvious that CV conjecture requires an arbitrary length scale $\ell_{\rm bulk}$ in its definition in order to obtain a dimensionless complexity. Different from the CV conjecture, another holographic complexity proposal called the complexity=action (CA) conjecture was proposed in [57, 58]. The CA proposal states that the complexity is given by evaluating the gravitational action on a region of spacetime, known as the Wheeler-DeWitt (WDW) patch,

which can be regarded as the causal development of a space-like bulk surface anchored on the boundary time slice Σ. The CA conjecture then suggests

$$\mathcal{C}_{\rm A}(\Sigma) = \frac{I_{\rm WDW}}{\pi} \,. \tag{2.64}$$

We note the factor $\frac{1}{\pi}$ was fixed for the sake of connecting the time growth of holographic complexity to a conjecture called Lloyd's bound, which states that computation rates of quantum system are bounded by its energy [130] . However, we need to point out that such a bound is not satisfied in general by any proposals of holographic complexity; see *e.g.,* [57, 58, 110, 131] for more discussion. At first glance, the advantage of the CA proposal is that it does not depend on an overall arbitrary dimensionful factor, which differs from the CV conjecture. However, an arbitrary length scale also appears in the calculations for the action of a WDW patch as we show in the following.

It is known that evaluating the Einstein-Hilbert action with spacelike/timelike boundaries requires the Gibbons-Hawking-York surface term [132, 133] in order to have a well defined variational principle. As showing in figure 2.3, the WDW patch (after introducing the cut-off surfaces) contains not only spacelike surfaces but also null surfaces as boundaries, calling for an analogous contribution for null boundaries [134, 135]. Furthermore, there are also some codimension-2 joints where such null boundaries intersect with other boundary surfaces. Their contributions have been addressed in [136, 137] for joints that do not involve null surfaces, and in [134] for joints that involve at least one null surface. As a result, the action of the WDW patch in eq. (2.64) needs a careful analysis for various boundary terms, which must be added to the gravitational action to have a well-posed variational principle for the whole patch. We refers readers to [134, 135] for more details about gravitational action with different boundaries.

As a summary, the action $I_{\rm WDW}$ including these gravitational boundary terms consists of

$$I_{\rm WDW} = I_{\rm bulk} + I_{\rm GHY} + I_{\rm null} + I_{\rm ct} + I_{\rm joints} \,, \tag{2.65}$$

with

$$
\begin{aligned}
I_{\text{bulk}} &= \frac{1}{16\pi G_{\text{N}}}\int d^{d+1}y\sqrt{|g|}\left(\mathcal{R}+\frac{d(d-1)}{L^2}\right)+I_{\text{matter}}\\
I_{\text{GHY}} &= +\frac{1}{8\pi G_{\text{N}}}\int_{\text{regulator}} d^{d}x\,\sqrt{|h|}\,K\,,\\
I_{\text{null}} &= \frac{1}{8\pi G_{\text{N}}}\int_{\partial\text{WDW}} d\lambda\,d\Omega_{d-1}\,\sqrt{\gamma}\,\kappa\,,\\
I_{\text{ct}} &= \frac{1}{8\pi G_{\text{N}}}\int_{\partial\text{WDW}} d\lambda\,d\Omega_{d-1}\,\sqrt{\gamma}\,\Theta\log(\ell_{\text{ct}}\Theta)\,,\\
I_{\text{joints}} &= \frac{1}{8\pi G_{\text{N}}}\int_{\text{joints}} d\Omega_{d-1}\,\sqrt{\sigma}\,a_{\text{jt}}\,.
\end{aligned}
\tag{2.66}
$$

The full prescription can be found in [134], or in appendix A of [114]. As a example for bulk action, here we only consider the Einstein-Hilbert action with a negative cosmological constant, and I_{matter}, describing the contributions from matter fields. The remaining terms are surface terms evaluated on the different pieces of the boundary of the WDW patch: I_{GHY} is the usual Gibbons-Hawking-York term [132, 133] defined on the AdS boundary regulator surface, I_{null} and I_{ct} involve integration over the null boundaries of the WDW patch, whereas I_{joints} is the null joint term evaluated where the null boundaries of the WDW patch intersect the AdS boundary regulator surface [134]. In the corresponding surface term for null boundaries, the constant κ is defined by the equation

$$
k^{\mu}\nabla_{\mu}k_{\nu}=\kappa k_{\nu}\,,
\tag{2.67}
$$

where $\mathbf{k}=k_{\mu}dx^{\mu}$ is the outward directed null normal. We remark that the constant κ measures the failure of the surface parameter (denoted by λ) to be an affine parameter on the null generators of the null boundary and it can be chosen to be zero by choosing the normalization appropriately. For null boundaries, one must also include the null counterterm I_{ct} introduced in [134] to restore reparametrization invariance along the null generators. For joints terms I_{joints}, Θ is the expansion scalar of the null generator, *i.e.,* $\Theta=\partial_{\lambda}\ln\sqrt{\gamma}$, γ is the induced metric on the null boundary and ℓ_{ct} is an arbitrary constant representing the freedom in the definition of this counterterm. Let us add that the expansion Θ only depends on the intrinsic geometry of the null boundaries and so I_{ct} is not required for a well-defined variational principle of gravitational action. Correspondingly, the counterterm I_{ct} introduces a new arbitrary length scale ℓ_{ct} and the choice of this length scale influences various properties of the complexity. While this extra length scale looks unnatural, it may be traced back to the ambiguities in the definition of circuit complexity. Furthermore,

comparing the structure of the UV singularities in holographic and QFT calculations of complexity leads to the suggestion that the choice of this length scale may be related to the choice of microscopic scales in defining the reference state and the gates in the complexity model of the boundary theory (*e.g.,* μ in our QFT construction) [62, 69, 112].

Similar to the time growth of CV, one can also examine the time dependence of CA for an eternal black hole (2.55) in asymptotically AdS spacetime by using the full action shown in eq. (2.65). The full analysis is shown in [110]. To summarize, the time dependence of CA (with $t_{\rm L} = t_{\rm R} = t/2$) is given by

$$\frac{d\mathcal{C}_{\rm A}}{dt} = \begin{cases} 0, & 0 \le t \le t_c\,, \\ \frac{1}{\pi}\left(2M + \frac{\Omega_{k,d-1}(d-1)r_m^{d-2}f(r_m)}{16\pi G_{\rm N}}\left[\log\left(|f\left(r_m\right)|\right) - 2\log\left(\frac{r_m}{(d-1)\ell_{\rm ct}}\right)\right]\right)\,, & t > t_c\,, \end{cases} \tag{2.68}$$

where t_c is the critical time when the past light sheets from left and right boundaries intersect on the singularity at $r = 0$ and r_m indicates the radius of the intersection (behind the past horizon) after the critical time as shown in the right plot in figure 2.3. Taking the late-time limit, it is obvious that $r_m \to r_h$ and $f(r_m) \to 0$. So the growth of holographic complexity from the CA conjecture approaches a constant and is simply proportional to the black hole mass, *i.e.,*

$$\left.\frac{d\mathcal{C}_{\rm A}}{dt}\right|_{t\to\infty} = \frac{2M}{\pi}\,, \tag{2.69}$$

which is independent of the dimension and also the geometry of the horizon. This simple result reproduces the expected linear growth of complexity at late times [57, 58]. While we only sketch the basic ingredients in evaluating the action of WdW patch in this section, the CA conjecture has inspired a lot of studies on various aspects of holographic complexity, *e.g.,* [64, 71, 110–114, 117–119, 123, 129, 131, 134, 138–170].

Chapter 3

Circuit Complexity of Mixed States

Our aim in this thesis is to explore the complexity of mixed states. Specially in this chapter, we will examine the so-called "*purification complexity*" [171], defined as the minimal complexity of a pure state that purifies our mixed state, see eq. (3.1). Our analysis in this chapter will focus on Gaussian mixed states and the main content is adapted from sections 3-5 in [2].

3.1 Optimal Purification and Purification Complexity

Quantum information concepts and their embedding in gravitational holography [172] have proved very useful for developing our understanding of the bulk-boundary map, *e.g.,* see [40,173–175]. One particular notion, which has captured increasing attention, is computational complexity. The complexity of a quantum state is defined as the minimal number of simple operations required in order to construct the state starting from a simple unentangled product state [176, 177]. There exist several proposals for the holographic dual of computational complexity [54–58, 115], however, at the moment, we can only test them at a phenomenological level due to the absence of a well-posed definition for the complexity for quantum field theory states. One front, in which progress has been made is that of Gaussian and nearly Gaussian states, *e.g.,* [62, 69, 70, 178, 179]. Most of those studies, however, focused on pure states, and very little is known about the complexity of mixed states. Several proposals were made to define mixed-state complexity in [171] and our goal here is to examine one of these, the purification complexity, in detail for mixed Gaussian states. Let us also mention that in holography, several proposals have been made for the

gravitational dual of the complexity of mixed states associated with reduced density matrices on subregions of the boundary of asymptotically AdS spaces [114, 180] and we will also compare our QFT results with those coming from holography, at least at the qualitative level.

Circuits with Ancillae and Purification Complexity: Preparing a mixed state $\hat{\rho}_{\mathcal{A}}$ on some Hilbert space $\mathcal{A}$, starting from a pure reference state, cannot be achieved using only unitary gates. Instead, we should think of preparing the state using a set of allowed universal (non-unitary) gates, which consist of completely positive trace-preserving maps acting on the reference state. However, this approach is equivalent to extending the Hilbert space to include **ancillary** degrees of freedom and working with unitary gates acting on this extended Hilbert space, *e.g.,* see [176, 181, 182] and chapter 8 in [42]. One can think that the set of unitary gates is extended to include **ancillary gates**, which introduce a new ancillary degree of freedom (in some simple product state) as needed, and **erasure gates**, which erase or trace out a single degree of freedom whenever is convenient. Alternatively, as illustrated in figure 3.1, we can think that the reference state is an unentangled product state on all of the needed or available auxiliary degrees of freedom, as well as the physical degrees of freedom, *i.e.,* the reference state (and all of the intermediate pure states) live on an extended Hilbert space $\mathcal{A} \otimes \mathcal{A}^c$. Then after applying a unitary circuit to this extended state, the ancillae are all traced out of the final pure state to produce the desired mixed state on the physical Hilbert space $\mathcal{A}$ alone.

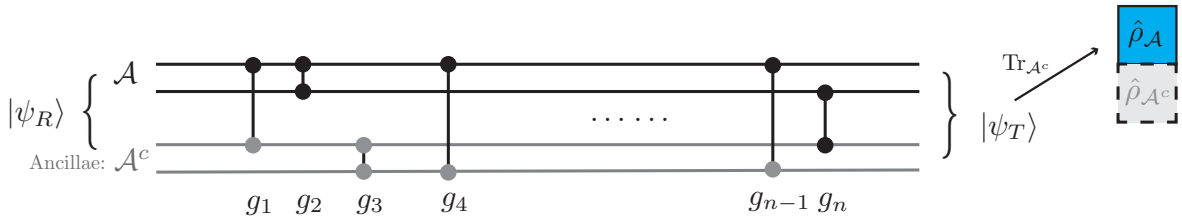

Figure 3.1: Circuit with the ancillary degrees of freedom. The mixed state $\hat{\rho}_{\mathcal{A}}$ that we want to prepare is obtained at the final step after tracing out the ancillae.

Following this discussion, we can define the complexity of mixed states by considering the complexity of pure states that purify them. Obviously, the purifications of a given mixed state are not unique. However, a natural definition of mixed state complexity – the so-called **purification complexity** [171] is defined as the minimal pure state complexity among all possible purifications of our mixed state, *i.e.,* as usual, we are optimizing over the circuits that take the reference state to a target state $|\Psi_{\mathcal{A}\mathcal{A}^c}\rangle$, which is a purification of the desired mixed state $\hat{\rho}_{\mathcal{A}}$, but we must also optimize over the possible purifications of

$\hat{\rho}_{\mathcal{A}}$, *i.e.*,

$$\mathcal{C}\left(\hat{\rho}_{\mathcal{A}}\right) \equiv \min_{\mathcal{A}^c} \mathcal{C}\left(|\Psi_{\mathcal{A}\mathcal{A}^c}\rangle\right), \quad \text{such that} \quad \hat{\rho}_{\mathcal{A}} = \mathrm{Tr}_{\mathcal{A}^c} |\Psi_{\mathcal{A}\mathcal{A}^c}\rangle \langle\Psi_{\mathcal{A}\mathcal{A}^c}| \ . \tag{3.1}$$

Recall that we are applying this analysis to study mixed Gaussian states. A simplifying assumption in our analysis will be that the purified states are also Gaussian. This allows us to use the prescription of [62] for evaluating the complexity of the possible purifications,[1] and we then minimize over the parameters of the purifications, as in eq. (3.1) above.[2]

Completing our complexity model requires specifying the cost function.[3] A variety of cost-functions have been considered in the literature for the complexity of pure Gaussian states (*e.g.,* see [1, 62, 69, 70]). As was pointed out in [62, 69], the F_1 cost function (see eq. (2.6)) seems most closely related to complexity in holography because the structures of the UV divergences match. Hence we will focus our analysis on this choice in the following. However, the precise results are also found to depend on the basis chosen for the fundamental gates. For example, a recent study of the complexity of the thermofield double (TFD) state [68] has shown the importance of choosing a basis that is not entirely diagonal when two systems are involved.[4] Hence, we also explore the possibility of working in a basis that distinguishes the ancillary degrees of freedom from the physical degrees of freedom of the original reduced density matrix. We refer to such basis as the **physical basis**, as opposed to the **diagonal basis** that mixes the two sets of degrees of freedom.

At this point, let us add that it is natural to think of the auxiliary degrees of freedom as a resource in the preparation of the desired mixed states and hence in differentiating possible purifications, one would assign an additional cost for including more ancillae, *i.e.,* we can assign an extra cost for the ancillary and erasure gates commented on above. However, we will not consider the effect of such an additional cost for the bulk of our analysis, but we return to this issue briefly in chapter 6.

[1] The results of [62] used a $\mathrm{GL}(N, \mathbb{R})$ subgroup of the group $\mathrm{Sp}(2\mathrm{N}, \mathbb{R})$ of transformations between the Gaussian states and our results below are restricted to this case.

[2] We might mention that this assumption also appeared in a recent discussion [183] of the entanglement of purification [183–185] for Gaussian states.

[3] The cost functions assign a cost to different trajectories in the space of unitary transformations between the different states — see section 2.1.1.1 for further details.

[4] The TFD state is a purification of the thermal density matrix on a given QFT_L (the "Left" copy) in terms of another identical QFT_R (the "Right" copy). When studying the complexity of this state, it is important to work with a basis which distinguishes the "Left" and "Right" degrees of freedom to reproduce qualitative features of the holographic complexity of the double-sided AdS black hole.

3.2 Warm-Up: Purification Complexity of a Single Harmonic Oscillator

3.2.1 Gaussian Purifications of One-Mode Mixed States

Turning to the purification complexity of mixed states, we begin by considering Gaussian density matrices for a single oscillator and explore their purifications. Consider a single harmonic oscillator in a mixed state $\hat{\rho}$, such that

$$\rho(x,x') \equiv \langle x|\,\hat{\rho}\,|x'\rangle = \left(\frac{a-b}{\pi}\right)^{1/2} e^{-\frac{1}{2}\left(ax^2+ax'^2-2bxx'\right)} \tag{3.2}$$

where we will assume that a and b are real. Note that this is compatible with ρ being a Hermitian operator, *i.e.*, $\rho^\dagger = \rho$ or $\rho^*(x',x) = \rho(x,x')$. The overall normalization constant was chosen to ensure $\mathrm{Tr}[\rho] = \int dx\,\rho(x,x) = 1$. In order for the Gaussian integral in this norm to be well defined, we need $a > b$. Further, in order that the density matrix be positive semi-definite (*i.e.*, $\langle\psi|\,\hat{\rho}\,|\psi\rangle \geqslant 0$ for arbitrary wavefunctions $\psi(x)$) we should require that $b \geqslant 0$.[5]

Next, we consider purifications of the density matrix (3.2) by pure Gaussian states with two degrees of freedom

$$\psi_{12}(x,y) \equiv \langle x,y|\psi\rangle = \left(\frac{\omega_1\omega_2-k^2}{\pi^2}\right)^{1/4} e^{-\frac{1}{2}\left(\omega_1 x^2+\omega_2 y^2+2k\,xy\right)} \tag{3.3}$$

where again we will assume for simplicity that $\omega_{1,2}$ and k are all real. For this wavefunction to be normalizable, *i.e.*, $1 = \int dx\,dy\;|\psi(x,y)|^2$, we need $\omega_2 > 0$ and $\omega_1\,\omega_2 - k^2 > 0$. The density matrix corresponding to $|\psi\rangle$ is simply given by

$$\rho_{12}(x,y,x',y') = \left(\frac{\omega_1\omega_2-k^2}{\pi^2}\right)^{1/2} e^{-\frac{1}{2}\left(\omega_1 x'^2+\omega_2 y'^2+2kx'y'\right)} e^{-\frac{1}{2}\left(\omega_1 x^2+\omega_2 y^2+2kxy\right)}\,. \tag{3.4}$$

Tracing out the auxiliary oscillator, we find

$$\rho_1(x',x) = \int dy\,\rho_{12}(x,y,x',y) = \frac{\sqrt{\omega_1\omega_2-k^2}}{\sqrt{\pi\,\omega_2}}\, e^{-\frac{1}{2}\left[\left(\omega_1-\frac{k^2}{2\omega_2}\right)(x^2+x'^2)-\frac{k^2}{\omega_2}\,xx'\right]}. \tag{3.5}$$

[5]Since probabilities are all either zero or positive, the density matrix is positive semidefinite, *e.g.*, see section III of [186]. We will see below that $b \geqslant 0$ ensures that the purifying wavefunction also has real parameters.

Therefore comparing the above density matrix to eq. (3.2), we find

$$a = \omega_1 - \frac{k^2}{2\omega_2}\,, \qquad b = \frac{k^2}{2\omega_2}\,. \tag{3.6}$$

From the second equation, we see that $b \geq 0$ ensures a real purification. Note that for $b = 0$, we simply get

$$a = \omega_1\,, \qquad k = 0 \tag{3.7}$$

and ω_2 is unconstrained. That is, for the density matrix (3.2) of an already pure state (*i.e.,* $\rho(x,x') = \psi_1(x)\psi_1^\dagger(x')$), the purification in eq. (3.3) is itself simply the product of two decoupled wavefunctions (*i.e.,* $\psi_{12}(x,y) = \psi_1(x)\psi_2(y)$). For non-zero b, we may solve for ω_1 and ω_2 in terms of a, b and k to find

$$\omega_1 = a + b\,, \qquad \omega_2 = \frac{k^2}{2b}\,. \tag{3.8}$$

Hence we arrive at the one-parameter family of wavefunctions

$$\psi_{12}(x,y) = \left(\frac{(a-b)}{2b}\frac{k^2}{\pi^2}\right)^{1/4} e^{-\frac{1}{2}\left[(a+b)x^2 + \frac{k^2}{2b}y^2 + 2kxy\right]}\,, \tag{3.9}$$

all of which produce the same density matrix (3.2) upon tracing out the auxiliary position y. The purification complexity is then found by optimizing the usual pure state complexity over the free parameter k distinguishing these different purifications.

3.2.2 Alternative Description of the Purifications

Before we evaluate the purification complexity of the density matrix in eq. (3.2), it will be convenient to introduce a second representation of the Gaussian states in order to simplify the optimization and to make clear the role of the ancillae for our Gaussian examples. Hence let us work in terms of the energy eigenstates of a given Hamiltonian

$$H = \frac{1}{2}\hat{p}^2 + \frac{1}{2}\omega^2\hat{x}^2 = \omega\left(a^\dagger a + \frac{1}{2}\right)\,, \tag{3.10}$$

where we have set the mass to one.[6] The annihilation and creation operators are defined as usual with

$$a \equiv \sqrt{\frac{\omega}{2}}\left(\hat{x} + i\frac{\hat{p}}{\omega}\right)\,, \qquad a^\dagger \equiv \sqrt{\frac{\omega}{2}}\left(\hat{x} - i\frac{\hat{p}}{\omega}\right) \tag{3.11}$$

[6]The frequency ω of the oscillator is an arbitrary choice here, but of course, the result of our analysis will only depend on this choice through the parameters of the density matrix (3.2).

and satisfy the commutation relations $[a, a^\dagger] = 1$. The corresponding energy eigenstates can be written as

$$|n\rangle = \frac{(a^\dagger)^n}{\sqrt{n!}}|0\rangle \tag{3.12}$$

where $|0\rangle$ is the vacuum state of the Hamiltonian (3.10).

It is well known in the literature of quantum information, *e.g.,* see [46–48], that Gaussian states can be decomposed in terms of standard operators defined using these creation and annihilation operators. In particular, the most general real density matrix of a one-mode Gaussian state can be decomposed according to[7]

$$\hat{\rho}_1 = \hat{S}_1(r)\, \hat{v}_{\rm th}(\beta, \omega)\, \hat{S}_1^\dagger(r)\,. \tag{3.13}$$

The operator $\hat{S}_1(r)$ is the one-mode squeezing operator, acting on our oscillator which we denote by the subscript 1 (in anticipation for introducing a second oscillator for the purification, which we will denote by a subscript 2), which for real values of r reads[8]

$$\hat{S}_1(r) \equiv e^{-\frac{r}{2}\left(a_1^{\dagger 2} - a_1^2\right)} = e^{i\frac{r}{2}(\hat{x}_1\hat{p}_1 + \hat{p}_1\hat{x}_1)}\,. \tag{3.14}$$

This squeezing operator acts on the wavefunction $\psi(x) \equiv \langle x|\psi\rangle$ by rescaling the coordinate x according to $\langle x|\hat{S}_1(r)|\psi\rangle = e^{r/2}\,\psi(e^r x)$. The remaining operator $\hat{v}_{th}(\beta, \omega)$ is a thermal density matrix for the canonical ensemble with temperature $1/\beta$, *i.e.,*

$$\hat{v}_{\rm th}(\beta, \omega) \equiv \frac{e^{-\beta\omega\, a^\dagger a}}{{\rm Tr}(e^{-\beta\omega\, a^\dagger a})} = \left(1 - e^{-\beta\omega}\right) \sum_{n=0}^{\infty} e^{-\beta\omega\, n}\, |n\rangle\langle n|\,. \tag{3.15}$$

We can evaluate the position space representation of the density matrix $\hat{\rho}$ in eq. (3.13), *i.e.,* $\langle x|\hat{\rho}|x'\rangle$, using Mehler's formula [187], *e.g.,*

$$\sum_{n=0}^{\infty} \frac{u^n}{2^n n!} H_n(x) H_n(y) = \frac{1}{\sqrt{1-u^2}} \exp\left(-\frac{u^2(x^2+y^2) - 2uxy}{1-u^2}\right), \tag{3.16}$$

[7] In this paper, we only consider Gaussian states with $\langle x\rangle = 0 = \langle p\rangle$, which implies that the exponent of the Gaussian wavefunction does not contain a term linear in x. If such terms were present, we would have to extend eq. (3.13) by conjugating with the displacement operator, *e.g.,* see the discussion of complexity of coherent states in [1].

[8] Note that the frequency ω from the definition of a, $a^\dagger$ in eq. (3.11) does not appear here. The infinitesimal version of this squeezing operator is simply the scaling gate (with $a = b$) in eq. (2.15).

where $H_n(x)$ is referred to as the Hermite polynomials. Of course, this yields a Gaussian density matrix of the form in eq. (3.2) with the following parameters

$$a = \frac{e^{2r}\,\omega\,\cosh\beta\omega}{\sinh\beta\omega} > 0\,, \qquad b = \frac{e^{2r}\,\omega}{\sinh\beta\omega} > 0\,, \qquad \frac{a}{b} = \cosh\beta\omega \geq 1\,. \tag{3.17}$$

Demanding that the temperature and frequency are positive is then equivalent to the previous restrictions, $a > b \geqslant 0$, discussed around eq. (3.2). We note that while the parameter ω was introduced as a dimensional scale here, our result for the complexity will only depend on the dimensionless combinations $\beta\omega$ and μ/ω, as well as the (dimensionless) squeezing parameter r.[9] However, the parameter ω will still play an important role later on when considering different modes of a free QFT on the lattice in sections 3.4 and 3.5.[10] When the temperature is set to zero, *i.e.,* $\beta\omega \to \infty$, eq. (3.13) reduces to a pure state. From eq. (3.17), we see that this corresponds to the limit $b/a \to 0$.

The decomposition (3.13) suggests that in order to purify this mixed state, one must purify the thermal part $\hat{v}_{\rm th}$ of the density matrix.[11] This can be done in terms of the thermofield double state, *e.g.,* see [68]

$$|\text{TFD}\rangle_{12} \equiv S_{12}(\alpha)\;|0\rangle_1\,|0\rangle_2 = \left(1-e^{-\beta\omega}\right)^{1/2}\sum_{n=0}^{\infty} e^{-\frac{1}{2}\,\beta\omega\,n}\,|n\rangle_1\,|n\rangle_2 \tag{3.18}$$

where we have introduced the two-mode squeezing operator which entangles the two degrees of freedom,

$$S_{12}(\alpha) \equiv e^{\alpha\left(a_1^\dagger a_2^\dagger - a_1 a_2\right)} = e^{-i\alpha(\hat{x}_1\hat{p}_2+\hat{p}_1\hat{x}_2)}\,. \tag{3.19}$$

The (real) squeezing parameter α for eq. (3.18) is given by

$$\tanh\alpha = e^{-\beta\omega/2}\,, \qquad \alpha = \frac{1}{2}\ln\frac{1+e^{-\beta\omega/2}}{1-e^{-\beta\omega/2}}\,. \tag{3.20}$$

[9] Below, we will see that the complexity only depends on two parameters, namely $\beta\omega$ and a particular combination of μ/ω and r. The latter reduction can be traced back to a symmetry of complexity, *i.e.,* the 'distance' between the reference state and target state is left unchanged if we rescale μ and shift r simultaneously.

[10] As we noted above, ω does not appear in the squeezing operator and further, ω only appears in the dimensionless combination $\beta\omega$ in the thermal density matrix (3.15) (and implicitly in the definition of $|n\rangle$ in that same equation). However, from eq. (3.17), we see that it sets the scale of the dimensionful parameters, a and b, in eq. (3.2). Further, it will set the scale of the dimensionful parameters in the purified state (3.3) — see eq. (3.24) below.

[11] It is noted that the thermal part of eq. (3.13) also determines the (entanglement) entropy of the mixed Gaussian state.

The thermal density matrix $\hat{v}_{\rm th}$ in eq. (3.15) is then produced by tracing out the auxiliary degree of freedom

$$\mathrm{Tr}_2(|\mathrm{TFD}\rangle_{12}\,\langle\mathrm{TFD}|_{12}) = \left(1-e^{-\beta\omega}\right)\sum_n^\infty e^{-\beta\omega\, n}\,|n\rangle_1\langle n|_1 = \hat{v}_{th}(\beta,\omega)\,. \tag{3.21}$$

However, we may also act with any unitary operator on the second oscillator in eq. (3.18) and then this trace would yield an identical thermal density matrix. Hence we can write the most general two-mode purification of eq. (3.13) as

$$|\psi\rangle_{12} = S_1(r)\,S_2(s)\,S_{12}(\alpha)\;|0\rangle_1\,|0\rangle_2\;, \tag{3.22}$$

where we have introduced a second one-mode squeezing operator $S_2(s)$ to account for the freedom noted above in defining the purification of $\hat{v}_{\rm th}(\beta,\omega)$. Eq. (3.22) is the most general two-mode purification using Gaussian states with real parameters. This can be seen by writing the position-space wavefunction

$$\begin{aligned}\psi_{12}(x,y) &\equiv \langle x,y\,|\psi\rangle_{12} = \\ =&\sqrt{\frac{\omega}{\pi}}\,e^{\frac{r+s}{2}}\;\exp\left[-\frac{\omega}{2}\left(\cosh 2\alpha\,(e^{2r}x^2+e^{2s}y^2)-2\,e^{r+s}x\,y\sinh 2\alpha\right)\right]\,.\end{aligned} \tag{3.23}$$

This wavefunction has precisely the same form as given in eq. (3.3), and we identify the parameters as

$$\omega_1 = \omega\,e^{2r}\cosh 2\alpha\,,\qquad \omega_2 = \omega\,e^{2s}\cosh 2\alpha\,,\qquad k = -\omega\,e^{r+s}\sinh 2\alpha\,. \tag{3.24}$$

Of course, substituting these relations into eq. (3.6) yields the same values for a, b as shown in eq. (3.17), where we have used the following identities following from eq. (3.20)

$$\cosh 2\alpha = \frac{1}{\tanh(\beta\omega/2)}\,,\qquad \sinh 2\alpha = \frac{1}{\sinh(\beta\omega/2)}\;,\qquad \tanh^2\alpha = e^{-\beta\omega}\,. \tag{3.25}$$

In the representation (3.23), the squeezing parameter s encodes the freedom in defining the purification, which was previously captured by k in eq. (3.9). Hence with this description, the purification complexity will be found by optimizing the usual pure state complexity over s.

To close here, we note that the expressions in eqs. (3.23) and (3.24), as well as throughout the next section, can easily be written in terms of the parameter $\beta\omega$, which appears in the thermal density matrix (3.15) using the relations (3.25). However, we continue to write

our results in terms of the squeezing parameter α appearing in the purification (3.22). One reason for this is that it simplifies the expressions for the limits of validity of the different regimes in our final result for the purification complexity — see eq. (3.36). Further, α will also be a convenient parameter in our discussion of the purification complexity of a thermal density matrix (and in comparing it to the complexity of the thermofield double state [68]) in section 3.4.

3.2.3 Purification Complexity in the Diagonal Basis

According to the definition of purification complexity [171], see also eq. (3.1), we evaluate the complexity of the mixed state by optimizing the purification to have the minimal circuit complexity as a pure state. We emphasize that we are simplifying this problem here by focusing on Gaussian mixed states and constraining ourselves to only considering Gaussian purifications. As mentioned before, throughout the following, we focus on the complexity defined with the F_1 cost function (2.6). Recall that the $\mathcal{C}_1$ complexity for Gaussian states was found to replicate the behaviours of holographic complexity most closely [62, 68, 69]. However, as was also mentioned in section 2.1.1, the F_1 cost function is basis dependent, and so we must specify that in this subsection, we evaluate the $\mathcal{C}_1$ complexity in the diagonal basis. We will explore the results using the physical basis, which does not mix the original degree of freedom with the ancilla, in the next subsection.

The coefficient matrix $M_{\rm T}^{ab}$ in eq. (2.9) for the purifying wavefunction $|\psi_{12}\rangle$ in eq. (3.23) is given by

$$M_{\rm T}^{ab} = \omega \begin{pmatrix} e^{2r}\cosh 2\alpha & -e^{r+s}\sinh 2\alpha \\ -e^{r+s}\sinh 2\alpha & e^{2s}\cosh 2\alpha \end{pmatrix} . \tag{3.26}$$

Again, the free parameter s specifies a family of purifications of the same mixed state $\hat{\rho}_1$ in eq. (3.13). The prescription for evaluating the complexity of pure states was briefly reviewed in section 2.1.1.1, and the $\mathcal{C}_1$ complexity was given in eq. (2.19). Hence, the complexity of the Gaussian state (3.22) becomes[12]

$$\mathcal{C}_1^{\rm diag}\left(|\psi\rangle_{12}\right) = \frac{1}{2}\left|\ln\frac{\omega_+}{\mu}\right| + \frac{1}{2}\left|\ln\frac{\omega_-}{\mu}\right| , \tag{3.27}$$

where $\omega_\pm$ are the eigenvalues of the matrix M^{ab}, *i.e.,*

$$\omega_\pm = \omega\, e^{r+s}\left(\cosh 2\alpha\, \cosh(r-s) \pm \sqrt{\cosh^2 2\alpha\, \cosh^2(r-s) - 1}\right) . \tag{3.28}$$

[12] We note again that the superscript 'diag' indicates that we are working with the diagonal basis, *i.e.,* with gates acting on the eigenmodes which mix the physical and auxiliary degrees of freedom.

Now according to the definition of purification complexity (3.1), the complexity of the corresponding mixed state (3.13) is given by[13]

$$\mathcal{C}_1^{\text{diag}}\left(\hat{\rho}_1\right) = \min_s \mathcal{C}_1^{\text{diag}}\left(|\psi\rangle_{12}\right) , \tag{3.29}$$

where the dependence on the squeezing parameter s is hidden in the eigenfrequencies $\omega_\pm$ in eq. (3.28).

Before proceeding, we must consider that there are three possibilities in eq. (3.27) depending on the relative magnitudes of the frequencies,

$$\begin{aligned}
&\text{case 1:} \quad \mathcal{C}_1^{\text{diag}} = \frac{1}{2}\ln\frac{\mu^2}{\omega_+\omega_-} = -(\bar{r}+\bar{s})\,, && \mu \geq \omega_\pm\,,\\
&\text{case 2:} \quad \mathcal{C}_1^{\text{diag}} = \frac{1}{2}\ln\frac{\omega_+}{\omega_-} = \cosh^{-1}\big[\cosh 2\alpha \cosh(\bar{r}-\bar{s})\big]\,, && \omega_- \leq \mu \leq \omega_+,\\
&\text{case 3:} \quad \mathcal{C}_1^{\text{diag}} = \frac{1}{2}\ln\frac{\omega_+\omega_-}{\mu^2} = \bar{r}+\bar{s}\,, && \mu \leq \omega_\pm\,.
\end{aligned} \tag{3.30}$$

These results have been simplified by the introduction of the shifted squeezing parameters,

$$\bar{r} \equiv r + \frac{1}{2}\ln\frac{\omega}{\mu} \qquad \text{and} \qquad \bar{s} \equiv s + \frac{1}{2}\ln\frac{\omega}{\mu}\,. \tag{3.31}$$

Now in order to perform the minimization in eq. (3.29), we must identify the different regimes in eq. (3.30) in terms of the parameters of the purifying wavefunction,[14]

$$\begin{aligned}
&\text{case 1:} \quad \tanh^2\alpha \leq \tanh\bar{r}\,\tanh\bar{s} \quad \text{and} \quad \bar{r}+\bar{s} \leq 0\,,\\
&\text{case 2:} \quad \tanh^2\alpha \geq \tanh\bar{r}\,\tanh\bar{s}\,,\\
&\text{case 3:} \quad \tanh^2\alpha \leq \tanh\bar{r}\,\tanh\bar{s} \quad \text{and} \quad \bar{r}+\bar{s} \geq 0\,.
\end{aligned} \tag{3.32}$$

We see immediately that for case 1, both $\bar{r}$ and $\bar{s}$ will be negative, while for case 3, both will be positive. Let us next identify the value of $\bar{s}$ that yields a minimal complexity within each regime. For case 1, the complexity in eq. (3.30) is monotonically decreasing as a function of $\bar{s}$, and hence the minimal complexity is obtain by the maximal allowed value of $\bar{s}$, which can be found from eq. (3.32). Similarly for case 3, the complexity is monotonically

[13] Note that we only optimize over the purification of the target state. We assume that the reference state is fixed as a factorized Gaussian, where both the physical and auxiliary degrees of freedom appear with the same reference frequency.

[14] This is done by analyzing the functional dependence of $\frac{\omega_\pm}{\mu}$ on $\cosh(2\alpha)\cosh(\bar{r}-\bar{s})$ separately for each sign of $\bar{r}+\bar{s}$.

increasing with $\bar{s}$, and so the minimal complexity is associated with the minimal value of $\bar{s}$ allowed according to the inequalities in eq. (3.32).[15] Incidentally, these two critical values of $\bar{s}$ coincide and are given by[16]

$$\text{case 1,3:} \quad \bar{s}_{\text{crit}} = \tanh^{-1}\left(\frac{\tanh^2\alpha}{\tanh\bar{r}}\right) = \frac{1}{2}\ln\left(\frac{e^{2\bar{r}}\cosh 2\alpha - 1}{e^{2\bar{r}} - \cosh 2\alpha}\right) . \tag{3.33}$$

Hence the minimal complexity in these two regimes is given by

$$\text{case 1,3:} \quad \mathcal{C}_1^{\text{diag}} = \pm\frac{1}{2}\ln\left(\frac{1 - e^{-2\bar{r}}\cosh 2\alpha}{e^{2\bar{r}}\cosh 2\alpha - 1}\right) . \tag{3.34}$$

For case 2, the minimal complexity is obtained by minimizing the function in eq. (3.30), which leads to

$$\text{case 2:} \quad \bar{s}_{\text{min}} = \bar{r} \qquad \longrightarrow \qquad \mathcal{C}_1^{\text{diag}} = 2\alpha\,. \tag{3.35}$$

Now the final step is to clarify which one of these minimal complexities is the relevant one for given values of $\bar{r}$ and α. If $\bar{r} < 0$ for instance, both cases 1 and 2 could be in principle relevant, as long as $e^{2\bar{r}}\cosh(2\alpha) < 1$. However for $0 > \bar{r} > -\alpha$, the lowest complexity is that in case 2 and hence the final answer for the purification complexity is given by eq. (3.35). A similar argument can be given in the overlapping regime of cases 2 and 3. We finally arrive at the purification complexity (5.78) for the one-mode Gaussian mixed states (3.13),

$$\mathcal{C}_1^{\text{diag}}(\hat{\rho}_1) = \begin{cases} \frac{1}{2}\ln\left(\frac{e^{-2\bar{r}}\cosh 2\alpha - 1}{1 - e^{2\bar{r}}\cosh 2\alpha}\right), & 0 \le \alpha \le -\bar{r}\,, \\ 2\alpha, & \alpha \ge |\bar{r}|\,, \\ \frac{1}{2}\ln\left(\frac{e^{2\bar{r}}\cosh 2\alpha - 1}{1 - e^{-2\bar{r}}\cosh 2\alpha}\right), & 0 \le \alpha \le \bar{r}\,. \end{cases} \tag{3.36}$$

One interesting point about this result is that the complexity of the mixed state $\hat{\rho}_1$ generally depends on both the thermal parameter $\beta\omega$ (or alternatively, α), and the shifted squeezing

[15] Recall that the boundary of the allowed values for $\bar{s}$ in each of these cases are precisely those for which $\omega_+ = \mu$ or $\omega_- = \mu$ for case 1 and 3 respectively. Thus, the optimal purification in case 1 will have $\omega_+ = \mu$, and similarly the optimal purification in case 3 will have $\omega_- = \mu$.

[16] Let us note that when $\bar{r} < 0$ and $e^{2\bar{r}}\cosh(2\alpha) > 1$, $\bar{s}_{\text{crit}}$ is pushed to minus infinity. Therefore case 1 is not valid for any value of $\bar{s}$ and we are left with case 2 only. Similarly, for $\bar{r} > 0$ and $e^{-2\bar{r}}\cosh(2\alpha) > 1$, $\bar{s}_{\text{crit}}$ is pushed to infinity, case 3 is not valid for any value of $\bar{s}$ and we are once again left with case 2 only.

parameter $\bar{r}$ (which has absorbed the ratio μ/ω), whereas the (entanglement) entropy of this state only depends on the combination $\beta\omega$.

At this point, we can also point out the various benefits of the parametrization introduced in subsection 3.2.2. First, α and r are natural dimensionless parameters associated with the thermal state and its squeezing. The state described by those parameters is always physical, which means we do not need to impose extra constraints on those parameters. In particular, the density matrix is automatically positive semi-definitive and Hermitian for any positive temperature and frequency. For $r = 0$, the density matrix corresponds to a thermal state at temperature $1/\beta$ for a single harmonic oscillator of frequency ω. More generally, for non-zero r, one can think of it as the thermal density matrix with an inverse temperature $\beta' = e^{-2r}\beta$ for a harmonic oscillator of frequency $\omega' = e^{2r}\omega$. That is, using eq. (3.17), one can easily show that

$$\hat{\rho}_1 = \hat{S}_1(r)\,\hat{v}_{\rm th}(\beta,\omega)\,\hat{S}_1^\dagger(r) = \hat{v}_{\rm th}(e^{-2r}\beta, e^{2r}\omega)\,. \tag{3.37}$$

In addition, these parameters simplify the analytical analysis of the minimization, and bring the final result for the complexity and, in particular, the limits of validity of each regime into a (much more) compact form. Further, the physical meaning of the purification becomes clear — in order to purify the Gaussian state, we only need to purify its thermal component, and the extra freedom in the optimization comes from the squeezing operator $S_2(s)$ on the ancilla. Finally, the parametrization is closely related to the thermofield double state at temperature $1/\beta$ which is defined by $r = s = 0$; and for $r = s \neq 0$, it is the thermofield double at temperature $1/\beta'$ of a harmonic oscillator of frequency ω' (where β' and ω' are the same as defined above).

3.2.4 Purification Complexity in the Physical Basis

Next, we explore the sensitivity of our previous results to the choice of the basis. In particular, we re-examine the purification complexity of the one-mode mixed Gaussian state, defined in eq. (3.2) or (3.13), with the F_1 cost function but using the physical basis. That is, here the gates implicitly act directly on the original and auxiliary degrees of freedom, rather than on the linear combinations comprising the eigenmodes of $M_{\rm T}$ describing the purification. This change of basis is accomplished with the orthogonal transformation described in eq. (2.20).

To begin, we re-express the wavefunction matrix (3.26) for the purification $|\psi_{12}\rangle$ in terms of the shifted squeezing parameters in eq. (3.31) as follows

$$M_{\rm T}^{ab} = \mu \begin{pmatrix} e^{2\bar{r}}\cosh 2\alpha & -e^{\bar{r}+\bar{s}}\sinh 2\alpha \\ -e^{\bar{r}+\bar{s}}\sinh 2\alpha & e^{2\bar{s}}\cosh 2\alpha \end{pmatrix}. \tag{3.38}$$

Similarly, the eigenvalues (3.28) become

$$\omega_\pm = \mu\, e^{\bar{r}+\bar{s}} \left(\cosh 2\alpha\, \cosh(\bar{r}-\bar{s}) \pm \sqrt{\cosh^2 2\alpha\, \cosh^2(\bar{r}-\bar{s}) - 1} \right) . \tag{3.39}$$

Now, in order to evaluate the $\mathcal{C}_1^{\rm phys}$ complexity as in eq. (2.20), we need to determine the orthogonal transformation that brings the matrix (3.38) to its diagonal form, see eq. (2.11). That is,

$$\tilde{M}_{\rm T} = \begin{pmatrix} \omega_- & 0 \\ 0 & \omega_+ \end{pmatrix} = O^T\, M_{\rm T}\, O \qquad \text{with} \quad O \equiv \begin{pmatrix} \cos\theta & -\sin\theta \\ \sin\theta & \cos\theta \end{pmatrix} , \tag{3.40}$$

where $\theta \in [0, \frac{\pi}{2}]$ and

$$\begin{aligned} &\sin\theta = \frac{1}{\sqrt{X^2+1}} , \qquad \cos\theta = \frac{X}{\sqrt{X^2+1}} , \\ &X \equiv \frac{1}{\sinh 2\alpha} \left(\sqrt{\cosh^2 2\alpha \cosh^2(\bar{r}-\bar{s}) - 1} - \cosh 2\alpha \sinh(\bar{r}-\bar{s}) \right) \geq 0 . \end{aligned} \tag{3.41}$$

The next step is to rotate the generator $\tilde{H}$ in eq. (2.18), *i.e.*,

$$\tilde{H} = \frac{1}{2} \begin{pmatrix} \ln\frac{\omega_-}{\mu} & 0 \\ 0 & \ln\frac{\omega_+}{\mu} \end{pmatrix} , \tag{3.42}$$

as in eq. (2.20), which defines the circuit generator in the physical basis[17]

$$H = O\, \tilde{H}\, O^T = \frac{1}{2} \begin{pmatrix} \cos^2\theta \ln\frac{\omega_-}{\mu} + \sin^2\theta \ln\frac{\omega_+}{\mu} & -\sin\theta\cos\theta\, \ln\frac{\omega_+}{\omega_-} \\ -\sin\theta\cos\theta\, \ln\frac{\omega_+}{\omega_-} & \cos^2\theta \ln\frac{\omega_+}{\mu} + \sin^2\theta \ln\frac{\omega_-}{\mu} \end{pmatrix} . \tag{3.43}$$

Again using eq. (2.20), $\mathcal{C}_1$ for the purified state corresponding to the wavefunction matrix (3.38) in the physical basis becomes

$$\begin{aligned} \mathcal{C}_1^{\rm phys}(|\psi_{12}\rangle) = \frac{1}{4} \Bigg(& 2\, \sin 2\theta \ln\frac{\omega_+}{\omega_-} + \left| \ln\frac{\omega_+\omega_-}{\mu^2} - \cos 2\theta \ln\frac{\omega_+}{\omega_-} \right| \\ & + \left| \ln\frac{\omega_+\omega_-}{\mu^2} + \cos 2\theta \ln\frac{\omega_+}{\omega_-} \right| \Bigg) . \end{aligned} \tag{3.44}$$

[17] As an aside, we note that the circuit generator H is easily expressed in terms of the "relative wavefunction" matrix $M_{\rm T} M_{\rm R}^{-1}$ directly in the physical basis as $H = \frac{1}{2} \ln\left(M_{\rm T} M_{\rm R}^{-1}\right)$.

It will be convenient to optimize the purification by varying the angle θ rather than working with the squeezing parameter s. Hence we use eq. (3.41) to replace

$$\sinh(\bar{r}-\bar{s}) = -\tanh 2\alpha \, \cot 2\theta \, . \tag{3.45}$$

Note that the sign of $\sinh(\bar{r}-\bar{s})$ will be positive for $\theta > \pi/4$ and negative for $\theta < \pi/4$. Combining this expression with eqs. (3.39) and (3.41), we can also express the other factors in eq. (3.44) in terms of θ as follows

$$\begin{aligned} \frac{1}{2}\ln\frac{\omega_+}{\omega_-} &= \cosh^{-1}(\cosh 2\alpha \cosh(\bar{r}-\bar{s})) = \sinh^{-1}(\sinh 2\alpha \, \csc 2\theta) \, , \\ \frac{1}{2}\ln\frac{\omega_+\omega_-}{\mu^2} &= \bar{r}+\bar{s} = 2\bar{r} + \sinh^{-1}(\tanh 2\alpha \, \cot 2\theta) \, . \end{aligned} \tag{3.46}$$

Using these expressions and examining eq. (3.44) according to the different possible signs in the absolute values, we obtain

$$\begin{aligned} (a) \;\; -- \; : \quad & \mathcal{C}_1^{\text{phys}} = -2\bar{r} + \sin 2\theta \, \sinh^{-1}\left(\frac{\sinh 2\alpha}{\sin 2\theta}\right) - \sinh^{-1}(\tanh 2\alpha \, \cot 2\theta) \\ (b) \;\; +- \; : \quad & \mathcal{C}_1^{\text{phys}} = \sqrt{2}\sin\left(2\theta - \frac{\pi}{4}\right) \sinh^{-1}\left(\frac{\sinh 2\alpha}{\sin 2\theta}\right) \\ (c) \;\; -+ \; : \quad & \mathcal{C}_1^{\text{phys}} = \sqrt{2}\sin\left(2\theta + \frac{\pi}{4}\right) \sinh^{-1}\left(\frac{\sinh 2\alpha}{\sin 2\theta}\right) \\ (d) \;\; ++ \; : \quad & \mathcal{C}_1^{\text{phys}} = 2\bar{r} + \sin 2\theta \, \sinh^{-1}\left(\frac{\sinh 2\alpha}{\sin 2\theta}\right) + \sinh^{-1}(\tanh 2\alpha \, \cot 2\theta) \end{aligned} \tag{3.47}$$

where for instance $+-$ indicates that the sign of the expression inside the first absolute value in eq. (3.44) is positive and the sign of the expression inside the second absolute value is negative. Finally, the purification complexity in the physical basis for the one-mode Gaussian mixed state is given by minimizing this expression with respect to the free parameter θ

$$\mathcal{C}_1^{\text{phys}}(\hat{\rho}_1) = \min_\theta \mathcal{C}_1^{\text{phys}}(|\psi\rangle_{12}) \, . \tag{3.48}$$

Unfortunately, the exact analytical minimization of eq. (3.48) is not possible since it would require solving a transcendental equation. Hence, in order to develop some intuition, let us consider the simple case $\mu = \omega e^{2r}$, *i.e.*, $\bar{r} = 0$ where the purification complexity reduces to

$$\mathcal{C}_1^{\text{phys}} = \begin{cases} \sqrt{2}\sin\left(2\theta - \frac{\pi}{4}\right) \sinh^{-1}\left(\frac{\sinh 2\alpha}{\sin 2\theta}\right) & : \quad +- \, , \\ \sqrt{2}\sin\left(2\theta + \frac{\pi}{4}\right) \sinh^{-1}\left(\frac{\sinh 2\alpha}{\sin 2\theta}\right) & : \quad -+ \, . \end{cases} \tag{3.49}$$

That is, $\mathcal{C}_1^{\text{phys}}$ is given be either cases (b) or (c) in eq. (3.47). We are able to rule out cases (a) and (d) (*i.e.,* $++$ and $--$) by verifying that the product of the terms in the absolute values in eq. (3.44) is negative using the identity[18]

$$\sinh^{-1}\left(\tanh 2\alpha\,|\cot 2\theta\,|\right) - |\cos 2\theta|\,\sinh^{-1}\left(\sinh 2\alpha\,|\csc 2\theta\,|\right) < 0\,. \tag{3.50}$$

To proceed further, let us point out an interesting way to identify which set of signs of the terms in the absolute values is relevant for the evaluation of complexity. We can regard the expressions for each of the cases in eq. (3.47) as evaluating the expression in eq. (3.44), but without the absolute values; rather we are inserting the specified signs in front of the last two terms. Hence for a given value of θ, we can evaluate all four of these expressions. However, the correct result will correspond to the largest value because in this case with the specified signs, both of the second and third terms must be making a positive contribution to the complexity, as required by the absolute values in eq. (3.44). Using this reasoning in eq. (3.49) with $\bar{r} = 0$, we can see that when $\theta < \pi/4$, case (c) is the correct choice, while for $\theta > \pi/4$, the relevant case is (b). This fact will also be useful when performing the numerical analysis of more general cases later on. We may also use the identity $a\sinh^{-1}(x) > \sinh^{-1}(ax)$ for $a > 1$, $x > 0$,[19] with $a = \sin(2\theta) \pm \cos(2\theta) > 1$ for $0 < \theta < \pi/4$ and $\pi/4 < \theta < \pi/2$ respectively, as well as the monotonicity of $\sinh^{-1}(x)$, in order to demonstrate that the minimal value for the complexity is obtained for $\theta = \frac{\pi}{4}$ (which corresponds to $\bar{s} = \bar{r} = 0$), see eq. (3.45). This yields the following purification complexity

$$\mathcal{C}_1^{\text{phys}}\left(\hat{\rho}_1(\bar{r}=0)\right) = \min_\theta \mathcal{C}_1^{\text{phys}}\left(|\psi\rangle_{12}\right) = 2\alpha\,. \tag{3.51}$$

We may also point out, that for $r = 0$, this is simply the TFD purification of a state with temperature β and frequency $\omega = \mu$. The addition of the squeezing parameter r leads to the TFD purification of a state with temperature $\beta' = e^{-2r}\beta$ and frequency $\omega' = \omega e^{2r}$ which is equal to the reference frequency μ, according to the logic described around eq. (3.37).

Next, we return to the general case for which we examine the optimization (3.48) numerically. Without loss of generality, let us assume that $\mu \geq \omega e^{2r}$, or equivalently $\bar{r} < 0$.[20] We will try to use the same logic as above in order to identify the ranges of θ

[18] This identity can be verified separately in each region $0 < \theta < \pi/4$ and $\pi/4 < \theta < \pi/2$ by using the fact that for $\alpha = 0$ we obtain an equality together with the fact that the derivative of the left hand side with respect to α has a definite sign in each region, namely, it is negative for $0 < \theta < \pi/4$ and positive for $\pi/4 < \theta < \pi/2$.

[19] This is due to the fact that $\sinh^{-1}(x)$ is concave down.

[20] Note that the system is symmetric under the exchange $\bar{r} \to -\bar{r}$, $\theta \to \frac{\pi}{2} - \theta$, and (a)$\leftrightarrow$(d), (b)$\leftrightarrow$(c). As a consequence, though the details of the analysis will slightly vary, the value of the complexity obtained by minimizing (3.44) will only depend on the absolute value of $\bar{r}$.

in which the different sets of signs in eq. (3.47) are valid. It is useful to start by looking at a plot of all possible sign combinations given by the four cases (a)–(d), for all values of $0 < \theta < \pi/2$ — see figure 3.2. As noted before, the relevant sign combination for the complexity will always be the highest of the four lines, since that possibility takes into account the correct (positive) signs for all the absolute values. Therefore, we must minimize the complexity over the uppermost envelope of the plots in figure 3.2. Let us proceed with this graphical understanding in mind. For a non-zero value of $\bar{r} < 0$, the different cases in eq. (3.47) are shifted up (case (a)), down (case (d)) or not modified (cases (b) and (c)). Using the same inequalities mentioned above, it is straightforward to see that case (d) becomes irrelevant and is smaller than at least one of the other cases for all values of θ. Therefore, in each region of θ, we should consider two competing sign combinations:

$$\mathcal{C}_1^{\text{phys}}\left(|\psi\rangle_{12}\right) = \begin{cases} \text{case } (a) \text{ or } (b) & \text{for } \frac{\pi}{4} \leq \theta \leq \frac{\pi}{2}\,, \\ \\ \text{case } (a) \text{ or } (c) & \text{for } 0 \leq \theta \leq \frac{\pi}{4}\,. \end{cases} \tag{3.52}$$

We have examined these cases numerically, see figure 3.2. The minimal purification complexity is obtained for a value of θ that either lies at minimal points of the curves (a), (b) or (c) or at the intersections of the curves (a) and (c) or of the curves (a) and (b) depending on the values of $\bar{r}$ and α considered. These values can be identified by solving transcendental equations. For example, in the regime where α is small or $-\bar{r}$ is large, the minimal complexity is obtained at the point where the curves for cases (a) and (c) intersect, which corresponds to solving the equation

$$-2\bar{r} = \sinh^{-1}(\tanh 2\alpha \, \cot 2\theta_c) + \cos 2\theta_c \, \sinh^{-1}\left(\frac{\sinh 2\alpha}{\sin 2\theta_c}\right)\,, \tag{3.53}$$

and the purification complexity reads

$$\mathcal{C}_{1,c}^{\text{phys}}\left(\hat{\rho}_1\right) = (\sin 2\theta_c + \cos 2\theta_c) \, \sinh^{-1}\left(\frac{\sinh 2\alpha}{\sin 2\theta_c}\right)\,. \tag{3.54}$$

When the parameter α is large enough, we can find that the minimal complexity corresponds to the minimal point along the curve (c) rather than to the intersection of curves (c) and (a). This is illustrated in figure 3.3 which plots the difference $\mathcal{C}_{1,c}^{\text{phys}} - \mathcal{C}_1^{\text{phys}}$. The non-zero values in the middle of this plot mean that the minimization is obtained at the local minimal point of curve (c) where the complexity is given by

$$\mathcal{C}_1^{\text{phys}}\left(\hat{\rho}_1\right) = \sqrt{2}\sin\left(2\theta_{\text{min}} + \frac{\pi}{4}\right) \, \sinh^{-1}\left(\frac{\sinh 2\alpha}{\sin 2\theta_{\text{min}}}\right) \tag{3.55}$$

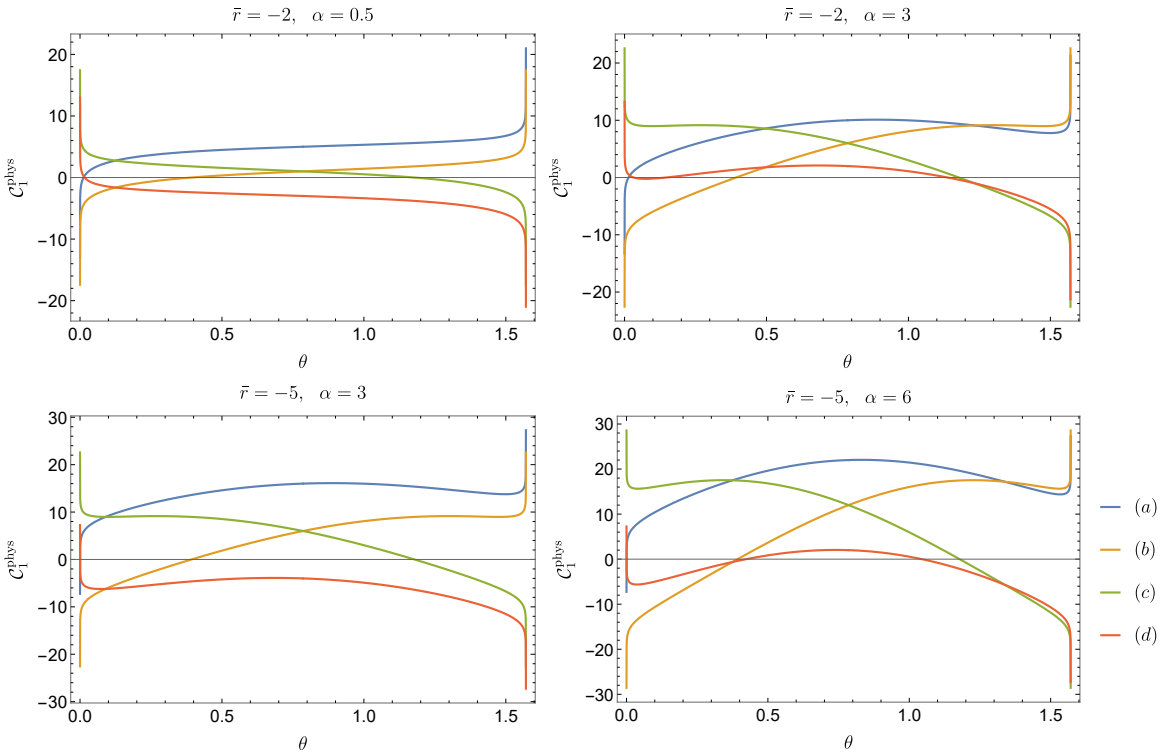

Figure 3.2: Possible values for the pure state complexity $\mathcal{C}_1^{\text{phys}}(|\psi_{12}\rangle)$ in the physical basis as a function of θ, for all possible sign combinations according to eq. (3.47) for fixed values of $\bar{r}$ and α. The complexity of the mixed state purified by $|\psi_{12}\rangle$ is obtained by minimizing over the uppermost envelope of each of these plots.

where

$$\partial_\theta \left(\sin\left(2\theta + \frac{\pi}{4}\right) \sinh^{-1}\left(\frac{\sinh 2\alpha}{\sin 2\theta}\right)\right)\Big|_{\theta_{\text{min}}} = 0, \qquad 0 \leq \theta_{\text{min}} \leq \theta_c \,. \tag{3.56}$$

Although we cannot solve for θ_c or θ_{min} analytically, we may evaluate them numerically. Similar equations can be written for other possible positions of the minimum. Figure 3.4 contains results for $\mathcal{C}_1^{\text{phys}}(\hat{\rho}_1)$ from numerical minimization with fixed value of $\bar{r}$.

3.2.4.1 Differences between the two bases

We must stress again that with the physical basis, the gates act directly on the original and auxiliary degrees of freedom. This contrasts with the diagonal basis where the gates act on

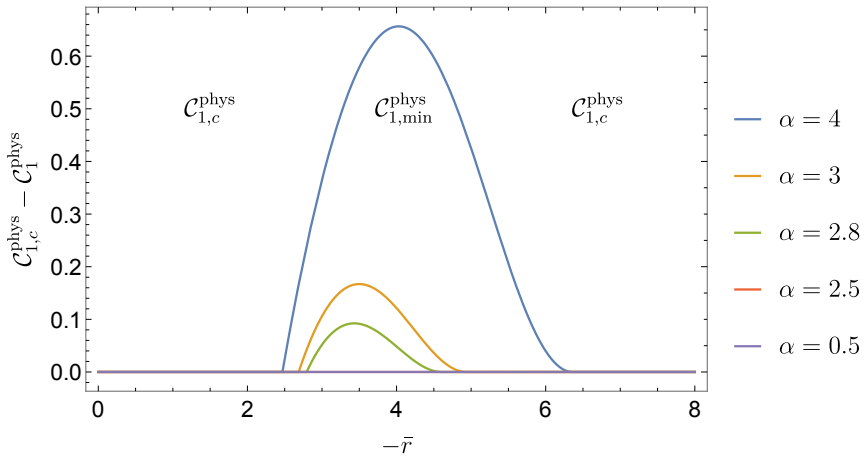

Figure 3.3: The difference between the complexity obtained for θ_c at the intersection of cases (a) and (c) and the exact purification complexity of one-mode Gaussian states in the physical basis $\mathcal{C}^{\text{phys}}_{1,c}(\hat{\rho}_1) - \mathcal{C}^{\text{phys}}_{1}(\hat{\rho}_1)$ as a function of $\bar{r}$ for some fixed values of α. We see that the complexity obtained at the intersection between cases (a) and (c) with $\mathcal{C}^{\text{phys}}_{1,c}(\hat{\rho}_1)$ in eq. (3.54) ceases to be optimal for some region of the parameter $\bar{r}$ for large enough values of α.

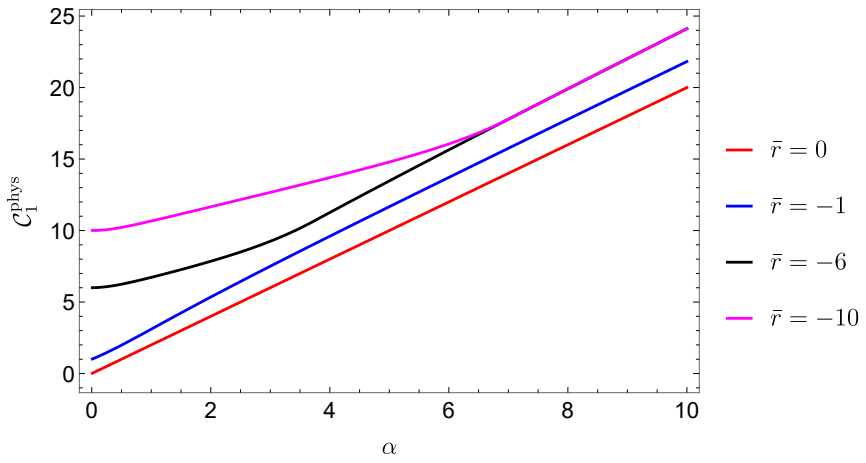

Figure 3.4: Purification complexity of one-mode Gaussian states in the physical basis $\mathcal{C}^{\text{phys}}_{1}(\hat{\rho}_1)$ as a function of α for some fixed values of $\bar{r}$. The fact that the curves with $\bar{r} = -6$ and $\bar{r} = -10$ coincide after a certain value of α is due to the fact that this minimization is obtained at the minimum of case (c) which is $\bar{r}$ independent.

the linear combinations comprising the eigenmodes of $M_{\rm T}$ describing the purification. In particular, then, one of the diagonal generators is precisely aligned with the generator $\tilde{H}$ of the optimal circuit in eq. (2.18). As a consequence, one expects that with other choices of basis, the purification complexity of mixed states (as well as the complexity of pure states) will not be smaller than in the diagonal basis.

Comparing our results for of the one-mode Gaussian mixed states in the physical basis (3.44) to those in the diagonal basis (3.30), we can show

$$\begin{aligned}\mathcal{C}_1^{\rm phys} &= \frac{1}{2}\left(\sin 2\theta \ln\frac{\omega_+}{\omega_-} + \left|\cos 2\theta \frac{1}{2}\ln\frac{\omega_+}{\omega_-} - \frac{1}{2}\ln\frac{\omega_+\omega_-}{\mu^2}\right| + \left|\frac{1}{2}\ln\frac{\omega_+\omega_-}{\mu^2} + \cos 2\theta\frac{1}{2}\ln\frac{\omega_+}{\omega_-}\right|\right) , \\ &\geq (\sin 2\theta + |\cos 2\theta|)\,\frac{1}{2}\ln\frac{\omega_+}{\omega_-} \geq \mathcal{C}_1^{\rm diag}(\text{case 2}) ,\end{aligned} \tag{3.57}$$

and

$$\begin{aligned}\mathcal{C}_1^{\rm phys} &= \frac{1}{2}\left(\sin 2\theta \ln\frac{\omega_+}{\omega_-} + \left|\frac{1}{2}\ln\frac{\omega_+\omega_-}{\mu^2} - \cos 2\theta \frac{1}{2}\ln\frac{\omega_+}{\omega_-}\right| + \left|\frac{1}{2}\ln\frac{\omega_+\omega_-}{\mu^2} + \cos 2\theta\frac{1}{2}\ln\frac{\omega_+}{\omega_-}\right|\right) , \\ &\geq \sin 2\theta\,\frac{1}{2}\ln\frac{\omega_+}{\omega_-} + \frac{1}{2}\left|\ln\frac{\omega_+\omega_-}{\mu^2}\right| \geq \mathcal{C}_1^{\rm diag}(\text{case 1,3}) ,\end{aligned} \tag{3.58}$$

where we used the inequality $|a-c|+|c-b| \geq |a-b|$. Hence, we conclude

$$\mathcal{C}_1^{\rm phys}(|\psi_{12}\rangle) \geq \mathcal{C}_1^{\rm diag}(|\psi_{12}\rangle) , \qquad \mathcal{C}_1^{\rm phys}(\hat{\rho}_1) \geq \mathcal{C}_1^{\rm diag}(\hat{\rho}_1) , \tag{3.59}$$

as expected. It is also easy to demonstrate that the latter inequality holds in various examples by numerical minimization.

3.3 Optimal Purification of Mixed Gaussian States

In the previous section, our mixed state (3.2) described a single physical degree of freedom, and it was purified by introducing a single ancilla. When trying to evaluate the purification complexity for a mixed state with many modes, one must ask the question of how many ancillae are needed to produce the minimal complexity. In subsection 3.3.1, we began by identifying the minimum number of extra degrees of freedom that are needed to purify a given mixed state. We will refer to such purifications with only the essential number of

ancillae as **essential purifications**. Note that as we introduce additional ancillae, the number of free parameters over which one would optimize increases, and so one might expect that this will also reduce the corresponding purification complexity. However, we will argue that this intuition is incorrect for Gaussian mixed states and that the optimal purification should be an essential purification. Further, in identifying the minimum number of ancillae, our approach is to construct a 'diagonal' basis in which the density matrix takes a canonical form where each eigenmode is separately either in a mixed or pure state. Each of the mixed state modes can then be purified by a single ancilla in a purification, which we refer to as a **mode-by-mode purification** (see figure 3.5). In the next section 3.4 and 3.5, we consider the purification complexity in some examples of Gaussian mixed states in quantum field theory. Adopting the conclusion from this section, the purifications over which we optimize there will be both essential and mode-by-mode purifications [21].

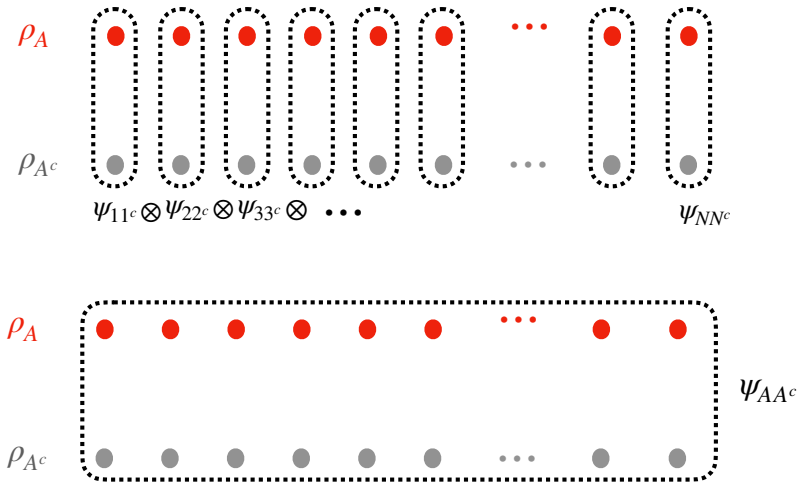

Figure 3.5: Illustration of the different ways to purify a multi-mode Gaussian state $\hat{\rho}_A$. We refer to the purifications of the form $\Psi_{11^c} \otimes \Psi_{22^c} \otimes \cdots \otimes \Psi_{NN^c}$ as mode-by-mode purifications.

[21] Without assuming the mode-by-mode purification, the purification complexity with F_2 cost function and the most general Gaussian purification is studied in [188] for 2D free CFTs.

3.3.1 Purifying General Gaussian States

In this subsection, we study Gaussian purifications of Gaussian density matrices with an arbitrary number of modes. The discussion will follow closely the one in [183], and as before, we will focus on density matrices and wavefunctions with real parameters for simplicity. We start with the wavefunction of a pure Gaussian state

$$\Psi_{\mathcal{A}\mathcal{A}^c} = \mathcal{N}_{\mathcal{A}\mathcal{A}^c} \ \exp\left[-\frac{1}{2}(\vec{q}_{\mathcal{A}}, \vec{q}_{\mathcal{A}^c}) \begin{pmatrix} \Gamma & K \\ K^T & \Omega \end{pmatrix} \begin{pmatrix} \vec{q}_{\mathcal{A}} \\ \vec{q}_{\mathcal{A}^c} \end{pmatrix}\right], \tag{3.60}$$

where the degrees of freedom were divided into the "inside" region $\mathcal{A}$ containing the $N_{\mathcal{A}}$ coordinates $\vec{q}_{\mathcal{A}}$, and the "outside" region $\mathcal{A}^c$ containing the $N_{\mathcal{A}^c}$ coordinates $\vec{q}_{\mathcal{A}^c}$. The wavefunction matrix in eq. (3.60) has to be positive definite in order for the wavefunction to be normalizable. The square matrices Γ and Ω are real, symmetric and positive definite.[22] Further, the rectangular $N_{\mathcal{A}} \times N_{\mathcal{A}^c}$ matrix K is also real[23] and $\mathcal{N}_{\mathcal{A}\mathcal{A}^c}$ is the normalization factor (ensuring that the wavefunction has unit norm). The reduced density matrix describing the mixed state on the subsystem $\mathcal{A}$ is obtained by tracing out the degrees of freedom in the outside region $\mathcal{A}^c$, as follows

$$\hat{\rho}_{\mathcal{A}} = \mathrm{Tr}_{\mathcal{A}^c}\big(\, |\Psi_{\mathcal{A}\mathcal{A}^c}\rangle \langle \Psi_{\mathcal{A}\mathcal{A}^c}| \,\big) \,. \tag{3.61}$$

This amounts to the Gaussian integral

$$\begin{aligned} \rho_{\mathcal{A}}\left(\vec{q}_{\mathcal{A}}, \vec{q}\,'_{\mathcal{A}}\right) &= \int d\, q_{\mathcal{A}^c} \ \Psi_{\mathcal{A}\mathcal{A}^c}(\vec{q}_{\mathcal{A}}, \vec{q}_{\mathcal{A}^c}) \, \Psi^{\dagger}_{\mathcal{A}\mathcal{A}^c}(\vec{q}\,'_{\mathcal{A}}, \vec{q}_{\mathcal{A}^c}) \\ &= \mathcal{N}_{\mathcal{A}} \ \exp\left[-\frac{1}{2}(\vec{q}_{\mathcal{A}}, \vec{q}\,'_{\mathcal{A}}) \begin{pmatrix} \Gamma - \frac{1}{2}K\Omega^{-1}K^T & -\frac{1}{2}K\Omega^{-1}K^T \\ -\frac{1}{2}K\Omega^{-1}K^T & \Gamma - \frac{1}{2}K\Omega^{-1}K^T \end{pmatrix} \begin{pmatrix} \vec{q}_{\mathcal{A}} \\ \vec{q}\,'_{\mathcal{A}} \end{pmatrix}\right]. \end{aligned} \tag{3.62}$$

Following the reverse logic, let us start with a general mixed Gaussian state of $N_{\mathcal{A}}$ modes with the (real) density matrix

$$\rho_{\mathcal{A}}\left(\vec{q}_{\mathcal{A}}, \vec{q}\,'_{\mathcal{A}}\right) = \mathcal{N}_{\mathcal{A}} \ \exp\left[-\frac{1}{2}(\vec{q}_{\mathcal{A}}, \vec{q}\,'_{\mathcal{A}}) \begin{pmatrix} A & -B \\ -B & A \end{pmatrix} \begin{pmatrix} \vec{q}_{\mathcal{A}} \\ \vec{q}\,'_{\mathcal{A}} \end{pmatrix}\right], \tag{3.63}$$

where the $N_{\mathcal{A}} \times N_{\mathcal{A}}$ matrices A and B are both real and symmetric. Further, we must require B to be positive semi-definite to ensure that the density matrix is non-negative, and $A - B$ to be a strictly positive matrix to ensure that the density matrix can be normalized.[24]

[22] Note that sub-matrices of positive definite matrices are also positive definite. It will also be important that positive definite matrices are invertible.

[23] The restriction to real matrices here and above are a choice that we impose to simplify our analysis. In contrast, the positivity of Γ and Ω is required to ensure that the wavefunction is normalizable.

[24] This also implies that A is a strictly positive matrix, since the sum of two positive definite matrices is also positive definite.

In this case, a wavefunction of the form (3.60) will purify $\rho_{\mathcal{A}}$ if the two following constraints are satisfied

$$\Gamma = A + B\,, \qquad \frac{1}{2} K \Omega^{-1} K^T = B\,. \tag{3.64}$$

In this situation, the $\vec{q}_{\mathcal{A}}$ are the physical degrees of freedom while the $\vec{q}_{\mathcal{A}^c}$ are now auxiliary degrees of freedom. While Γ is completely fixed by the first constraint above, it should be clear that the second constraint leaves a great deal of freedom in the choice of Ω and K. Assuming K has a left inverse (and B is invertible),[25] we can rewrite the constraints (3.64) as

$$\Gamma = A + B\,, \qquad \Omega = \frac{1}{2}\, K^T B^{-1} K\,, \tag{3.65}$$

where Ω is completely determined by B and K. Hence we can think of the freedom in choosing the purification as being parameterized by the choice of the $N_{\mathcal{A}} N_{\mathcal{A}^c}$ components of K. Of course, this is the multi-mode generalization of the freedom found in eq. (3.9), where the single parameter k parameterized the purifications of the density matrix (3.2) for a single degree of freedom. Hence with many modes (and ancillae), the purification complexity will be found by optimizing the usual complexity of the purification (3.60) over the freedom in choosing the matrix K.

However, it is natural to first ask what is the minimum number of ancillae $N_{\mathcal{A}^c}$ required to purify the mixed state $\rho_{\mathcal{A}}$. In order to count the degrees of freedom needed for the purification, we start by bringing the matrices A and B in eq. (3.63) to a canonical form by performing a sequence of coordinate transformations: First, we find an orthogonal matrix O_A that diagonalizes A, *i.e.,* $D_A = O_A^T \cdot A \cdot O_A$. We then rescale the coordinates $\vec{q}_A$ such that A becomes the unit matrix. Finally, we diagonalize the transformed B matrix with a second orthogonal transformation O_B. The complete coordinate transformation reads

$$\vec{q}_{\mathcal{A}} = O_A \cdot D_A^{-1/2} \cdot O_B \cdot \tilde{\vec{q}}_{\mathcal{A}}\,, \tag{3.66}$$

and of course, the same equation holds for $\vec{q}\,'_{\mathcal{A}}$. In this basis,[26] the quadratic form describing

[25] We stress that these conditions are not achieved for generic purifications. For example, a linear transformation $K : \mathcal{A}^c \to \mathcal{A}$ has a left inverse if and only if it is injective (*i.e.,* one-to-one). This immediately implies that $N_{\mathcal{A}^c} = \dim(\mathcal{A}^c) \leq \dim(\mathcal{A}) = N_{\mathcal{A}}$. This constraint does not hold in general since we can introduce as many ancillae as we wish in purifying a given mixed state. However, it does hold for essential mode-by-mode purifications, which will be the focus of our analysis in the following. Similar comments apply for the conditions under which B is invertible.

[26] As an aside, we note that eq. (3.66) is not an orthogonal transformation and as a consequence, the reference state (2.14), which we are implicitly choosing for the purified $\mathcal{A}\mathcal{A}^c$ system,

$$\Psi_R\left(\vec{q}_{\mathcal{A}}, \vec{q}_{\mathcal{A}^c}\right) = \mathcal{N}_R \;\exp\left[-\frac{\mu}{2}(\vec{q}_{\mathcal{A}}, \vec{q}_{\mathcal{A}^c}) \begin{pmatrix} \mathbb{I}_{N_{\mathcal{A}}} & 0 \\ 0 & \mathbb{I}_{N_{\mathcal{A}^c}} \end{pmatrix} \begin{pmatrix} \vec{q}_{\mathcal{A}} \\ \vec{q}_{\mathcal{A}^c} \end{pmatrix}\right], \tag{3.67}$$

the density matrix (3.63) is given in terms of matrices $\tilde{A}$ and $\tilde{B}$ which read

$$\tilde{A} = \mathbb{1}_{N_{\mathcal{A}}}, \quad \tilde{B} = O_B^T \cdot D_A^{-1/2} \cdot O_A^T \cdot B \cdot O_A \cdot D_A^{-1/2} \cdot O_B = D_B \,. \tag{3.69}$$

In this canonical form, the matrix B has become

$$\tilde{B} = D_B = \begin{pmatrix} b_1 & & & & & & \\ & b_2 & & & & & \\ & & \ddots & & & & \\ & & & b_{n_B} & & & \\ & & & & 0 & & \\ & & & & & \ddots & \\ & & & & & & 0 \end{pmatrix}, \tag{3.70}$$

with $n_B = \mathrm{rank}(\tilde{B}) = \mathrm{rank}(B)$ non-zero components. Therefore written in terms of the transformed coordinates $\tilde{\vec{q}}_{\mathcal{A}}$, the density matrix $\rho_{\mathcal{A}}$ has been decomposed into n_B two-by-two blocks describing modes in a mixed state, *i.e.,*

$$\begin{pmatrix} 1 & b_i \\ b_i & 1 \end{pmatrix}, \tag{3.71}$$

and $N_{\mathcal{A}} - n_B$ two-by-two unit matrices describing modes in a pure state. Now it is possible to follow the procedure in section 3.2.1 to purify each of the mixed-state modes with a single ancilla, and finally transform back with eq. (3.66) to obtain a purification of the density matrix $\rho_{\mathcal{A}}$ in the original $\vec{q}_{\mathcal{A}}$ basis. As illustrated in figure 3.5, we refer to such purifications as **mode-by-mode purifications**.

It is also straightforward to show that we cannot purify $\rho_{\mathcal{A}}$ with less than n_B additional degrees of freedom, namely $N_{\mathcal{A}^c} \geq n_B$. Towards this goal, we consider the following theorem regarding the rank of the product of two matrices

$$\mathrm{rank}(M \cdot N) \leq \min(\mathrm{rank}(M), \mathrm{rank}(N)) \,. \tag{3.72}$$

transforms nontrivially. The transformed reference state becomes

$$\Psi_R\left(\tilde{\vec{q}}_{\mathcal{A}}, \vec{q}_{\mathcal{A}^c}\right) = \mathcal{N}_R \det(D_A) \ \exp\left[-\frac{\mu}{2}(\tilde{\vec{q}}_{\mathcal{A}}, \vec{q}_{\mathcal{A}^c}) \begin{pmatrix} O_B^T \cdot D_A^{-1} \cdot O_B & 0 \\ 0 & \mathbb{1}_{N_{\mathcal{A}^c}} \end{pmatrix} \begin{pmatrix} \tilde{\vec{q}}_{\mathcal{A}} \\ \vec{q}_{\mathcal{A}^c} \end{pmatrix}\right], \tag{3.68}$$

which is no longer an unentangled product state. However, this point is irrelevant for our argument determining the minimal value of degrees of freedom $N_{\mathcal{A}^c}$ required for the purification.

Hence applying this theorem to the second constraint in eq. (3.64), *i.e.*, $\frac{1}{2}K\,\Omega^{-1}K^T = B$, we see that if a solution exists then we must have $\text{rank}(B) \leq \min(\text{rank}(\Omega^{-1}), \text{rank}(K))$. Next we observe that since the $N_{\mathcal{A}^c} \times N_{\mathcal{A}^c}$ matrix Ω is invertible, $\text{rank}(\Omega^{-1}) = \text{rank}(\Omega) = N_{\mathcal{A}^c}$. Furthermore, $\text{rank}(K) \leq \min(N_{\mathcal{A}}, N_{\mathcal{A}^c}) \leq N_{\mathcal{A}^c}$ since K is an $N_{\mathcal{A}} \times N_{\mathcal{A}^c}$ matrix. Hence we arrive at

$$N_{\mathcal{A}^c} \geq n_B\,, \tag{3.73}$$

where $n_B \equiv \text{rank}(B)$. That is, we will need at least n_B ancillae in the $\mathcal{A}^c$ system in order to purify the mixed Gaussian state $\rho_{\mathcal{A}}$. However, having explicitly constructed a purification with $N_{\mathcal{A}^c} = n_B$ above, we know that it is possible to saturate this bound and we may conclude that this is the minimum number of extra degrees of freedom needed for the purification. We refer to these purifications containing only the essential number of ancillae as **essential purifications**.[27]

Generally, it is a challenge to determine what is the optimal purification for a general Gaussian mixed state with a given complexity measure. In [2], we numerically examine the role of extra ancillae in the purification of a one-mode Gaussian state. Our analysis yields a clear result that adding extra ancillae will not improve the purification complexity considering either a diagonal basis or a physical basis. Throughout the following, we are emboldened to interpret this result as an indication that the optimal purification for a Gaussian mixed state for many oscillators is an essential purification, *i.e.*, the number of ancillae saturates eq. (3.73) with $N_{\mathcal{A}^c} = n_B$. On the other hand, we also test the optimality of the mode-by-mode purification with taking Gaussian mixed states for two degree of freedom as an explicit example in [2]. Motivated by our numerical results for two-mode Gaussian states, we arrive at the second conjecture that for the general $N_{\mathcal{A}}$-mode Gaussian state $\rho_{\mathcal{A}}$ whose density matrix elements satisfy

$$[A, B] = 0\,, \tag{3.74}$$

the optimal purification will be a mode-by-mode purification (in both diagonal and physical basis). Further, when $[A, B] \neq 0$ but these matrices are still close to commuting, the mode-by-mode purification will still be a good approximation to the true optimal purification.

3.4 Circuit Complexity of Thermal States

Now we wish to apply the techniques developed in the previous sections in order to evaluate the purification complexity for examples in quantum field theory (QFT). In particular,

[27] We chose this name to distinguish this class of purifications from the *optimal* purifications, which are defined to be the purifications yielding the minimal complexity.

we start in this section with a thermal mixed state for a free scalar field theory. As a simple exercise, we begin by considering the thermal state of a single harmonic oscillator. One question we ask here is while the thermofield-double (TFD) state for two harmonic oscillators provides a natural purification of the thermal state, is it ever the optimal purification for this state? Next, we briefly review the lattice regularization of a free scalar field theory, which reduces to a family of coupled harmonic oscillators. We then apply our results for the single oscillator case to examine the purification complexity for a thermal mixed state in the free scalar QFT, both in the diagonal basis and in the physical basis. In Chapter 4, we follow up with a comparison of our results here with the analogous results from holographic complexity.

3.4.1 Exercise: One-mode Thermal States

For simplicity, we start by analyzing the purification complexity of the thermal state for a single oscillator, *i.e.,* $\hat{v}_{\rm th}(\beta,\omega)$ in eq. (3.15). For this exercise, we limit ourselves to considering the diagonal basis. In fact, this is a simple case of the one-mode mixed states (3.13) studied in section 3.2.3, where we set the squeezing parameter $r=0$. Hence the purification complexity is given by simply substituting $r=0$ into eq. (3.36),

$$\mathcal{C}^{\rm diag}_{1,\rm th}(\beta,\omega,\mu)=\begin{cases} \frac{1}{2}\ln\frac{\mu}{\omega}+\frac{1}{2}\ln\left(\frac{\frac{\mu}{\omega}\coth(\beta\omega/2)-1}{\frac{\mu}{\omega}-\coth(\beta\omega/2)}\right), & \text{for}\quad \coth(\frac{\beta\omega}{4})\leq\frac{\mu}{\omega}\,, \\ \ln\coth\left(\frac{\beta\omega}{4}\right), & \text{for}\quad \tanh(\frac{\beta\omega}{4})\leq\frac{\mu}{\omega}\leq\coth(\frac{\beta\omega}{4})\,, \\ \frac{1}{2}\ln\frac{\omega}{\mu}+\frac{1}{2}\ln\left(\frac{\frac{\omega}{\mu}\coth(\beta\omega/2)-1}{\frac{\omega}{\mu}-\coth(\beta\omega/2)}\right), & \text{for}\quad \frac{\mu}{\omega}\leq\tanh(\frac{\beta\omega}{4})\,. \end{cases} \tag{3.75}$$

Here we have substituted $\bar{r}=\frac{1}{2}\ln\frac{\omega}{\mu}$ from setting $r=0$ in eq. (3.31), and we have used the definition of α given in eq. (3.20). The interplay between the different regimes of eq. (3.75) is explored in figure 3.6.

Of course, one well-known purification of the thermal state (3.15) is the TFD state, see eq. (3.21). However, this is not necessarily the optimal purification that leads to a minimal complexity. Examining eq. (3.75), it turns out that the optimal purification is in fact the TFD state for the intermediate regime, *i.e.,* $\tanh(\beta\omega/4)\leq\frac{\mu}{\omega}\leq\coth(\beta\omega/4)$. This can be seen by observing that eqs. (3.35) and (3.31) yield $s=0$ when $r=0$ in this case and therefore the purification (3.22) reduces to the TFD state in eq. (3.18). For example, this case will be of relevance when the reference frequency μ and the oscillator frequency ω are equal.

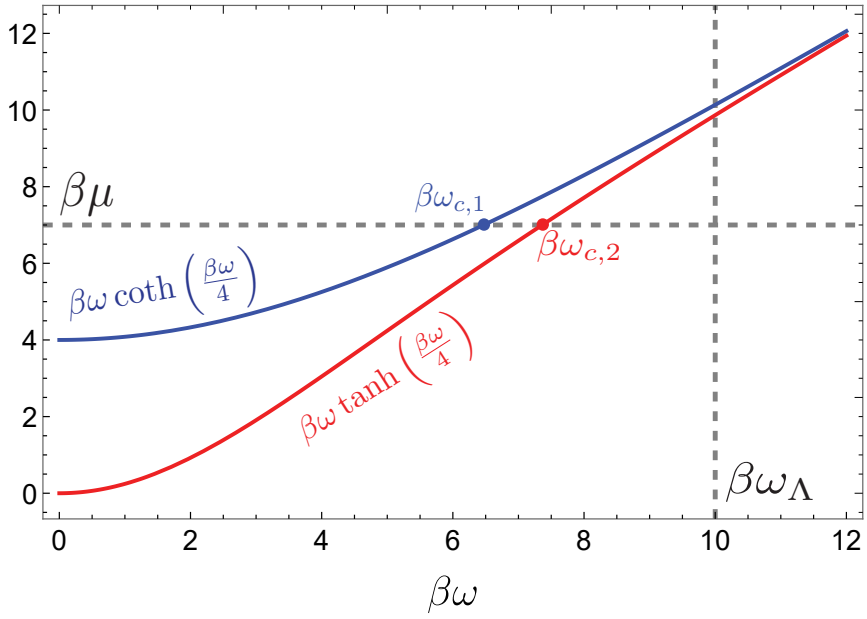

Figure 3.6: Different regimes of eq. (3.75): values of $\beta\mu$ above the blue curve, *i.e.*, $\beta\omega \coth(\beta\omega/4)$, correspond to the first regime in this equation; below the red curve *i.e.*, $\beta\omega \tanh(\beta\omega/4)$, correspond to the third regime; while between the blue and red curves correspond to the second regime. We observe that when $\beta\mu \gg 1$, there is a very narrow range of frequencies $\beta\omega$ between the blue and red lines (since both curves converge towards $\beta\omega$) for which the intermediate regime applies.

We may also consider two other interesting limits: First, for $\omega \coth \frac{\beta\omega}{4} \ll \mu$, the first line in eq. (3.75) applies and this limit yields

$$\mathcal{C}^{\rm diag}_{1,\rm th} \simeq \frac{1}{2}\,\ln\left(\frac{\mu}{\omega}\,\coth\frac{\beta\omega}{2}\right) \qquad \text{with} \quad s \simeq \frac{1}{2}\,\ln\left(\frac{\mu}{\omega}\,\tanh\frac{\beta\omega}{2}\right)\,, \tag{3.76}$$

see eq. (3.33) and (3.31). Hence the optimal purification is far from being the TFD state, for which $s = 0$. Next, in the opposite limit with $\mu \ll \omega \tanh \frac{\beta\omega}{4}$, the third case in eq. (3.75) applies. This limit then yields

$$\mathcal{C}^{\rm diag}_{1,\rm th} \approx \frac{1}{2}\,\ln\left(\frac{\omega}{\mu}\coth\frac{\beta\omega}{2}\right) \qquad \text{with} \quad s \simeq \frac{1}{2}\,\ln\left(\frac{\mu}{\omega}\,\coth\frac{\beta\omega}{2}\right)\,. \tag{3.77}$$

Hence, the optimal purification is again far from the TFD state.

While we have limited our attention to the diagonal basis here, the analogous results for the physical basis can be found by using $r = 0$ in section 3.2.4.

3.4.2 Discretization of the Free Scalar

In order to apply our results from the last several sections to a QFT, we follow [62] and consider a free massive scalar theory with Hamiltonian

$$H = \frac{1}{2}\int d^{d-1}x \left[\pi(x)^2 + (\vec{\nabla}\phi(x))^2 + m^2\,\phi(x)^2\right] . \tag{3.78}$$

We start by regulating the theory by placing it on a periodic 'square' lattice with lattice spacing δ and where each side has a linear length L. Therefore the total number of sites is given by $N^{d-1} \equiv (L/\delta)^{d-1}$. The lattice Hamiltonian is then the Hamiltonian for N^{d-1} coupled harmonic oscillators, which can be written as[28]

$$H = \sum_{\vec{n}} \left\{ \frac{\bar{p}(\vec{n})^2}{2M} + \frac{1}{2}M\left[\bar{\omega}^2\bar{x}(\vec{n})^2 + \Omega^2 \sum_i \left(\bar{x}(\vec{n}) - \bar{x}(\vec{n}-\hat{x}_i)\right)^2\right]\right\} , \tag{3.79}$$

where in the second line, we have defined $\bar{x}(\vec{n}) = \delta^{d/2}\phi(\vec{n})$, $\bar{p}(\vec{n}) = \delta^{(d-2)/2}\pi(\vec{n})$, $\bar{\omega} = m$ and $\Omega = 1/\delta = M$, see, e.g., [62]. Further, periodic boundary conditions are imposed with $\bar{x}(\vec{n} + N\hat{x}_i) \equiv \bar{x}(\vec{n})$ for any i. Next we rewrite the Hamiltonian in terms of the normal modes

$$x_{\vec{k}} \equiv \frac{1}{N^{\frac{d-1}{2}}} \sum_{\vec{n}} \exp\left(\frac{2\pi i\vec{k}\cdot\vec{n}}{N}\right)\bar{x}(\vec{n}) , \quad \omega_{\vec{k}}^2 = m^2 + 4\Omega^2 \sum_i \sin^2\frac{\pi k_i}{N} , \tag{3.80}$$

where $\vec{k} = (k_1, \cdots, k_{d-1})$ with $k_i = 1, 2, \cdots N$. The Hamiltonian then becomes

$$H = \frac{1}{2M}\sum_{\vec{k}} \left(|p_{\vec{k}}|^2 + M^2\omega_{\vec{k}}^2\,|x_{\vec{k}}|^2\right) , \tag{3.81}$$

where we have used that $x_{\vec{k}}^\dagger = x_{-\vec{k}}$. This means that we can think of the system as a system of N^{d-1} decoupled real harmonic oscillators with frequencies as indicated by eq. (3.80) and with masses $1/\delta$. Of course, the diagonalization process can also be performed directly for

[28] The lattice sites are designated with $\vec{n} = n_i\,\hat{x}^i$, where $\hat{x}^i$ are unit normals along the spatial axes.

the continuum Hamiltonian and in the infinite volume limit,[29] in which case one obtains the eigenfrequencies $\omega_{\vec{k}} = \sqrt{\vec{k}^2 + m^2}$ and the sum over the (dimensionless) k_i is replaced by the (dimensionful) momentum integral $V_{d-1} \int \frac{d^{d-1}k}{(2\pi)^{d-1}}$. Here $V_{d-1} = L^{d-1}$ was introduced as an IR regulator for the spatial volume of the system.

It is natural to interpret the reference state as the ground state of an ultralocal Hamiltonian of the form

$$H = \frac{1}{2} \int d^{d-1}x \left[\pi(x)^2 + \mu^2 \, \phi(x)^2\right] \, . \tag{3.82}$$

That is, we have dropped the usual term with spatial derivatives here and so in the ground state, the field is not correlated at different spatial points. On the lattice, this Hamiltonian (3.82) becomes

$$H = \frac{1}{2M} \sum_{\vec{k}} \left(|p_{\vec{k}}|^2 + M^2\mu^2 \, |x_{\vec{k}}|^2\right) \, . \tag{3.83}$$

Finally, recall that we have implicitly set the mass parameter M to one in all our previous expressions, *e.g.,* in eqs. (2.10) and (2.14). It is easy to restore the dependence on the mass by merely multiplying the frequencies by M. This does not influence the various expressions for the complexity since those were given in terms of ratios of frequencies.

3.4.3 Purification Complexity in the Diagonal Basis

As we noted above, the Hamiltonian (3.81) consists of a sum of decoupled harmonic oscillators. As a consequence, the corresponding thermal density matrix for the QFT factorizes into a product of thermal density matrices, one for each mode. In other words, one can find the simple mixed state

$$\hat{\rho}_{\rm th}(\beta) = \bigotimes_{\vec{k}} \, \hat{\upsilon}_{\rm th}(\beta, \omega_{\vec{k}}) \, , \tag{3.84}$$

[29] Recall that there are two independent limits here. The continuum limit refers to taking the lattice spacing δ small compared to the other physical parameters in the problem, *e.g.,* $\delta m \to 0$ and $\delta/L \to 0$. In that case, the sum over lattice points becomes an integral over positions on a square torus, given the boundary conditions under eq. (3.79). The infinite volume takes the limit $L = N\delta \to \infty$ while holding δ fixed. Hence in this limit, L is large compared to the other dimensionful parameters, *e.g.,* $mL \to \infty$ and $L/\delta \to \infty$. Recall that the difference between adjacent values of the dimensionful momenta in eq. (3.80) is $\Delta k = \frac{2\pi}{N\delta} = \frac{2\pi}{L}$, and hence the momentum sums are replaced with integrals in the infinite volume limit. The results of this section will all involve both the continuum and infinite volume limits, while those of section 3.5 are given on the circle (*i.e.,* $d = 2$) with finite L.

where $\hat{v}_{\rm th}$ denotes the thermal density matrix of a single oscillator with frequency $\omega_{\vec{k}}$ and inverse temperature β, as defined in eq. (3.15). In proceeding with our evaluation of the purification complexity, we will focus here on the diagonal basis and save a discussion of the physical-basis complexity for section 3.4.4. Given a mixed state with a product structure as in eq. (3.84), we recall from section 3.3 that we expect the optimal purification will be both an essential purification and a mode-by-mode purification.[30] Hence we expect that the final result for the purification complexity eq. (3.84) is simply obtained by summing the complexities for the individual modes,

$$\mathcal{C}^{\rm diag,tot}_{\rm 1,th}(\beta,\mu) = \sum_{\vec{k}} \mathcal{C}^{\rm diag}_{\rm 1,th}(\beta,\omega_{\vec{k}},\mu)\,, \tag{3.85}$$

where $\mathcal{C}^{\rm diag}_{\rm 1,th}(\beta,\omega_{\vec{k}},\mu)$ is given in eq. (3.75). Alternatively, in the continuum formulation, we have

$$\mathcal{C}^{\rm diag,tot}_{\rm 1,th}(\beta,\mu) = V_{d-1}\int_{|\vec{k}|<\Lambda}\frac{d^{d-1}k}{(2\pi)^{d-1}}\,\mathcal{C}^{\rm diag}_{\rm 1,th}(\beta,\omega_{\vec{k}},\mu)\,, \tag{3.86}$$

where the momentum cutoff Λ was introduced to regulate the system in the UV.[31]

To proceed, we define two critical frequencies with

$$\omega_{c,1}: \quad \beta\mu = \beta\omega_{c,1}\coth\left(\frac{\beta\omega_{c,1}}{4}\right), \qquad \omega_{c,2}: \quad \beta\mu = \beta\omega_{c,2}\tanh\left(\frac{\beta\omega_{c,2}}{4}\right). \tag{3.87}$$

These correspond to the frequencies where there is a transition between the three different regimes in eq. (3.75) — see the blue and red points indicated in figure 3.6. The critical frequencies are functions of β and μ, and of course, they can be converted to a corresponding momentum with $k^2_{c,1} = \omega^2_{c,1} - m^2$ and $k^2_{c,2} = \omega^2_{c,1} - m^2$. Now we will evaluate eq. (3.86) for the three cases distinguished by the relation between the critical frequencies and the cutoff frequency $\omega_\Lambda \equiv \sqrt{\Lambda^2 + m^2}$:

1. $\omega_\Lambda < \omega_{c,1}$:

$$\mathcal{C}^{\rm diag,tot}_{\rm 1,th}(\beta,\mu) = \frac{\Omega_{d-2}V_{d-1}}{2}\int_0^\Lambda \frac{k^{d-2}\,dk}{(2\pi)^{d-1}}\left[\ln\frac{\mu}{\omega_{\vec{k}}} + \ln\left(\frac{\mu\,\coth(\beta\omega_{\vec{k}}/2) - \omega_{\vec{k}}}{\mu - \omega_{\vec{k}}\,\coth(\beta\omega_{\vec{k}}/2)}\right)\right] \tag{3.88}$$

[30] To connect directly to the discussion in section 3.3, we can write the thermal density matrix in the form given in eq. (3.63) using the expressions in eq. (3.17) with $r = 0$. In this form, we would find that A and B are commuting matrices with $A = \mathrm{diag}(\omega_{\vec{k}}\coth\beta\omega_{\vec{k}})$ and $B = \mathrm{diag}(\omega_{\vec{k}}\,\mathrm{csch}\beta\omega_{\vec{k}})$.

[31] This regulator is different than the lattice regularization introduced above in that the momentum integration bound is a sphere, while the edge of the momentum integration of the lattice regularization is a cube given by the edges of the first Brillouin zone. The continuum limit corresponds to Λ being much greater than any dimensionful parameter in the problem, *e.g.*, $\beta\Lambda \to \infty$.

2. $\omega_{c,1} < \omega_\Lambda < \omega_{c,2}$:

$$\begin{aligned}\mathcal{C}_{1,\text{th}}^{\text{diag,tot}}(\beta,\mu) =& \frac{\Omega_{d-2}V_{d-1}}{2}\int_0^{k_{c,1}} \frac{k^{d-2}\,dk}{(2\pi)^{d-1}}\left[\ln\frac{\mu}{\omega_{\vec{k}}} + \ln\left(\frac{\mu\,\coth(\beta\omega_{\vec{k}}/2)-\omega_{\vec{k}}}{\mu-\omega_{\vec{k}}\,\coth(\beta\omega_{\vec{k}}/2)}\right)\right] \\ &+ \Omega_{d-2}V_{d-1}\int_{k_{c,1}}^{\Lambda}\frac{k^{d-2}dk}{(2\pi)^{d-1}}\,\ln\coth\left(\frac{\beta\omega_{\vec{k}}}{4}\right)\end{aligned} \tag{3.89}$$

3. $\omega_{c,2} < \omega_\Lambda$:

$$\begin{aligned}\mathcal{C}_{1,\text{th}}^{\text{diag,tot}}(\beta,\mu) =& \frac{\Omega_{d-2}V_{d-1}}{2}\int_0^{k_{c,1}} \frac{k^{d-2}\,dk}{(2\pi)^{d-1}}\left[\ln\frac{\mu}{\omega_{\vec{k}}} + \ln\left(\frac{\mu\,\coth(\beta\omega_{\vec{k}}/2)-\omega_{\vec{k}}}{\mu-\omega_{\vec{k}}\,\coth(\beta\omega_{\vec{k}}/2)}\right)\right] \\ &+ \Omega_{d-2}V_{d-1}\int_{k_{c,1}}^{k_{c,2}}\frac{k^{d-2}dk}{(2\pi)^{d-1}}\,\ln\coth\left(\frac{\beta\omega_{\vec{k}}}{4}\right) \\ &+ \frac{\Omega_{d-2}V_{d-1}}{2}\int_{k_{c,2}}^{\Lambda}\frac{k^{d-2}dk}{(2\pi)^{d-1}}\left[\ln\frac{\omega_{\vec{k}}}{\mu} + \ln\left(\frac{\omega_{\vec{k}}\,\coth(\beta\omega_{\vec{k}}/2)-\mu}{\omega_k-\mu\,\coth(\beta\omega_{\vec{k}}/2)}\right)\right],\end{aligned} \tag{3.90}$$

where $\Omega_{d-2} \equiv 2\pi^{\frac{d-1}{2}}/\Gamma(\frac{d-1}{2})$ is the volume of a unit $(d-2)$-sphere.

These results can be simplified in certain limits. In particular, here we will focus on the case of a massless scalar, *i.e.*, $m = 0$, in which case, the critical frequencies and momenta are equal to one another, *i.e.*, $k_{c,1} = \omega_{c,1}$ and $k_{c,2} = \omega_{c,2}$. We also focus on the case where the reference frequency is much larger than the temperature, *i.e.*, $\beta\mu \gg 1$. Working in this regime, eq. (3.87) can be solved for the critical momenta in a perturbative expansion yielding

$$k_{c,1} = \mu\left(1 - 2e^{-\frac{\beta\mu}{2}} + \cdots\right), \qquad k_{c,2} = \mu\left(1 + 2e^{-\frac{\beta\mu}{2}} + \cdots\right). \tag{3.91}$$

Hence we see that only the first case is relevant when $\mu \gtrsim \Lambda$ and that the third case becomes relevant as well when $\mu \lesssim \Lambda$. Further, since $k_{c,2} - k_{c,1} = 4\mu e^{-\frac{\beta\mu}{2}} + \cdots$, we see that the range of the integration in the second lines of eqs. (3.89) and (3.90) is extremely small and the corresponding contributions are exponentially suppressed for $\beta\mu \gg 1$. Therefore, it is reasonable to ignore the contribution of these integrals to the complexity in the following.

Let us also comment on the behaviour of the various integrals near their limits of integration. First, near $k = 0$, the integrands have at worst a logarithmic divergence in $d = 2$, while this is suppressed by the factor of k^{d-2} in higher dimensions, and so the integrals converge there. Logarithmic divergences also appear at $k_{c,1}$ and $k_{c,2}$, *i.e.*, $\ln(k_{c,1} - k)$ and $\ln(k - k_{c,2})$, and so the integrals are well behaved there. This leaves us with a UV divergence due to the terms proportional to $|\ln\mu/\omega_{\vec{k}}|$. In fact, this contribution

is identical to that for the vacuum state of the free scalar Hamiltonian (3.78), *e.g.,* see [62], and hence the UV divergence in the complexity is identical to that in the complexity of the vacuum state.

We note that the latter result is different from what happens for the TFD state for the same Hamiltonian (3.78), where the UV divergence is precisely double that of the vacuum, *e.g.,* see [68]. This doubling is natural if we think of the TFD state as an entangled state of two copies of the underlying QFT. In this case, the circuit constructing the state is introducing entanglement at short distance (*i.e.,* UV) scales in both copies of the QFT, which produces the UV divergences in the complexity. For the thermal mixed state, this short distance entanglement must be introduced for the physical degrees of freedom, but there is no need to do the same for the auxiliary degrees of freedom. Hence it is natural that the UV divergence in the purification complexity of the thermal state matches that in the complexity of the vacuum state. We return to comment on this point and explicitly evaluate eqs. (3.88)-(3.90) in section 3.4.5.

To close here, we note that the final result for the purification complexity (with $m = 0$) can be shown to be proportional to $V_{d-1}\, T^{d-1}$, or equivalently to the thermal entropy, where the proportionality factor is a function of $\beta\Lambda$ and $\beta\mu$. For later convenience, let us quote the result for the entropy of the thermal state for the massless theory,

$$S\left(\hat{\rho}_{\rm th}\right)\big|_{m=0} = \frac{\Omega_{d-2}}{(2\pi)^{d-1}}\,\frac{\zeta(d)\Gamma(d+1)}{d-1}\,V_{d-1}\,T^{d-1}\,. \tag{3.92}$$

We recall that ref. [68] showed that the complexity of formation for the TFD state is also proportional to the entropy when $m = 0$.

3.4.4 Purification Complexity in the Physical Basis

Recall from sections 3.2.3 and 3.2.4 that the complexity typically shows different properties in the diagonal and physical bases. Hence we investigate the purification complexity for the thermal mixed state in the physical basis in this section. However, for the free scalar field theory where the density matrix takes the simple product form shown in eq. (3.84), we still expect that in the physical basis, the optimal purification will be an essential purification and also a mode-by-mode purification. So the final result for the purification complexity is again obtained by summing the complexities for the individual modes, *i.e.,*

$$\mathcal{C}^{\rm phys,tot}_{1,\rm th}(\beta,\mu) = \sum_{\vec{k}} \mathcal{C}^{\rm phys}_{1,\rm th}(\beta,\omega_{\vec{k}},\mu)\,, \tag{3.93}$$

where $\mathcal{C}^{\text{phys}}_{1,\text{th}}(\beta,\omega_{\vec{k}},\mu)$ is the purification complexity of the one-mode thermal density matrix, *i.e.,* of eq. (3.13) with $r=0$. Alternatively, in the continuum formulation, we have

$$\mathcal{C}^{\text{phys,tot}}_{1,\text{th}}(\beta,\mu) = V_{d-1}\int_{|\vec{k}|<\Lambda}\frac{d^{d-1}k}{(2\pi)^{d-1}}\,\mathcal{C}^{\text{phys}}_{1,\text{th}}(\beta,\omega_{\vec{k}},\mu)\,, \tag{3.94}$$

where the momentum cutoff Λ regulates the UV portion of the integral.

Let us begin by examining $\mathcal{C}^{\text{phys}}_{1,\text{th}}(\beta,\omega,\mu)$, which is simply determined by setting $r=0$ or $\bar{r}=\frac{1}{2}\ln(\omega/\mu)$ in the results of section 3.2.4.[32] As shown in that section, we cannot find the full analytical results for the purification complexity in the physical basis. However, we can consider certain limits where the results are simplified. In particular, we now investigate the limit of small α, which corresponds either to a low-temperature limit or a high-frequency limit, *i.e.,* $\beta\omega\gg 1$. In this limit, eq. (3.20) yields $\alpha\simeq e^{-\beta\omega/2}\ll 1$. Further, for small α, the diagonal and physical bases are very close, *i.e.,* the orthogonal transformation in eq. (3.40) is close to the identity. The latter follows from evaluating the expressions in eq. (3.41) with $\alpha\to 0$ and assuming $\sinh(\bar{r}-\bar{s})=-\sinh s<0$, which yields[33]

$$\theta\simeq\alpha/\sinh s+\mathcal{O}(\alpha^3)\,. \tag{3.95}$$

Now since we want to expand our expressions for small α, it is easiest to use s as the optimization parameter in evaluating the purification complexity, in analogy to eq. (5.78).[34]

In the physical basis, the single mode purification complexity is given by minimizing eq. (3.44). Hence we must evaluate the expressions there in terms of s and in a small α expansion using eqs. (3.46) and (3.95) as well as $r=0$. We find[35]

$$\frac{1}{2}\ln\frac{\omega_+\omega_-}{\mu^2}=2\bar{r}+s\,,\qquad \frac{1}{2}\ln\frac{\omega_+}{\omega_-}=s+\mathcal{O}(\alpha^2)\,. \tag{3.96}$$

Now we see that eq. (3.44) reduces to

$$\mathcal{C}^{\text{phys}}_{1,\text{th}}\left(|\psi\rangle_{12}\right)=|\bar{r}|+|\bar{r}+s|+\frac{2\,\alpha\,s}{\sinh s}+\mathcal{O}(\alpha^2)\,. \tag{3.97}$$

At the leading order in α, this is minimized when the second absolute value vanishes, which fixes $s=-\bar{r}=\frac{1}{2}\ln(\mu/\omega)$ (which implies $\bar{s}=0$). Further, we note that consistency with

[32] We have dropped the subscript $\vec{k}$ on the frequency here to reduce the clutter in our formulae for the time being. Further recall that the result for $\bar{r}$ follows from eq. (3.31).

[33] That is, we are assuming that the auxiliary squeezing parameter is positive, *i.e.,* $s>0$. Later, we see that this corresponds to $\mu>\omega$. Footnote 36 comments on the regime $s<0$, which corresponds to $\mu<\omega$.

[34] This contrasts with section 3.2.4, where we optimized with respect to θ as in eq. (3.48).

[35] Note that the first equation is exact because $\bar{r}+\bar{s}=2\bar{r}+s$ with $r=0$.

our assumption that $s > 0$ requires that we are in the regime $\mu > \omega$.[36] Hence in the region $\beta\omega \gg 1$, we find that the purification complexity becomes[37]

$$\mathcal{C}^{\text{phys}}_{1,\text{th}}(\hat{v}_{\text{th}}) = \frac{1}{2}\left|\ln\frac{\mu}{\omega}\right| + \frac{2\alpha\,\ln\frac{\mu}{\omega}}{\sqrt{\mu/\omega}-\sqrt{\omega/\mu}} + \mathcal{O}(\alpha^2)\,. \tag{3.99}$$

This result is very close to the complexity for the (pure) vacuum state of a single harmonic oscillator at frequency ω, as expected. Now let us turn to the purification complexity of the mixed thermal state for the free scalar field theory. As noted above, we expect that it takes the simple form given in eq. (3.93) or (3.94) given the simple product structure of the thermal state (3.84). At this point, let us recall the definitions of our parameters for the thermal state

$$\alpha = \frac{1}{2}\,\ln\left(\coth\frac{\beta\omega_{\vec{k}}}{4}\right)\,, \qquad \bar{r} = \frac{1}{2}\,\ln\frac{\omega_{\vec{k}}}{\mu}\,. \tag{3.100}$$

As the combination $\beta\omega_{\vec{k}}$ grows, the value of α rapidly decreases, *e.g.*, $\frac{1}{2}\ln\left(\coth\left(10^{-2}\right)\right) \approx 2.3$, $\frac{1}{2}\ln\left(\coth(10^2)\right) \approx 10^{-87}$. Now the momentum integral in eq. (3.94) is dominated by the phase space near the UV cutoff $|\vec{k}| \sim \Lambda$ and hence with $\beta\Lambda \ll 1$, α will be very small over a majority of this integration. Further, if the reference frequency μ is large enough, *e.g.*, near the cutoff Λ, we will have $-\bar{r}$ very large over the complementary part of the momentum integral. Hence, we can expect in a physically interesting setting that, over the entire integral, either α is small or $|\bar{r}|$ is large, and this is precisely the regime where the single-mode purification complexity in the physical basis is given by the simplified expression in eq. (3.54). Hence we can simplify eq. (3.94) to the following

$$\mathcal{C}^{\text{phys,tot}}_{1,\text{th}}(\beta,\mu) = \Omega_{d-2}V_{d-1}\int_0^\Lambda \frac{k^{d-2}dk}{(2\pi)^{d-1}}\,(\sin 2\theta_c + \cos 2\theta_c)\,\sinh^{-1}\left(\frac{\sinh 2\alpha}{\sin 2\theta_c}\right)\,, \tag{3.101}$$

[36] Let us add that if we assume $s < 0$, we are lead to the following approximation

$$\begin{gathered}\theta = \frac{\pi}{2} - \frac{\alpha}{\sinh|s|} + \mathcal{O}(\alpha^3)\,, \qquad \text{with} \\ \frac{1}{2}\ln\frac{\omega_+\omega_-}{\mu^2} = 2\bar{r} + s\,, \qquad \frac{1}{2}\ln\frac{\omega_+}{\omega_-} = |s| + \mathcal{O}(\alpha^2)\,.\end{gathered} \tag{3.98}$$

The expression for the complexity in eq. (3.97) remains unchanged, and it is again minimized by setting the second term to zero. Hence, we find $s = -\bar{r} = \frac{1}{2}\ln(\mu/\omega)$ as before, but consistency with $s < 0$ now requires that we are in the regime $\mu < \omega$. The final expression for the purification complexity (3.99) also remains unchanged in this regime.

[37] Note that the $\omega \to \mu$ limit of this expression agrees with the complexity of the thermofield double $\mathcal{C}^{\text{phys}}_{1,th} \to 2\alpha$, as expected from the results of section 3.2: namely, that the optimal purification for states with $\omega = \mu$ is the thermofield double.

where both θ_c and α are implicitly functions of k — see eqs. (3.53) and (3.100). However, it is still hard to explicitly do the remaining integral without any further assumptions. If we assume the small α limit is valid over most of the momentum integral, we can use eq. (3.99) to simplify the purification complexity to

$$\mathcal{C}^{\text{phys,tot}}_{1,\text{th}}(\beta,\mu) \simeq \Omega_{d-2}V_{d-1}\int_0^\Lambda \frac{k^{d-2}dk}{(2\pi)^{d-1}}\left[\frac{1}{2}\left|\ln\frac{\mu}{\omega_k}\right| + \frac{\ln\left(\coth\frac{\beta\omega_k}{4}\right)\,\ln\frac{\mu}{\omega_k}}{\sqrt{\mu/\omega_k}-\sqrt{\omega_k/\mu}}\right], \tag{3.102}$$

where we use the notation $\omega_k = \sqrt{k^2+m^2}$ and where we have only dropped the higher order terms in the α expansion. Note that this approximation of the integrand is valid in the UV portion of the integration. In this case, the first term simply reproduces the vacuum complexity (*i.e.,* the zero temperature complexity) and hence the purification complexity has precisely the same UV divergences as the vacuum complexity (for one copy of the underlying QFT). Of course, this feature is identical to what we found for the diagonal basis. Further, this approximation is valid more generally in the full range of integration in the situation where $\beta m \gg 1$. In this case, the second term gives the leading finite temperature corrections to the vacuum complexity, which are suppressed by factors of $e^{-\beta m/2}$.

3.4.5 Mutual Complexity of TFD States

In this section, we compare the purification complexity of a thermal mixed state with the complexity of the corresponding TFD state, using a quantity known as the mutual complexity. We follow the nomenclature introduced by [189] in considering the holographic complexity of subregions.

Consider a pure state $|\Psi_{\mathcal{AB}}\rangle$ on a collection of degrees of freedom comprised of two subsystems, $\mathcal{A}$ and $\mathcal{B}$. There are two mixed states that are naturally constructed here, namely, the reduced density matrices,

$$\hat{\rho}_{\mathcal{A}} = \text{Tr}_{\mathcal{B}}(|\Psi_{\mathcal{AB}}\rangle\langle\Psi_{\mathcal{AB}}|)\,, \qquad \hat{\rho}_{\mathcal{B}} = \text{Tr}_{\mathcal{A}}(|\Psi_{\mathcal{AB}}\rangle\langle\Psi_{\mathcal{AB}}|)\,. \tag{3.103}$$

It is clear that each of the purification complexities for $\hat{\rho}_{\mathcal{A}}$ and $\hat{\rho}_{\mathcal{B}}$ is less than the complexity of the original pure state. That is, since $|\Psi_{\mathcal{AB}}\rangle$ provides one particular purification of $\hat{\rho}_{\mathcal{A}}$, it is unlikely to be the optimal purification and so we have the inequality

$$\mathcal{C}(\hat{\rho}_{\mathcal{A}}) = \min \mathcal{C}(|\Psi_{\mathcal{AA}^c}\rangle) \leq \mathcal{C}(|\Psi_{\mathcal{AB}}\rangle)\,, \tag{3.104}$$

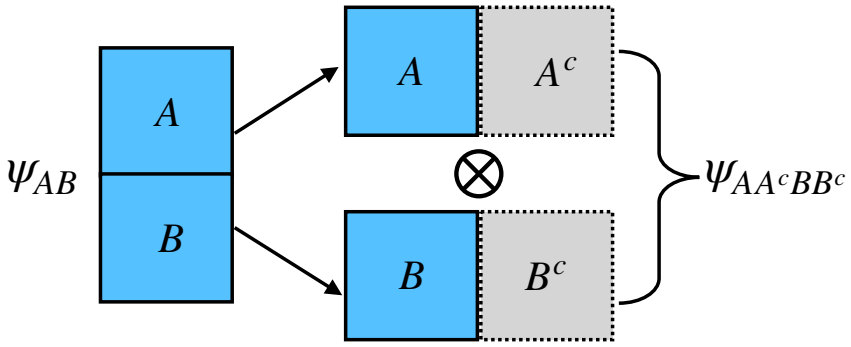

Figure 3.7: Illustration of the optimal purification of two mixed states in two complementary subsystems $\mathcal{A}$ and $\mathcal{B}$ of an original pure state $|\Psi\rangle_{\mathcal{AB}}$. The state in the subsystem $\mathcal{A}$ is purified by a state $|\Psi\rangle_{\mathcal{AA}^c}$ and the one in the subsystem $\mathcal{B}$ is purified by $|\Psi\rangle_{\mathcal{BB}^c}$. Even though the direct product of the purifying systems $|\Psi\rangle_{\mathcal{AA}^c} \otimes |\Psi\rangle_{\mathcal{BB}^c}$ generally has a larger number of degrees of freedom than the original state $|\Psi\rangle_{\mathcal{AB}}$, the mutual complexity eq. (3.105) can have either sign.

as well as the analogous inequality for $\hat{\rho}_{\mathcal{B}}$. Implicitly, we chose the same cost function and basis to define the circuit complexity of the pure state $|\Psi_{\mathcal{AB}}\rangle$.[38]

As illustrated in figure 3.7, it is also obvious that in building the pure state, *e.g.*, $|\Psi_{\mathcal{AA}^c}\rangle$, from the corresponding unentangled reference state, the circuit should only work hard enough to establish the correlations found in $\hat{\rho}_{\mathcal{A}}$ amongst the physical degrees of freedom. However, it need not establish an analogous set of correlations (in particular, analogous UV correlations) amongst the ancillary degrees of freedom. Similarly, the correlations between $\mathcal{A}$ and $\mathcal{A}^c$ in $|\Psi_{\mathcal{AA}^c}\rangle$ need not precisely mirror those between $\mathcal{A}$ and $\mathcal{B}$ in $|\Psi_{\mathcal{AB}}\rangle$. As discussed in the introduction, the **mutual complexity** is constructed to quantify the additional correlations in the original pure state with the following difference of complexities,

$$\Delta\mathcal{C} = \mathcal{C}(\hat{\rho}_{\mathcal{A}}) + \mathcal{C}(\hat{\rho}_{\mathcal{B}}) - \mathcal{C}(|\Psi_{\mathcal{AB}}\rangle) \ . \tag{3.105}$$

This quantity was introduced in [189], where it was studied for subregions in the context of holographic complexity. The structure in eq. (3.105) was chosen to parallel that of the mutual information, which can be defined by a similar difference of entanglement entropies. However, whereas the mutual information is always positive (or zero), we cannot prove that

[38] Note the choice of basis is important in establishing the inequality for the F_1 cost function, which we are implicitly using here. For example, in eq. (3.104), we are *not* claiming that $\mathcal{C}_1^{\text{phys}}(\hat{\rho}_{\mathcal{A}}) \leq \mathcal{C}_1^{\text{diag}}(|\Psi_{\mathcal{AB}}\rangle)$, even though $\mathcal{C}_1^{\text{diag}}(|\Psi_{\mathcal{AB}}\rangle)$ may seem the natural definition for the complexity of the pure state. Of course, the basis choice does not play a role for covariant cost functions such as F_2.

$\Delta\mathcal{C}$ is always positive or negative from the basic definitions of complexity and purification complexity. Hence the sign of the mutual complexity is nontrivial.

In the present case, the pure state of interest will be a TFD state, *i.e.,* $|\Psi_{\mathcal{AB}}\rangle = |\text{TFD}\rangle$, which can be regarded as an entangled state of two copies, *i.e.,* the left and right copies, of the underlying QFT. The corresponding mixed states will both be the thermal state (3.84), which is produced by tracing over either the left or right degrees of freedom, *i.e.,* $\hat{\rho}_{\mathcal{A}} = \hat{\rho}_{\mathcal{B}} = \hat{\rho}_{\text{th}}(\beta)$. That is, we will consider

$$\Delta\mathcal{C} = 2\,\mathcal{C}(\hat{\rho}_{\text{th}}(\beta)) - \mathcal{C}(|\text{TFD}\rangle) \ . \tag{3.106}$$

Again, while the TFD state provides one purification of the thermal mixed state, it will not generally be the optimal purification.[39]

Another noteworthy feature of the mutual complexity (3.106) is that we expect it to be UV finite for the TFD state. This expectation arises from our previous observation that the UV divergences in the purification complexity of $\hat{\rho}_{\text{th}}(\beta)$ precisely matched those found in the vacuum state of one copy of the QFT, while the TFD state doubles the prefactors in those UV divergences. Hence we will see that these divergences cancel in our calculations below.

We refer to complexity models with the property that the mutual complexity is always positive as satisfying **subadditivity** since in these cases the complexity of the combined state $\Psi_{\mathcal{AB}}$ is less than the sum of the complexities of the two reduced density matrices, $\hat{\rho}_{\mathcal{A}}$, and $\hat{\rho}_{\mathcal{B}}$ [171] — see also the discussion in [190]. In the same way, we refer to complexity models as satisfying **superadditivity** if $\Delta\mathcal{C}$ is always negative. Further, in Chapter 4, we will also see that the mutual complexity plays a role in distinguishing different holographic conjectures for the complexity of mixed states.

3.4.5.1 Mutual complexity in the diagonal basis

Let us begin with the TFD state entangling two modes. Eq. (3.18) shows that $|\text{TFD}\rangle_{12}$ is the two-mode squeezed state with $r = s = 0$, and from eq. (3.30), we can see that its

[39] Let us point out that by examining figure 3.6, we find that there exist situations for which the TFD state is the optimal purification, but this requires $\beta\Lambda$ to be an order one number. However, we regard such a situation where the temperature is of the same order as the UV cutoff as unphysical.

circuit complexity with the F_1 cost function in the diagonal basis reads [68]

$$\begin{aligned}\mathcal{C}_1^{\text{diag}}\left(|\text{TFD}\rangle_{12}\right) &= \left|\frac{1}{2}\ln\frac{\omega}{\mu}+\alpha\right| + \left|\frac{1}{2}\ln\frac{\omega}{\mu}-\alpha\right| , \\ &= \begin{cases} \ln\frac{\mu}{\omega} & \text{for} \quad \coth(\frac{\beta\omega}{4}) \leq \frac{\mu}{\omega} , \\ \ln\coth\left(\frac{\beta\omega}{4}\right) & \text{for} \quad \tanh(\frac{\beta\omega}{4}) \leq \frac{\mu}{\omega} \leq \coth(\frac{\beta\omega}{4}) , \\ \ln\frac{\omega}{\mu} & \text{for} \quad \frac{\mu}{\omega} \leq \tanh(\frac{\beta\omega}{4}) . \end{cases}\end{aligned} \tag{3.107}$$

Here we have expressed the three parameter regimes in the same way as they appears in eq. (3.75) for the purification complexity of the thermal mixed state. Obviously, the results in the intermediate regime are the same in both cases because the optimal purification for the thermal state in this region coincides with the TFD state, as shown in section 3.4.1. As noted in eq. (3.106), the two subsystems are described by the same mixed state, *i.e.*, $\hat{\rho}_{1,2} = \hat{v}_{th}$, and hence the mutual complexity of this TFD state in the diagonal basis becomes

$$\Delta\mathcal{C}_1^{\text{diag}}(|\text{TFD}\rangle_{12}) = 2\,\mathcal{C}_1^{\text{diag}}(\hat{v}_{\text{th}}) - \mathcal{C}_1^{\text{diag}}(|\text{TFD}\rangle_{12}) . \tag{3.108}$$

Combining eqs. (3.75) and (3.107), we find

$$\Delta\mathcal{C}_1^{\text{diag}}(|\text{TFD}\rangle_{12}) = \begin{cases} \ln\left(\frac{\mu\coth(\beta\omega/2)-\omega}{\mu-\omega\coth(\beta\omega/2)}\right) & \text{for} \quad \omega\coth(\frac{\beta\omega}{4}) \leq \mu , \\ \ln\coth(\beta\omega/4) & \text{for} \quad \omega\tanh(\frac{\beta\omega}{4}) \leq \mu \leq \omega\coth(\frac{\beta\omega}{4}) , \\ \ln\left(\frac{\omega\coth(\beta\omega/2)-\mu}{\omega-\mu\coth(\beta\omega/2)}\right) & \text{for} \quad \mu \leq \omega\tanh(\frac{\beta\omega}{4}) . \end{cases} \tag{3.109}$$

It is straightforward to show that this result for $\Delta\mathcal{C}_1^{\text{diag}}(|\text{TFD}\rangle_{12})$ is positive and decays exponentially with increasing frequency (yielding zero in the limit $\beta\omega \to \infty$). Using the nomenclature introduced above, we have found that in the diagonal basis, the $\mathcal{C}_1$ complexity is subadditive for these thermal states. In order to be able to compare with the equivalent results in the physical basis which will appear in section 3.4.5.2, we plot $\Delta\mathcal{C}_1^{\text{diag}}(|\text{TFD}\rangle_{12})$ in figure 3.8.

Now let us evaluate the mutual complexity (3.106) of the TFD state in the free scalar theory. Because of the product form of the TFD state and the corresponding thermal density matrices (3.84), the mutual complexity simply requires summing eq. (3.109) over

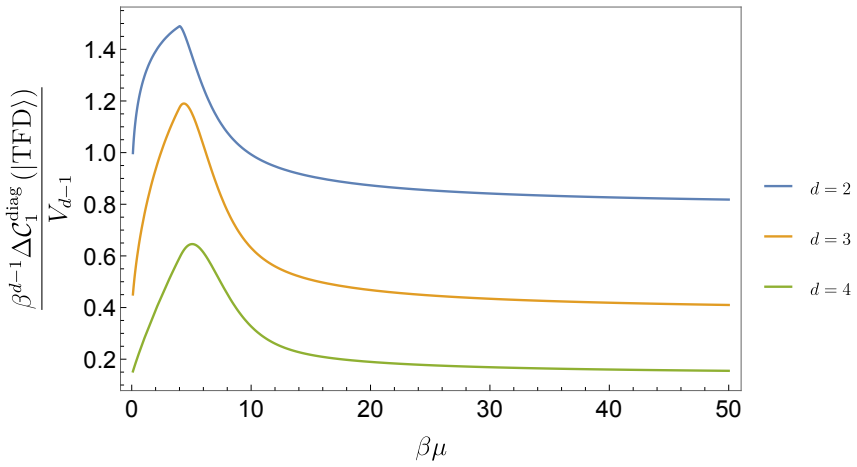

Figure 3.8: The integrated mutual complexity in the diagonal basis, *i.e.*, $\Delta\mathcal{C}_1^{\rm diag}(|{\rm TFD}\rangle)$ defined in eq. (3.111) for a massless field theory in different dimensions.

all of the modes, *i.e.*,

$$\Delta\mathcal{C}_1^{\rm diag}(|{\rm TFD}\rangle;\beta,\mu)=\Omega_{d-2}V_{d-1}\int_{|\vec{k}|<\Lambda}\frac{k^{d-2}dk}{(2\pi)^{d-1}}\,\Delta\mathcal{C}_1^{\rm diag}\left(|{\rm TFD}\rangle_{12};\beta,\omega_{\vec{k}},\mu\right)\,. \tag{3.110}$$

Using our previous results, it is easy to show that there are three possible expressions depending on the relation between the cutoff frequency ω_Λ and the critical frequencies, $\omega_{c,1}$ and $\omega_{c,2}$, defined in eq. (3.87). We find

$$\begin{aligned}\Delta\mathcal{C}_1^{\rm diag}(|{\rm TFD}\rangle)(\beta,\mu)&=\Omega_{d-2}V_{d-1}\int_0^\Lambda\frac{k^{d-2}dk}{(2\pi)^{d-1}}\,\ln\coth\left(\frac{\beta\omega_{\vec{k}}}{2}\right)\\&+\begin{cases}\Omega_{d-2}V_{d-1}\int_0^\Lambda\frac{k^{d-2}dk}{(2\pi)^{d-1}}\,I_1 & \text{for}\quad \omega_\Lambda\le\omega_{c,1}\,,\\ \Omega_{d-2}V_{d-1}\left(\int_0^{k_{c,1}}\frac{k^{d-2}dk}{(2\pi)^{d-1}}\,I_1+\int_{k_{c,1}}^\Lambda\frac{k^{d-2}dk}{(2\pi)^{d-1}}\,I_2\right) & \text{for}\quad \omega_{c,1}\le\omega_\Lambda\le\omega_{c,2}\,,\\ \Omega_{d-2}V_{d-1}\left(\int_0^{k_{c,1}}\frac{k^{d-2}dk}{(2\pi)^{d-1}}\,I_1+\int_{k_{c,1}}^{k_{c,2}}\frac{k^{d-2}dk}{(2\pi)^{d-1}}\,I_2+\int_{k_{c,2}}^\Lambda\frac{k^{d-2}dk}{(2\pi)^{d-1}}\,I_3\right) & \text{for}\quad \omega_{c,2}\le\omega_\Lambda\,.\end{cases}\end{aligned} \tag{3.111}$$

The first line is a "universal contribution," which is common to all three cases, and the expression on the second line is determined by the relationship between the cut-off and the

critical frequencies, with

$$I_1 = \ln\left(\frac{\mu-\omega_{\vec{k}}\tanh(\beta\omega_{\vec{k}}/2)}{\mu-\omega_{\vec{k}}\coth(\beta\omega_{\vec{k}}/2)}\right), \qquad I_2=\ln\left(\frac{\coth(\beta\omega_{\vec{k}}/4)}{\coth(\beta\omega_{\vec{k}}/2)}\right),$$
$$I_3=\ln\left(\frac{\omega_{\vec{k}}-\mu\tanh(\beta\omega_{\vec{k}}/2)}{\omega_{\vec{k}}-\mu\coth(\beta\omega_{\vec{k}}/2)}\right). \tag{3.112}$$

First, let us observe that as expected the mutual complexity $\Delta_1^{\rm diag}(|\text{TFD}\rangle)$ is finite. In particular, the terms that could potentially produce UV divergences, *i.e.*, $|\ln\frac{\mu}{\omega_{\vec{k}}}|$, and that would appear in the complexity of the TFD state and the thermal state (as well as the vacuum state) separately, have been fully canceled in the mutual complexity.

In order to produce explicit results, let us focus on the massless field theory. For simplicity, we also assume that $\mu \gg \Lambda$ (as well as $\mu\beta \gg 1$), which assures us that we are in the first regime, *i.e.*, $\omega_\Lambda < \omega_{c,1}$, in eq. (3.111). Further, this assumption allows us to use k/μ as an expansion parameter in the second integral below. Now the universal contribution coming from the first line of eq. (3.111) yields[40]

$$\begin{aligned}\Delta\mathcal{C}_1^{\text{diag},(0)}(|\text{TFD}\rangle)\big|_{m=0} &= \Omega_{d-2}V_{d-1}\int_0^\Lambda \frac{k^{d-2}dk}{(2\pi)^{d-1}}\,\ln\coth(\beta k/2)\\ &= \frac{\Omega_{d-2}}{(4\pi)^{d-1}}\,(2^d-1)\zeta(d)\Gamma(d-1)\,V_{d-1}T^{d-1}\\ &= \frac{2^d-1}{2^{d-1}d}\,S\left(\hat\rho_{\rm th}\right)\big|_{m=0},\end{aligned} \tag{3.114}$$

where the expression for the thermal entropy was given in eq. (3.92). Note that because the integral is UV finite, we have taken the upper limit of the integration to infinity. Turning

[40] Certain integrals relevant for the complexity can be evaluated analytically with $m=0$, *e.g.*,

$$\begin{aligned}\int_0^\infty k^n\,\ln\coth(\beta k/2)\,dk &= \frac{(2^{n+2}-1)\Gamma(n+2)\zeta(n+2)}{(n+1)(2\beta)^{n+1}}, \qquad \text{for } n\geq 0,\\ \int_0^\infty \frac{k^n}{\sinh\beta k}\,dk &= \frac{(2^{n+1}-1)\Gamma(n+1)\zeta(n+1)}{2^n\beta^{n+1}}, \qquad \text{for } n\geq 1.\end{aligned} \tag{3.113}$$

to the second contribution, we find[41]

$$\begin{aligned}\Delta\mathcal{C}_1^{\text{diag},(1)}(|\text{TFD}\rangle)\big|_{m=0} &= \Omega_{d-2}V_{d-1}\int_0^\Lambda \frac{k^{d-2}dk}{(2\pi)^{d-1}}\,\ln\left(\frac{\mu-k\,\tanh(\beta k/2)}{\mu-k\,\coth(\beta k/2)}\right)\\ &\simeq \Omega_{d-2}V_{d-1}\int_0^\Lambda \frac{k^{d-2}dk}{(2\pi)^{d-1}}\left[\frac{k}{\mu}\,\frac{2}{\sinh\beta k}+\mathcal{O}\big(k^2/\mu^2\big)\right] \qquad (3.115)\\ &= \Delta\mathcal{C}_1^{\text{diag},(0)}(|\text{TFD}\rangle)\big|_{m=0}\left[2(d-1)\,\frac{T}{\mu}+\mathcal{O}\big(T^2/\mu^2\big)\right].\end{aligned}$$

Hence for the massless theory, the universal contribution (3.114) is proportional to the thermal entropy, while the second integral modifies this result with a series of corrections suppressed by powers of T/μ. Note that both eq. (3.114) and the leading correction in eq. (3.115) are positive, and hence the mutual complexity of the thermofield double state exhibits subadditivity, for the massless scalar in the diagonal basis. Of course, this had to be the case since eq. (3.109) is always positive.

For a small mass, we can also evaluate the integrals for the massive theory to find additional corrections suppressed by powers of m/T. The leading contribution comes from the universal correction, which can be rewritten as

$$\begin{aligned}\Delta\mathcal{C}_1^{\text{diag},(0)}(|\text{TFD}\rangle) &= \Omega_{d-2}V_{d-1}\int\frac{k^{d-2}dk}{(2\pi)^{d-1}}\,\ln\frac{e^{\beta\omega_k}+1}{e^{\beta\omega_k}-1}\,,\\ &= \frac{\Omega_{d-2}}{(2\pi)^{d-1}}\,V_{d-1}T^{d-1}\int_{\beta m}^\infty dx\;x\left(x^2-\beta^2m^2\right)^{\frac{d-3}{2}}\ln\coth(x/2)\,,\end{aligned} \qquad (3.116)$$

where as usual, $\omega_k^2=k^2+m^2$, and in the second line, we defined $x\equiv\beta\omega_k$. For $d=3$, the integral yields a relatively simple analytical answer

$$\begin{aligned}\Delta\mathcal{C}_1^{\text{diag},(0)}(|\text{TFD}\rangle)\big|_{d=3} &= \frac{V_2\,T^2}{2\pi}\Bigg[-\beta^2m^2\left(\frac{1}{3}\,\beta m+i\frac{\pi}{2}\right)\\ &\qquad -\beta m\left[\text{Li}_2\big(e^{\beta m}\big)+\text{Li}_2\big(-e^{-\beta m}\big)+\text{Li}_3\big(e^{\beta m}\big)-\text{Li}_3\big(-e^{-\beta m}\big)\right]\Bigg]\\ &\simeq \frac{V_2\,T^2}{8\pi}\left[7\,\zeta(3)+\frac{m^2}{T^2}\left(2\,\ln\Big(\frac{m}{2T}\Big)-1\right)+\mathcal{O}\left(m^3/T^3\right)\right], \qquad (3.117)\end{aligned}$$

[41] The term we have neglected in the second line, *i.e.*, $\mathcal{O}\big(k^2/\mu^2\big)$, is also proportional to $e^{-k\beta}$ when the momentum is large with respect to the temperature, which makes it convergent.

where Li_n denotes the polylogarithm function. For $d > 3$ (and $m/T \ll 1$ again), one finds

$$\begin{aligned}\Delta\mathcal{C}_1^{\mathrm{diag},(0)}(|\mathrm{TFD}\rangle)\big|_d &\simeq \frac{\Omega_{d-2}\,V_{d-1}T^{d-1}}{(2\pi)^{d-1}}\int_{m\beta}^{\infty}dx\left[x^{d-2}-\frac{d-3}{2}\beta^2m^2\,x^{d-4}\right]\ln\coth(x/2)\\ &\simeq \frac{\Omega_{d-2}\,V_{d-1}T^{d-1}}{(4\pi)^{d-1}}\Bigg[(2^d-1)\zeta(d)\Gamma(d-1)\\ &\qquad -(2^{d-1}-2)\zeta(d-2)\Gamma(d-2)\,\frac{m^2}{T^2}+\mathcal{O}(m^3/T^3)\Bigg]\,.\end{aligned} \tag{3.118}$$

Of course, the leading contribution above (and in eq. (3.117)) matches the universal result for $m = 0$ in eq. (3.114). Note that the m^2/T^2 correction to the integrand in eq. (3.118) vanishes for $d = 3$. Hence in eq. (3.117), the correction at this order comes entirely from the modification to the lower limit of the range of integration. In contrast for $d > 3$, the change in the lower limit of integration yields a higher order correction of order $(\beta m)^{d-1}$, *i.e.,* this contribution is higher order than the $(\beta m)^2$ term retained in eq. (3.118). We also note that for both $d = 3$ and $d > 3$, the leading correction is always negative. However, in this regime with $m/T \ll 1$, the mutual complexity is still dominated by the leading term (3.114), which is positive. Hence the complexity of the TFD state remains subadditive in this limit. Of course, this had to be the case given the positivity of eq. (3.109).

3.4.5.2 Mutual complexity in the physical basis

We now turn to evaluating the mutual complexity of the TFD state in the physical basis. For a single mode, the TFD state (3.18) is obtained from the general purification (3.22) by setting $r = s = 0$. Using eqs. (3.31) and (3.40), we can demonstrate that this corresponds to

$$X_- = 1\,,\quad \theta = \frac{\pi}{4},\quad \omega_\pm = \omega e^{\pm 2\alpha},\quad \frac{1}{2}\ln\frac{\omega_+}{\omega_-} = 2\alpha,\quad H = \frac{1}{2}\begin{pmatrix}\ln\frac{\omega}{\mu} & -2\alpha\\ -2\alpha & \ln\frac{\omega}{\mu}\end{pmatrix}. \tag{3.119}$$

It is then straightforward to show that the complexity of the TFD state (3.18) is given by

$$\mathcal{C}_1^{\mathrm{phys}}\left(|\mathrm{TFD}\rangle_{12}\right) = \left|\ln\frac{\omega}{\mu}\right| + 2\alpha = \begin{cases}\ln\frac{\mu}{\omega} + \ln\coth\left(\frac{\beta\omega}{4}\right), & \omega \le \mu\,,\\ \ln\frac{\omega}{\mu} + \ln\coth\left(\frac{\beta\omega}{4}\right), & \omega \ge \mu\,.\end{cases} \tag{3.120}$$

This result is consistent with the complexity derived in [68] using the F_1 cost function — see eq. (138) in [68] with $C_1^{\mathrm{LR}} = |\ln\lambda| + 2|\alpha|$ and note that the physical basis was denoted as the LR basis there.

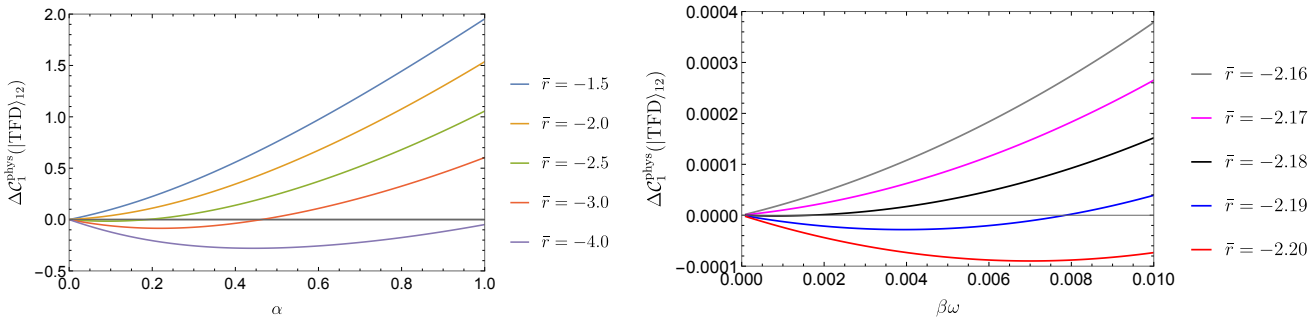

Figure 3.9: The mutual complexity $\Delta\mathcal{C}_1^{\rm phys}\left(|{\rm TFD}\rangle_{12}\right)$ as defined in eq. (3.121) with fixed $\bar{r} = \frac{1}{2}\ln\frac{\omega}{\mu} < 0$ as a function of α. We find that the quantity $\Delta\mathcal{C}_1^{\rm phys}$ can be either positive or negative. The right plot is the region with $\bar{r}$ near the transition point $\bar{r} = -2.177$.

As before, the two reduced density matrices are $\hat{\rho}_{1,2} = \hat{v}_{\rm th}$, and we wish to evaluate the mutual complexity of the TFD state but now in the physical basis:

$$\Delta\mathcal{C}_1^{\rm phys}\left(|{\rm TFD}\rangle_{12}\right) = 2\,\mathcal{C}_1^{\rm phys}\left(\hat{v}_{\rm th}\right) - \mathcal{C}_1^{\rm phys}\left(|{\rm TFD}\rangle_{12}\right) . \tag{3.121}$$

The purification complexity $\mathcal{C}_1^{\rm phys}(\hat{v}_{\rm th})$ is defined using eq. (3.48) and $\mathcal{C}_1^{\rm phys}\left(|{\rm TFD}\rangle_{12}\right)$ is given in eq. (3.120). This expression is evaluated numerically in figure 3.9, and we note that in the physical basis, $\Delta\mathcal{C}_1^{\rm phys}\left(|{\rm TFD}\rangle_{12}\right)$ does not have a definite sign. That is, eq. (3.121) may be positive or negative depending on the parameters, which contrasts with the corresponding expression for the mutual complexity always being positive in the diagonal basis.

One can gain some analytical insight into the above result by focusing on the limit of small α, *i.e.*, large $\beta\omega$. Combining eqs. (3.99) and (3.120), the single-mode mutual complexity (3.121) becomes

$$\begin{aligned}\Delta\mathcal{C}_1^{\rm phys}(|{\rm TFD}\rangle_{12}) &= 2\,\mathcal{C}_1^{\rm phys}(\hat{v}_{\rm th}) - \mathcal{C}_1^{\rm phys}\left(|{\rm TFD}\rangle_{12}\right) \\ &= 2\alpha\left(\frac{2\,\ln\frac{\mu}{\omega}}{\sqrt{\mu/\omega} - \sqrt{\omega/\mu}} - 1\right) + \mathcal{O}(\alpha^2)\,.\end{aligned} \tag{3.122}$$

Comparing to figure 3.9, we see that this leading expression captures the linear behaviour in the vicinity of $\alpha = 0$, and that the sign of the slope determines whether the corresponding mutual complexity will be negative over some range. Further, eq. (3.122) shows that the slope is determined by the ratio μ/ω (or alternatively by $\bar{r} = \frac{1}{2}\ln(\omega/\mu)$). We also observe that this slope (*i.e.*, the function multiplying 2α) is invariant under $\frac{\mu}{\omega} \to \frac{\omega}{\mu}$. The transition between positive and negative values of the slope occurs at

$$2\,|\bar{r}_c| = \left|\ln\frac{\omega_c}{\mu}\right| \simeq 4.35464\cdots . \tag{3.123}$$

That is, $\Delta\mathcal{C}_1^{\text{phys}}(|\text{TFD}\rangle_{12})$ is entirely positive (for all values of α) in the region $0.01285 \lesssim \omega/\mu \lesssim 77.84$, or alternatively $|\bar{r}| \lesssim 2.177$, and it has negative contributions (for small values of α) outside of this range. Of course, these results precisely match those found numerically, as shown in figure 3.9.

Now because of the factorization of the thermal state in free field theory, the corresponding mutual complexity is given by simply summing eq. (3.121) over each of the modes,

$$\Delta\mathcal{C}_1^{\text{phys}}\left(|\text{TFD}\rangle\right) = V_{d-1}\int \frac{d^{d-1}k}{(2\pi)^{d-1}}\left[2\,\mathcal{C}_1^{\text{phys}}(\hat{v}_{\text{th}}) - \mathcal{C}_1^{\text{phys}}(|\text{TFD}\rangle_{12})\right] . \tag{3.124}$$

It is possible to demonstrate that this expression for the mutual complexity in the physical basis is finite by considering the small α limit in eq. (3.122), which demonstrates that the mutual complexity is exponentially suppressed for large momentum, hence resulting in a convergent integral. Although evaluating this expression analytically is a challenge, it is straightforward to evaluate this mutual complexity numerically. Figure 3.10 shows the mutual complexity $\Delta\mathcal{C}_1^{\text{phys}}\left(|\text{TFD}\rangle\right)$ for a massless free scalar in $d = 2$, as an example. Varying the reference frequency from IR scales to UV scales, we see that mutual complexity begins with negative values for $\beta\mu \ll 1$, then rises to positive values at intermediate scales with $\beta\mu \sim 1$, and finally becomes negative again for $\beta\mu \gg 1$. In other words, the mutual complexity $\Delta\mathcal{C}_1^{\text{phys}}(|\text{TFD}\rangle)$ can be **negative** when the reference frequency is very large or extremely small. This again stands in contrast with the diagonal basis, where the corresponding mutual complexity was found to be positive for all values of the reference frequency.

Using a change of variables $\tilde{k} = \beta k$ in the integral in eq. (3.124), it is possible to extract an overall coefficient proportional to the entropy (3.92) of the massless theory, *i.e.*, $V_{d-1}T^{d-1} \sim S_{\text{th}}$. The remaining integral is a function of the dimensionless parameter $\beta\mu$. Finiteness of the result in the limit $\beta\mu \gg 1$ requires that this function will approach a constant.[42] Hence, the resulting mutual complexity is proportional to the entropy in this limit.

3.5 Circuit Complexity of Vacuum Subregions

In the previous section, we considered the purification complexity for thermal states of a free scalar QFT. In this section, we proceed with the QFT applications by considering

[42] Though it is not immediately obvious from the plot in the right panel of figure 3.10, we were able to confirm that in the limit of large $\beta\mu$, the result approaches a constant.

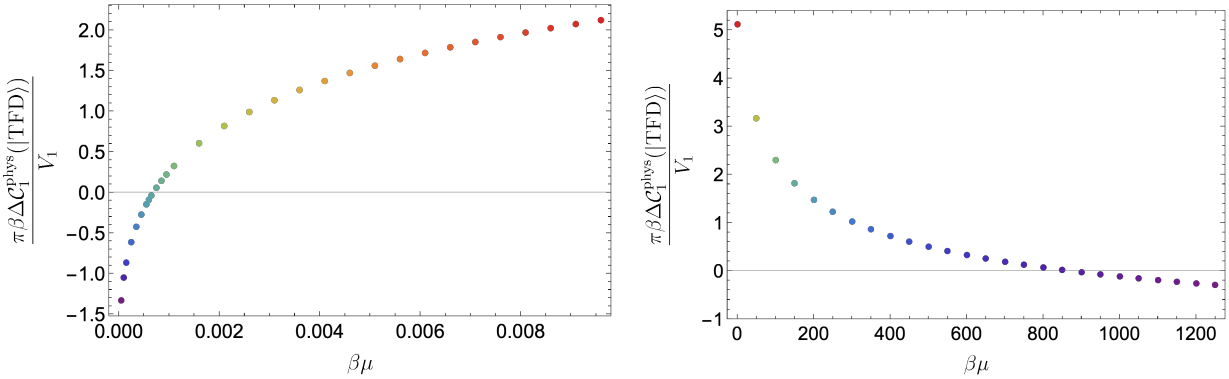

Figure 3.10: The integrated mutual complexity in the physical basis $\Delta\mathcal{C}_1^{\rm phys}(|{\rm TFD}\rangle)$ in eq. (3.124) for a massless free scalar field theory in $d = 2$ as a function of $\beta\mu$. The two plots show different regimes of the parameter $\beta\mu$. The integrated mutual complexity is negative when $\beta\mu$ is very small or very large.

mixed states on finite subregions of the vacuum state of a free scalar QFT. As in section 3.4.2, we regulate our field theory on a spatial lattice in order to obtain a finite result for the purification complexity. We evaluate the complexity and the mutual complexity both in the diagonal basis, and also in the physical basis, and comment on the sign of the mutual complexity in both cases. Our results are primarily evaluated numerically, and so we limit ourselves to considering the free scalar in two dimensions on a circular lattice. To illustrate the different bases relevant to this problem, in appendix A, we study analytically examples of small lattices with four coupled oscillators and reduced density matrices associated with subregions consisting of half of the oscillators.

3.5.1 Purification Complexity in the Diagonal Basis

Here we study the diagonal basis complexity and mutual complexity of density matrices of different subregions of the vacuum state of a discretized free scalar theory in two dimensions. We focus on a circular lattice of oscillators. We state the problem in terms of matrices on this lattice, and then describe the algorithm we used in order to find the complexity numerically. We then present our results for the complexity and the mutual complexity. Further, in discussing our results, we focus on the case of a very small mass in order that the results might mimic those of a holographic CFT.

3.5.1.1 Set-up

We begin with the lattice of harmonic oscillators (3.79) realizing a regularization of a free quantum field theory (3.78) on a one-dimensional circle of length L with N oscillators and lattice spacing $\delta = L/N$. The various oscillators are located at sites $\bar{x}_a$ where $a = 1, \ldots, N$ and we impose periodic boundary conditions $\bar{x}_{N+1} := \bar{x}_1$. The Hamiltonian in normal mode coordinates x_k defined in eq. (3.80) is given by eq. (3.83) and the complex coordinates are related according to $x_k^\dagger = x_{N-k}$.

The ground state wavefunction of this system of harmonic oscillators is straightforward to find in normal mode basis[43]

$$\Psi_0(x_k) = \prod_{k=1}^{N} \left(\frac{\omega_k}{\pi}\right)^{1/4} \exp\left(-\frac{1}{2}\omega_k |x_k|^2\right) . \tag{3.125}$$

This can be explicitly written in the physical basis using the transformation (3.80)

$$\Psi_0(\bar{x}_a) = \left(\det\left(\frac{M}{\pi}\right)\right)^{1/4} \exp\left[-\frac{1}{2} M_{ab} \bar{x}_a \bar{x}_b\right] , \tag{3.126}$$

where

$$M_{ab} = \frac{1}{N} \sum_{k=1}^{N} \omega_k \exp\left[-\frac{2\pi i k}{N}(a-b)\right] . \tag{3.127}$$

Next, we partition the system into two subregions $\mathcal{A} = \{\bar{x}_1, \bar{x}_2, \cdots, \bar{x}_J\}$ and $\mathcal{B} = \{\bar{x}_{J+1}, \cdots, \bar{x}_N\}$ and decompose the matrix M as in eq. (3.60)

$$M = \begin{pmatrix} \Gamma & K \\ K^\dagger & \Omega \end{pmatrix} \tag{3.128}$$

where Γ links the oscillators in the subregion $\mathcal{A}$ while Ω links the oscillators in subregion $\mathcal{B}$. The K matrices link the two subregions and are responsible for the entanglement between $\mathcal{A}$ and $\mathcal{B}$. Tracing out the oscillators in $\mathcal{B}$ then gives us a density matrix of the form (3.62)-(3.63), where the matrices A and B are related to M by (3.64)

$$A = \Gamma - \frac{1}{2} K \Omega^{-1} K^\dagger , \quad B = \frac{1}{2} K \Omega^{-1} K^\dagger . \tag{3.129}$$

[43] Note that eq. (3.125) differs from (2.10) in that we have the magnitude squared of x_k instead of simply the squared of each $\tilde{x}_k$. This is because while we assumed $\tilde{x}_k$ is real, the transformation (3.80) defining x_k is complex. It is possible to use instead the real Fourier transformations involving trigonometric functions in which case we would find real normal modes $\tilde{x}_k$ and the ground state would be given by (2.10), but we opt instead to use the simpler transformation (3.80) at the cost of having complex x_k.

If $K = 0$ then $B = 0$ and we have a pure state. This is to be expected since without K there is no entanglement between the two regions and both wave-functions are pure: $\Psi_{\mathcal{AB}} = \Psi_{\mathcal{A}} \otimes \Psi_{\mathcal{B}}$.

In this section, our goal is to calculate the purification complexity of the density matrix (3.62) obtained by the procedure above. Although the numerical minimization for purification complexity is always possible in principle, the number of free parameters will increase rapidly with the size of the subsystem, which means that we will need much more time in order to perform the numerical minimization for a larger lattice. Instead, we have claimed in section 3.3 that even for density matrices that are not simple products of single modes, mode-by-mode purifications can be used to provide a good approximation of the optimal purifications. Hence, here we have taken the strategy to focus on mode-by-mode purifications in the numerical minimization for the complexity of the mixed state in a given subregion $\hat{\rho}_{\mathcal{A}}$. We expect our results presented later will approximate the purification complexity $\mathcal{C}_1^{\text{diag}}$ for subregions of the vacuum.

In order to find the purification complexity using a mode-by-mode approximation, we have followed the following algorithm. We begin by computing the parameter matrix M_{ab} in eq. (3.127). Next, given a partition of our system $\mathcal{A}\cup\mathcal{B}$, we compute A and B using (3.129). We then diagonalize A with an orthogonal transformation O_A by $D_A = O_A A O_A^T$, and proceed to rescale the entries of A by $D_A^{-1/2}$. We then diagonalize the $\tilde{B} = D_A^{1/2} O_A B O_A^T D_A^{1/2}$ matrix in this new non-orthogonal basis[44] with an orthogonal transformation O_B by $D_B = O_B \tilde{B} O_B^T$. The density matrix in the non-orthogonal basis $\tilde{x} = O_B D_A^{1/2} O_A \bar{x} \equiv R\bar{x}$ now takes the following form

$$\rho_{\mathcal{A}}(\tilde{x}_i, \tilde{x}_i') = |\det R|^{-1} \sqrt{\det\left(\frac{A-B}{\pi}\right)} \prod_i \exp\left[-\frac{1}{2}(\tilde{x}_i^2 + (\tilde{x}_i')^2) + b_i \tilde{x}_i \tilde{x}_i'\right] ,$$

where the number of non-zero eigenvalues b_i indicates the number of ancillary oscillators which are necessary in order to purify the density matrix. We proceed to purify the mixed state $\hat{\rho}_{\mathcal{A}}$ with a mode-by-mode purification in this non-orthogonal basis, *i.e.,*

$$\hat{\rho}_{\mathcal{A}} = \text{Tr}_{\mathcal{A}^c} \hat{\rho}_{\mathcal{A}\mathcal{A}^c} , \quad \hat{\rho}_{\mathcal{A}\mathcal{A}^c} = |\Psi_{\mathcal{A}\mathcal{A}^c}\rangle\langle\Psi_{\mathcal{A}\mathcal{A}^c}| , \tag{3.130}$$

with

$$\Psi_{\mathcal{A}\mathcal{A}^c}(\tilde{x}_i, y_i) = \mathcal{N} \prod_i \exp\left[-\frac{1}{2}(1+b_i)\tilde{x}_i^2 - \frac{k_i^2}{4b_i} y_i^2 - k_i \tilde{x}_i y_i\right] . \tag{3.131}$$

[44]The basis is non-orthogonal for non-commuting A and B because of the rescaling by D_A between the two orthogonal transformations O_A and O_B.

We return to the orthogonal basis $\bar{x} = R^{-1}\tilde{x}$ with

$$\Psi_{\mathcal{A}\mathcal{A}^c}(\bar{x}_i, y_i) = \mathcal{N}' \exp\left[-\frac{1}{2}(\bar{x}, y)\cdot M_{\mathcal{A}}\cdot \begin{pmatrix} \bar{x} \\ y \end{pmatrix}\right], \tag{3.132}$$

and find the eigenvalues λ_i of $M_{\mathcal{A}}$. Finally, we minimize the complexity $\mathcal{C}_1^{\text{diag}} = \frac{1}{2}\sum_i |\ln\frac{\lambda_i}{\mu}|$ over the free parameters k_i. For some of the subregions considered, this minimization has to be done over an $\mathcal{O}(10^2)$ number of parameters. Fortunately, in our problem at hand, dividing this minimization into a sequence of minimizations over $\mathcal{O}(1)$ parameters indeed reaches the global minima of the function to be optimized.[45]

Obviously, we can follow the same process to derive the purification complexity for the complementary subregion $\hat{\rho}_{\mathcal{B}}$. Following the analysis in section 3.4.5, we can define the mutual complexity for subregions in the diagonal basis as

$$\Delta\mathcal{C}_1^{\text{diag}} \equiv \mathcal{C}_1^{\text{diag}}(\rho_{\mathcal{A}}) + \mathcal{C}_1^{\text{diag}}(\rho_{\mathcal{B}}) - \mathcal{C}_1^{\text{diag}}(|\Psi_0\rangle)\,. \tag{3.133}$$

3.5.1.2 Numerical results in the diagonal basis

Throughout the following discussion, we have set the mass to $mL = 0.01$. Again, our aim is that by setting the mass to such a small value, our QFT results might resemble those found in holography where the boundary theory is conformal. A comparison of the results for the free scalar theory and for holography will be considered in Chapter 4.

Dependence on the size of the subregion: First, we find the subregion complexity as a function of the subregion size for a lattice of 1000 harmonic oscillators for different values of the reference frequency and plot the results in figure 3.11. For all cases, the complexity grows linearly with the subregion size up to the expected complexity of the vacuum. The slope of the plot decreases with increasing reference frequency.

Structure of divergences in purification complexity: For subregions with fixed size, we plot the cutoff dependence of the purification complexity in figure 3.12. The large N (or equivalently, the small δ) behavior of the subregion complexity with $\ell/L =$

[45] Indeed, even taking the minimization over one parameter at a time gives the global minima *most* of the time. We found that minimizing over 2 or 3 parameters at a time gave accurate enough results without requiring too much more computational power.

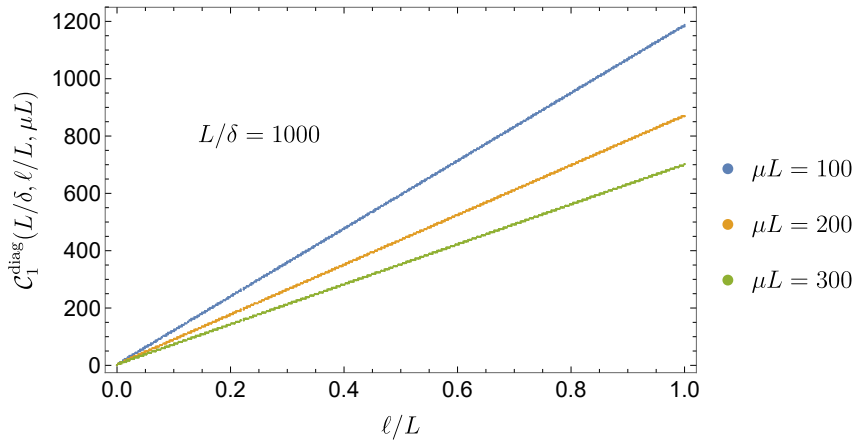

Figure 3.11: Purification complexity in the diagonal basis for subregions of the vacuum as a function of the subregion size. The cutoff was set to $N = L/\delta = 1000$ and the mass to $mL = 0.01$. The purification complexity for the subregion with $\ell \to L$ agrees with the complexity of the ground state in diagonal basis.

1/20, 1/10, 9/10 and 19/20 is given by

$$\begin{aligned}
\mathcal{C}_1^{\rm diag}(\ell/L = 0.05, \mu L, \delta/L) &\approx \frac{\ell}{2\,\delta} \ln \frac{1}{\mu\delta} + 0.232 \ln \frac{L}{\delta} + 0.307\,\mu\ell + 2.08\,, \\
\mathcal{C}_1^{\rm diag}(\ell/L = 0.10, \mu L, \delta/L) &\approx \frac{\ell}{2\,\delta} \ln \frac{1}{\mu\delta} + 0.241 \ln \frac{L}{\delta} + 0.312\,\mu\ell + 2.11\,, \\
\mathcal{C}_1^{\rm diag}(\ell/L = 0.90, \mu L, \delta/L) &\approx \frac{\ell}{2\,\delta} \ln \frac{1}{\mu\delta} + (0.542 - 0.304\mu\ell)\, \ln \frac{L}{\delta} + 0.340\,\mu\ell - 0.308\,, \\
\mathcal{C}_1^{\rm diag}(\ell/L = 0.95, \mu L, \delta/L) &\approx \frac{\ell}{2\,\delta} \ln \frac{1}{\mu\delta} + (0.383 - 0.147\,\mu\ell)\, \ln \frac{L}{\delta} + 0.329\,\mu\ell + 0.688\,.
\end{aligned} \tag{3.134}$$

These suggest a divergence structure of the form[46]

$$\mathcal{C}_1^{\rm diag}(\ell/L, \mu L, \delta/L) \approx \frac{\ell}{2\,\delta} \left| \ln \frac{1}{\mu\delta} \right| + f_1(\mu L, \ell/L) \ln \frac{L}{\delta} + f_2(\mu L, \ell/L) \tag{3.135}$$

[46]Note that the fits in eq. (3.134) were obtained using the data for large values of L/δ, *i.e.*, $L/\delta > 300$ in figure 3.12. Furthermore, we kept μL fixed in these fits (and plots). Therefore, the fits correspond to a region where $\mu\delta$ is small. More generally, one could consider reference frequencies of the order of the cutoff, or even larger. The intuition from the pure state results (see footnote 47) leads to the conclusion that there should be an absolute value on the logarithmic factor, as we write in eq. (3.135).

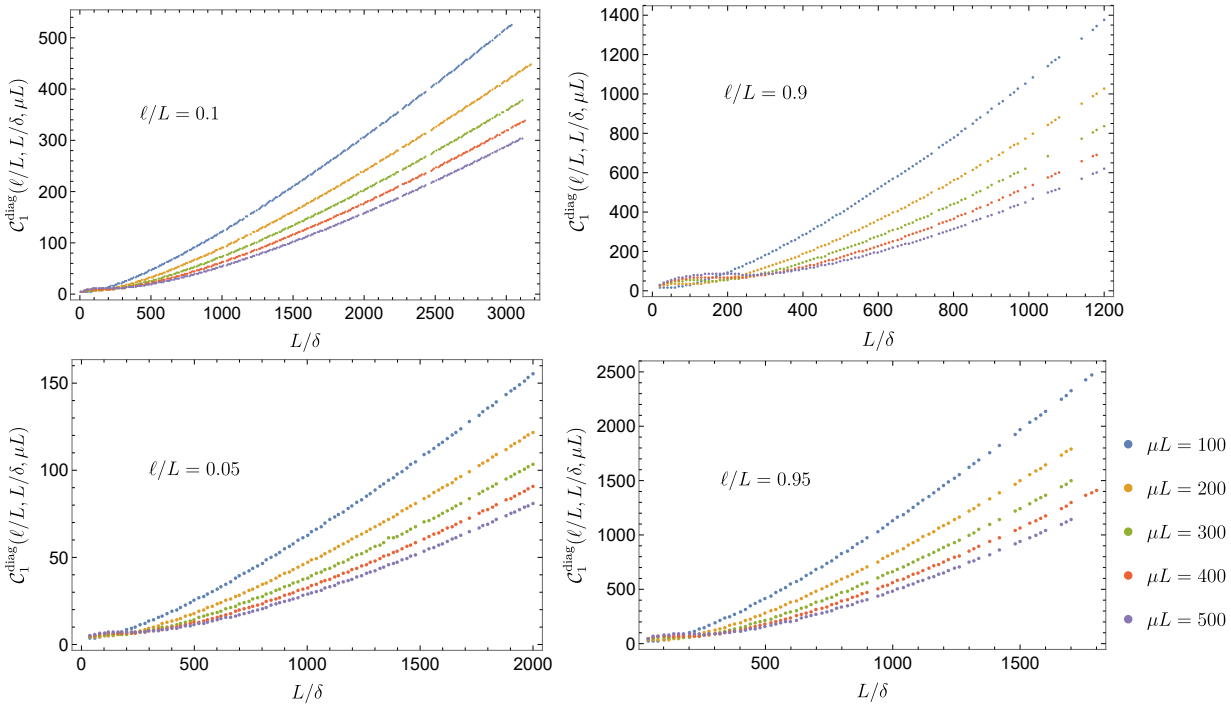

Figure 3.12: Purification complexity in the diagonal basis for subregions of the vacuum as a function of the lattice cutoff. The mass was set to $mL = 0.01$. The different plots correspond to different subregion sizes $\ell/L = 0.05$, 0.1, 0.9 and 0.95 as indicated and each plot contains five different reference frequencies of $\mu L = 100$, 200, 300, 400 and 500 respectively.

where f_1 and f_2 are dimensionless functions, which are independent of the cutoff scale δ. We note that the leading divergence matches the results found in [62,69] for the full system with $\ell \to L$.

In eq. (3.135), we have found the structure of divergences for our system with $mL = 0.01$, which was chosen to emulate a massless field theory. In the case of a massive theory, *i.e.*, $mL \gtrsim 1$, we expect that the divergence structure is again as in eq. (3.135), except that the coefficients f_1 and f_2 would now also depend on the additional mass parameter, *e.g.*, $f_1 = f_1(\mu L, \ell/L, mL)$ and $f_2 = f_2(\mu L, \ell/L, mL)$. On the other hand, we expect that the UV divergence in the first term is a universal volume term, as in the massless theory. This contribution represents the cost required to prepare the ground state entanglement at very

short scales, while the other terms depend on the details of the QFT (*e.g.,* the mass).[47] The structure of UV divergences is similar for holographic complexity, as we examine in section 4.3.

Mutual complexity in the diagonal basis for subregions: The numerical results for the mutual complexity (3.133) are shown in figures 3.13 and 3.14. We observe that the mutual complexity in the diagonal basis is positive for all of the subregion sizes shown there. However, we do not have an analytic argument that proves that this should be the case in general. The mutual complexity rises dramatically for small subregion sizes in figure (3.133), and then it continues to increase as the subregion size grows until the subregion reaches half of the system. Further, $\Delta\mathcal{C}$ is symmetric under $\ell \to L - \ell$. It has a positive logarithmic dependence on the cutoff which comes from the subleading divergence in the complexities. Looking at eq. (3.134), we observe that while $f_1(\mu\ell) + f_1(\mu(L-\ell))$ becomes negative for large enough reference frequency, this contribution is offset by the negative coefficient of the logarithmic term in the vacuum complexity (see footnote 47) to produce an overall positive cutoff dependence in the mutual complexity, as can be seen in figure 3.14.

3.5.2 Purification Complexity in the Physical Basis

In this subsection, we investigate the behaviour of the physical basis purification complexity $\mathcal{C}_1^{\text{phys}}$ for subregions of the vacuum for a two-dimensional free scalar QFT on a circular lattice. The procedure to do this is very similar to the algorithm introduced in the previous section. In fact, the only difference comes after finding the purification matrix in the

[47] In particular, we found that the complexity of the *full* ground state is, using eqs. (2.19) and (3.80),

$$\mathcal{C}_1^{\text{diag}}(\hat{\rho}_0) = \frac{L}{2\delta}\ln(\mu\delta) + \frac{1}{2}\ln\left(\frac{1}{mL}\right) - \frac{m^2L^2}{48} + \mathcal{O}(m^4, m^2\delta^2)\,, \tag{3.136}$$

where here we assumed $\mu \geq \sqrt{\frac{4}{\delta^2} + m^2}$ in order to obtain this simple analytic form. Alternatively, for $\mu < m$, the same result is obtained up to an overall minus sign. For the values we chose, $\frac{1}{2}\ln\left(\frac{1}{mL}\right) - \frac{m^2L^2}{48} \approx \frac{1}{2}\ln\left(\frac{1}{mL}\right) \approx 2.30$, although this zero mode contribution would diverge in the $m \to 0$ limit. For intermediate values of the reference frequency $m < \mu < \sqrt{\frac{4}{\delta^2} + m^2}$, numerical fitting show the same leading divergence and a subleading logarithmic divergence $\mathcal{C}_1^{\text{diag}}(\hat{\rho}_0) = \frac{L}{2\delta}|\ln(\mu\delta)| - \tilde{f}(\mu L)|\ln(\mu\delta)| + \text{finite}$, with $\tilde{f}(\mu L) \approx 4.10 \times 10^{-7}(\mu L)^{1.85} > 0$. We used the parameters $mL = 0.01$, $\mu L = 20, 40, 60, 80, 100, 200, 300, 400, 500$ for data with $L/\delta = 1$ to 10^4, and found fits for the large L/δ behaviour.

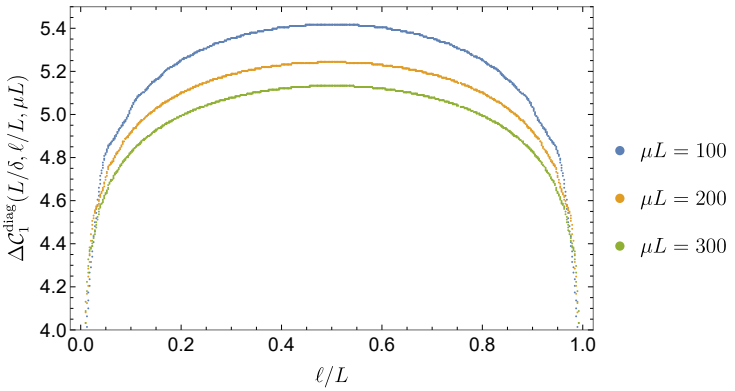

Figure 3.13: Subregion size dependence of the mutual complexity in the diagonal basis $\Delta\mathcal{C}_1^{\rm diag}$ for different reference frequencies $\mu L = 100$, 200 and 300. The cutoff was set to $\delta/L = 1/N = 1/1000$ and the mass to $mL = 0.01$.

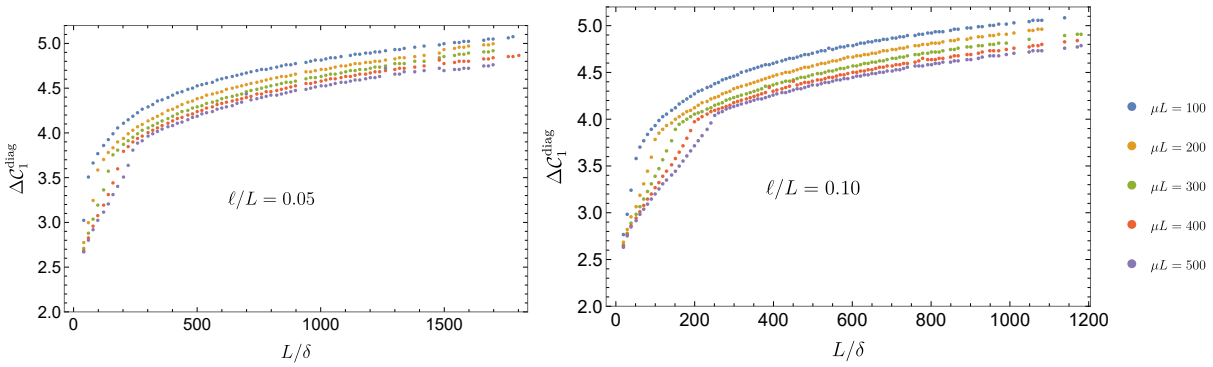

Figure 3.14: Cutoff dependence of the mutual complexity in the diagonal basis $\Delta\mathcal{C}_1^{\rm diag}$ for different reference frequencies $\mu L = 100$, 200, 300, 400 and 500. The subregion sizes were fixed to $\ell/L = 0.1$ and 0.05 and the mass to $mL = 0.01$.

position basis in eq. (3.132). From the purification matrix in the position basis

$$M_{\mathcal{A}} = \begin{pmatrix} \Gamma^{\rm pos} & K^{\rm pos} \\ (K^{\rm pos})^T & \Omega^{\rm pos} \end{pmatrix} , \tag{3.137}$$

we rotate the physical modes and the ancilla modes independently to diagonalize $\Gamma^{\rm pos}$ and $\Omega^{\rm pos}$ according to

$$M_{\mathcal{A}} \to M_{\mathcal{A}}^{\rm phys} = R_{\rm phys} M_{\mathcal{A}} R_{\rm phys}^T , \quad R_{\rm phys} = \begin{pmatrix} R_{\mathcal{A}} & 0 \\ 0 & R_{\mathcal{A}^c} \end{pmatrix} , \tag{3.138}$$

where $R_{\mathcal{A}} \in SO(N_{\mathcal{A}}, \mathbb{R})$ and $R_{\mathcal{A}^c} \in SO(N_{\mathcal{A}^c}, \mathbb{R})$ such that $\Gamma^{\text{phys}} = R_{\mathcal{A}} \Gamma^{\text{pos}} R_{\mathcal{A}}^T$ and $\Omega^{\text{phys}} = R_{\mathcal{A}^c} \Omega^{\text{pos}} R_{\mathcal{A}^c}^T$ are diagonal. Finally, the generator matrix H^{phys} can be found by taking the matrix logarithm of the parameter matrix in this basis as

$$H^{\text{phys}} = \frac{1}{2} \ln\left(\frac{M_{\mathcal{A}}^{\text{phys}}}{\mu}\right) . \tag{3.139}$$

The physical basis complexity of these purifications is defined by

$$\mathcal{C}_1^{\text{phys}}\left(\hat{\rho}_{\mathcal{A}}\right) = \min \sum_{a,b=1}^{N_{\mathcal{A}}+N_{\mathcal{A}^c}} |H_{ab}^{\text{phys}}| \,, \tag{3.140}$$

where we need to minimize the purification complexity over the free parameters k_i which were introduced in eq. (3.131).

3.5.2.1 Numerical results in the physical basis

Again, we set $mL = 0.01$ throughout the following. By setting the mass to such a small value, we expect that our QFT results might behave similar to those found for a holographic CFT.

Dependence on the size of the subregion: We plot the purification complexity in the physical basis as a function of the subregion size for a lattice of 100 harmonic oscillators for different values of the reference frequency in figure 3.15. Unlike the diagonal basis complexity, we find that for subregions approaching the full system, the physical basis purification complexity can increase beyond the complexity of the full system before decreasing rapidly to the full system complexity. At first sight, this might seem contradictory, since the ground state is one of the possible purifications over which the purification complexity is minimized. However, the complexity of the ground state in the physical basis partitioned by $\mathcal{A}$ and $\mathcal{A}^c$ can be greater than the complexity of the ground state itself. In fact, the purification complexity in the physical basis should be less than the complexity of the ground state *in that same basis*. In the right panel of figure 3.15, we compare the purification complexity in the physical basis $\mathcal{C}_1^{\text{phys}}(\rho_{\mathcal{A}})$ to the complexity of the ground state $\mathcal{C}_1^{\mathcal{AB}}(|\Psi_0\rangle)$ in the basis which does not mix the degrees of freedom in the subsystem $\mathcal{A}$ with the modes in the complementary region $\mathcal{B}$. Indeed, we find that $\mathcal{C}_1^{\text{phys}}(\rho_{\mathcal{A}}) \leq \mathcal{C}_1^{\mathcal{AB}}(|\Psi_0\rangle)$ for all subregions $\mathcal{A}$ and the inequality is only saturated when $\mathcal{A}$ encompasses the entire system (*i.e.*, $\ell/L = 1$). Note that comparing $\mathcal{C}_1^{\text{phys}}(\rho_{\mathcal{A}})$ with the complexity of the ground state $\mathcal{C}_1^{\text{diag}}(|\Psi_0\rangle)$ in the diagonal basis, we find that the above bound does not hold. In

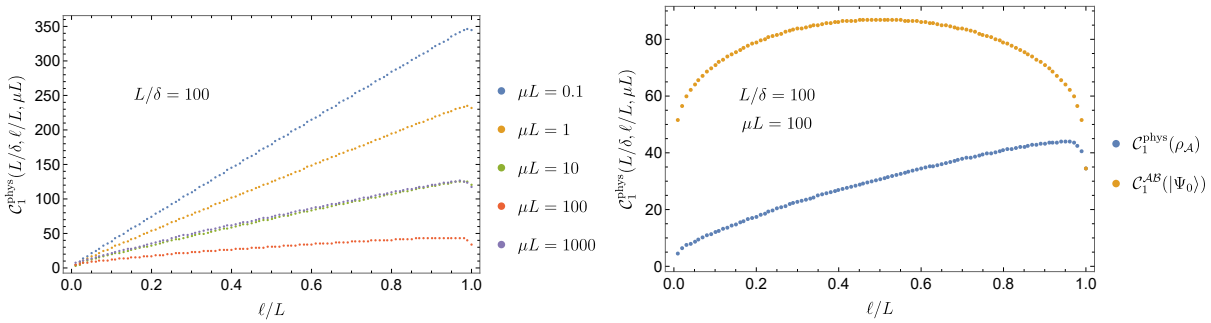

Figure 3.15: Left panel: subregion complexity as a function of the subregion size in physical basis for reference frequencies $\mu L = 0.1,\ 1,\ 10,\ 100,\ 1000$. Right panel: comparison of the subregion complexity to the complexity of the ground state in the physical basis for $\mu L = 100$. In both plots, the cutoff was set to to $L/\delta = N = 100$ and the mass to $mL = 0.01$.

particular, the figure shows that for large subregions (*i.e.,* $\ell/L \gtrsim 0.6$), the subregion complexity exceeds that of the ground state in diagonal basis (but, of course, they coincide at $\ell/L = 1$). There is no contradiction in finding $\mathcal{C}_1^{\rm phys}(\rho_{\mathcal{A}}) > \mathcal{C}_1^{\rm diag}(|\Psi_0\rangle)$ for some subregions since the two complexities are evaluated using different gate sets. As noted above, when the complexities are evaluated using the same basis, the subregion complexity is smaller than that of the vacuum.

Structure of divergences in purification complexity: For subregions with fixed size, we plot the cutoff dependence of the purification complexity in figure 3.16. The large N (or equivalently, the small δ) behavior of the subregion complexity with $\ell/L = 1/10,\ 9/10,\ 1/20$ and $19/20$ is

$$\begin{aligned}
\mathcal{C}_1^{\rm phys}(\ell/L = 0.05, \mu L, \delta/L) &\approx \frac{\ell}{2\,\delta} \ln \frac{1}{\mu\delta} + 3.31 \ln \frac{L}{\delta} + 0.149\,\mu\ell - 6.54\,, \\
\mathcal{C}_1^{\rm phys}(\ell/L = 0.10, \mu L, \delta/L) &\approx \frac{\ell}{2\,\delta} \ln \frac{1}{\mu\delta} + 3.60 \ln \frac{L}{\delta} + 0.253\,\mu\ell - 5.79\,, \\
\mathcal{C}_1^{\rm phys}(\ell/L = 0.90, \mu L, \delta/L) &\approx \frac{\ell}{2\,\delta} \ln \frac{1}{\mu\delta} + 4.74 \ln \frac{L}{\delta} + 0.343\,\mu\ell - 13.1\,, \\
\mathcal{C}_1^{\rm phys}(\ell/L = 0.95, \mu L, \delta/L) &\approx \frac{\ell}{2\,\delta} \ln \frac{1}{\mu\delta} + 5.04 \ln \frac{L}{\delta} + 0.333\,\mu\ell - 14.5\,.
\end{aligned} \tag{3.141}$$

These fits suggest a divergence structure for the subregion complexities in the physical

basis of the form[48]

$$\mathcal{C}_1^{\text{phys}}(\mu L, \delta/L) \approx \frac{\ell}{2\,\delta}\left|\ln\frac{1}{\mu\delta}\right| + f_1(\mu L, \ell/L)\ln\frac{L}{\delta} + f_2(\mu L, \ell/L)\,. \tag{3.142}$$

Similarly to the discussion for the diagonal basis, we expect the structure of divergences in the physical basis to be the same as in eq. (3.142) for more general cases, except that the coefficients f_1 and f_2 will depend on the other parameters of the system. For example, for a massive scalar QFT, we expect $f_i = f_i(\mu L, \ell/L, mL)$.

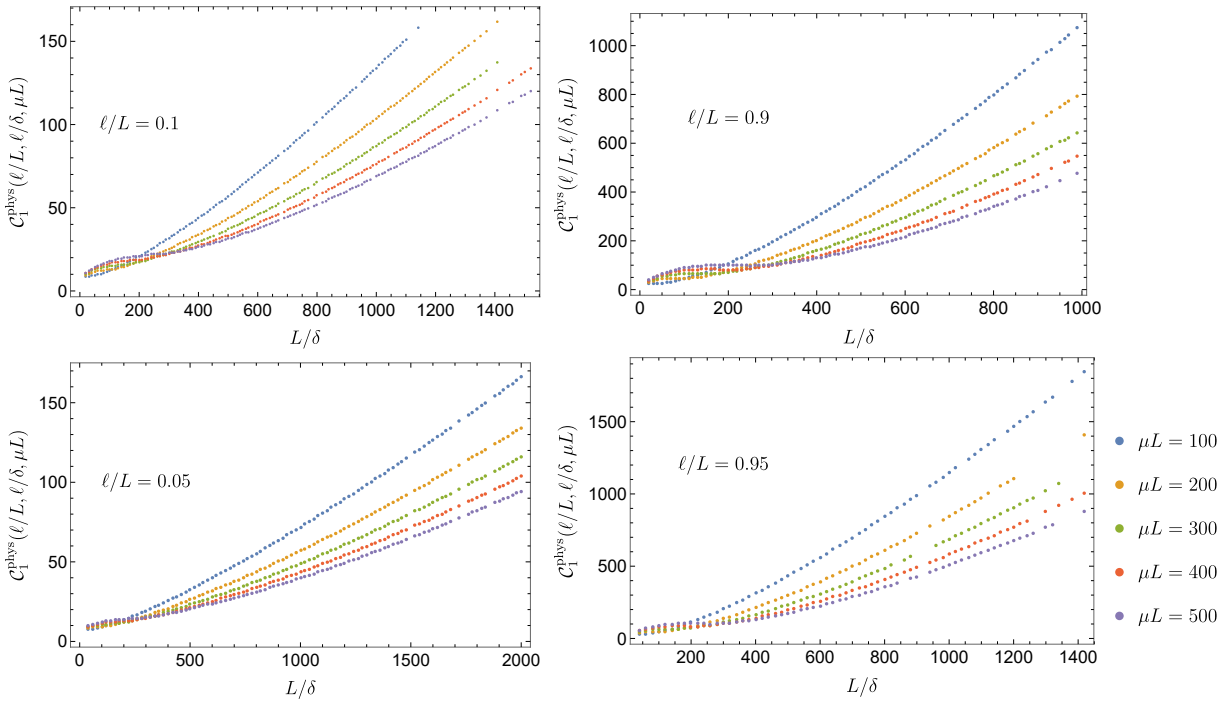

Figure 3.16: Subregion complexity in the physical basis as a function of the cutoff $N = L/\delta$ for $\ell/L = 0.05$, 0.1, 0.9 and 0.95. The mass was set to $mL = 0.01$.

Mutual complexity in physical basis: We plot the mutual complexity in the physical basis

$$\Delta\mathcal{C}_1^{\text{phys}} \equiv \mathcal{C}_1^{\text{phys}}(\rho_{\mathcal{A}}) + \mathcal{C}_1^{\text{phys}}(\rho_{\mathcal{B}}) - \mathcal{C}_1^{\text{phys}}(|\Psi_0\rangle)\,, \tag{3.143}$$

[48] As mentioned in footnote 46, our fits were made for small δ/L with μL fixed. In general, we expect the leading term to be the absolute value of the logarithmic term. Our resolution in the physical basis fits was not high enough to rule out a term of the form $f_0(\mu L, \ell/L)\,\frac{\ell}{\delta}$ where $f_0(\mu L, \ell/L) \lesssim \mathcal{O}(10^{-2})$.

in figure 3.17, which we observe to be negative for all of the subregion sizes shown there. However, some explanation is required here. The mutual complexity (3.143) will be different depending on whether the physical basis for the three states considered is fixed to be one which separates $\mathcal{A}$ and/or $\mathcal{B}$ from the rest of the degrees of freedom, or if the physical basis is considered for each state independently. More precisely, the physical basis for $\rho_{\mathcal{A}}$ (and $\rho_{\mathcal{B}}$) will be a basis in which the $\mathcal{A}$ and $\mathcal{A}^c$ (and the $\mathcal{B}$ and $\mathcal{B}^c$, respectively) degrees of freedom are kept separate. However, for the ground state, there is no natural partition of the system into $\mathcal{A} \cup \mathcal{B}$ independently of the density matrices $\rho_{\mathcal{A}}$ and $\rho_{\mathcal{B}}$. Therefore, if the physical basis in the evaluation of the complexity of the ground state were to be considered independently of the other two complexities, we would find that the physical basis for the ground state corresponds to all of the degrees of freedom in the system, and the physical basis would coincide with the diagonal basis. Therefore, to be more explicit, we define two mutual complexities in the physical basis

$$\begin{aligned} \Delta\mathcal{C}_1^{\text{phys}} &\equiv \mathcal{C}_1^{\mathcal{A}\mathcal{A}^c}(\rho_{\mathcal{A}}) + \mathcal{C}_1^{\mathcal{B}\mathcal{B}^c}(\rho_{\mathcal{B}}) - \mathcal{C}_1^{\mathcal{A}\mathcal{B}}(|\Psi_0\rangle)\,, \\ \Delta\tilde{\mathcal{C}}_1^{\text{phys}} &\equiv \mathcal{C}_1^{\mathcal{A}\mathcal{A}^c}(\rho_{\mathcal{A}}) + \mathcal{C}_1^{\mathcal{B}\mathcal{B}^c}(\rho_{\mathcal{B}}) - \mathcal{C}_1^{\text{diag}}(|\Psi_0\rangle)\,, \end{aligned} \tag{3.144}$$

where $\mathcal{C}^{\mathcal{A}\mathcal{B}}$ denotes the physical basis complexity of a state given a partition of the system into $\mathcal{A} \cup \mathcal{B}$. It is natural to expect that $\Delta\mathcal{C}_1^{\text{phys}} < \Delta\tilde{\mathcal{C}}_1^{\text{phys}}$, since the difference between the two definitions in eq. (3.144) is the subtraction of the vacuum complexity in two different bases. More precisely, the $\mathcal{C}_1^{\mathcal{A}\mathcal{B}}(|\Psi_0\rangle)$ evaluates the complexity of the ground state subject to the additional constraint that the $\mathcal{A}$ and $\mathcal{B}$ degrees of freedom remain separated. Being a minimization with additional constraints compared to $\mathcal{C}_1^{\text{diag}}(|\Psi_0\rangle)$, it follows that $\mathcal{C}_1^{\mathcal{A}\mathcal{B}}(|\Psi_0\rangle) > \mathcal{C}_1^{\text{diag}}(|\Psi_0\rangle)$ from which the above conclusion follows.

Just like the mutual complexity in the diagonal basis, we observe that both of the mutual complexities in the physical basis increase in magnitude as a function of the subregion size, reaching maximum at $\ell/L = 1/2$, and are symmetric about this point. The $\Delta\tilde{\mathcal{C}}_1^{\text{phys}}$ shows similar behaviour to the diagonal basis mutual complexity: it is positive and depends logarithmically on the cutoff. Again, this logarithmic dependence comes from the subleading logarithmic divergence of the complexities. The subleading divergence in the subregion complexities in the physical basis are positive, while the subleading divergence of the complexity of the ground state is negative for all cases studied here (see footnote 47). On the other hand, the $\Delta\mathcal{C}_1^{\text{phys}}$ is negative and decreases linearly as a function of the cutoff. This contrasts with the logarithmic cutoff dependence of the mutual complexity in the diagonal basis in figure 3.14. The negative linear dependence of $\Delta\mathcal{C}_1^{\text{phys}}$ on the cutoff is due to the vacuum complexity in the $\mathcal{A}\mathcal{B}$ basis having a subleading positive linear divergence, which is not present for the diagonal basis.

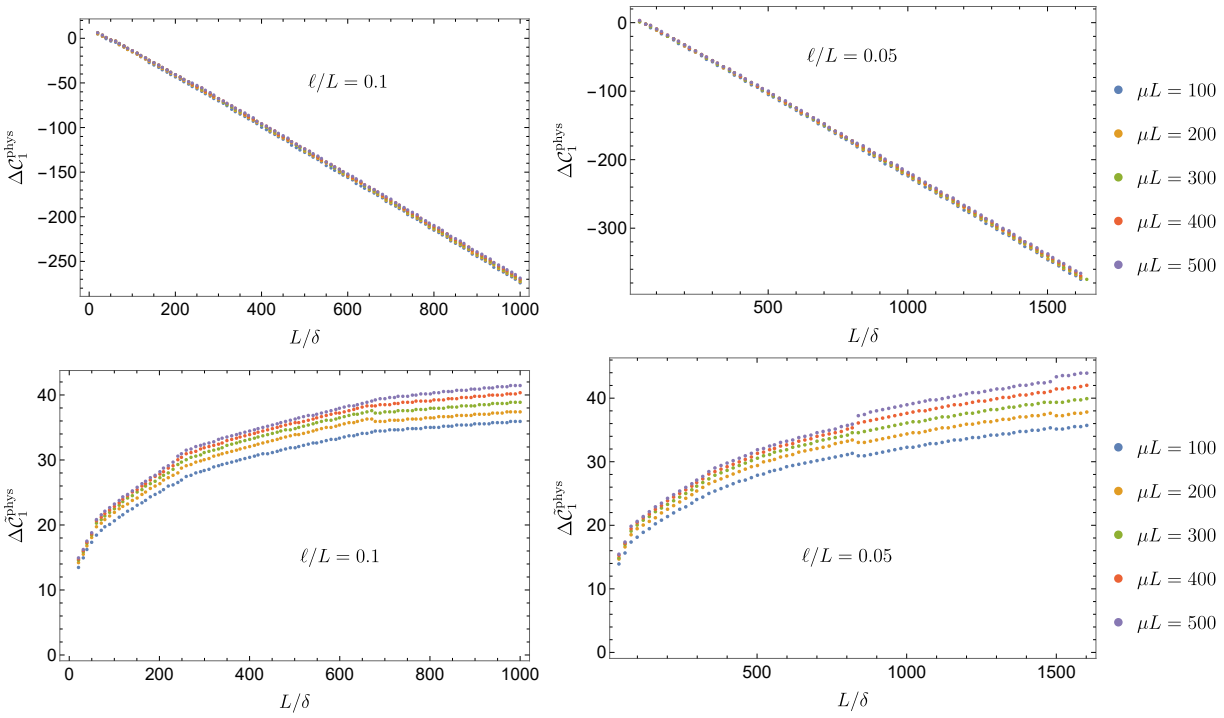

Figure 3.17: The two definitions of mutual complexity in the physical basis $\Delta\mathcal{C}_1^{\text{phys}}$ and $\Delta\tilde{\mathcal{C}}_1^{\text{phys}}$ as a function of the cutoff for various reference frequencies $\mu L = 100$, 200, 300, 400 and 500. The mass was set to $mL = 0.01$.

Chapter 4

Holographic Complexity of Mixed States

In the previous chapter, we investigated the purification complexity for Gaussian mixed states in free scalar quantum field theory. In particular, we focused on two examples: the complexity of thermal states and the complexity of subregions in the vacuum state. The purpose of this chapter is to review and compare some general features of these results to those obtained using the proposals for holographic complexity.

In holography, there have been two different proposals for the gravitational dual of subregion complexity. These proposals are extensions of the complexity=volume (CV) [55, 56] and complexity=action proposals [57, 58], and they were motivated by entanglement wedge reconstruction, *i.e.,* the understanding that the reduced density matrix of a boundary subregion encodes the dual entanglement wedge in the bulk [191–193].[1] We denote the two proposals as the subregion complexity=volume (subregion-CV) [114, 180] and the subregion complexity=action (subregion-CA) [114] conjectures. A third approach for holographic complexity was also proposed with the complexity = spacetime volume (CV2.0) conjecture [115]. Hence in the following, we also discuss the natural extension of this proposal for the case of subregions, which we designate the subregion-CV2.0 conjecture. Note that all three approaches for subregion complexity recover the corresponding original proposal for the holographic complexity of a pure state in the limit in which the subregion becomes the whole boundary.

Let us add that subregion complexity in holography has been widely explored. See

[1] The latter can be proven with the assumption that the bulk and boundary relative entropies are exactly equal [194, 195].

e.g., [2, 114, 147, 156, 161, 162, 164, 165, 169, 171, 180, 190, 196, 196–204]. These include, to name only a few, general studies of the structure of divergences [114, 114, 180], multiple subregions [147], subregions whose boundary includes kinks/corners [196, 198], subregions of systems with defects [162], subregion complexity in eternal black hole backgrounds for subregions consisting of a single boundary [171], and the opposite limit of small subregions in eternal black hole geometry [169]. We begin below with a brief review of the different approaches described above and their main properties. We will then review the results of evaluating these proposals for two examples, which are relevant for the comparison to the QFT results in the two previous sections: a subregion consisting of a single boundary of the TFD state (eternal black hole), where we are evaluating the complexity associated to the thermal state; and a boundary subregion of the CFT vacuum state (empty AdS).

This chapter is adapted from section 6 in [2].

4.1 Review of the Holographic Proposals

The subregion-CV conjecture [114, 180] suggests that the complexity associated with a boundary subregion $\mathcal{A}$ on a given time slice is given by the maximal spatial volume of a codimension-one surface $\mathcal{R}_{\mathcal{A}}$, bounded by the boundary subregion and its Hubeny-Rangamani-Takayanagi (HRT) surface $\mathcal{E}_{\mathcal{A}}$ [26–28, 51]:

$$\mathcal{C}_{\rm V}(\mathcal{A}) = \max_{\partial\mathcal{R}_{\mathcal{A}}=\mathcal{A}\cup\mathcal{E}_{\mathcal{A}}} \left[\frac{\mathcal{V}(\mathcal{R}_{\mathcal{A}})}{G_N\,\ell_{\rm bulk}}\right] . \tag{4.1}$$

The appearance of an arbitrary bulk length scale, $\ell_{\rm bulk}$, is a somewhat undesirable feature. In the following, we assume that $\ell_{\rm bulk} = L$, the AdS curvature radius. Note that while a more sophisticated prescription to define $\ell_{\rm bulk}$ for black hole geometries was given in [109], it still yields $\ell_{\rm bulk} \sim L$ for the planar AdS black holes that we consider below, *i.e.,* see eq. (4.8).

A second proposal is the subregion-CA conjecture [114], which suggests that the subregion complexity is given by the on-shell gravitational action on a particular bulk region $\widetilde{W}_{\mathcal{A}}$, which is defined as the intersection of the Wheeler-DeWitt (WDW) patch and the entanglement wedge of the boundary region $\mathcal{A}$ [191–193]:

$$\mathcal{C}_{\rm A}(\mathcal{A}) = \frac{I_{\rm grav}(\widetilde{W}_{\mathcal{A}})}{\pi} . \tag{4.2}$$

In addition to the codimension-one boundary surfaces, the boundary of $\widetilde{W}$ also contains codimension-two joints at the intersection of the boundary surfaces. Similar to evaluation

of the gravitational action in the WDW patch shown in (2.65), the gravitational action $I_{\rm grav}(\widetilde{W_{\mathcal{A}}})$ also contains various boundary terms and joint terms, *i.e.,*

$$I_{\rm grav}(\widetilde{W_{\mathcal{A}}}) = I_{\rm bulk} + I_{\rm GHY} + I_{\rm null} + I_{\rm ct} + I_{\rm joints}\,. \tag{4.3}$$

We point out again that one must also include the null counterterm $I_{\rm ct}$ introduced in [134] to restore reparametrization invariance along the null generators.

The complexity = spacetime volume (CV2.0)[2] conjecture [115] simplifies the CA conjecture by proposing that the complexity can be determined by evaluating the spacetime volume of the WDW patch. The simplification still displays all of the properties expected of holographic complexity. Our subregion-CV2.0 conjecture is the natural generalization of this proposal to boundary subregions. That is, the complexity of a subregion $\mathcal{A}$ is given by the spacetime volume of the region appearing in eq. (4.2), *i.e.,* the intersection of the WDW patch and the entanglement wedge,[3]

$$\mathcal{C}_{\rm V2.0}(\mathcal{A}) = \frac{\mathcal{V}(\widetilde{W_{\mathcal{A}}})}{G_N\, L^2}\,. \tag{4.4}$$

As a pragmatic point, we note that in our calculations below, the integrand of the bulk action, *i.e.,* the Einstein-Hilbert term, is simply constant with $R - 2\Lambda = -\frac{2d}{L^2}$. Hence, the complexity in eq. (4.4) and the bulk action evaluated for eq. (4.2) are simply related by

$$\mathcal{C}_{\rm V2.0}(\mathcal{A}) = -\frac{8\pi}{d}\, I_{\rm bulk}(\widetilde{W_{\mathcal{A}}})\,. \tag{4.5}$$

Additivity properties: The various holographic proposals for subregion complexity differ in several important respects. $\mathcal{C}_{\rm V}$ is superadditive — see section 2.1 of [171]. That is, let σ be the Cauchy slice on which a pure state is defined, and divide this surface into a subregion $\mathcal{A}$ and its complement $\mathcal{B}$. Then the corresponding holographic complexities evaluated satisfy,

$$\mathcal{C}_{\rm V}(\mathcal{A}) + \mathcal{C}_{\rm V}(\mathcal{B}) \leq \mathcal{C}_{\rm V}(\sigma = \mathcal{A}\cup\mathcal{B})\,, \tag{4.6}$$

i.e., the mutual complexity (3.105) is negative. Intuitively, superadditivity in $\mathcal{C}_{\rm V}$ is the result of dealing with positive definite volumes and the fact that the requirement to pass

[2] An update to the complexity = spacetime volume conjecture, denoted 'CA2.0', was proposed in [126]. However, for Einstein-Hilbert gravity with minimally coupled matter, this approach simply reduces to the CV2.0 proposal. As such, we will not consider it further here.

[3] The units are naturally absorbed by the AdS curvature scale in the definition here following [109]. Their approach uses the relation $\mathcal{C} \sim \mathcal{P}\,\mathcal{V}_{\rm WDW}$ where $\mathcal{P} = -\frac{\Lambda}{8\pi G_N} \sim 1/(G_N L^2)$ is the 'bulk' pressure [205]. Note that the application of these arguments is not straightforward for solutions with nontrivial scalar hair [126].

through the HRT surface adds an additional constraint in maximizing the volume. Let us add that this inequality is saturated in simple examples where the boundary Cauchy slice defines a time-reversal symmetric state (for which the HRT surface for $\mathcal{A}$ and $\mathcal{B}$ lies within the corresponding extremal bulk surface).

Similarly, the subregion-CV2.0 conjecture yields superadditive results. This follows because the spacetime volume is always positive and further the intersection of the entanglement wedge and the WDW patch is a subregion within the WDW patch of σ. Hence it becomes evident that the mutual complexity (3.105) will always be negative using this proposal. Let us emphasize that there are no obvious simple examples where the corresponding inequality would be saturated, *i.e.,* we *cannot* easily achieve $\Delta\mathcal{C}_{\text{V2.0}} = 0$, unless one of the subregions vanishes.

On the other hand, recall that the calculation of $\mathcal{C}_{\text{A}}$ in eq. (4.2) involves the length scale ℓ_{ct} associated with the null boundary counterterm. Different values of this length scale result in $\mathcal{C}_{\text{A}}$ being subadditive or superadditive in different situations [171] — see also [190]. However, one should expect that the complexity, and hence the leading divergence, is positive, which partially fixes this ambiguity and further results in $\mathcal{C}_{\text{A}}$ being superadditive.

Structure of divergences: All three proposals have a leading UV divergence proportional to the volume of the boundary subregion, *i.e.,* $V(\mathcal{A})/\delta^{d-1}$ but the subleading divergences are quite different. The subregion-CA conjecture yields subleading divergences with any power of δ. In particular, in [114], a class of subleading divergences associated with the boundary of the subregion were identified for the subregion-CA approach, *e.g.,* $V(\partial\mathcal{A})/\delta^{d-2}$. Similarly, subleading divergences with any power of delta appear for subregion-CV2.0, as is easily inferred from the results of [114] and the relation in eq. (4.5). In contrast, it was shown that the subregion-CV approach yields power-law divergences involving only odd or even powers of the cutoff δ for an even- or odd-dimensional boundary theory, respectively. Hence the $V(\partial\mathcal{A})/\delta^{d-2}$ term does not appear with the subregion-CV approach.

Before closing let us add that one could easily modify the three proposals in eqs. (4.1), (4.2) and (4.4) by including additional surface terms on the boundaries associated with the entanglement wedge. Because these bulk boundaries vanish when the subregion expands to fill the entire Cauchy slice on the holographic boundary, these surface contributions would disappear, and one would still recover the original proposal for holographic complexity of a pure state. For example, in the subregion-CV conjecture, one could add an extra term proportional to the volume of HRT surface $\mathcal{E}_A$ to produce the revised conjecture,

$$\mathcal{C}'_{\text{V}}(\mathcal{A}) = \mathcal{C}_{\text{V}}(\mathcal{A}) + \eta\,\frac{\mathcal{V}(\mathcal{E}_{\mathcal{A}})}{4G_N}\,, \tag{4.7}$$

where $\mathcal{C}_{\rm V}(\mathcal{A})$ is the maximal volume expression in eq. (4.1) and η is a (dimensionless) constant that remains to be determined. Our normalization of the second term makes it clear that we are simply adding a term proportional to the entanglement entropy of the subregion $\mathcal{A}$, *i.e.*, $\mathcal{C}'_{\rm V}(\mathcal{A}) = \mathcal{C}_{\rm V}(\mathcal{A}) + \eta\, S_{\rm EE}(\mathcal{A})$. With this revised proposal, the form of the UV divergences becomes closer to that found with the subregion-CA and the subregion-CV2.0 approaches, *i.e.,* new subleading divergences associated with the boundary of $\mathcal{A}$ appear. Further, choosing a negative η will ensure that the inequality in eq. (4.6) is never saturated with $\mathcal{C}'_{\rm V}(\mathcal{A})$. On the other hand, if η is chosen to be positive, this revised proposal (4.7) will typically be superadditive (because the mutual complexity will be dominated by the subleading divergence associated with the $S_{\rm EE}(\mathcal{A})$ contribution). See section 6.3 for more discussion about this proposal.

4.2 Holographic Complexity of Thermal States

Here, we apply these holographic prescriptions to evaluate the complexity of the thermal state, *i.e.,* where the subregion is taken to be one boundary of an (uncharged) eternal black hole, and to evaluate the mutual complexity of the corresponding thermofield double state. This system was already studied in [171] and we review their results here.[4] The holographic calculation is performed for a two-sided AdS_{d+1} black hole with the boundary dimension $d \geq 2$ and with metric

$$ds^2 = \frac{L^2}{z^2}\left(-f(z)\,dt^2 + \frac{dz^2}{f(z)} + d\vec{x}^2\right), \qquad \text{where} \quad f(z) = 1 - \left(\frac{z}{z_0}\right)^d . \tag{4.8}$$

Note that the boundary and horizon geometries are taken to be flat in this geometry. This eternal black hole in the bulk is dual to a thermofield double state in the boundary theory with temperature $T = \frac{d}{4\pi z_0}$. As noted above, we choose the subregion to be a constant time slice on one of the boundaries and so the corresponding reduced state in the boundary theory is the thermal mixed state with the same temperature. With this choice, the HRT surface is simply the bifurcation surface on the horizon (which is reached with $z \to z_0$ holding t fixed), and the entanglement wedge is simply the static patch outside of the horizon, *i.e.,* $z \geq z_0$.

[4] Note that our notation, *e.g.,* in eqs. (4.9) and (4.12), is not identical to that in [171], however, our results are in complete agreement with theirs. The only exception is that we have accounted for a factor of 4 typo in the second term in eq. (2.17) of [171].

Subregion-CV: The result for subregion-CV (4.1), obtained in eq. (2.16) of [171], is

$$\mathcal{C}_{\rm V}(\mathcal{A}) = \frac{L^{d-1}}{(d-1)G_N}\,\frac{L}{\ell_{\rm bulk}}\,\frac{V(\mathcal{A})}{\delta^{d-1}} + b(d)\,\frac{L}{\ell_{\rm bulk}}\,S\,, \tag{4.9}$$

where $\ell_{\rm bulk}$ is the extra length scale appearing in eq. (4.1), and $V(\mathcal{A})$ is the spatial volume of the boundary theory. Further, $b(d)$ is a positive dimension-dependent coefficient given by

$$b(d) = 2\sqrt{\pi}\,\frac{d-2}{d-1}\,\frac{\Gamma(\frac{d+1}{d})}{\Gamma(\frac{d+2}{2d})}\,. \tag{4.10}$$

Hence the finite term in eq. (4.9) is positive and proportional to $S = \frac{L^{d-1}}{4G_N\, z_0^{d-1}}\,V(\mathcal{B})$, the black hole entropy. Of course, S can also be interpreted as the entropy of the thermal state in the boundary theory.

In the simplest situation where $t_{\rm L} = t_{\rm R} = 0$,[5] the mutual complexity (3.105) vanishes, *i.e.*,

$$\Delta\mathcal{C}_{\rm V} \equiv \mathcal{C}_{\rm V}(\mathcal{L}) + \mathcal{C}_{\rm V}(\mathcal{R}) - \mathcal{C}_{\rm V}(\mathcal{L}\cup\mathcal{R}) = 0\,, \tag{4.11}$$

because of the symmetry of the two-sided geometry. Hence, in this case, the inequality (4.6) is exactly saturated. More generally, the same result arises if we choose $t_{\rm L} + t_{\rm R} = 0$, which ensures that the full boundary state is still the TFD state without any additional time evolution. On the other hand, if we allow for some time evolution with t_L, $t_R > 0$, then $\mathcal{C}_{\rm V}(\mathcal{L})$ and $\mathcal{C}_{\rm V}(\mathcal{R})$ remain invariant while $\mathcal{C}_{\rm V}(\mathcal{L}\cup\mathcal{R})$ increases. Therefore the mutual complexity becomes negative, and the complexity of the time-evolved TFD state is superadditive.

Subregion-CA: The final result for subregion-CA (4.2) is[6]

$$\mathcal{C}_{\rm A}(\mathcal{A}) = a(d)\,\frac{L^{d-1}}{16\pi^2 G_N}\,\frac{V(\mathcal{A})}{\delta^{d-1}} - \frac{a(d)+g_0}{4\pi^2}\,S \tag{4.12}$$

where the constants, $a(d)$ and g_0, are given by

$$\begin{aligned} a(d) &= 4\,\ln\left[\frac{\ell_{\rm ct}}{L}(d-1)\right]\,, \\ g_0 &= 2\left[\psi_0(1) - \psi_0\left(\frac{1}{d}\right)\right]\,, \end{aligned} \tag{4.13}$$

[5] Here, $t_{\rm L}$ and $t_{\rm R}$ denote the times on the left and right boundaries, respectively.

[6] Compare to eq. (2.14) of [171].

with $\psi_0(z) = \Gamma'(z)/\Gamma(z)$. Note that g_0 is positive for $d > 1$ (while, of course, it vanishes for $d = 1$). The constant $a(d)$ involves the scale $\ell_{\rm ct}$ appearing in the boundary counterterm in the gravitational action (4.3) — see also eq. (4.27). Note that we must choose that $\ell_{\rm ct} > L/(d-1)$ to ensure that $a(d)$, and hence the complexity $\mathcal{C}_{\rm A}(\mathcal{B})$, is positive. Therefore, the finite contribution in eq. (4.12) is negative and proportional to the entropy of the thermal state.

Using the subregion-CA approach, the mutual complexity (3.106) for the TFD state with $t_{\rm L} = t_{\rm R} = 0$ becomes[7]

$$\Delta\mathcal{C}_{\rm A} \equiv \mathcal{C}_{\rm A}(\mathcal{L}) + \mathcal{C}_{\rm A}(\mathcal{R}) - \mathcal{C}_{\rm A}(\mathcal{L}\cup\mathcal{R}) = -\frac{g_d}{2\pi^2}\, S \tag{4.14}$$

where

$$g_d = a(d) + g_0 + 4\pi\,\frac{d-1}{d}\,. \tag{4.15}$$

Since each of the terms contributing to g_d is itself positive, the mutual complexity is negative and hence the complexity of the TFD state is superadditive. If we evolve the system forward in time with $t_{\rm L}$, $t_{\rm R} > 0$, then $\mathcal{C}_{\rm A}(\mathcal{L})$ and $\mathcal{C}_{\rm A}(\mathcal{R})$ are again invariant while generally $\mathcal{C}_{\rm A}(\mathcal{L}\cup\mathcal{R})$ increases. A detailed analysis [110] shows that the complexity remains constant up to a critical time, at which point it briefly dips down slightly before beginning to grow linearly. We show in appendix B that the mutual complexity will remain negative even in this short time period where $\mathcal{C}_{\rm A}(\mathcal{L}\cup\mathcal{R})$ decreases from its value at $t = 0$ and therefore the complexity of the time-evolved TFD state is always superadditive as well.

Subregion-CV2.0: It is easy to extract the results for the subregion-CV2.0 using eq. (4.5). Some results for the bulk portion of the gravitational action appear in eqs. (2.26), (B.10) and (B.16) of [171]. After accounting for the relevant proportionality factor, we obtain

$$C_{\rm V2.0}(\mathcal{A}) = \frac{2\,V(\mathcal{A})L^{d-1}}{d(d-1)G_N}\left(\frac{1}{\delta^{d-1}} - \frac{1}{z_0^{d-1}}\right), \tag{4.16}$$

for the complexity of the thermal state, and

$$\Delta C_{\rm V2.0} = -\frac{16}{d}\left(\frac{1}{d-1} + \frac{\pi}{d}\,\cot\frac{\pi}{d}\right) S\,, \tag{4.17}$$

for the mutual complexity. This result for the mutual complexity is once again negative for $d \geq 2$, and this means that the complexity of the TFD state according to the subregion-CV2.0 proposal is again superadditive. We also note that, as with the other proposals, the mutual complexity is proportional to the entropy.

[7] Again, we may choose $t_{\rm L} + t_{\rm R} = 0$ more generally. This result appears in eqs. (2.7)-(2.8) of [171].

4.3 Holographic Complexity of Vacuum Subregions

4.3.1 Holographic Complexity in the Poincaré Patch

In this section, we summarize and extend the results in the literature regarding subregion complexity in holography. We start by summarizing the volume results from [114, 180] for a ball-shaped subregion in general dimensions. After that, we discuss the subregion-CA complexity in the Poincaré patch, regulated in such a way that the WDW patch starts at the cutoff surface $z = \delta$ in Fefferman-Graham coordinates. This calculation was outlined in [114]. However, at the time the paper was written it was still not clear if the counterterm restoring reparametrization invariance is an essential ingredient of the complexity=action proposal. This later became clear, among other things, due to the fact that the counterterm is essential for obtaining the expected behavior in the presence of shocks, see [111, 112]. We briefly review the results of [114] and then extend them to include the counter term.

4.3.1.1 Subregion-CV

Here we summarize the results of [180] (see eq. (5)-(7)) as well as [114] (see eq. (4.9)) for the subregion complexity using the CV conjecture for a ball shaped region on the boundary of AdS_{d+1} in Poincaré coordinates. The bulk spacetime is described by the metric

$$ds^2 = \frac{L^2}{z^2}\left[dz^2 - dt^2 + d\rho^2 + \rho^2 d\Omega_{d-2}^2\right]. \tag{4.18}$$

For a ball-shaped region on a constant time slice with $\rho \leq R$, the complexity is given by performing the following integral

$$C_{\text{V}} = \frac{L^{d-1}\Omega_{d-2}}{(d-1)G_N}\int_{\delta}^{R} dz \frac{(R^2 - z^2)^{\frac{d-1}{2}}}{z^d} \tag{4.19}$$

where $\Omega_{d-2} = 2\pi^{\frac{d-1}{2}}/\Gamma\left(\frac{d-1}{2}\right)$ is the volume of the S^{d-2} sphere and R is the radius of the ball (or half the size of the interval for a two dimensional boundary). The explicit results of this integration for $d = 2$ (AdS_3) and $d = 3$ (AdS_4) are presented in the next section in eqs. (4.33) and (4.34).

4.3.1.2 Subregion-CA

The form of the intersection $\widetilde{W}$ between the WDW patch (starting at the cutoff surface) and the entanglement wedge is illustrated in figure 4.1, together with its projection on the

$t = 0$ time slice, where we label the various surfaces and joints required for the calculation. The region $\widetilde{W}$ is bounded by four surfaces. $S^{\pm}$ are the boundaries of the WDW patch and $C^{\pm}$ are the boundaries of the entanglement wedge. They are described by the following constraints

$$S^{\pm}: \quad t = \pm(z - \delta), \qquad C^{\pm}: \quad t = \pm(R - \sqrt{\rho^2 + z^2}), \tag{4.20}$$

where R is the radius of the ball shaped subregion for which we evaluate the complexity. The affinely parameterized normals to the various surfaces are[8]

$$S^{\pm}: \quad k_{1,2} = \alpha(-dt \pm dz), \qquad C^{\pm}: \quad k_{3,4} = \beta\left(-dt \mp \frac{\rho d\rho + z dz}{\sqrt{\rho^2 + z^2}}\right). \tag{4.21}$$

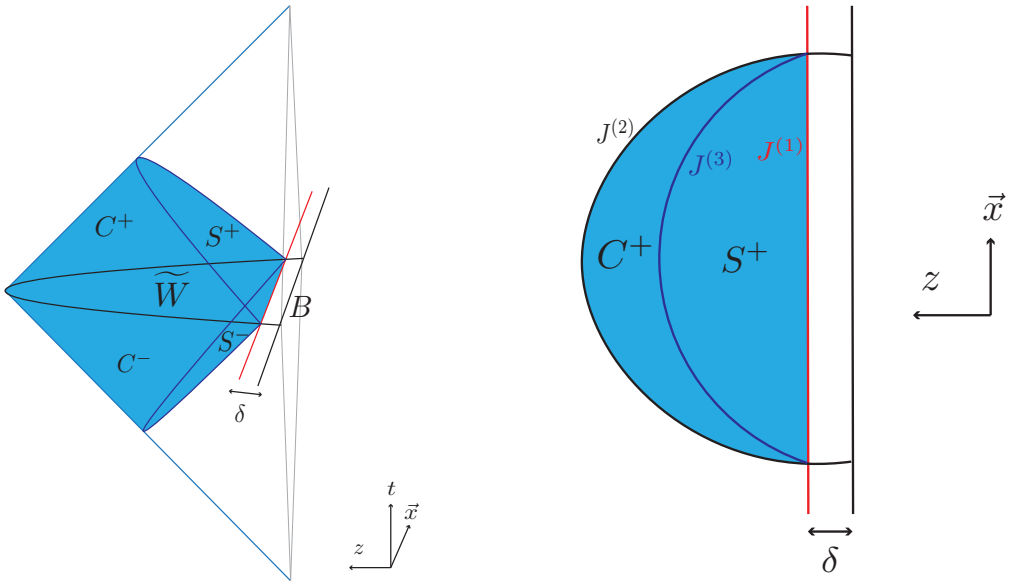

Figure 4.1: The intersection of the entanglement wedge and the WDW patch defines the region $\widetilde{\mathcal{W}}$ that is relevant for the evaluation of $\mathcal{C}_{\text{A}}(B)$.

The subregion-CA conjecture consists of evaluating the gravitational action of the region $\widetilde{W}$. When the normals to the null surfaces are affinely parametrized the relevant contributions are: the bulk contribution I_{bulk}, the joints $J^{(1)}$, $J^{(2)}$ and (twice) $J^{(3)}$ (see figure 4.1), whose contributions we label $I^{(1)}$, $I^{(2)}$ and $I^{(3)}$, respectively, and finally the counterterm contribution required to render the result independent of the normalization

[8]Here we chose the direction such that the normal vectors are future oriented, in order to be consistent with the conventions of appendix C of [134] which we use throughout the following.

constants α and β. Since the boundary of the entanglement wedge is a killing horizon with vanishing expansion [34, 50] we only have to include the counter term on the boundaries of the WDW patch $S^{\pm}$. Finally the complexity is given by

$$\mathcal{C}_{\rm A}(B) = \frac{1}{\pi}\left(I_{\rm bulk} + I^{(1)} + I^{(2)} + 2I^{(3)} + 2I_{\rm ct}\right). \tag{4.22}$$

Most of the contributions above were already evaluated in [134] and we quote the results here (fixing a few small typos). For the bulk contribution we have

$$I_{\rm bulk} = -\frac{d\,\Omega_{d-2}L^{d-1}}{4\pi G_{\rm N}}\int_0^{\frac{R-\delta}{2}} dt\int_{t+\delta}^{R-t}\frac{dz}{z^{d+1}}\frac{((R-t)^2-z^2)^{\frac{d-1}{2}}}{d-1}. \tag{4.23}$$

For the various joints we have[9]

$$\begin{aligned}
I^{(1)} &= -\frac{\Omega_{d-2}L^{d-1}}{4\pi(d-1)G_{\rm N}}\frac{(R^2-\delta^2)^{\frac{d-1}{2}}}{\delta^{d-1}}\ln\left(\frac{\alpha\delta}{L}\right),\\
I^{(2)} &= -\frac{L^{d-1}\Omega_{d-2}}{4\pi G_{\rm N}}\int_\delta^R\frac{dz}{z^{d-1}}R(R^2-z^2)^{\frac{d-3}{2}}\ln\left(\frac{\beta z}{L}\right),\\
I^{(3)} &= \frac{L^{d-1}\Omega_{d-2}}{8\pi G_{\rm N}}\int_\delta^{\frac{R+\delta}{2}}\frac{d\bar{z}}{\bar{z}^{d-1}}(R+\delta)^{\frac{d-1}{2}}(R+\delta-2\bar{z})^{\frac{d-3}{2}}\ln\left(\frac{\alpha\beta\bar{z}^2(R+\delta)}{2L^2(R+\delta-\bar{z})}\right),
\end{aligned} \tag{4.24}$$

where in $I^{(3)}$ we have relabeled the integration variable as $\bar{z}$ for reasons that will become clear in a moment. Recall that the boundaries of the WDW patch had vanishing expansion and so no counterterm was needed in order to cancel the dependence on the normalization constant β. To make this observation manifest let us use the following change of variables

$$\bar{z} = \frac{z(R+\delta)}{R+z}, \qquad z = \frac{R\,\bar{z}}{R+\delta-\bar{z}}, \tag{4.25}$$

which relabels the various points on the joint $J^{(3)}$ by the corresponding value of z on the joint $J^{(2)}$ along the same light ray originating from the point $z=\rho=0$, $t=R$. After this change of variables we are able to combine the contributions of the joints $J^{(2)}$ and $J^{(3)}$ as follows

$$I^{(2)} + 2I^{(3)} = \frac{L^{d-1}\Omega_{d-2}}{4\pi G_{\rm N}}\int_\delta^R\frac{dz}{z^{d-1}}R\,(R^2-z^2)^{\frac{d-3}{2}}\ln\left(\frac{\alpha z(R+\delta)^2}{2(R+z)LR}\right), \tag{4.26}$$

[9] We have fixed the following factors: overall factor of R in $I^{(2)}$ was missing, upper limit of integration in $I^{(3)}$ was changed to $\frac{R+\delta}{2}$.

where we see explicitly that all the dependence on β canceled out.

Next, we evaluate the contribution of the counterterm. We remind the readers the definition of the counterterm [134]

$$I_{\rm ct} = -\frac{1}{8\pi G_{\rm N}} \int d\lambda\, d^{d-1}x \sqrt{\gamma}\, \Theta \ln\left(\ell_{\rm ct}|\Theta|\right), \tag{4.27}$$

where the expansion parameter is $\Theta = \partial_\lambda \ln\sqrt{\gamma}$, γ is the metric on the light surface modulo light rays and $\ell_{\rm ct}$ is an arbitrary constant representing the freedom in the definition of this counter term. First, we identify the light-ray parameter $\lambda = -L^2/\alpha z$, which is consistent with the normal definition $k_1^\mu = dx^\mu/d\lambda$, see eq. (4.21), along the surface S^+, see eq. (4.20). We then evaluate the expansion

$$\Theta = \partial_\lambda \ln\sqrt{\gamma} = -\frac{\alpha(d-1)z}{L^2}. \tag{4.28}$$

Finally the counter term contribution reads

$$I_{\rm ct} = \frac{\Omega_{d-2}L^{d-1}}{8\pi G_{\rm N}} \int_\delta^{\frac{R+\delta}{2}} \frac{d\bar{z}}{\bar{z}^d} (R+\delta)^{\frac{d-1}{2}} (R+\delta-2\bar{z})^{\frac{d-1}{2}} \ln\left(\frac{\ell_{\rm ct}\,\alpha(d-1)\bar{z}}{L^2}\right). \tag{4.29}$$

Once again, it will be useful to use the change of coordinates (4.25), which brings this contribution to the form

$$I_{\rm ct} = \frac{\Omega_{d-2}L^{d-1}}{8\pi G_{\rm N}} \int_\delta^{R} \frac{dz}{z^d} R\,(R+z)^{\frac{d-3}{2}} (R-z)^{\frac{d-1}{2}} \ln\left(\frac{\ell_{\rm ct}\,\alpha(d-1)z(R+\delta)}{L^2(R+z)}\right). \tag{4.30}$$

Combining all the joints and the counter term and using integration by parts together with the identity $\int \frac{dz}{z^d} R^2 (R^2-z^2)^{\frac{d-3}{2}} = -\frac{1}{z^{d-1}} \frac{(R^2-z^2)^{\frac{d-1}{2}}}{d-1}$ finally yields

$$\begin{aligned} I_{\rm s,j,ct} \equiv 2I_{\rm ct} + I^{(1)} + I^{(2)} + 2I^{(3)} = \frac{\Omega_{d-2}L^{d-1}}{4\pi G_{\rm N}} \int_\delta^R dz \frac{R\,(R^2-z^2)^{\frac{d-3}{2}}}{z^{d-1}} \times \\ \times \left[\frac{(R-z)}{z}\left[\frac{1}{(d-1)} + \ln\left(\frac{\ell_{\rm ct}(d-1)}{L}\right)\right] + \ln\left(\frac{R+\delta}{2R}\right)\right], \end{aligned} \tag{4.31}$$

and we see that all the dependence on α has canceled. The final result for the complexity is then given by combining eqs. (4.23) and (4.31), *i.e.*,

$$\mathcal{C}_{\rm A} = \frac{1}{\pi}\left(I_{\rm bulk} + I_{\rm s,j,ct}\right). \tag{4.32}$$

We evaluated this expression explicitly for the cases of $d = 2$ and $d = 3$ and the final results are given by eqs. (4.35) and (4.38).

4.3.2 Holographic Complexity of Vacuum Subregions

Below we summarize the results from all three approaches for a subregion of the CFT vacuum in two dimensions, *i.e.,* an interval in the boundary of AdS_3. These are the holographic results that are most relevant for the comparison with the QFT results in section 3.5. We also consider a disk-shaped subregion in the CFT vacuum in three dimensions, *i.e.,* on the boundary of AdS_4, to gain some intuition about the behaviour with an odd number of boundary dimensions.

Subregion-CV: With the subregion-CV approach for the case of AdS_3, both in global coordinates and in the Poincaré patch, we have

$$AdS_3, \text{G/P} : \quad \mathcal{C}_{\text{V}}(\mathcal{A}) = \frac{2c}{3}\left(\frac{\ell}{\delta} - \pi\right) \tag{4.33}$$

where $c = 3L/(2G_{\text{N}})$ is the central charge of the two-dimensional boundary CFT [206], ℓ is the size of the interval and δ is the UV cutoff. For global coordinates in AdS_3, this result comes from [147], and for the Poincaré patch, it was found in [180]. The constant term (*i.e.,* $-\pi$) is a topological term studied in [147].

For a ball-shaped subregion with radius R on the boundary of AdS_{d+1}, the calculation of $\mathcal{C}_V$ is outlined in eqs. (5) and (7) of [180] — see also eq. (4.9) of [114] and our eq. (4.19). For example, for the case of a disk on the boundary of AdS_4, one obtains

$$AdS_4, \text{P} : \quad \mathcal{C}_{\text{V}}(\mathcal{A}) = \frac{\pi^4 c_T}{3}\left(\frac{R^2}{2\delta^2} - \ln\left(\frac{R}{\delta}\right) - \frac{1}{2}\right) \tag{4.34}$$

where $c_T = 3L^2/(\pi^3 G_{\text{N}})$ is the central charge appearing in the OPE of two stress tensors in the boundary theory, *e.g.,* see [207].

Subregion-CA: Next, we turn to the subregion-CA results. For the case of a flat boundary (in the Poincaré patch), the divergence structure of the subregion complexity in vacuum AdS was studied in [114]. However, these results did not include the boundary counterterms I_{ct}, which restore the reparametrization invariance on the null surfaces. We evaluated the contribution of I_{ct} in our calculations in the last subsection 4.3.1. We have also corrected a number of typos in the original calculation of [114], and explicitly demonstrated the cancellation of the normalization constants of the null normals. Combining eqs. (4.23), (4.31) and (4.32) for the case of AdS_3 yields

$$AdS_3, \text{P} : \quad \mathcal{C}_{\text{A}}(\mathcal{A}) = \frac{c}{3\pi^2}\left(\frac{\ell}{2\delta}\ln\left(\frac{\ell_{\text{ct}}}{L}\right) - \ln\left(\frac{2\ell_{\text{ct}}}{L}\right)\ln\left(\frac{\ell}{\delta}\right) + \frac{\pi^2}{8}\right), \tag{4.35}$$

where ℓ is again the size of the boundary interval. Further, we note that the UV divergences were regulated in the above calculation by anchoring the WDW patch at the UV cutoff surface. Repeating these calculations in global coordinates [162], we find[10]

$$\mathrm{AdS}_3, \mathrm{G}: \quad \mathcal{C}_{\mathrm{A}}(\mathcal{A}) = \frac{c}{3\pi^2}\left(\frac{\ell}{2\delta}\,\ln\left(\frac{\ell_{\mathrm{ct}}}{L}\right) - \ln\left(\frac{2\ell_{\mathrm{ct}}}{L}\right)\ln\left(\frac{C}{\delta}\right)\right) + f(\ell/C)\,, \tag{4.36}$$

where C is the circumference of a time slice on the boundary. Here, $f(\ell/C)$ is some finite contribution, whose precise form we did not determine analytically. However, we do know that in the limit $\ell/C \to 0$, eq. (4.36) should reduce to the previous expression in eq. (4.35) and hence

$$\frac{\ell}{C} \ll 1 \;:\quad f(\ell/C) \simeq \frac{c}{3\pi^2}\left(\ln\left(\frac{2\ell_{\mathrm{ct}}}{L}\right)\ln\left(\frac{C}{\ell}\right) + \frac{\pi^2}{8}\right) + \mathcal{O}(\ell/C)\,. \tag{4.37}$$

For more discussion about this finite part, see the discussion section in [2].

For a disk-shaped region (of radius R) on the boundary of AdS_4 using Poincaré coordinates, we obtain

$$\mathrm{AdS}_4, \mathrm{P}: \; \mathcal{C}_{\mathrm{A}}(\mathcal{A}) = \frac{\pi^2 c_T}{12}\left(\frac{R^2}{\delta^2}\ln\left(\frac{2\ell_{\mathrm{ct}}}{L}\right) - \frac{2R}{\delta}\ln\left(\frac{4\ell_{\mathrm{ct}}}{L}\right) + 2\ln\frac{R}{\delta} + \ln\left(\frac{\ell_{\mathrm{ct}}}{2L}\right)\right). \tag{4.38}$$

This calculation can also be seen as the smooth limit of the result obtained in [198] for subregions with kinks/corners, *i.e.,* compare with eq. (5.8) of [198].

Subregion-CV2.0: Again, it is straightforward to extract the results for the subregion-CV2.0 proposal using eq. (4.5). We have the results for the bulk portion of the gravitational action in eq. (4.23) for AdS_3 in Poincaré coordinates (*i.e.,* $d = 2$) and so after accounting for the relevant proportionality factor we obtain

$$\mathrm{AdS}_3, \mathrm{P}: \quad \mathcal{C}_{\mathrm{V2.0}}(\mathcal{A}) = \frac{4\,c}{3}\left(\frac{\ell}{2\delta} - \ln\frac{\ell}{\delta} - \frac{\pi^2}{8}\right). \tag{4.39}$$

[10] We note that this result can be obtained either by anchoring the WDW patch at the cutoff surface, or by anchoring it at the boundary of AdS_3 (as in [162]) but adding the usual counterterms of the kind often used in holographic renormalization (*e.g.,* see [208]) on the cutoff surface.

Further the analogous result for AdS_3 in global coordinates [162],[11]

$$AdS_3, G: \quad \mathcal{C}_{V2.0}(\mathcal{A}) = \frac{4\,c}{3}\left(\frac{\ell}{2\delta} - \ln\frac{C}{\delta}\right) + \tilde{f}(\ell/C)\,, \tag{4.41}$$

where C is again the circumference of a time slice on the boundary and $\tilde{f}(\ell/C)$ is a finite contribution. We return to examine this contribution in more detail in section 6.3. However, let us observe here that in the limit $\ell/C \to 0$, eq. (4.41) must reduce to the previous expression in eq. (4.39) and hence we expect to find

$$\frac{\ell}{C} \ll 1 \;: \quad \tilde{f}(\ell/C) \simeq \frac{4\,c}{3}\left(\ln\left(\frac{C}{\ell}\right) - \frac{\pi^2}{8}\right) + \mathcal{O}(\ell/C)\,. \tag{4.42}$$

We can also use eq. (4.23) to evaluate the complexity for a disk-shaped region on the boundary of AdS_4 in Poincaré coordinates,

$$AdS_4, P: \quad \mathcal{C}_{V2.0}(\mathcal{A}) = \frac{\pi^4 c_T}{9}\left(\frac{R^2}{\delta^2} - \frac{2R}{\delta} - 4\ln\frac{R}{4\delta} + 1\right)\,. \tag{4.43}$$

With all three proposals, the leading divergence is proportional to the volume of the boundary region $V(\mathcal{A})$, *i.e.*, $V(\mathcal{A}) = \ell$ with $d = 2$ while $V(\mathcal{A}) = \pi R^2$ with $d = 3$. However, the subleading divergences are quite different for subregion-CV compared to subregion-CA and subregion-CV2.0. With either of the latter two, the subleading contribution is a negative term proportional to the area of the boundary of $\mathcal{A}$, *e.g.*, $V(\partial\mathcal{A}) = 2\pi R$ with $d = 3$. In contrast, no comparable contribution appears in the subregion-CV results. Similar boundary contributions with a negative sign were found in [198] for subregion-CA. Such subleading divergences appear to be a generic feature of both the subregion-CA and subregion-CV2.0 approaches, and can be understood as a contribution to the complexity proportional to the entanglement entropy [209] – see also the discussion around eq. (4.7).[12]

[11] This result was obtained by anchoring the WDW patch at the cutoff surface. The result for another regularization scheme where the WDW patch is anchored at the boundary of AdS_3 can be read from eq. (B.18) of [162]

$$AdS_3, G: \quad \mathcal{C}_{V2.0}(\mathcal{A}) = \frac{4}{3}c\left(\frac{\ell}{\delta} - \ln\frac{\ell}{\delta} + \text{finite}\right), \tag{4.40}$$

where we notice that the leading divergence has changed by a factor of 2, however, the universal logarithmic piece remains unchanged.

[12] We should also mention that additional relations between the entanglement entropy and complexity for AdS_3/CFT_2 using the complexity=volume proposal have been developed in the context of the kinematic space in [147, 197], see, *e.g.*, eqs. (46) and (4.6), respectively.

Mutual Complexity: Now we can use the previous results together with the results for the complexity of the full boundary time slice to evaluate the mutual complexity. The first observation is that in our examples here, we are considering the vacuum state and subregions of the vacuum for the boundary CFT on a constant time slice. Hence for the CV and subregion-CV proposals, the maximal volume slices also all lie in the constant time slice in the bulk. Hence the two bulk volumes corresponding to a subregion and its complement precisely add up to equal the volume for the full vacuum state. That is, we are in a situation where we saturate the inequality in eq. (4.6) and the mutual complexity vanishes.[13] Of course, if we choose to examine the vacuum state on a more general Cauchy slice in the boundary, we expect the mutual complexity to be negative, *i.e.,* the complexity would be superadditive. It would be interesting to understand the precise form of $\Delta\mathcal{C}_V$ in these situations.

The results are more interesting for the CA and CV2.0 proposals. Here we will focus our discussion on the case of a flat boundary, *i.e.,* with Poincaré coordinates in the bulk, since they are easily generalized to higher dimensions. We illustrate the discussion with the example of AdS_4, where we begin by evaluating the complexity of the full vacuum state (see the appendix D in [2]), *i.e.,*

$$\begin{aligned} AdS_4, P: \quad \mathcal{C}_{A}(\text{vac}) &= \frac{\pi\, c_T}{12}\frac{V(\Sigma)}{\delta^2}\,\ln\frac{2\ell_{ct}}{L}\,, \\ AdS_4, P: \quad \mathcal{C}_{V2.0}(\text{vac}) &= \frac{\pi^3 c_T}{9}\frac{V(\Sigma)}{\delta^2}\,, \end{aligned} \tag{4.44}$$

where $V(\Sigma)$ is the spatial volume of the entire time slice in the boundary.[14] Next, we gave the results for a disk-shaped region in eqs. (4.38) and (4.43) for the subregion-CA and subregion-CV2.0, respectively, which we re-express here as

$$\begin{aligned} AdS_4, P: \quad \mathcal{C}_{A}(\mathcal{A}) &= \frac{\pi\, c_T}{12}\left(\frac{V(\mathcal{A})}{\delta^2}\,\ln\left(\frac{2\ell_{ct}}{L}\right) - \frac{V(\partial\mathcal{A})}{\delta}\ln\left(\frac{4\ell_{ct}}{L}\right) + 2\pi\,\ln\frac{L}{\delta} + \text{finite}\right)\,, \\ AdS_4, P: \quad \mathcal{C}_{V2.0}(\mathcal{A}) &= \frac{\pi^3 c_T}{9}\left(\frac{V(\mathcal{A})}{\delta^2} - \frac{V(\partial\mathcal{A})}{\delta} - 4\pi\,\ln\frac{L}{\delta} + \text{finite}\right)\,, \end{aligned} \tag{4.45}$$

where $V(\mathcal{A}) = \pi R^2$ is the area of the disk and $V(\partial\mathcal{A}) = 2\pi R$ is the circumference of the boundary of the disk. This leaves us to evaluate the complexity of the exterior of the disk, which we denote $\mathcal{B}$. While this calculation may seem more formidable because $\mathcal{B}$ has an infinite extent in this flat boundary geometry, the geometric interpretation of

[13] As for the previous discussion of the CV proposal for the TFD state with $t_L = 0 = t_R$.

[14] In fact, the time slice is two-dimensional and so $V(\Sigma)$ is an area in this specific example.

the two leading singularities would be precisely as in eq. (4.45). Further, we would have $V(\mathcal{A}) + V(\mathcal{B}) = V(\Sigma)$ and $V(\partial\mathcal{A}) = V(\partial\mathcal{B})$ and hence the mutual complexity becomes

$$\begin{aligned} \text{AdS}_4, \text{P}: \qquad \Delta\mathcal{C}_{\text{A}} &= -\frac{\pi\, c_T}{6} \ln\left(\frac{4\ell_{\text{ct}}}{L}\right) \frac{V(\partial\mathcal{A})}{\delta} + \cdots, \\ \text{AdS}_4, \text{P}: \qquad \Delta\mathcal{C}_{\text{V2.0}} &= -\frac{2\pi^3 c_T}{9} \frac{V(\partial\mathcal{A})}{\delta} + \cdots. \end{aligned} \tag{4.46}$$

In fact, this result can be extended to any (smooth) bipartition of the two-dimensional time slice in the boundary theory, and $V(\partial\mathcal{A})$ will denote the length of the boundary between the subregion $\mathcal{A}$ and its complement $\mathcal{B}$. Given the sign of the results above, we see that the complexity of the vacuum is superadditive for both the subregion-CA and subregion-CV2.0 approaches. We might also note that the leading singularity in eq. (4.46) has the same form as that in the entanglement entropy for the same bipartition. Hence, at least to leading order here, the mutual complexity is again proportional to the entanglement entropy between the two subregions.

Using the results of appendix 4.3.1 and of [114], these calculations are easily extended to higher dimensions, where we find for $d > 2$

$$\begin{aligned} \text{AdS}_{d+1}, \text{P}: \qquad \Delta\mathcal{C}_{\text{A}} &= -\frac{L^{d-1}}{2\pi^2(d-2)G_N} \ln\left(\frac{2(d-1)\ell_{\text{ct}}}{L}\right) \frac{V(\partial\mathcal{A})}{\delta^{d-2}} + \cdots, \\ \text{AdS}_{d+1}, \text{P}: \qquad \Delta\mathcal{C}_{\text{V2.0}} &= -\frac{4L^{d-1}}{d(d-1)(d-2)G_N} \frac{V(\partial\mathcal{A})}{\delta^{d-2}} + \cdots. \end{aligned} \tag{4.47}$$

Of course, using our previous results for subregions on the boundary of AdS_3, these calculations are easily extended to $d = 2$. In this case, we find that the mutual complexity becomes

$$\begin{aligned} \text{AdS}_3, \text{P}: \qquad \Delta\mathcal{C}_{\text{A}} &= -\frac{2\,c}{3\pi^2} \ln\left(\frac{2\ell_{\text{ct}}}{L}\right) \ln\frac{\ell}{\delta} + \cdots, \\ \text{AdS}_3, \text{P}: \qquad \Delta\mathcal{C}_{\text{V2.0}} &= -\frac{8\,c}{3} \ln\frac{\ell}{\delta} + \cdots. \end{aligned} \tag{4.48}$$

Hence these general results again show that the mutual complexity is negative and hence that the complexity of the vacuum state is superadditive. We may also note that to leading order, the mutual complexity is proportional to the entanglement entropy of the subregions.

Chapter 5

Purification Complexity without Purification

In chapter 2, we have reviewed various proposals toward defining the computational complexity of states in quantum field theory, *e.g.,* Nielsen's geometric approach [59–62] in section 2.1.1, the Fubini-Study metric approach [69] in section 2.1.2 and path-integral complexity [92, 93] in section 2.1.3. In light of the definitions for the complexity between two pure states, it is natural to generalize it to the case of mixed states. More explicitly, we focus on exploring the mixed-state complexity between arbitrary quantum states, *viz.*

$$\mathcal{C}\left(\hat{\sigma}_{\mathrm{R}}, \hat{\rho}_{\mathrm{T}}\right) : \hat{\sigma}_{\mathrm{R}} \longrightarrow \hat{\rho}_{\mathrm{T}} \,, \tag{5.1}$$

in this thesis. Different from the complexity of pure states, *i.e.,* $\mathcal{C}\left(\left|\Phi_{\mathrm{R}}\right\rangle, \left|\Psi_{\mathrm{T}}\right\rangle\right)$ for which the unitary operations are sufficient to construct the transformation from a reference state to a target state, we need to introduce non-unitary operations if the target state is a mixed state in the Hilbert space $\mathcal{H}_{\mathcal{A}}$, *e.g.,* the quantum states associated with a subregion in QFT. The non-unitary operations call for the ancillae. In order to respect unitary evolution, we can consider complexity for purified states with the help of an auxiliary system $\mathcal{H}_{\mathcal{A}^c}$. More generally, we can also start from a purified reference state if it is also not pure. In light of the non-uniqueness of the purification, a natural definition of mixed-state complexity between the reference $\hat{\sigma}_{\mathrm{R}}$ and the target state $\hat{\rho}_{\mathrm{T}}$ is called *purification complexity* $\mathcal{P}$ that is defined to be [1]

$$\begin{aligned} &\mathcal{P}\left(\hat{\sigma}_{\mathrm{R}}, \hat{\rho}_{\mathrm{T}}\right) \equiv \min_{\Phi} \min_{\Psi} \mathcal{C}\left(\left|\Phi_{\mathrm{R}}\right\rangle, \left|\Psi_{\mathrm{T}}\right\rangle\right) \,, \\ \text{with} \qquad &\mathrm{Tr}\left(\left|\Phi_{\mathrm{R}}\right\rangle\left\langle\Phi_{\mathrm{R}}\right|\right) = \hat{\sigma}_{\mathrm{R}} \,, \quad \mathrm{Tr}\left(\left|\Psi_{\mathrm{T}}\right\rangle\left\langle\Psi_{\mathrm{T}}\right|\right) = \hat{\rho}_{\mathrm{T}} \,, \end{aligned} \tag{5.2}$$

[1] To avoid confusion in this chapter, we refer to a new notation $\mathcal{P}$ as the purification complexity.

where the minimization is performed over all possible purifications $|\Phi_{\mathrm{R}}\rangle, |\Psi_{\mathrm{T}}\rangle$ of $\hat{\sigma}_{\mathrm{R}}, \hat{\rho}_{\mathrm{T}}$, respectively, and $\mathcal{C}$ denotes a specific pure-state complexity we are interested in. Taking Nielsen's geometric method, the purification complexity of Gaussian mixed states with F_1 cost functions has been explored in [2] as described in chapter 3.

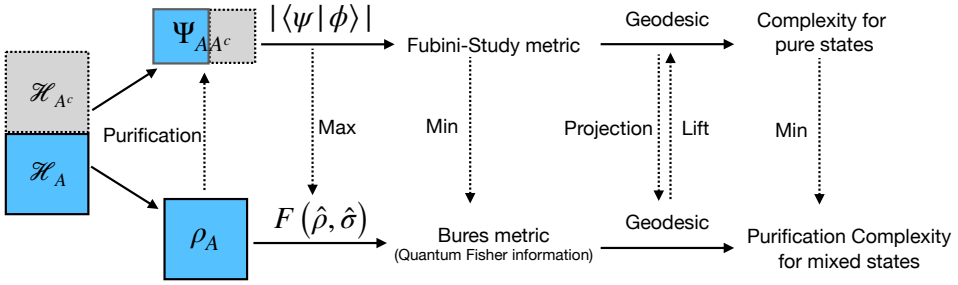

Figure 5.1: The connections between pure-state complexity from the Fubini-Study metric and purification complexity derived from the Bures metric (or quantum Fisher information metric). The Hilbert space consisting of quantum states $\hat{\rho}_{\mathcal{A}}$ that we are interested in is denoted by $\mathcal{H}_{\mathcal{A}}$ and the extended Hilbert space with introducing auxiliary system is represented by $\mathcal{H}_{\mathcal{A}} \otimes \mathcal{H}_{\mathcal{A}^c}$.

However, purification complexity is based on the triple minimizations. First of all, we need to minimize all paths to find the optimal circuit for a given purified reference state and target state. Second, we also have to search for the optimal purifications twice by minimizing the complexity for all free parameters due to the freedom in purification. With these tips from the purification complexity based on Nielsen's geometric method, it is natural to explore a similar purification complexity by taking account of the Fubini-Study metric as the complexity measure for purified states. As shown in chapter 3, finding the optimal purification for mixed states in QFT is a challenging task even for Gaussian states due to the huge number of free parameters in purification. See also [188] for the optimal purification with respect to F_2 cost function.

In view of the difficulties in the minimization for purification complexity, it would be great to find a better way to deal with the optimization explicitly. On the other hand, one may also wonder how to generalize the Fubini-Study metric method for pure-state complexity to arbitrary quantum states $\hat{\rho}_{\mathcal{A}}$, *i.e.,* defining the geodesic distance in the space of density matrices equipped with a special metric as the complexity measure for mixed states. Different from pure states where the Fubini-Study metric serves as one unique definition [210], there are too many similar definitions of finite distance and also corresponding local metrics for mixed states [42, 210, 211]. In this chapter, we propose to

consider the dubbed **Bures metric** or **quantum Fisher information metric** (QFIM) as the complexity measure for generic quantum states. Thanks to Uhlmann's fidelity theorem [42,212], we find that the complexity from the quantum Fisher information metric can be exactly explained as the purification complexity $\mathcal{P}$ with the Fubini-Study metric acting as the complexity measure of purified states. Consequently, our proposal avoids the explicit process for purification and also minimization. As an overview, the connections are summarized in figure 5.1.

This chapter is adapted from [3].

5.1 Uhlmann's fidelity and Quantum Fisher Information Metric

Stating from a family of pure states $|\Psi(\lambda)\rangle$ with parameters λ^μ, one can derive the quantum information metric (fidelity susceptibility) $g_{\mu\nu}$, *e.g.,* [42, 213] by

$$F(\lambda, \lambda + d\lambda) = 1 - \frac{1}{2} g_{\mu\nu}\, d\lambda^\mu\, d\lambda^\nu + \mathcal{O}(d\lambda^3)\,, \tag{5.3}$$

where $F(\lambda, \lambda')$ is the quantum fidelity defined as the inner product between two states, *i.e.,* $F(\lambda, \lambda') = |\langle\Psi(\lambda)|\Psi(\lambda')\rangle|$. It is known that Fubini-Study metric $g^{\text{FS}}_{\mu\nu}$ defined in eq. (2.23) agrees with the quantum information metric for pure states. In the sense of distance, one can consider $g^{\text{FS}}_{\mu\nu}$ as the infinitesimal version of the finite distance $(1 - F(\lambda, \lambda'))$ between arbitrary two pure states $|\Psi(\lambda)\rangle\,, |\Psi(\lambda')\rangle$. As reviewed in section 2.1.2, the Fubini-Study metric approach [69] identifies the complexity of pure states as the length of the geodesic $\lambda^\mu(s)$ connecting a reference state $|\Phi_{\text{R}}\rangle$ and a target state $|\Psi_{\text{R}}\rangle$, *i.e.,*

$$\mathcal{C}_{\text{FS}}\left(|\Phi_{\text{R}}\rangle\,, |\Psi_{\text{R}}\rangle\right) = \int_0^1 d\sigma\, \sqrt{2 g^{\text{FS}}_{\mu\nu}\left(\lambda\right)\, \dot{\lambda}^\mu\, \dot{\lambda}^\nu}\,, \tag{5.4}$$

where the boundary conditions are determined by the reference state and target state, $\dot{\lambda}^\mu(\sigma) = \frac{d\lambda^\mu(\sigma)}{d\sigma}$ denotes the tangent vector to the trajectory. It noted that we artificially add a factor 2 to make this definition consistent with the results from the F_2 norm in Nielson's geometric method [1] for Gaussian states (see eqs. (2.38) and (2.40)).

Equipped with the complexity measure $\mathcal{C}_{\text{FS}}$ for pure states, one can also define the specific purification complexity as

$$\mathcal{P}_{\text{FS}}\left(\hat{\sigma}_{\mathcal{A}}, \hat{\rho}_{\mathcal{A}}\right) = \min_{\Phi} \min_{\Psi} \mathcal{C}_{\text{FS}}\left(|\Phi_{\mathcal{A}\mathcal{A}^c}\rangle\,, |\Psi_{\mathcal{A}\mathcal{A}^c}\rangle\right)\,, \tag{5.5}$$

where $|\Phi_{\mathcal{A}\mathcal{A}^c}\rangle, |\Psi_{\mathcal{A}\mathcal{A}^c}\rangle$ denote the purifications of two density operators $\hat{\sigma}_{\mathcal{A}}, \hat{\rho}_{\mathcal{A}}$, respectively. Then we still end up with the same optimization problem. However, we will show in next section that this purification complexity can be derived without any purifications and minimization.

Inspired by the connections between quantum fidelity and the circuit complexity proposal with the Fubini-Study metric approach [69], we first extend the Fubini-Study method to more generic quantum states, but avoiding the challenges in purification complexity due to the minimization over all purifications. Obviously, the key question is how to define an analog of the Fubini-Study metric for mixed states. We ask for the help of the quantum fidelity [2] between two general quantum states. In this paper, we focus on the fidelity of two quantum states $\hat{\rho}$ and $\hat{\sigma}$ defined by [42] [3]

$$F(\hat{\rho},\hat{\sigma}) \equiv \mathrm{Tr}\left(\sqrt{\sqrt{\hat{\rho}}\hat{\sigma}\sqrt{\hat{\rho}}}\right) = ||\sqrt{\hat{\rho}}\sqrt{\hat{\sigma}}||_1 \,. \tag{5.6}$$

If at least one of the two states is pure, the quantum fidelity F reduces to the overlap between two density matrices

$$F(\hat{\rho},\hat{\sigma}) = \sqrt{\mathrm{Tr}\left(\hat{\rho}\,\hat{\sigma}\right)} = \sqrt{\langle\psi|\,\hat{\rho}\,|\psi\rangle}\,, \qquad \hat{\sigma} = |\psi\rangle\langle\psi| \,. \tag{5.7}$$

This quantum fidelity $F(\hat{\rho},\hat{\sigma})$ can be naturally interpreted as a generalization of the transition probability for pure states. For later use, we also list some interesting and nice properties of the quantum fidelity as follows:

a) $0 \leq F(\hat{\rho},\hat{\sigma}) \leq 1$;

b) $F(\hat{\rho},\hat{\sigma}) = 1 \Longleftrightarrow \hat{\rho} = \hat{\sigma}; \quad F(\hat{\rho},\hat{\sigma}) = 0 \Longleftrightarrow \hat{\rho} \perp \hat{\sigma}$;

c) Symmetric : $F(\hat{\rho},\hat{\sigma}) = F(\hat{\sigma},\hat{\rho})$;

d) Concavity : $F\left(\hat{\sigma},\sum_i p_i\hat{\rho}_i\right) \geq \sum_i p_i F\left(\hat{\sigma},\hat{\rho}_i\right)$ for all $0 \leq p_i \leq 1$ such that $\sum_i p_i = 1$;

e) Strong Concavity: $F\left(\sum_i p_i\hat{\sigma}_i,\sum_i q_i\hat{\rho}_i\right) \geq \sum_i \sqrt{p_i q_i} F\left(\hat{\sigma}_i,\hat{\rho}_i\right)$ for all $0 \leq p_i, q_i \leq 1$ such that $\sum_i p_i = 1 = \sum_i q_i$;

f) Multiplicativity : $F\left(\hat{\rho}_1\otimes\hat{\rho}_2,\hat{\sigma}_1\otimes\hat{\sigma}_2\right) = F\left(\hat{\rho}_1,\hat{\sigma}_1\right)F\left(\hat{\rho}_2,\hat{\sigma}_2\right)$;

g) Unitary invariance : $F(\hat{\rho},\hat{\sigma}) = F(U\hat{\rho}U^\dagger, U\hat{\sigma}U^\dagger)$.

[2] In some literatures, the quantum fidelity may be defined as $F(\hat{\rho},\hat{\sigma})^2$.

[3] For a positive semi-definite operator, its square root uniquely exits and is also positive semi-definite.

The proofs for those properties can be found in textbooks on quantum information, *e.g.,* [42–44] or original references *e.g.,* [214–216]. There are also some other definitions for the quantum fidelity or distance between two density matrices. However, we prefer the definition in (5.6) because there is an important theorem called *Uhlmann's theorem*, which states that

Uhlmann's theorem. *For any possible purification* $|\psi\rangle$ *and* $|\phi\rangle$ *in system* $\mathcal{A}\mathcal{A}^c$ *with respect to* $\hat{\rho}$ *and* $\hat{\sigma}$ *in system* $\mathcal{A}$*, respectively* [4]*, the quantum fidelity satisfies*

$$F(\hat{\rho},\hat{\sigma}) \equiv Tr\left(\sqrt{\sqrt{\hat{\rho}}\hat{\sigma}\sqrt{\hat{\rho}}}\right) = \max_{|\psi\rangle,|\phi\rangle} |\langle\phi|\psi\rangle| \geq |\langle\phi|\psi\rangle|\,, \tag{5.8}$$

where the maximization is over all purifications of $\hat{\rho},\hat{\sigma}$ *and the last inequality can always be saturated by some appropriate purifications (called parallel purification).*

Uhlmann's theorem plays an important role in connecting the complexity from quantum Fisher information metric to the purification complexity $\mathcal{P}$. Another crucial property for the quantum fidelity is associated with the lowest bound of fidelity and its meaning in distinguishing states. Letting $\{E_a\}$ with $\sum_a E_a = \mathbb{I}$ be an arbitrary generalized measurement, *i.e., positive operator-valued measure* (POVM), the quantum fidelity between two density operators satisfies

$$F(\hat{\rho},\hat{\sigma}) = \min_{\{E_a\}} \sum_a \sqrt{\mathrm{Tr}(\hat{\rho}E_a)}\sqrt{\mathrm{Tr}(\hat{\sigma}E_a)}\,, \tag{5.9}$$

where the minimization is performed with respect to all sets of positive operators $\{E_a\}$ and we can call the POVM saturating the bound as the optimal POVM. Considering two distributions $P_1(a) = \mathrm{Tr}(\hat{\rho}E_a)$ and $P_2(a) = \mathrm{Tr}(\hat{\sigma}E_a)$, it is clear that the definition of quantum fidelity in (5.6) is the analogue of the statistical overlap and is actually the minimal overlap between these two probability distributions. In view of the importance of this inequality, let's sketch the proof to convince the readers who are not familiar with it. Starting from any POVM and unitary operator U, one can find [215]

$$\begin{aligned}\sum_a \sqrt{\mathrm{Tr}\left(\hat{\rho}E_a\right)}\sqrt{\mathrm{Tr}\left(\hat{\sigma}E_a\right)} &= \sum_a \sqrt{\mathrm{Tr}\left(U\sqrt{\hat{\rho}}E_a\sqrt{\hat{\rho}}U^\dagger\right)}\sqrt{\mathrm{Tr}\left(\sqrt{\hat{\sigma}}E_a\sqrt{\hat{\sigma}}\right)} \\ &\geq \sum_a \left|\mathrm{Tr}\left(U\sqrt{\hat{\rho}}\sqrt{E_a}\sqrt{E_a}\sqrt{\hat{\sigma}}\right)\right| = \left|\mathrm{Tr}\left(U\sqrt{\hat{\rho}}\sqrt{\hat{\sigma}}\right)\right|\end{aligned}, \tag{5.10}$$

[4] So it means that we have the constrains $\mathrm{Tr}_{\mathcal{A}^c}|\psi\rangle\langle\psi| = \hat{\rho}$ and $\mathrm{Tr}_{\mathcal{A}^c}|\phi\rangle\langle\phi| = \hat{\sigma}$.

where we only need the cyclic property of the trace and the Schwarz inequality (*i.e.,* the Schatten 2-norm is sub-multiplicative.). In consideration of the fact that the maximization over all unitary operator U, namely

$$\max_{U} \left|\mathrm{Tr}\left(UO\right)\right| = \mathrm{Tr}\left(\sqrt{O^{\dagger}O}\right) , \tag{5.11}$$

is saturated if and only if $UO = e^{i\phi}\sqrt{O^{\dagger}O}$, we finally arrive at the conclusion for the quantum fidelity, *i.e.,* eq. (5.9), by applying that maximization to operator $\sqrt{\hat{\rho}}\sqrt{\hat{\sigma}}$. Furthermore, one can also find that the optimal POVM is the special positive semi-definite operator with spectral decomposition

$$\hat{E} \equiv \sum_{a} \lambda_a E_a = \sum_{a} \lambda_a \left|a\right\rangle \left\langle a\right| = \left(\hat{\sigma}\right)^{-\frac{1}{2}} \sqrt{\sqrt{\hat{\sigma}}\hat{\rho}\sqrt{\hat{\sigma}}} \left(\hat{\sigma}\right)^{-\frac{1}{2}} , \tag{5.12}$$

which is nothing but the geometric mean of $\hat{\rho}$ and $\hat{\sigma}^{-1}$. Interpreting the quantum fidelity (5.6) as the minimization of statical overlap, one can prove some other interesting properties, *e.g.,* the non-broadcasting of non-commuting mixed states [215]. Here we stress its another application that the quantum fidelity $F\left(\hat{\sigma},\hat{\rho}\right)$ is non-decreasing under any quantum operations. Similar to the purifications of mixed states, we can introduce the bipartite system $\mathcal{H}_{\mathcal{A}} \otimes \mathcal{H}_{\mathcal{B}}$ and have the corresponding density matrices in the two subsystems such that

$$\hat{\rho}_{\mathcal{AB}} \in \mathcal{H}_{\mathcal{A}} \otimes \mathcal{H}_{\mathcal{B}} , \quad \mathrm{Tr}_{\mathcal{B}}\left(\hat{\rho}_{\mathcal{AB}}\right) = \hat{\rho}_{\mathcal{A}} , \qquad \mathrm{Tr}_{\mathcal{A}}\left(\hat{\rho}_{\mathcal{AB}}\right) = \hat{\rho}_{\mathcal{B}} . \tag{5.13}$$

The minimization in eq. (5.9) implies we have the monotonicity of quantum fidelity [5]

$$F\left(\hat{\rho}_{\mathcal{AB}},\hat{\sigma}_{\mathcal{AB}}\right) \leq F\left(\hat{\rho}_{\mathcal{A}},\hat{\sigma}_{\mathcal{A}}\right) , \tag{5.14}$$

which means that any partial trace can not reduce Uhlmann's fidelity and also indicates that the density operators in a subsystem are less distinguishable than those in a larger system. More generally, we can also explain this property in the way associated with quantum operation. As it is known [42], the quantum operation (quantum channel) $\mathcal{E}$ defined by *completely positive trace-preserving* (CPTP) map can be explained in different ways (see appendix C.2 for more details). For example, we can realize quantum operations $\mathcal{E}\left(\hat{\rho}_{\mathcal{A}}\right)$ on density operators $\hat{\rho}_{\mathcal{A}}$ by the unitary transformations acting on the extended Hilbert space $\mathcal{H}_{\mathcal{A}} \otimes \mathcal{H}_{\mathcal{A}^c}$ with some ancillae (or environment), *i.e.,*

$$\mathcal{E}\left(\hat{\rho}_{\mathcal{A}}\right) = \mathrm{Tr}_{\mathcal{A}^c}\left(U_{\mathcal{AA}^c}\left(\hat{\rho}_{\mathcal{A}} \otimes \hat{\rho}_{\mathcal{A}^c}\right) U_{\mathcal{AA}^c}^{\dagger}\right) , \tag{5.15}$$

[5] Obviously, this monotonicity is a consequence of Uhlmann's theorem. Although the optimal purification of $\hat{\rho}_{\mathcal{AB}}$ and $\hat{\sigma}_{\mathcal{AB}}$ are also the purification of $\hat{\rho}_{\mathcal{A}}$ and $\hat{\sigma}_{\mathcal{A}}$, respectively, they may not be the optimal ones with respect to $\hat{\rho}_{\mathcal{A}}$ and $\hat{\sigma}_{\mathcal{A}}$.

where the $\hat{\rho}_{\mathcal{A}^c}$ is the initial state for the ancillae and $\mathrm{Tr}_{\mathcal{A}^c}$ refers to tracing out the ancilla part. On the other hand, we can also rewrite the equivalent quantum operations in the operator sum representation by

$$\mathcal{E}\left(\hat{\rho}_{\mathcal{A}}\right)=\sum_{a}\hat{M}_{a}\hat{\rho}_{\mathcal{A}}\hat{M}_{a}^{\dagger}\,,\quad\sum_{a}\hat{M}_{a}^{\dagger}\hat{M}_{a}=\mathbb{I}\,,\tag{5.16}$$

where $\mathbb{I}$ denotes the identity matrix. So finally, in the sense of quantum operations, one can understand the non-decreasing of quantum fidelity as

$$F\left(\mathcal{E}\left(\hat{\rho}_{\mathcal{A}}\right),\mathcal{E}\left(\hat{\sigma}_{\mathcal{A}}\right)\right)\geq F\left(\hat{\rho}_{\mathcal{A}}\otimes\hat{\rho}_{\mathcal{A}^c},\hat{\sigma}_{\mathcal{A}}\otimes\hat{\sigma}_{\mathcal{A}^c}\right)=F\left(\hat{\rho}_{\mathcal{A}},\hat{\sigma}_{\mathcal{A}}\right)F\left(\hat{\rho}_{\mathcal{A}^c},\hat{\sigma}_{\mathcal{A}^c}\right)\,,\tag{5.17}$$

where we use the non-decrease of the quantum fidelity under partial trace and its unitary invariance in the first inequality and its multiplicativity to derive the second equality. Taking the ancilla part for the two density operators as the same, we can arrive at a monotonic form

$$F\left(\mathcal{E}\left(\hat{\rho}_{\mathcal{A}}\right),\mathcal{E}\left(\hat{\sigma}_{\mathcal{A}}\right)\right)\geq F\left(\hat{\rho}_{\mathcal{A}},\hat{\sigma}_{\mathcal{A}}\right)\geq F\left(\hat{\rho}_{\mathcal{AB}},\hat{\sigma}_{\mathcal{AB}}\right)\,,\tag{5.18}$$

indicating the quantum operation can not decrease the fidelity. Physically, the above inequality also implies that physical process can not increase the distinguishability between quantum states. The first inequality holds for any trace-preserving quantum operation (quantum channel) defined by $\mathcal{E}:\hat{\rho}\rightarrow\mathcal{E}\left(\hat{\rho}\right)$ and can be understood as the quantum analog of the classical information-processing inequality.

After introducing the quantum fidelity between density matrices, we move on to our new proposal for the circuit complexity between two generic quantum states. Similar to the pure-state complexity based on the Fubini-Study metric, we can parametrize the space of quantum states by density operators $\hat{\rho}\left(\lambda^{\mu}\right)$ with independent parameters λ^{μ}. Then our proposal to the complexity from any reference state $\hat{\sigma}_{\mathrm{R}}\left(\lambda_{0}^{\mu}\right)$ to any target state $\hat{\rho}_{\mathrm{T}}\left(\lambda_{1}^{\mu}\right)$ is the following

$$\begin{aligned}\mathcal{C}_{\mathrm{IM}}\left(\hat{\sigma}_{\mathrm{R}},\hat{\rho}_{\mathrm{T}}\right)&=\int_{0}^{1}d\sigma\,\sqrt{2g_{\mu\nu}^{\mathrm{IM}}\,\dot{\lambda}^{\mu}\,\dot{\lambda}^{\nu}}\,,\qquad\dot{\lambda}^{\mu}=\frac{d\lambda^{\mu}(\sigma)}{d\sigma}\,,\\\mathcal{C}_{\mathrm{IM}}^{\kappa=2}\left(\hat{\sigma}_{\mathrm{R}},\hat{\rho}_{\mathrm{T}}\right)&=2\int_{0}^{1}d\sigma\,g_{\mu\nu}^{\mathrm{IM}}\,\dot{\lambda}^{\mu}\,\dot{\lambda}^{\nu}=\left(\mathcal{C}_{\mathrm{IM}}\right)^{2}\,,\end{aligned}\tag{5.19}$$

where the integral is taken along the optimal circuit *i.e.,* the geodesic γ_{IM} measured by the fidelity susceptibility $g_{\mu\nu}^{\mathrm{IM}}$ with reference state and target state as the endpoints. If the geodesics are not unique, we should choose the one minimizing the distance between the

reference state and the target state. The quantum fidelity susceptibility $g^{\rm IM}_{\mu\nu}$ can be derived from the expansion of Uhlmann's fidelity between two nearby quantum states, *i.e.,*

$$g^{\rm IM}_{\mu\nu}(\lambda)\, d\lambda^\mu d\lambda^\nu =_2 2\left(1 - F\left(\hat{\rho}(\lambda), \hat{\rho}(\lambda+\delta\lambda)\right) =_2 1 - F(\hat{\rho}, \hat{\rho}+\delta\hat{\rho})^2\right), \tag{5.20}$$

where the equality is taken at the second order of $\delta\lambda$ and the quantum fidelity F for mixed states is defined to be (5.6). We have used the superscript "IM" for this metric because it is equal to the *quantum Fisher information metric* (QFIM). For more explicit forms of QFIM, see appendix C.3 . Technically, it is also convenient to derive the quantum Fisher information metric by

$$g^{\rm IM}_{\mu\nu} = -\lim_{\lambda'\to\lambda} \frac{\partial^2 F(\lambda,\lambda')}{\partial\lambda^\mu \partial\lambda^\nu}, \tag{5.21}$$

which has the same spirit as the derivation shown in eq. (2.24) for the Fubini-Study metric. For mixed states, the quantum Fisher information metric or quantum fidelity susceptibility is also known as the Bures metric [210,211,214,217,218], [6] which is derived from the finite Bures distance defined by $1 - F(\hat{\rho}, \hat{\sigma})$.

To close this subsection, we stress that the choice $\hat{\rho}(\lambda^\mu)$ is not arbitrary and in principle, it is determined by the set of gates on the whole system. From the viewpoint of the quantum circuit with ancillae (*e.g.,* figure 5.2), the whole Hilbert space is defined by $\hat{\rho}(\lambda^\mu) = {\rm Tr}_{\mathcal{A}^c}\left(|\Psi_{\mathcal{A}\mathcal{A}^c}\rangle\langle\Psi_{\mathcal{A}\mathcal{A}^c}|\right)$ where the pure states are constrained by the set of gates, *i.e.,* all possible unitary operations $U_{\mathcal{A}\mathcal{A}^c}$ from $|\Psi_{\mathcal{A}\mathcal{A}^c}\rangle = U_{\mathcal{A}\mathcal{A}^c}|\Phi_{\rm R}\rangle$. The last thing we want to point out is the different meanings of "optimal" states. Uhlmann's fidelity provides a criterion for the optimal purification with respect to any two states. However, the circuit complexity is based on the optimal path in the space of states, *i.e.,* geodesic $\gamma_{\rm IM}$. The quantum fidelity only quantifies the local measure while the geodesic length indicates a global optimization for a given reference state and a target state.

5.2 Properties of Purification Complexity

5.2.1 Purification Complexity without Purifications

In the last subsection, we have seen that Uhlmann's theorem (5.8) naturally relates the quantum fidelity between two mixed states to the fidelity from their "optimal" purifications. It may remind you of the idea about purification complexity [2,161] by introducing

[6] In the literature in quantum information, quantum Fisher information metric and the Bures metric are different by a factor 4. Because we need to normalize the metric in order to measure complexity, we ignore this factor and do not distinguish the two metrics.

ancillae in the quantum circuit and defining the minimal complexity of optimal purifications as the complexity for respective mixed states. Here, we will show that the complexity derived from the quantum Fisher information metric is actually the purification complexity, where the pure-state complexity is measured by the Fubini-Study metric. Generally, we can take arbitrary mixed states $\hat{\sigma}_{\mathcal{A}}, \hat{\rho}_{\mathcal{A}}$ in system $\mathcal{A}$ as our reference state and target state, respectively. First of all, let's think that we have found a specific purification $|\Psi_{\mathcal{A}\mathcal{A}^c}\rangle$ by introducing an ancillary system $\mathcal{A}^c$. Considering the Fubini-Study metric as the complexity measure for pure states, we can search for the optimal purification and define the corresponding purification complexity as

$$\mathcal{P}_{\text{FS}}\left(\hat{\sigma}_{\mathcal{A}}, \hat{\rho}_{\mathcal{A}}\right) = \min_{\Phi} \min_{\Psi} \mathcal{C}_{\text{FS}}\left(|\Phi_{\mathcal{A}\mathcal{A}^c}\rangle, |\Psi_{\mathcal{A}\mathcal{A}^c}\rangle\right) = \min_{\Phi} \min_{\Psi} \int_0^1 d\sigma \sqrt{2 g^{\text{FS}}_{\mu\nu} \dot{\lambda}^{\mu} \dot{\lambda}^{\nu}}\,, \tag{5.22}$$

where $g^{\text{FS}}_{\mu\nu}$ is the Fubini-Study metric defined in (2.23) and the minimization is employed over all purifications for the target state $\hat{\rho}_{\mathcal{A}}$ and reference state $\hat{\sigma}_{\mathcal{A}}$. We can assume the optimal purification from this point of view as $\left|\tilde{\Psi}_{\mathcal{A}\mathcal{A}^c}\right\rangle$. Let's just focus on an arbitrary infinitesimal step in the optimal quantum circuit, *i.e.,* the geodesic on the space of $|\Psi_{\mathcal{A}\mathcal{A}^c}\rangle$. From the definition of the Fubini-Study metric (2.23), the cost for this step is related to the quantum fidelity between two extremely nearby pure states, *i.e.,*

$$\begin{aligned} \delta\mathcal{C}_{\text{FS}}\left(|\Psi_{\mathcal{A}\mathcal{A}^c}(\sigma)\rangle\right) &\equiv \sqrt{2\left(1 - |\langle\Psi_{\mathcal{A}\mathcal{A}^c}(\sigma)|\Psi_{\mathcal{A}\mathcal{A}^c}(\sigma+d\sigma)\rangle|^2\right)}\,, \\ \delta\mathcal{P}_{\text{FS}}\left(\hat{\rho}_{\mathcal{A}}(\sigma)\right) &= \sqrt{2\left(1 - |\langle\tilde{\Psi}_{\mathcal{A}\mathcal{A}^c}(\sigma)|\tilde{\Psi}_{\mathcal{A}\mathcal{A}^c}(\sigma+d\sigma)\rangle|^2\right)}\,, \end{aligned} \tag{5.23}$$

where the purification complexity $\mathcal{P}_{\text{FS}}$ from the Fubini-Study metric is associated with the optimal purification $\left|\tilde{\Psi}_{\mathcal{A}\mathcal{A}^c}\right\rangle$. On the other hand, we can also consider the same infinitesimal step and define the complexity of mixed states by considering the quantum Fisher information metric. It is clear that Uhlmann's theorem ensures the inequality

$$\begin{aligned} \delta\mathcal{D}_{\text{IM}}\left(\hat{\rho}_{\mathcal{A}}(\sigma)\right) &\equiv \sqrt{2 g^{\text{IM}}_{\mu\nu}\, d\lambda^{\mu}\, d\lambda^{\nu}} = \sqrt{2(1 - F\left(\hat{\rho}_{\mathcal{A}}, \hat{\rho}_{\mathcal{A}}(\sigma+d\sigma)\right))}\,, \\ &\leq \delta\mathcal{P}_{\text{FS}}\left(\hat{\rho}_{\mathcal{A}}(\sigma)\right)\,, \end{aligned} \tag{5.24}$$

where we obtain the two near mixed states associated with pure states $\left|\tilde{\Psi}_{\mathcal{A}\mathcal{A}^c}(\sigma+d\sigma)\right\rangle$ and $\left|\tilde{\Psi}_{\mathcal{A}\mathcal{A}^c}(\sigma)\right\rangle$ by tracing out the ancillary system $\mathcal{A}^c$. Repeating this projection from optimal pure states $\left|\tilde{\Psi}_{\mathcal{A}\mathcal{A}^c}(\sigma)\right\rangle$ to the space of mixed states $\hat{\rho}_{\mathcal{A}}(\sigma)$ in subsystem $\mathcal{H}_{\mathcal{A}}$, we must be able to find a path in the space of mixed states with its length as the lowest bound

of the purification complexity $\mathcal{P}_{\text{FS}}$ for arbitrary states $\hat{\sigma}_{\mathcal{A}}, \hat{\rho}_{\mathcal{A}}$. Recalling the fact that the complexity of mixed states from the quantum Fisher information metric is defined as the minimal geodesic length connecting a reference state and a target state, we finally arrive at the first conclusion for arbitrary mixed states,

$$\mathcal{C}_{\text{IM}}\left(\hat{\sigma}_{\mathcal{A}}, \hat{\rho}_{\mathcal{A}}\right) \leq \mathcal{D}_{\text{IM}}\left(\text{Projection of}\, \gamma_{\text{FS}}\right) \leq \mathcal{P}_{\text{FS}}\left(\hat{\sigma}_{\mathcal{A}}, \hat{\rho}_{\mathcal{A}}\right) \equiv \min_{\Phi} \min_{\Psi} \mathcal{C}_{\text{FS}}\left(|\Psi_{\mathcal{A}\mathcal{A}^c}\rangle\right) , \tag{5.25}$$

which means that the purification complexity $\mathcal{P}_{\text{FS}}$ is the upper bound of the complexity $\mathcal{C}_{\text{IM}}$ derived from the quantum Fisher information metric. The above argument is illustrated by the projection from Hilbert space $\mathcal{H}_{\mathcal{A}\mathcal{A}^c}$ to $\mathcal{H}_{\mathcal{A}}$ in the figure 5.3 . It was stressed before that the quantum fidelity can always be saturated by choosing specific purifications. Then you may immediately face a puzzle: why we can find a lower value than the purification complexity $\mathcal{P}_{\text{FS}}$ even when we have minimized the complexity from all possible purifications $|\Psi_{\mathcal{A}\mathcal{A}^c}\rangle$. Another natural question is that, by taking account of the inequality itself, when can we obtain the exact equality? All of these can be illustrated by stressing the difference between these two methods, which originates from the way of introducing the ancillae. The special point for purification complexity is that we only introduce one specific optimal ancillary system $\mathcal{A}^c$ at the beginning and keep it in the full circuit. For the circuit with complexity derived from the quantum Fisher information metric, it is possible that the quantum circuit may need different auxiliary systems after every step as shown in figure 5.2. From the viewpoint of optimal purification, this is because we have to introduce a special ancilla for every step to guarantee the fidelity between these purified states satisfying Uhlmann's fidelity, *i.e.,* (5.6) which is a maximum for the purified states.

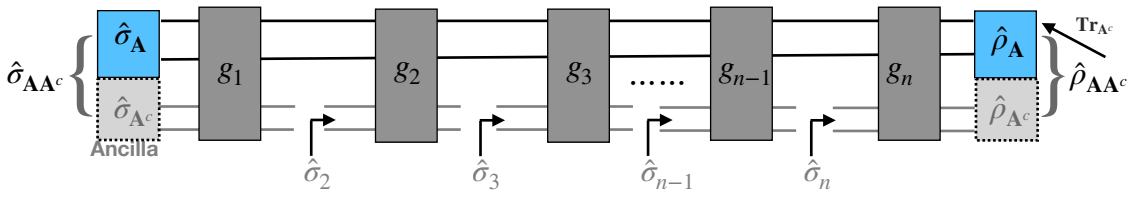

Figure 5.2: A lift of evolution $\hat{\rho}_{\mathcal{A}}(\sigma)$ to the extended Hilbert space: A general circuit connecting purified state $\hat{\sigma}_{\mathcal{A}\mathcal{A}^c}$ to $\hat{\rho}_{\mathcal{A}\mathcal{A}^c}$ with different ancillae after every step because we do not count the cost of introducing ancilla and tracing out the auxiliary system. More importantly, it is based on the fact that any trace-preserving quantum operation is equivalently described by the unitary evolution with ancilla.

However, Uhlmann's theorem also claims that the fidelity bound can be always saturated by taking some special purifications. In other words, we can find a continuous lift

mapping from the geodesic in the space of quantum states $\hat{\rho}_{\mathcal{A}}$ to a path in the Hilbert space $\mathcal{H}_{\mathcal{A}\mathcal{A}^c}$ of purified states $|\Psi_{\mathcal{A}\mathcal{A}^c}\rangle$ [7]. Due to the same infinitesimal complexity measure, it is obvious that the image after lift-map has the same distance as $\mathcal{C}_{\text{IM}}(\hat{\rho}_{\mathcal{A}})$. It is shown in the map from the left blue curve to the right blue curve in figure 5.3[8]. Again, we note that the purification complexity from the Fubini-Study metric is also defined as the minimal geodesic length. Comparing the geodesic distance with respect to the Fubini-Study metric and the distance of the image after the lift-map, we can also obtain another inequality

$$\mathcal{C}_{\text{IM}}(\hat{\sigma}_{\mathcal{A}}, \hat{\rho}_{\mathcal{A}}) = \mathcal{D}_{\text{FS}}(\text{Lift of}\,\gamma_{\text{IM}}) \geq \mathcal{P}_{\text{FS}}(\hat{\sigma}_{\mathcal{A}}, \hat{\rho}_{\mathcal{A}}) \ . \tag{5.26}$$

Combining this new inequality with the first inequality from Uhlmann's theorem, we finally conclude that the complexity $\mathcal{C}_{\text{IM}}(\hat{\sigma}_{\mathcal{A}}, \hat{\rho}_{\mathcal{A}})$ derived from the quantum Fisher information metric is exactly the purification complexity measured by the Fubini-Study metric on purified states [9], *i.e.,*

$$\mathcal{C}_{\text{IM}}(\hat{\sigma}_{\mathcal{A}}, \hat{\rho}_{\mathcal{A}}) = \mathcal{P}_{\text{FS}}(\hat{\sigma}_{\mathcal{A}}, \hat{\rho}_{\mathcal{A}}) \equiv \min_{\Phi} \min_{\Psi} \mathcal{C}_{\text{FS}}(|\Phi_{\mathcal{A}\mathcal{A}^c}\rangle, |\Psi_{\mathcal{A}\mathcal{A}^c}\rangle) \ , \tag{5.27}$$

where the target state and reference state are related to purified states in the extended system $\mathcal{H}_{\mathcal{A}\mathcal{A}^c}$ by $\hat{\rho}_{\mathcal{A}} = \text{Tr}_{\mathcal{A}^c}(|\Psi_{\mathcal{A}\mathcal{A}^c}\rangle\langle\Psi_{\mathcal{A}\mathcal{A}^c}|)$ and $\hat{\sigma}_{\mathcal{A}} = \text{Tr}_{\mathcal{A}^c}(|\Phi_{\mathcal{A}\mathcal{A}^c}\rangle\langle\Phi_{\mathcal{A}\mathcal{A}^c}|)$, respectively. In the next section, we will take Gaussian mixed states as an explicit example to show that how the first equality holds after minimization and find the special purifications satisfying the bound from Uhlmann's fidelity along the whole geodesic $\hat{\rho}_{\mathcal{A}}(\sigma)$.

5.2.2 The Non-increase of Purification Complexity

Instead of considering the optimal purified state $|\Psi_{\mathcal{A}\mathcal{A}^c}\rangle$ in the extended Hilbert space, we can start from generic mixed states $\hat{\rho}_{\mathcal{A}\mathcal{B}}$ with $\text{Tr}_{\mathcal{B}}(\hat{\rho}_{\mathcal{A}\mathcal{B}}) = \hat{\rho}_{\mathcal{A}}$ in a bipartite Hilbert space $\mathcal{H}_{\mathcal{A}} \otimes \mathcal{H}_{\mathcal{B}}$ and assume the complexity from $\hat{\sigma}_{\mathcal{A}\mathcal{B}}$ to $\hat{\rho}_{\mathcal{A}\mathcal{B}}$ is associated with the geodesic $\gamma(\hat{\rho}_{\mathcal{A}\mathcal{B}}(\sigma))$. In order to show the consequence of partial trace on the complexity $\mathcal{C}_{\text{IM}}(\hat{\sigma}_{\mathcal{A}\mathcal{B}}, \hat{\rho}_{\mathcal{A}\mathcal{B}})$, we can similarly trace out the system $\mathcal{B}$ along the geodesic $\gamma(\hat{\rho}_{\mathcal{A}\mathcal{B}}(\sigma))$,

[7] Especially, I would like to thank Juan Hernandez for illuminating discussions on that point.

[8] As discussed in figure 5.2, there are many ways to introduce the ancillae and simultaneously make Uhlmann's fidelity saturated (the lift-map is not injective). However, most of them after the lift-map only make discontinuous lines in $\mathcal{H}_{\mathcal{A}\mathcal{A}^c}$ but with the same length.

[9] This equivalence is based on our definitions that the two complexities are both defined as the geodesic length on the corresponding state space. It is also possible to define the complexity as the length of a non-geodesic path by constraining the allowed motions in the space of states, which corresponds to reducing the set of gates. Then our proof in the main content for the equivalence between $\mathcal{C}_{\text{IM}}$ and $\mathcal{P}_{\text{FS}}$ would not work. I would like to thank Simon Ross for pointing out this.

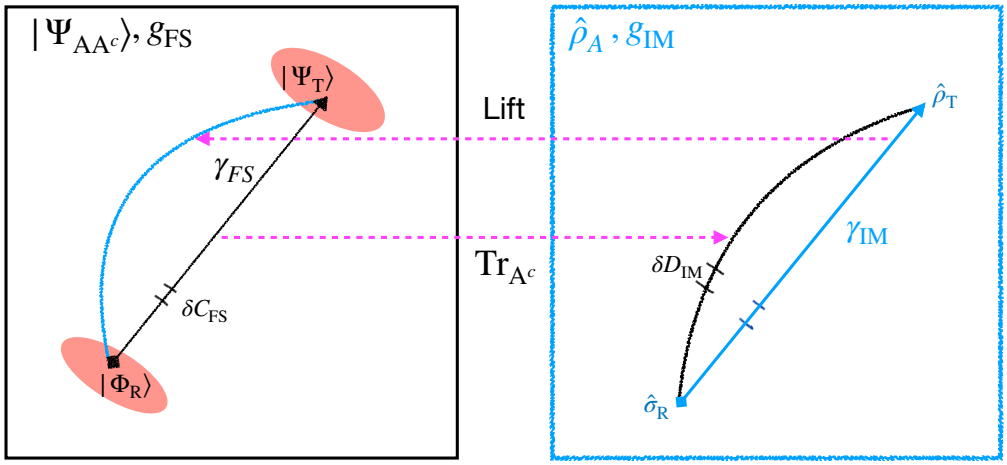

Figure 5.3: Left side is the Hilbert space $\mathcal{H}_{\mathcal{A}\mathcal{A}^c}$ of purified state $|\Psi_{\mathcal{A}\mathcal{A}^c}\rangle$, which is equipped with the Fubini-study metric g_{FS} as the complexity measure. The black line is referred to as the geodesic γ_{FS} in this space. The right side represents the Hilbert space $\mathcal{H}_{\mathcal{A}}$ for density matrices $\hat{\rho}_{\mathcal{A}}$ with the quantum Fisher information metric g_{IM} defined in (5.20) as the complexity measure. The corresponding geodesic γ_{IM} is indicated by the blue line. By tracing out the ancillary part $\mathcal{A}^c$, we can find the projection-map from γ_{FS} to a path in the space of $\hat{\rho}_{\mathcal{A}}$ which is shown as the black curve. According to Uhlmann's theorem, we can also construct a lift-map from $\mathcal{H}_{\mathcal{A}}$ to $\mathcal{H}_{\mathcal{A}\mathcal{A}^c}$ with the fidelity bound is always saturating.

mapping the geodesic connecting $\sigma_{\mathcal{A}\mathcal{B}}$ and $\hat{\rho}_{\mathcal{A}\mathcal{B}}$ to a special path in $\mathcal{H}_{\mathcal{A}}$. The non-decrease of fidelity under partial trace (5.18) gives rise to the monotone for circuit complexity by

$$\mathcal{C}_{\mathrm{IM}}\left(\hat{\sigma}_{\mathcal{A}\mathcal{B}}, \hat{\rho}_{\mathcal{A}\mathcal{B}}\right) \geq \mathcal{D}_{\mathrm{IM}}\left(\text{Projection of}\, \gamma\left(\hat{\rho}_{\mathcal{A}\mathcal{B}}(\sigma)\right)\right) \geq \mathcal{C}_{\mathrm{IM}}\left(\hat{\sigma}_{\mathcal{A}}, \hat{\rho}_{\mathcal{A}}\right) . \tag{5.28}$$

where $\mathcal{D}_{\mathrm{IM}}$ denotes the length measured by the QFIM and we have used the fact that the projection of geodesic $\gamma\left(\hat{\rho}_{\mathcal{A}\mathcal{B}}(\sigma)\right)$ may not be a geodesic on the space of $\hat{\rho}_{\mathcal{A}}$ to obtain the second inequality. This non-increasing property of complexity $\mathcal{C}_{\mathrm{IM}}$ is obviously in accord with our intuition because it is reasonable to expect the complexity for reduced states in a smaller Hilbert space to be smaller. Furthermore, we can also consider the map of the geodesic $\gamma\left(\hat{\rho}_{\mathcal{A}}(\sigma)\right)$ under any arbitrary quantum operation $\mathcal{E}$. From the non-decrease of quantum fidelity $F\left(\hat{\sigma}_{\mathcal{A}}, \hat{\rho}_{\mathcal{A}}\right)$ under $\mathcal{E}$, one can also arrive at the most general non-increasing

property of purification complexity $\mathcal{C}_{\text{IM}}$ by

$$\mathcal{C}_{\text{IM}}\left(\hat{\sigma}_{\mathcal{A}},\hat{\rho}_{\mathcal{A}}\right)\geq\mathcal{D}_{\text{IM}}\left(\mathcal{E}\left(\left(\hat{\rho}_{\mathcal{A}}(\sigma)\right)\right)\geq\mathcal{C}_{\text{IM}}\left(\mathcal{E}\left(\hat{\sigma}_{\mathcal{A}}\right),\mathcal{E}\left(\hat{\rho}_{\mathcal{A}}\right)\right)\right. . \tag{5.29}$$

As a straightforward application, we can find that a reversible quantum operation does not change the complexity since

$$\mathcal{C}_{\text{IM}}\left(\hat{\sigma}_{\mathcal{A}},\hat{\rho}_{\mathcal{A}}\right)\geq\mathcal{C}_{\text{IM}}\left(\mathcal{E}\left(\hat{\sigma}_{\mathcal{A}}\right),\mathcal{E}\left(\hat{\rho}_{\mathcal{A}}\right)\right)\geq\mathcal{C}_{\text{IM}}\left(\mathcal{E}^{-1}\circ\mathcal{E}\left(\hat{\sigma}_{\mathcal{A}}\right),\mathcal{E}^{-1}\circ\mathcal{E}\left(\hat{\rho}_{\mathcal{A}}\right)\right)=\mathcal{C}_{\text{IM}}\left(\hat{\sigma}_{\mathcal{A}},\hat{\rho}_{\mathcal{A}}\right) . \tag{5.30}$$

For example, any unitary operator is a reversible quantum operation and then we naturally have the unitary invariance of purification complexity

$$\mathcal{C}_{\text{IM}}\left(\hat{\sigma}_{\mathcal{A}},\hat{\rho}_{\mathcal{A}}\right)=\mathcal{C}_{\text{IM}}\left(U\hat{\sigma}_{\mathcal{A}}U^{\dagger},U\hat{\rho}_{\mathcal{A}}U^{\dagger}\right) , \tag{5.31}$$

which can also be derived from the unitary invariance of the quantum fidelity and the fact that the geodesic associated with complexity is chosen to be the one minimizing the distance.

Similar to the non-decreasing property of Uhlmann's fidelity in (5.18), we summarize our observation as a universal conclusion that the purification complexity $\mathcal{C}_{\text{IM}}\left(\hat{\sigma}_{\mathcal{A}},\hat{\rho}_{\mathcal{A}}\right)$ (for both pure states and mixed states) derived from the quantum Fisher information metric is **non-increasing** under any trace-preserving quantum operations (quantum channel) acting on the reference state and target state simultaneously, *i.e.,*

$$\mathcal{C}_{\text{IM}}\left(\hat{\sigma}_{\mathcal{AB}},\hat{\rho}_{\mathcal{AB}}\right)\geq\mathcal{C}_{\text{IM}}\left(\hat{\sigma}_{\mathcal{A}},\hat{\rho}_{\mathcal{A}}\right)=\mathcal{C}_{\text{IM}}\left(U\hat{\sigma}_{\mathcal{A}}U^{\dagger},U\hat{\rho}_{\mathcal{A}}U^{\dagger}\right)\geq\mathcal{C}_{\text{IM}}\left(\mathcal{E}\left(\hat{\sigma}_{\mathcal{A}}\right),\mathcal{E}\left(\hat{\rho}_{\mathcal{A}}\right)\right) . \tag{5.32}$$

Naively, a similar conclusion also holds for $\mathcal{C}_{\text{IM}}^{\kappa=2}$. Analogous to the triangle inequality of Von Neumann entropy or entanglement entropy

$$\left|S_{\text{vN}}\left(\hat{\rho}_{\mathcal{A}}\right)-S_{\text{vN}}\left(\hat{\rho}_{\mathcal{B}}\right)\right|\leq S_{\text{vN}}\left(\hat{\rho}_{\mathcal{AB}}\right)\leq S_{\text{vN}}\left(\hat{\rho}_{\mathcal{A}}\right)+S_{\text{vN}}\left(\hat{\rho}_{\mathcal{B}}\right) , \tag{5.33}$$

the monotonicity of the purification complexity simply implies

$$\left|\mathcal{C}_{\text{IM}}\left(\hat{\sigma}_{\mathcal{A}},\hat{\rho}_{\mathcal{A}}\right)-\mathcal{C}_{\text{IM}}\left(\hat{\sigma}_{\mathcal{B}},\hat{\rho}_{\mathcal{B}}\right)\right|\leq\mathcal{C}_{\text{IM}}\left(\hat{\sigma}_{\mathcal{AB}},\hat{\rho}_{\mathcal{AB}}\right) . \tag{5.34}$$

However, the subadditivity for purification complexity does not hold in general and will be discussed in the next subsection in detail.

Instead of applying quantum operations on both reference states and target states, we can also discuss the effect of quantum operations only on the target states or the reference

states. In the space of quantum states in any Hilbert space $\mathcal{H}_{\mathcal{A}}$, there is an extremely simple state called the *maximally mixed state* defined by

$$\hat{\sigma}_{0,\mathcal{A}} = \sum_{i}^{N_{\mathcal{A}}} \frac{1}{N_{\mathcal{A}}} |\psi_i\rangle \langle\psi_i| = \frac{\mathbb{I}}{N_{\mathcal{A}}}\,, \tag{5.35}$$

where $N_{\mathcal{A}}$ denotes the dimension of the Hilbert space $\mathcal{H}_{\mathcal{A}}$. It is easy to see the maximally mixed state has a fully degenerate spectrum (*i.e.,* Schmidt coefficients take the same value) and its entropy

$$S_{\text{vN}}\left(\hat{\sigma}_{0,\mathcal{A}}\right) = \text{Tr}_{\mathcal{A}}\left(\hat{\sigma}_0 \log \hat{\sigma}_0\right) = \log N_{\mathcal{A}}\,, \tag{5.36}$$

reaches the maximum entropy in a $N_{\mathcal{A}}$-dimensional Hilbert space. As a result, this is a completely random state with zero information. For example, we can approach the maximally mixed state by taking the inverse temperature of a thermal state $\hat{\upsilon}_{\text{th}}$ to zero, *i.e.,*

$$\lim_{\beta\to 0} \hat{\upsilon}_{\text{th}}(\beta,\omega) = \lim_{\beta\to 0} \frac{1}{Z\left(\beta\omega\right)} \sum_{n=0}^{N_{\mathcal{A}}} e^{-\beta\omega\, n} |n\rangle\langle n| = \hat{\sigma}_{0,\mathcal{A}}\,. \tag{5.37}$$

Taking the reference state (or target state) in a system $\mathcal{A}$ as the maximally mixed state and considering the unital quantum channels [10], the monotonicity of purification complexity reduces to

$$\mathcal{C}_{\text{IM}}\left(\hat{\sigma}_{0,\mathcal{A}}, \hat{\rho}_{\mathcal{A}}\right) = \mathcal{C}_{\text{IM}}\left(\hat{\sigma}_{0,\mathcal{A}}, U\hat{\rho}_{\mathcal{A}}U^{\dagger}\right) \geq \mathcal{C}_{\text{IM}}\left(\hat{\sigma}_{0,\mathcal{A}}, \mathcal{E}\left(\hat{\rho}_{\mathcal{A}}\right)\right)\,, \tag{5.38}$$

due to the invariance of maximally mixed states over any unital quantum channels.

From the above discussion, we have shown that the properties of the quantum fidelity are helpful in deriving related properties for the purification complexity. Instead of using the non-decrease of fidelity, we can also adopt other properties of fidelity. As a result of the strong concavity of fidelity

$$\sum_i p_i F\left(\hat{\sigma}_i, \hat{\rho}_i\right) \leq F\left(\sum_i p_i\hat{\sigma}_i, \sum_i p_i\hat{\rho}_i\right)\,, \qquad \text{with} \qquad \sum_i p_i = 1\,, \tag{5.39}$$

we can find that the infinitesimal distance measures satisfy

$$\sum_i p_i\, ds^2_{\text{IM}}\left(\hat{\rho}_i\left(\sigma\right), \hat{\rho}_i\left(\sigma + d\sigma\right)\right) \geq ds^2_{\text{IM}}\left(\sum_i p_i\hat{\rho}_i\left(\sigma\right), \sum_i p_i\hat{\rho}_i\left(\sigma + d\sigma\right)\right)\,. \tag{5.40}$$

[10]Not all quantum operations are unital. A quantum operation is unital if it preserves the identity operator. In the operator-sum representation, the unital quantum channels satisfy $\sum_k \hat{M}_k\hat{M}_k^{\dagger} = \mathbb{I}$.

Considering a sequence of reference states $\hat{\sigma}_i$ and targets states $\hat{\rho}_i$ such that

$$\hat{\sigma}_{\mathrm{R}} = \sum_i p_i \hat{\sigma}_i \,, \qquad \hat{\rho}_{\mathrm{T}} = \sum_i p_i \hat{\rho}_i \,, \tag{5.41}$$

and taking the integral along their respective geodesic γ_i which connects $\hat{\sigma}_i$ to $\hat{\rho}_i$, we can easily obtain another non-increasing behavior of the purification complexity

$$\sum_i p_i \mathcal{C}_{\mathrm{IM}}^{\kappa=2}\left(\hat{\sigma}_i, \hat{\rho}_i\right) \geq \mathcal{C}_{\mathrm{IM}}^{\kappa=2}\left(\hat{\sigma}_{\mathrm{R}}, \hat{\rho}_{\mathrm{T}}\right) \,. \tag{5.42}$$

It means that the complexity $\mathcal{C}_{\mathrm{IM}}^{\kappa=2}$ is jointly convex in reference states and target states. Taking the square root of the above inequality, we can find that the purification complexity $\mathcal{C}_{\mathrm{IM}}$ satisfies

$$\sum_i \sqrt{p_i} \mathcal{C}_{\mathrm{IM}}\left(\hat{\sigma}_i, \hat{\rho}_i\right) \geq \mathcal{C}_{\mathrm{IM}}\left(\hat{\sigma}_{\mathrm{R}}, \hat{\rho}_{\mathrm{T}}\right) \,, \tag{5.43}$$

which is reduced to

$$\sum_i \sqrt{p_i} \mathcal{C}_{\mathrm{IM}}\left(\hat{\sigma}_{\mathrm{R}}, \hat{\rho}_i\right) \geq \mathcal{C}_{\mathrm{IM}}\left(\hat{\sigma}_{\mathrm{R}}, \hat{\rho}_{\mathrm{T}}\right) \,, \quad \text{with} \qquad \hat{\rho}_{\mathrm{T}} = \sum_i p_i \hat{\rho}_i \,, \tag{5.44}$$

after taking $\hat{\sigma}_i = \hat{\sigma}_{\mathrm{R}}$.

Finally, we would like to remark that these properties of the purification complexity $\mathcal{C}_{\mathrm{IM}}\left(\hat{\sigma}, \hat{\rho}\right)$ with respective two quantum states are also shared by the quantum relative entropy $S\left(\hat{\rho}||\hat{\sigma}\right) \equiv \mathrm{Tr}\left(\hat{\rho}\left(\log\hat{\rho} - \log\hat{\sigma}\right)\right)$ in spirit. However, different from the complexity, quantum relative entropy is not symmetric and can not be considered as a distance measure between two quantum states.

5.2.3 More on Purification Complexity of Mixed States

5.2.3.1 Pure-State limit

First of all, let's point out the differences between pure-state complexity from the Fubini-Study metric and that from the quantum Fisher information metric. Applying our previous conclusion on purification complexity to pure states, we can find

$$\mathcal{C}_{\mathrm{IM}}\left(\left|\Phi_{\mathcal{A}}\right\rangle, \left|\Psi_{\mathcal{A}}\right\rangle\right) = \min_{\Phi} \min_{\Psi} \mathcal{C}_{\mathrm{FS}}\left(\left|\Phi_{\mathcal{A}\mathcal{A}^c}\right\rangle, \left|\Psi_{\mathcal{A}\mathcal{A}^c}\right\rangle\right) \leq \mathcal{C}_{\mathrm{FS}}\left(\left|\Phi_{\mathcal{A}}\right\rangle, \left|\Psi_{\mathcal{A}}\right\rangle\right) \,. \tag{5.45}$$

The above inequality implies that the pure-state limit of purification complexity may be different from the pure-state complexity derived from the Fubini-Study metric. You may

feel surprised that the pure-state limit of purification complexity does not reduce to the Fubini-Study complexity, in view of the fact that the quantum Fisher information metric for pure states is exactly equivalent to the Fubini-Study metric. However, it should fulfill the expectation because the geodesic in a higher dimensional manifold is not smaller than that on a reduced hypersurface. Furthermore, we can find two (equivalent) physical explanations for that discrepancy. First, it is due to the fact that the geodesic for $\mathcal{C}_{\text{FS}}\left(|\Phi_{\mathcal{A}}\rangle, |\Psi_{\mathcal{A}}\rangle\right)$ is constrained on the space with only pure states in $\mathcal{H}_{\mathcal{A}}$. However, with the help of the ancillae, we are allowed to use all pure states in the extended Hilbert space $\mathcal{H}_{\mathcal{A}} \otimes \mathcal{H}_{\mathcal{A}^c}$. Since any product state $|\Psi_{\mathcal{A}}\rangle \otimes |\Psi_{\mathcal{A}^c}\rangle$ is also a "purification" of $|\Psi_{\mathcal{A}}\rangle$, the two complexities for pure states are consistent if and only if the optimal purifications of $|\Phi_{\mathcal{A}}\rangle, |\Psi_{\mathcal{A}}\rangle$ are themselves. In other words, this equivalence only appears when the ancillae and entangled gates between $\mathcal{H}_{\mathcal{A}}$ and $\mathcal{H}_{\mathcal{A}^c}$ for pure states are useless. Without introducing the auxiliary system and purifications of pure states, we can focus on the subsystem $\mathcal{H}_{\mathcal{A}}$ and interpret the smaller complexity from $\mathcal{C}_{\text{IM}}\left(|\Phi_{\mathcal{A}}\rangle, |\Psi_{\mathcal{A}}\rangle\right)$ as the fact that we are allowed to evolve the pure reference state to a pure target state by some mixed states. Again, we can find that the two complexities will be the same if the geodesic only goes along pure states, which equivalently means that we do not need entangled gates between the physical system and ancilla system from the view in the extended Hilbert space. In later examples, we will find that the Gaussian states happen to be that simple case because the circuit complexity of the factorized reference state and target state is just a direct sum of the complexity from every single mode as shown in [62].

5.2.3.2 Simplify the minimization

Although the pure-state limit of purification complexity does not always agree with the Fubini-Study complexity for pure states, we can further use this upper bound to simplify the process of minimization. Based on the monotonicity of purification complexity with respect to the partial trace, we can find the increasing sequence

$$\mathcal{C}_{\text{IM}}\left(\hat{\sigma}_{\mathcal{A}}, \hat{\rho}_{\mathcal{A}}\right) \leq \mathcal{C}_{\text{IM}}\left(|\Phi_{\mathcal{A}\mathcal{A}^c}\rangle, |\Psi_{\mathcal{A}\mathcal{A}^c}\rangle\right) \leq \mathcal{C}_{\text{FS}}\left(|\Phi_{\mathcal{A}\mathcal{A}^c}\rangle, |\Psi_{\mathcal{A}\mathcal{A}^c}\rangle\right) . \tag{5.46}$$

in discarding of the subsystem $\mathcal{A}^c$. Because we have shown that the minimization of $\mathcal{C}_{\text{FS}}$ over all purifications exactly agrees with the purification complexity $\mathcal{C}_{\text{IM}}\left(\hat{\sigma}_{\mathcal{A}}, \hat{\rho}_{\mathcal{A}}\right)$, the minimum of $\mathcal{C}_{\text{IM}}\left(|\Phi_{\mathcal{A}\mathcal{A}^c}\rangle, |\Psi_{\mathcal{A}\mathcal{A}^c}\rangle\right)$ has to locate at the same value, *i.e.,*

$$\begin{aligned}\mathcal{C}_{\text{IM}}\left(\hat{\sigma}_{\mathcal{A}}, \hat{\rho}_{\mathcal{A}}\right) &= \min_{\Phi}\min_{\Psi} \mathcal{C}_{\text{FS}}\left(|\Phi_{\mathcal{A}\mathcal{A}^c}\rangle, |\Psi_{\mathcal{A}\mathcal{A}^c}\rangle\right) = \min_{\Phi}\min_{\Psi} \mathcal{C}_{\text{IM}}\left(|\Phi_{\mathcal{A}\mathcal{A}^c}\rangle, |\Psi_{\mathcal{A}\mathcal{A}^c}\rangle\right) \\ &= \min_{\Phi} \mathcal{C}_{\text{IM}}\left(|\Phi_{\mathcal{A}\mathcal{A}^c}\rangle, |\Psi_{\mathcal{A}\mathcal{A}^c}\rangle\right) = \min_{\Psi} \mathcal{C}_{\text{IM}}\left(|\Phi_{\mathcal{A}\mathcal{A}^c}\rangle, |\Psi_{\mathcal{A}\mathcal{A}^c}\rangle\right) .\end{aligned} \tag{5.47}$$

In order to simplify the double minimizations to one as shown in the above inequalities, we just note that the unitary invariance of purification complexity implies that we can relate the optimal purified states under the double minimizations to that with only one minimization. Taking the unitary operation $U_{\mathcal{A}\mathcal{A}^c}$ such that $U_{\mathcal{A}\mathcal{A}^c}\left|\tilde{\Phi}_{\mathcal{A}\mathcal{A}^c}\right\rangle = |\Phi_{\mathcal{A}\mathcal{A}^c}\rangle$, one can simplify the double minimizations by

$$\begin{aligned}
&\min_{\Phi}\min_{\Psi}\mathcal{C}_{\text{IM}}\left(|\Phi_{\mathcal{A}\mathcal{A}^c}\rangle, |\Psi_{\mathcal{A}\mathcal{A}^c}\rangle\right) = \mathcal{C}_{\text{IM}}\left(\left|\tilde{\Phi}_{\mathcal{A}\mathcal{A}^c}\right\rangle, \left|\tilde{\Psi}_{\mathcal{A}\mathcal{A}^c}\right\rangle\right) , \\
&= \mathcal{C}_{\text{IM}}\left(|\Phi_{\mathcal{A}\mathcal{A}^c}\rangle, U_{\mathcal{A}\mathcal{A}^c}\left|\tilde{\Psi}_{\mathcal{A}\mathcal{A}^c}\right\rangle\right) , \\
&= \min_{\Phi}\mathcal{C}_{\text{IM}}\left(|\Phi_{\mathcal{A}\mathcal{A}^c}\rangle, |\Psi_{\mathcal{A}\mathcal{A}^c}\rangle\right) ,
\end{aligned} \tag{5.48}$$

which also works for one minimization over all purified target states $|\Psi_{\mathcal{A}\mathcal{A}^c}\rangle$.

5.2.3.3 Mutual complexity of $\hat{\rho}_{\mathcal{A}\mathcal{B}}$

Starting from the target state represented by a density operator $\hat{\rho}_{\mathcal{A}\mathcal{B}}$ in the bipartite physical systems $\mathcal{H}_{\mathcal{A}\mathcal{B}}$, we can also define the mixed-state complexity for two reduced density matrices

$$\hat{\rho}_{\mathcal{A}} = \text{Tr}_{\mathcal{B}}\left(\hat{\rho}_{\mathcal{A}\mathcal{B}}\right) , \quad \hat{\rho}_{\mathcal{B}} = \text{Tr}_{\mathcal{A}}\left(\hat{\rho}_{\mathcal{A}\mathcal{B}}\right) , \tag{5.49}$$

in the subsystems $\mathcal{A}, \mathcal{B}$. From the non-increase of purification complexity under the partial trace in (5.32), it is direct to derive the inequality $\mathcal{C}_{\text{IM}}\left(\hat{\rho}_{\mathcal{A}}\right) \leq \mathcal{C}_{\text{IM}}\left(\hat{\rho}_{\mathcal{A}\mathcal{B}}\right)$ and also

$$\mathcal{C}_{\text{IM}}\left(\hat{\sigma}_{\mathcal{A}}, \hat{\rho}_{\mathcal{A}}\right) + \mathcal{C}_{\text{IM}}\left(\hat{\sigma}_{\mathcal{B}}, \hat{\rho}_{\mathcal{B}}\right) - 2\mathcal{C}_{\text{IM}}\left(\hat{\sigma}_{\mathcal{A}\mathcal{B}}, \hat{\rho}_{\mathcal{A}\mathcal{B}}\right) \leq 0 , \tag{5.50}$$

where the reference states are given by $\hat{\sigma}_{\mathcal{A}\mathcal{B}}$ in the system $\mathcal{A}\mathcal{B}$, $\hat{\sigma}_{\mathcal{A}} = \text{Tr}_{\mathcal{B}}\left(\hat{\sigma}_{\mathcal{A}\mathcal{B}}\right)$ in a subsystem $\mathcal{A}$, and $\hat{\sigma}_{\mathcal{B}} = \text{Tr}_{\mathcal{A}}\left(\hat{\sigma}_{\mathcal{A}\mathcal{B}}\right)$ in a subsystem $\mathcal{B}$, respectively. On the other hand, we are interested in the non-trivial concept called mutual complexity [2, 161]. As a generalization of the mutual complexity for pure states $|\Psi_{\mathcal{A}\mathcal{B}}\rangle$, the authors of [2] propose to extend the mutual complexity to more generic quantum states with bipartition as

$$\Delta\mathcal{C}_{\text{IM}} = \mathcal{C}_{\text{IM}}\left(\hat{\sigma}_{\mathcal{A}}, \hat{\rho}_{\mathcal{A}}\right) + \mathcal{C}_{\text{IM}}\left(\hat{\sigma}_{\mathcal{B}}, \hat{\rho}_{\mathcal{B}}\right) - \mathcal{C}_{\text{IM}}\left(\hat{\sigma}_{\mathcal{A}\mathcal{B}}, \hat{\rho}_{\mathcal{A}\mathcal{B}}\right) , \tag{5.51}$$

which quantifies the additional correlations between the subsystem $\mathcal{A}$ and $\mathcal{B}$. Taking the complexity of states as that derived from the quantum Fisher information metric makes the above definition calculable. When $\Delta\mathcal{C} > 0$ complexity is said to be subadditive, otherwise it is called to be superadditive when $\Delta\mathcal{C} < 0$. As discussed before, we have another definition

for pure-state complexity based on the Fubini-Study metric. Correspondingly, we can also define the mutual complexity for pure states $|\Psi_{\mathcal{AB}}\rangle$ by

$$\begin{aligned}\Delta\mathcal{C}_{\text{FS}} &= \mathcal{P}_{\text{FS}}\left(\hat{\sigma}_{\mathcal{A}},\hat{\rho}_{\mathcal{A}}\right)+\mathcal{P}_{\text{FS}}\left(\hat{\sigma}_{\mathcal{A}},\hat{\rho}_{\mathcal{B}}\right)-\mathcal{C}_{\text{FS}}\left(|\Phi_{\mathcal{AB}}\rangle,|\Psi_{\mathcal{AB}}\rangle\right),\\ &= \mathcal{C}_{\text{IM}}\left(\hat{\sigma}_{\mathcal{A}},\hat{\rho}_{\mathcal{A}}\right)+\mathcal{C}_{\text{IM}}\left(\hat{\sigma}_{\mathcal{A}},\hat{\rho}_{\mathcal{B}}\right)-\mathcal{C}_{\text{FS}}\left(|\Phi_{\mathcal{AB}}\rangle,|\Psi_{\mathcal{AB}}\rangle\right),\\ &\leq \Delta\mathcal{C}_{\text{IM}},\end{aligned} \tag{5.52}$$

where we have used the fact $\mathcal{C}_{\text{IM}}\left(\hat{\sigma}_{\mathcal{A}},\hat{\rho}_{\mathcal{A}}\right)=\mathcal{P}_{\text{FS}}\left((\hat{\sigma}_{\mathcal{A}},\hat{\rho}_{\mathcal{A}}\right)$ for purification complexity of mixed states and also $\mathcal{C}_{\text{FS}}\left(\Psi_{\mathcal{AB}}\right)\geq\mathcal{C}_{\text{IM}}\left(\Psi_{\mathcal{AB}}\right)$ for pure states.

Although we found that the mutual complexity (5.51) is either always superadditive or always subadditive in general, it is easy to get the subadditive mutual complexity in many simple cases due to the monotonicity of purification complexity $\mathcal{C}_{\text{IM}}$. If a quantum operation with $\mathcal{E}\left(\hat{\sigma}_{\mathcal{A}}\otimes\hat{\sigma}_{\mathcal{B}}\right)=\hat{\sigma}_{\mathcal{AB}},\mathcal{E}\left(\hat{\rho}_{\mathcal{A}}\otimes\hat{\rho}_{\mathcal{B}}\right)=\hat{\rho}_{\mathcal{AB}}$ exists, then one can easily confirm

$$\Delta\mathcal{C}_{\text{IM}}\geq\mathcal{C}_{\text{IM}}\left(\hat{\sigma}_{\mathcal{A}}\otimes\hat{\sigma}_{\mathcal{B}},\hat{\rho}_{\mathcal{A}}\otimes\hat{\rho}_{\mathcal{B}}\right)-\mathcal{C}_{\text{IM}}\left(\hat{\sigma}_{\mathcal{AB}},\hat{\rho}_{\mathcal{AB}}\right)\geq 0\,, \tag{5.53}$$

by using the simple fact $\mathcal{C}_{\text{IM}}\left(\hat{\sigma}_{\mathcal{A}}\otimes\hat{\sigma}_{\mathcal{B}},\hat{\rho}_{\mathcal{A}}\otimes\hat{\rho}_{\mathcal{B}}\right)\leq\mathcal{C}_{\text{IM}}\left(\hat{\sigma}_{\mathcal{A}},\hat{\rho}_{\mathcal{A}}\right)+\mathcal{C}_{\text{IM}}\left(\hat{\sigma}_{\mathcal{B}},\hat{\rho}_{\mathcal{B}}\right)$, and also applying the non-increase of purification complexity to derive the second inequality. For example, if the reference state and target state are both factorized (separable states) as $\hat{\sigma}_{\mathcal{AB}}=\hat{\sigma}_{\mathcal{A}}\otimes\hat{\sigma}_{\mathcal{B}},\hat{\rho}_{\mathcal{AB}}=\hat{\rho}_{\mathcal{A}}\otimes\hat{\rho}_{\mathcal{B}}$, we have $\Delta\mathcal{C}_{\text{IM}}\geq 0$.

It is intriguing to expect that the mutual complexity $\Delta\mathcal{C}_{\text{IM}}\left(\hat{\rho}_{\mathcal{AB}}\right)$ is always subadditive. However, we can easily find a counterexample by relating the reference state to the target state via $\sigma_{\mathcal{AB}}=\hat{\rho}_{\mathcal{A}}\otimes\hat{\rho}_{\mathcal{B}}$. Then it is obvious that

$$\Delta\mathcal{C}\left(\hat{\rho}_{\mathcal{A}}\otimes\hat{\rho}_{\mathcal{B}},\hat{\rho}_{\mathcal{AB}}\right)=\mathcal{C}\left(\hat{\rho}_{\mathcal{A}},\hat{\rho}_{\mathcal{A}}\right)+\mathcal{C}\left(\hat{\rho}_{\mathcal{B}},\hat{\rho}_{\mathcal{B}}\right)-\mathcal{C}\left(\hat{\rho}_{\mathcal{A}}\otimes\hat{\rho}_{\mathcal{B}},\hat{\rho}_{\mathcal{AB}}\right)=-\mathcal{C}\left(\hat{\rho}_{\mathcal{A}}\otimes\hat{\rho}_{\mathcal{B}},\hat{\rho}_{\mathcal{AB}}\right)\leq 0\,, \tag{5.54}$$

because of the non-negativity of complexity. Finally, we should point out that the above example with $\Delta\mathcal{C}\leq 0$ exists for any potential definitions of complexity between two density operators.

5.2.3.4 First Law of complexity for mixed states

Since we also define the complexity of mixed states as the geodesic distance, the idea about the first law of complexity [4] also directly applies to the mixed states because they can be both considered as a similar classical mechanics problem. Therefore, perturbing the target state $\hat{\rho}_{\mathcal{A}}$ by a small variation $\hat{\rho}_{\mathcal{A}}+\delta\hat{\rho}_{\mathcal{A}}\equiv\hat{\rho}_{\mathcal{A}}(\lambda+\delta\lambda)$ with a fixed reference state, one can

easily find that the variation of complexity for mixed states also satisfies *the first law of complexity* [4, 6]

$$\begin{aligned}\delta\mathcal{C}_{\text{IM}} &= \mathcal{C}_{\text{IM}}\left(\hat{\rho}_{\mathcal{A}}+\delta\hat{\rho}_{\mathcal{A}}\right)-\mathcal{C}_{\text{IM}}\left(\hat{\rho}_{\mathcal{A}}\right)\,,\\ &= \left(P_\mu\delta\lambda^\mu+\frac{1}{2}\delta P_\mu\delta\lambda^\mu+\cdots\right)\Big|_{s=1}\,,\end{aligned} \tag{5.55}$$

where the "momentum" P_μ is defined as

$$\begin{aligned}P_\mu &= \frac{\partial F_{\text{IM}}}{\partial\dot{\lambda}^\mu}=\frac{2g^{\text{IM}}_{\mu\nu}\,\dot{\lambda}^\nu}{F_{\text{IM}}}\,,\\ \delta P_\mu &= \delta\lambda^\nu\frac{\partial^2 F_{\text{IM}}}{\partial\lambda^\nu\partial\dot{\lambda}^\mu}+\delta\dot{\lambda}^\nu\frac{\partial^2 F_{\text{IM}}}{\partial\dot{\lambda}^\nu\partial\dot{\lambda}^\mu}\,,\end{aligned} \tag{5.56}$$

with respect to the complexity measure (cost function), *i.e.,* the proper distance with the QFIM, $F_{\text{IM}}=\sqrt{2g^{\text{IM}}_{\mu\nu}\,\dot{\lambda}^\mu\,\dot{\lambda}^\nu}$. However, except for the similarity in form, we also want to point out an obvious difference between the first law of complexity for pure states and that for mixed states. The former only works for the perturbation from unitary transformations. As described in [4, 6], the variation of complexity is traced back to the change on unitary operator

$$|\Psi_{\text{T}}\rangle\longrightarrow|\Psi_{\text{T}}+\delta\Psi\rangle\,,\quad\text{with}\quad U_{\text{TR}}\longrightarrow U'_{\text{T}'\text{R}}=U_{\text{TR}}+\delta U\,. \tag{5.57}$$

However, for the first law of complexity for mixed states, we can also interpret the change on target states as either unitary or non-unitary transformations. In a short sentence, the general quantum operation triggers a generic small variation of the mixed state by

$$\hat{\rho}_{\mathcal{A}}\longrightarrow\hat{\rho}'_{\mathcal{A}}=\hat{\rho}_{\mathcal{A}}+\delta\hat{\rho}_{\mathcal{A}}=\sum_i\hat{M}_i\hat{\rho}_{\mathcal{A}}\hat{M}_i^\dagger\,. \tag{5.58}$$

5.3 Application: Gaussian Mixed States

In the last section, we have shown that the complexity from the quantum Fisher information metric is the purification complexity in (5.27) and also (5.47) with a simpler minimization. In this section, we would like to use the Gaussian mixed states as an explicit example to illustrate that the equivalence holds after the minimization on the Fubini-Study complexity over all purified states.

5.3.1 Geodesic and Complexity

As the first application of the complexity $\mathcal{C}_{\text{IM}}$ from the quantum Fisher information metric, we start from the same one-mode Gaussian state as introduced in section 3.2.2, *i.e.*,

$$\hat{\rho}_1 = \hat{S}_1(r)\hat{\upsilon}_{\text{th}}(\beta,\omega)\hat{S}_1^\dagger(r)\,. \tag{5.59}$$

where the one-mode squeezing operator $S_1(r)$ with a real parameter r is defined in eq. (3.14) and $\hat{\upsilon}_{\text{th}}$ defined in eq. (3.15) denotes the thermal state with inverse temperature β. For convenience, we have introduced two new parameters in section 3.2, *viz.*

$$\alpha = \frac{1}{2}\ln\frac{1+e^{-\beta\omega/2}}{1-e^{-\beta\omega/2}}\,, \quad \bar{r} = r - \frac{1}{2}\ln\frac{\mu}{\omega}\,, \tag{5.60}$$

where the μ is the characteristic frequency of the reference state $|\psi_{\text{R}}\rangle \equiv |0(\mu)\rangle$ which is chosen to be a Gaussian pure state. First of all, we need the quantum fidelity for squeezed thermal states [219]

$$F(\hat{\rho}(\zeta_1,\beta_1),\hat{\rho}(\zeta_2,\beta_2)) = \sqrt{\frac{2\sinh\frac{\beta_1\omega}{2}\sinh\frac{\beta_2\omega}{2}}{\sqrt{Y}-1}}\,, \tag{5.61}$$

with complex squeezing parameters $\zeta_i = r_i e^{i\theta_i}$ and

$$\begin{aligned} Y =& \cos^2(\frac{\theta_1-\theta_2}{2})\left(\cosh^2(r_1-r_2)\cosh^2\left(\frac{\beta_1+\beta_2}{2}\omega\right) - \sinh^2(r_1-r_2)\cosh^2\left(\omega\frac{\beta_1-\beta_2}{2}\right)\right) + \\ & \sin^2(\frac{\theta_1-\theta_2}{2})\left(\cosh^2(r_1+r_2)\cosh^2\left(\frac{\beta_1+\beta_2}{2}\omega\right) - \sinh^2(r_1+r_2)\cosh^2\left(\omega\frac{\beta_1-\beta_2}{2}\right)\right). \end{aligned} \tag{5.62}$$

One can obtain the quantum Fisher information metric (Bures metric) by taking two nearby states

$$\begin{aligned} ds^2 =& {}_2\ 1 - F(\hat{\rho},\hat{\rho}+\delta\rho)^2 \\ =& \frac{\omega^2}{16\sinh^2\frac{\beta\omega}{2}}d\beta^2 + \frac{1}{8}\left(1+\frac{1}{\cosh(\beta\omega)}\right)\left(4dr^2+\sinh^2(2r)d\theta^2\right) \\ =& d\alpha^2 + \frac{1}{4}\left(1-\frac{2}{3+\cosh(4\alpha)}\right)\left(4dr^2+\sinh^2(2r)d\theta^2\right), \end{aligned} \tag{5.63}$$

which reduces to a hyperbolic geometry $\mathbb{H}^2$ for pure states with $\beta = \infty$. Similar to the assumption in [2], we can ignore the phase part associated with the angle θ and focus on the two dimensional metric

$$ds^2_{\text{IM}} = d\alpha^2 + \left(1 - \frac{2}{3 + \cosh(4\alpha)}\right) dr^2, \tag{5.64}$$

whose geodesic equations ($\sigma \in [0, 1]$) read

$$\frac{\dot{r}(\sigma)(\cosh(4\alpha(\sigma)) + 1)}{\cosh(4\alpha(\sigma)) + 3} = C_0\,, \quad \frac{4\dot{r}(\sigma)^2 \sinh(4\alpha(\sigma))}{(\cosh(4\alpha(\sigma)) + 3)^2} - \ddot{\alpha}(\sigma) = 0. \tag{5.65}$$

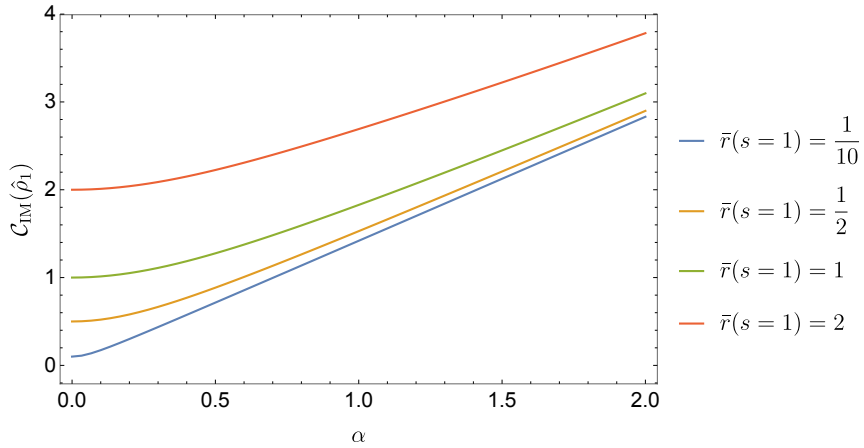

Figure 5.4: Circuit Complexity $\mathcal{C}_{\text{IM}}(\hat{\rho}_1)$ from the quantum Fisher information metric for one-mode Gaussian mixed state $\hat{\rho}_1\,(r(\sigma = 1), \alpha(\sigma = 1))$ with different boundary value $\bar{r}(\sigma = 1)$.

Taking the special initial conditions $\alpha(0) = 0, \bar{r}(0) = 0$ from our reference state $|\psi_{\text{R}}\rangle = |0(\mu)\rangle$, we can find the analytic solutions of geodesic equations

$$\begin{aligned} \alpha(\sigma) &= \frac{1}{2}\text{sech}^{-1}\left(\frac{\sqrt{C_1^2 \text{sech}^2\,(2C_1\sigma)}}{\sqrt{C_1^2 - C_0^2\tanh^2\,(2C_1\sigma)}}\right), \\ \bar{r}(\sigma) &= \frac{1}{2}\left(2C_0\sigma + \tanh^{-1}\left(\frac{C_0\tanh\,(2C_1\sigma)}{C_1}\right)\right). \end{aligned} \tag{5.66}$$

Imposing the boundary conditions, we can fix the constant C_0, C_1 as

$$C_0 = \pm\sqrt{C_1^2\left(\coth^2(2C_1) - \text{csch}^2(2C_1)\cosh^2(2\alpha(1))\right)}, \quad C_1 = \frac{C_0\tanh\,(2C_1)}{\tanh\,(2\bar{r}(1) - 2C_0)}, \tag{5.67}$$

where the sign of the first equation depends on the sign of $\bar{r}(\sigma = 1)$ and the second transcendental equation cannot be solved analytically. However, one can still find that the length of geodesic and complexity from the quantum Fisher information metric satisfy

$$g_{\mu\nu}\,\dot{\lambda}^{\mu}\dot{\lambda}^{\nu} = \frac{\dot{r}(\sigma)^2(\cosh(4\alpha(\sigma))+1)}{\cosh(4\alpha(\sigma))+3} + \dot{\alpha}(\sigma)^2 = C_0^2 + C_1^2, \tag{5.68}$$

and

$$\mathcal{C}_{\text{IM}}\left(|0(\mu)\rangle\,,\hat{\rho}_1\right) = \int_0^1 ds\,\sqrt{2g_{\mu\nu}\,\dot{\lambda}^{\mu}\dot{\lambda}^{\nu}} = \sqrt{2C_0^2+2C_1^2}\,, \tag{5.69}$$

which is derived from the semi-analytic geodesic solution (5.66). For later use, the geodesic solutions in (5.66) can be also rewritten as

$$\begin{aligned}
\alpha(\sigma) &= \frac{1}{2}\cosh^{-1}\left(\sqrt{\cosh^2(2C_1\sigma) - \frac{C_0^2}{C_1^2}\sinh^2(2C_1\sigma)}\right)\,,\\
\bar{r}(\sigma) &= C_0\sigma + \frac{1}{4}\ln\left(\frac{\cosh(2C_1\sigma)+\frac{C_0^2}{C_1^2}\sinh(2C_1\sigma)}{\cosh(2C_1\sigma)-\frac{C_0^2}{C_1^2}\sinh(2C_1\sigma)}\right)\,.
\end{aligned} \tag{5.70}$$

As a consistency check, we can consider the one-mode Gaussian pure state obtained by taking the following equivalent limits

$$\beta \longrightarrow \infty\,, \quad T \longrightarrow 0\,, \quad \alpha \longrightarrow 0\,. \tag{5.71}$$

It is easy to find that the geodesic solution (5.66) reduces to $C_1^2 = C_0^2$ and

$$\begin{aligned}
&\alpha(\sigma) = 0\,,\bar{r}(\sigma) = 2C_0\sigma = \bar{r}\,(\sigma=1)\,\sigma\,,\\
&\mathcal{C}_{\text{IM}}\left(|0(\mu)\rangle\,,|\psi_1\rangle\right) = \sqrt{2C_0^2+2C_1^2} = \bar{r}_1 = \frac{1}{2}\left|\ln\frac{\omega_1}{\mu}\right| = \mathcal{C}_{\text{FS}}\left(|0(\mu)\rangle\,,|\psi_1\rangle\right)\,,
\end{aligned} \tag{5.72}$$

which is the same as the results shown in [62] and [69]. Furthermore, we have pointed out an important result from [62] about pure Gaussian states, *i.e.,* the complexity of a pure Gaussian state factorizes in the normal basis. As a result, we can find that the pure-state limit of $\mathcal{C}_{\text{IM}}$ is equal to the complexity of any N-mode pure Gaussian state $|\psi_{\text{N}}\rangle$ (see *e.g.,* (2.9)) with Fubini-Study metric or F_2 cost function

$$\mathcal{C}_{\text{FS}}\left(|\psi_{\text{N}}\rangle\right) = \mathcal{C}_2\left(|\psi_{\text{N}}\rangle\right) = \mathcal{C}_{\text{IM}}\left(|\psi_{\text{N}}\rangle\right)\,, \tag{5.73}$$

which also implies that the ancillae for pure Gaussian state cannot decrease the complexity.

Except for the pure-state limit, we can also easily obtain the numerical solutions for (5.67) and the corresponding complexity by given $\bar{r}\,(\sigma=1)\,,\alpha\,(\sigma=1)$ for various target states. The numerical results are shown in the figure 5.4. From the geodesic solution (5.66), we actually identify the evolution of mixed states in the optimal circuit from $|0(\mu)\rangle$ to $\hat{\rho}_1$ as

$$\hat{\rho}_1(\sigma)=\hat{\rho}_1\left(r(\sigma),\alpha(\sigma)\right)\,, \tag{5.74}$$

without explicitly introducing the auxiliary system or performing any minimization process. In order to support our conclusion about the equivalence between purification complexity $\mathcal{P}_{\text{FS}}$ and mixes-state complexity $\mathcal{C}_{\text{IM}}$ from quantum Fisher information metric, we would like to show that the analytic trajectory for $\bar{r}(s),\alpha(s)$ can also be subtracted from the optimal circuit for purified states, *e.g.,* the two-mode Gaussian pure states whose complexity has been discussed in [62]. Comparing $\mathcal{C}_{\text{IM}}$ in (5.69) with the purification complexity derived by minimizing the complexity of purified states, we will show that the two results are the same in the next subsection.

Finally, we also note the mutual complexity of the TFD state is sub-additive, *i.e.,* $\Delta\mathcal{C}_{\text{IM}}\geq 0$ as shown in figure 5.5. From the viewpoint of purification complexity with F_2 cost function, the same result has been derived at section 7 in [2].

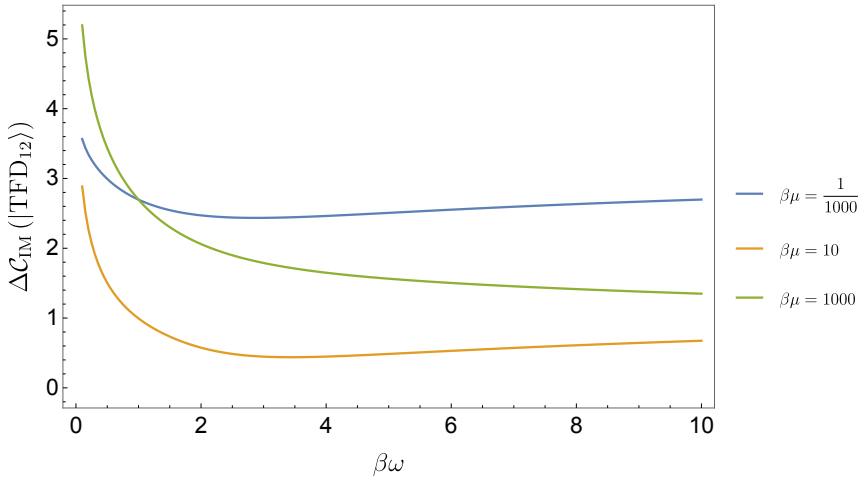

Figure 5.5: Mutual Complexity $\Delta\mathcal{C}_{\text{IM}}(|\text{TFD}_{12}\rangle)=\Delta\mathcal{C}_{\text{FS}}(|\text{TFD}_{12}\rangle)$ for TFD state is always subadditive.

5.3.2 Optimal Purifications and Purification Complexity

Given the mixed state $\hat{\rho}_{\mathcal{A}}$ for subsystem $\mathcal{A}$, we can obtain its purified state $|\Psi\rangle_{\mathcal{A}\mathcal{A}^c}$ by introducing ancillae, the auxiliary system $\mathcal{A}^c$. The purification complexity of $\hat{\rho}_{\mathcal{A}}$ is defined as the minimal complexity of purified states, *i.e.,*

$$\mathcal{P}\left(\hat{\rho}_{\mathcal{A}}\right)=\min_{\mathcal{A}^c}\mathcal{C}\left(|\Psi\rangle_{\mathcal{A}\mathcal{A}^c}\right)\,, \tag{5.75}$$

where the minimization is done over all possible purified states with $\mathrm{Tr}_{\mathcal{A}^c}\left(|\Psi\rangle_{\mathcal{A}\mathcal{A}^c}\langle\Psi|_{\mathcal{A}\mathcal{A}^c}\right)=\hat{\rho}_{\mathcal{A}}$. As we discussed around eq. (5.47), this minimization over all purified target states is enough to get the purification complexity, as we will explicitly show in this section.

Restricted on the Gaussian pure states, we have shown in subsections 3.2.1 and 3.2.2 that there is a one-parameter family of two-mode purified states, *i.e.,*

$$|\Psi_{\mathcal{A}\mathcal{A}^c}\rangle\rightarrow|\psi\rangle_{12}=\hat{S}_1(r)\,\hat{S}_2(s)\,\hat{S}_{12}(\alpha)\,|0\rangle_1\,|0\rangle_2\,, \tag{5.76}$$

whose position-space wavefunction is given by eq. (3.9) or eq. (3.23). In our the matrix representation (3.26), the purified Gaussian state is denoted by

$$M_{\mathrm{T}}^{ab}=\omega\begin{pmatrix}e^{2r}\cosh 2\alpha & -e^{r+s}\sinh 2\alpha\\ -e^{r+s}\sinh 2\alpha & e^{2s}\cosh 2\alpha\end{pmatrix}=\mu\begin{pmatrix}e^{2\bar{r}}\cosh 2\alpha & -e^{\bar{r}+\bar{s}}\sinh 2\alpha\\ -e^{\bar{r}+\bar{s}}\sinh 2\alpha & e^{2\bar{s}}\cosh 2\alpha\end{pmatrix}. \tag{5.77}$$

Fixing the reference state as the unentangled state $|0(\mu)\rangle\otimes|0(\mu)\rangle$, the purification complexity of Gaussian mixed state $\hat{\rho}_1$ is derived as

$$\mathcal{P}\left(|0(\mu)\rangle\,,\hat{\rho}_1\right)=\min_{s}\mathcal{C}\left(|0(\mu),0(\mu)\rangle\,,|\psi\rangle_{12}\right)\,, \tag{5.78}$$

where the complexity of Gaussian pure states depends on the choice of the cost function and minimization is performed among the free parameter s. For example, the purification complexity for the one-mode Gaussian mixed states with respect to the F_1-cost function has been discussed in detail in section 3.2.

In order to compare with the complexity from the quantum Fisher information metric, it is natural to consider the F_2-cost function or Fubini-Study metric. In subsection 2.1.2.1, we have discussed the pure-state complexity with the Fubini-Study metric approach. In this section, we take the optimal circuit for pure Gaussian states and apply the minimization to find the optimal trajectory for mixed states in the subsystem, *i.e.,* the one-mode state $\hat{\rho}_1(\sigma)$. From the matrix representation of the elements U_2 in $\mathrm{GL}(2,\mathbb{R})$ group shown in eq. (2.34),

the purified Gaussian state $\psi_{12}(x_+, x_-) = U_2\,\psi_{\rm R}(x_+, x_-)$ along the circuit (path) in this matrix representation is given by eq. (2.35), *i.e.,*

$$M_2(\sigma) = \mu \begin{pmatrix} e^{2y}(\cosh(2\rho) + \cos(2x)\sinh(2\rho)) & e^{2y}\sin(2x)\sinh(2\rho) \\ e^{2y}\sin(2x)\sinh(2\rho) & e^{2y}(\cosh(2\rho) - \cos(2x)\sinh(2\rho)) \end{pmatrix}, \tag{5.79}$$

with boundary conditions fixed by the specific target state. As advertised before, the optimal circuit is a straight line connecting the reference state and the target state in the norm basis, *i.e.,*

$$\rho(\sigma) = \rho_1\sigma\,, \quad x(\sigma) = x_0\,, \quad y(\sigma) = y_1\sigma\,, \tag{5.80}$$

with

$$y_1 = \frac{1}{4}\log\left(\frac{\omega_+\omega_-}{\mu^2}\right), \quad \rho_1 = \frac{1}{4}\log\frac{\omega_+}{\omega_-}\,. \tag{5.81}$$

and $\omega_\pm$ as the normal frequencies of the two-mode Gaussian state. According to the choice of cost functions, we can derive the complexity of two-mode Gaussian states as [11]

$$\begin{aligned} \mathcal{C}_{\rm FS}\left(|\psi_{12}\rangle\right) &= \mathcal{C}_2\left(|\psi_{12}\rangle\right) = \frac{1}{2}\sqrt{\left(\ln\frac{\omega_+}{\mu}\right)^2 + \left(\ln\frac{\omega_-}{\mu}\right)^2}\,, \\ \left(\mathcal{C}_{\rm FS}\left(|\psi_{12}\rangle\right)\right)^2 &= \mathcal{C}_{\kappa=2}\left(|\psi_{12}\rangle\right)\,. \end{aligned} \tag{5.82}$$

In addition, from the trajectory of two-mode Gaussian states, we can also explore the reduced trajectory of mixed Gaussian state $\hat{\rho}_1(\sigma)$ by tracing out one of the two modes. In the matrix representation, the purified states $|\psi_{12}\rangle$ for mixed states $\hat{\rho}_1$ is also given by $M_{\rm T}^{ab}$ as defined in eq. (5.77). Identifying the two matrix representations in eqs. (5.79) and (5.77), we can find the transformation

$$\begin{aligned} \bar{r} + \bar{s} &= 2y\,, \qquad \bar{r} - \bar{s} = \pm\frac{1}{2}\ln\left(\frac{\cosh 2\rho - \cos 2x\sinh 2\rho}{\cosh 2\rho + \cos 2x\sinh 2\rho}\right), \\ \alpha &= \frac{1}{2}\cosh^{-1}\left(\sqrt{\cosh^2 2\rho - \cos^2 2x\sinh^2 2\rho}\right). \end{aligned} \tag{5.83}$$

Recalling the geodesic solution (5.80) for pure Gaussian states, we then derive the trajectory of mixed Gaussian states $\hat{\rho}_1(\bar{r}, \alpha)$ as

$$\begin{aligned} \alpha(\sigma) &= \frac{1}{2}\cosh^{-1}\left(\sqrt{\cosh^2(2\rho_1\sigma) - \cos^2 2x_0\sinh^2(2\rho_1\sigma)}\right), \\ \bar{r}(\sigma) &= y_1\sigma + \frac{1}{4}\ln\left(\frac{\cosh(2\rho_1\sigma) + \cos 2x_0\sinh(2\rho_1\sigma)}{\cosh(2\rho_1\sigma) - \cos 2x_0\sinh(2\rho_1\sigma)}\right), \end{aligned} \tag{5.84}$$

[11] We adopt the definition shown in eq. (5.4) in order to exactly identify $\mathcal{C}_{\rm FS}\left(|\psi_{12}\rangle\right)$ and $\mathcal{C}_2\left(|\psi_{12}\rangle\right)$

which exactly matches the geodesic path (5.70) derived in 2D-manifold with the quantum Fisher information metric! But this is not the final answer for the purification complexity because we still need to find the optimal purification with a given target state $\hat{\rho}_1\left(\alpha\left(\sigma=1\right),\bar{r}\left(\sigma=1\right)\right)$ and then it will determine the free parameter $\bar{s}$ (decoded in the parameter ρ_1 via eq. (5.81)) for the optimal purification. Some analytical approximations have been discussed in [2]. Instead, we can also directly perform the numerical minimization. With all given target states $\hat{\rho}_1$ (as shown in figure 5.4 [12]), we find that the minimization leads us to the same minimum for complexity as (5.69). As a summary, the minimization for the purification complexity of the Gaussian mixed state $\hat{\rho}_1$ simply shows the equivalence, *i.e.,*

$$\mathcal{P}_{\text{FS}}\left(\left|0(\mu)\right\rangle,\hat{\rho}_1\right)\equiv\min_{\bar{s}}\mathcal{C}_{\text{FS}}\left(\left|\psi_{12}\right\rangle\right)=\min_{\bar{s}}\frac{1}{2}\sqrt{\left(\ln\frac{\omega_+}{\mu}\right)^2+\left(\ln\frac{\omega_-}{\mu}\right)^2}=\mathcal{C}_{\text{IM}}\left(\left|0(\mu)\right\rangle,\hat{\rho}_1\right)\,. \tag{5.85}$$

As shown in eqs. (5.70), (5.84), this equivalence also means that the optimal circuit found from the geodesic associated with the quantum Fisher information metric is the same as that from the optimal circuit for two-mode pure Gaussian state by tracing out one extra ancillary mode. This simple example illustrates our main conclusion that the mixed-state complexity (geodesic distance) associated with the quantum Fisher information metric is the purification complexity measured by the Fubini-Study metric. More generally, our proof in (5.27) also indicates the optimal purification for one-mode Gaussian state is actually the essential purification, *i.e.,* two-mode Gaussian state, confirming the expectation and assumption in [2].

5.3.3 Purified States with Uhlmann's fidelity

In the last subsection, we have shown the equivalence between purification complexity $\mathcal{P}_{\text{FS}}$ and mixed-state complexity $\mathcal{C}_{\text{IM}}$ based on the quantum Fisher information metric. In this subsection, we explicitly construct the optimal purified states and show that they saturate Uhlmann's fidelity. Furthermore, we also illustrate the quantum fidelity's bound, *i.e.,* Uhlmann's theorem for Gaussian state as stated in (5.8) is satisfied by taking the two-mode pure Gaussian state as purification. Taking two arbitrary mixed Gaussian states

[12] We find the difference between that and the results from numerical minimization is at the order 10^{-15} which is just the machine precision. Decreasing machine precision also correspondingly decreases the difference.

$\hat{\rho}_1\,(r_1,\alpha_1)$ and $\hat{\rho}_1'\,(r_2,\alpha_2)$, their quantum fidelity is found to be

$$F(\hat{\rho}_1,\hat{\rho}_1')=\sqrt{\frac{2\sinh\frac{\beta_1\omega}{2}\sinh\frac{\beta_2\omega}{2}}{\sqrt{\left(\cosh^2(r_1-r_2)\cosh^2\left(\frac{\beta_1+\beta_2}{2}\omega\right)-\sinh^2(r_1-r_2)\cosh^2\left(\omega\frac{\beta_1-\beta_2}{2}\right)\right)}-1}}\,, \tag{5.86}$$

which should be equivalent to the fidelity between specific purified states according to Uhlmann's theorem.

First of all, we start from the simplest purification, *i.e.,* the two-mode Gaussian states (3.22). Noting that we can parametrize the wavefunction of purified Gaussian states as (3.23)

$$\psi_{12}(x,y)=\sqrt{\frac{\omega}{\pi}}\,e^{\frac{r+s}{2}}\,\exp\left[-\frac{\omega}{2}\left(\cosh 2\alpha\,(e^{2r}x^2+e^{2s}y^2)-2\,e^{r+s}\sinh 2\alpha\,xy\right)\right]\,, \tag{5.87}$$

it is easy to find the quantum fidelity between pure Gaussian states $\psi_{12}(x,y;r_1,s_1,\alpha_1)$ and $\psi_{12}'(x,y;r_2,s_2,\alpha_2)$ as

$$\begin{aligned}F(\lambda_1,\lambda_2)=|\langle\psi\,|\psi'\rangle|&=\int_{-\infty}^{\infty}\int_{-\infty}^{\infty}\psi_{12}(x,y;r_1,s_1,\alpha_1)\psi_{12}'(x,y;r_2,s_2,\alpha_2)\,dx\,dy\,,\\&=\sqrt{\frac{2}{\cosh 2\alpha_1\cosh(2\alpha_2)\cosh(r_1-r_2-s_1+s_2)+\cosh(r_1-r_2+s_1-s_2)-\sinh 2\alpha_1\sinh 2\alpha_2}}\,,\end{aligned} \tag{5.88}$$

by a simple Gaussian integral. The maximal fidelity is decided by the saddle point with

$$\partial_{s_1}F(\lambda_1,\lambda_2)=0\qquad\text{and}\qquad\partial_{s_2}F(\lambda_1,\lambda_2)=0\,. \tag{5.89}$$

However, the above two derivative equations lead us to the same solution

$$s_2=s_1+\frac{1}{2}\log\left(\frac{e^{2r_1}+e^{2r_2}\cosh 2\alpha_1\cosh 2\alpha_2}{e^{2r_2}+e^{2r_1}\cosh 2\alpha_1\cosh 2\alpha_2}\right)\,. \tag{5.90}$$

Generally, the maximum of $F(\lambda_1,\lambda_2)$ should be given by critical point with $\partial_{s_1}F(\lambda_1,\lambda_2)=0$ and $\partial_{s_2}F(\lambda_1,\lambda_2)=0$ simultaneously. However, either condition is sufficient because of the unitary invariance of the fidelity. Plugging the solutions of s_1-s_2 into the fidelity between

pure states, we obtain the maximum fidelity

$$\max_{|\psi_{12}\rangle,|\psi'_{12}\rangle} F(\lambda_1,\lambda_2)$$
$$= \sqrt{\frac{2}{\sqrt{\cosh^2 2\alpha_1 \cosh^2 2\alpha_2 + 2\cosh 2\alpha_1 \cosh 2\alpha_2 \cosh(2r_1-2r_2)+1} - \sinh 2\alpha_1 \sinh 2\alpha_2}}, \tag{5.91}$$

which is nothing but Uhlmann's fidelity (5.86) derived from two Gaussian mixed states $\hat{\rho}(r_1,\alpha_1)$ and $\hat{\rho}(r_2,\alpha_2)$. From this viewpoint, we can claim that the purification restricted on pure Gaussian states is enough to achieve the optimal purification for mixed Gaussian state $\hat{\rho}_1$, *i.e.,* satisfying the fidelity bound in Uhlmann's theorem. That point illustrates why we can match the complexity and also the evolution of the path for mixed states $\hat{\rho}_1(\sigma)$ with those derived from only two-mode Gaussian pure states, which was explicitly shown in the last subsection.

To close this chapter, we summarize the main conclusions discussed in previous sections. First of all, we generalized the Fubini-Study method for circuit complexity to generic quantum states by using the quantum Fisher information metric $g^{\text{IM}}_{\mu\nu}$ in section 5.1. Due to the special properties of Uhlmann's fidelity (see (5.8)), we further find that the complexity $\mathcal{C}_{\text{IM}}$ defined in (5.19) between arbitrary two quantum states exactly equals the purification complexity measured by the Fubini-Study metric (or QFIM) on the extended Hilbert space for purified states, *i.e.,* (5.47)

$$\mathcal{C}_{\text{IM}}(\hat{\sigma}_{\mathcal{A}},\hat{\rho}_{\mathcal{A}}) = \min_{\Phi,\Psi} \mathcal{C}_{\text{FS}}(|\Phi_{\mathcal{A}\mathcal{A}^c}\rangle, |\Psi_{\mathcal{A}\mathcal{A}^c}\rangle) = \min_{\Phi,\Psi} \mathcal{C}_{\text{IM}}(|\Phi_{\mathcal{A}\mathcal{A}^c}\rangle, |\Psi_{\mathcal{A}\mathcal{A}^c}\rangle)\ . \tag{5.92}$$

Without explicitly introducing the auxiliary system and purifying the mixed states, our method avoids the challenging minimization over all purifications. This equivalence is illustrated by the example from Gaussian mixed states in section 5.3. Interestingly, we also prove that this purification complexity $\mathcal{C}_{\text{IM}}$ is always non-increasing under any quantum operations such as partial trace in (5.32). From this monotonicity, we also show the mutual complexity $\Delta\mathcal{C}_{\text{IM}}$ cannot be either subadditive or superadditive in general.

Chapter 6

Discussion

In this thesis, we examined the complexity of mixed states. After reviewing both circuit complexity and holographic complexity for pure states in chapter 2, we began with the purification complexity using the F_1 cost function, which was introduced in Nielsen's geometric approach to pure-state complexity. Our exploration in chapter 3 focused on the complexity of Gaussian mixed states in a free scalar field theory. We applied both the physical basis and the diagonal basis to study the purification complexity of a thermal density matrix and the reduced density matrix for a subregion of the vacuum. Next, we reviewed the holographic proposals for subregion complexity in the literature, *e.g.,* subregion-CV, subregion-CA, and subregion-CV2.0. Correspondingly, we explicitly presented the results in chapter 4 for the holographic complexity dual to a thermal state as well as subregions of the vacuum. Furthermore, in chapter 5, we also proposed a different approach to the circuit complexity of mixed states with the help of the quantum Fisher information metric or Bures metric. As a result of Uhlmann's theorem, we proved that the mixed-state complexity derived from QFIM is equivalent to the purification complexity obtained from Fubini-Study metric approach but without explicitly performing any purifications in our proposal.

In this final chapter, we would like to discuss some results that connect to the investigations in previous chapters. To finally close this thesis, we also briefly outline some possible directions for future studies.

6.1 Other Proposals for Mixed-State Complexity

Our exploration on the circuit complexity of mixed states in chapter 3 focused on a definition dubbed the **purification complexity** in [171]. That is, we considered the minimal complexity amongst the possible pure states that purify the desired mixed state $\hat{\rho}_{\mathcal{A}}$. Let us point out, however, that our perspective differs slightly from that of the authors of [171] in that the latter only consider essential purifications. The reason for this restriction was that they wanted the definition to collapse to the usual pure state complexity definition when the target state is pure. For the Gaussian mixed states considered in this thesis, we found that essential purifications are actually optimal and as a consequence this assumption becomes redundant. It would be interesting to explore whether including extra auxiliary degrees of freedom that appear in a simple tensor product in the final pure state could actually reduce the complexity of mixed states (or pure states) in more complicated situations.[1]

We might add that the purification complexity discussed here and in [171] is closely aligned with the standard approach developed in quantum information theory, *e.g.,* [176, 182]. However, in this setting, the auxiliary degrees of freedom are regarded as another resource required for the preparation of the desired mixed states, and hence an additional cost is associated with adding more ancillae. This cost was not considered in our analysis nor in [171]. This would be another feature that would favor essential purifications as the optimal purifications. Taking the one-mode Gaussian mixed state $\hat{\rho}_1$ as an example, we found the same complexity using either one or two ancillae, implying that the essential purification with one ancilla would clearly become the optimal one if we added an extra penalty for each ancilla that is introduced. Still, it would be interesting to investigate whether this simple result extends to, e.g., the case of interacting quantum field theories.

Before proceeding with a further discussion of our results, we would first like to briefly review some other proposals for mixed-state complexity and possible connections to our work:

Spectrum and Basis Complexity: One alternative [171] is to break the problem of preparing mixed states into two parts — creating the spectrum and creating the basis of eigenvectors. The spectrum complexity $\mathcal{C}_S$ is defined as the minimal purification complexity of some mixed state $\hat{\rho}_{\text{spec}}$ that has the same spectrum as $\hat{\rho}_{\mathcal{A}}$, where one also optimizes over the possible $\hat{\rho}_{\text{spec}}$. Since one possible $\hat{\rho}_{\text{spec}}$ with the required spectrum is simply $\hat{\rho}_{\mathcal{A}}$, we conclude that $\mathcal{C}_S \leq \mathcal{C}_P$, where $\mathcal{C}_P$ denotes the purification complexity of $\hat{\rho}$. In our analysis,

[1] We are reminded here of coherent (pure) states [1], where, in simple examples, the reference and target states had a tensor product structure which was not respected by the intermediate states.

the spectrum is defined by the eigenvalues of the matrix B in eq. (3.70).

The basis complexity can be defined in different ways: The first suggestion in [171] is simply the difference $\mathcal{C}_P - \mathcal{C}_S$. The second suggestion is to define $\mathcal{C}_B$ as the complexity (*i.e.,* minimal number of unitary gates) required to go from the optimal $\hat{\rho}_{\text{spec}}$ to our target state $\hat{\rho}$. The latter preparation can be made with unitary gates because the two mixed states share the same spectrum. We can easily demonstrate $\mathcal{C}_P \leq \mathcal{C}_S + \mathcal{C}_B$ since on the left-hand side, the preparation is constrained to pass through the intermediate state $\hat{\rho}_{\text{spec}}$.

Our construction using the physical basis seems closely related to this approach. To modify the spectrum, one must use "mixed" entangling gates acting between $\mathcal{A}$ and $\mathcal{A}^c$, and so these would appear in the circuit preparing (the purification of) $\hat{\rho}_{\text{spec}}$. The gates acting only on the $\mathcal{A}$ degrees of freedom modify the basis, and the circuit preparing $\hat{\rho}_{\mathcal{A}}$ from $\hat{\rho}_{\text{spec}}$ is comprised solely of these gates. However, it seems that there is no natural role for the gates acting only on $\mathcal{A}^c$. In this framework then, not using these gates may be the reason for the difference in the complexities, *i.e.,* $\mathcal{C}_P \leq \mathcal{C}_S + \mathcal{C}_B$. Let us also note that both the spectrum complexity and the entanglement entropy are both insensitive to the action of the gates acting only on $\mathcal{A}$ or only on $\mathcal{A}^c$. Only the $\mathcal{A}\mathcal{A}^c$ entangling gates change these quantities. For example, considering two mixed states of a single harmonic oscillator with the same entanglement entropies, this implies that the spectrum complexities must also be equal. It would be interesting to understand to what extent this property generalizes to states over many degrees of freedom, *e.g.,* the thermal state of a free scalar, studied in section 3.4.

Open System Complexity: Open system complexity studies the complexity of circuits that move through the space of density matrices using general CPTP maps, rather than only unitary transformations. This requires characterizing these general maps in terms of elementary operations and then assigning a cost to the latter. Of course, as discussed in the introduction, the dilation theorems [181] imply that the most general CPTP maps acting on a system of qubits can be realized as unitary evolution of the system coupled to ancillary qubits [176], which seems to bring this approach back to the framework used for the purification complexity. However, one potential difference for the open system complexity is that some of the ancillae may be introduced and traced out, *i.e.,* they are re-initialized, at every step. This would contrast with having a single reservoir of ancillae on which we can repeatedly act before tracing them at the very end of the unitary evolution, as described for the purification complexity.

Ensemble Complexity: The ensemble complexity is defined using a decomposition

of the mixed state over an ensemble of pure states as follows

$$\mathcal{C}_E = \min_{\{p_i,|\psi_i\rangle\}} \sum_i p_i \, \mathcal{C}(|\psi_i\rangle) \,, \qquad \text{where} \quad \hat{\rho} = \sum_i p_i |\psi_i\rangle\langle\psi_i| \,. \tag{6.1}$$

Of course, this notion reduces to the pure state complexity when the state $\hat{\rho}_{\mathcal{A}}$ is pure. Even with a Gaussian mixed state $\hat{\rho}_{\mathcal{A}}$, we would generally have to explore ensembles that are not constructed solely from Gaussian states. In the case of a thermal state, a decomposition is available in terms of coherent states and this allows to put a bound on the ensemble complexity of thermal states — see section 3.5 of [171] for further details.

Alternative Measures of Mixed-State Complexity: In chapter 5, we considered the quantum Fisher information metric or Bures metric as the measure for mixed-state complexity $\mathcal{C}_{\text{IM}}$. However, one may also consider alternative measures like choosing various cost functions in Nielsen's geometric method. In [3], we also examined some other distance measures in the space of density matrices, *e.g.,* trace distance, Hilbert-Schmidt distance. However, all these methods to evaluate the purification complexity or mixed-state complexity require solving the geodesic problem whose analytical solution may be absent.

As we shown in section 2.1.1, the circuit complexity of a Gaussian state with F_2 cost function is given by eq. (2.19). The result is also extended to any arbitrary Gaussian state in [65, 68]. Denoting the covariance matrices of reference state and target state as $\Sigma_{\text{R}}, \Sigma_{\text{T}}$, respectively, the circuit complexity of pure Gaussian states is given by a simple formula, namely

$$\mathcal{C}_2 = \frac{1}{2\sqrt{2}} \sqrt{\text{Tr}\left[(\log \Delta_{\text{TR}})^2\right]} \,, \tag{6.2}$$

with relative covariance matrix defined as $\Delta_{\text{TR}} \equiv \Sigma_{\text{T}} \Sigma_{\text{R}}^{-1}$. It is natural to expect that such a simple form can be generalized to any mixed Gaussian state because its covariance matrix is also well-defined. For unfamiliar readers, we refer them to appendix C for a minimal introduction to Gaussian states and their covariance matrices. Inspired by this compact formula (6.2) for pure Gaussian states, the authors in [220, 221] suggest the **Fisher-Rao distance** between covariance matrices Σ_{R} and Σ_{T} as the complexity of corresponding Gaussian states $\hat{\rho}_{\text{R}}, \hat{\rho}_{\text{T}}$, *i.e.,*

$$\mathcal{C}_2\left(\hat{\rho}_{\text{R}}, \hat{\rho}_{\text{T}}\right) \equiv \frac{1}{2\sqrt{2}} \sqrt{\text{Tr}\left[(\log \Delta_{\text{TR}})^2\right]} \equiv \frac{1}{2\sqrt{2}} \left\| \log\left(\Sigma_{\text{R}}^{-1/2} \Sigma_{\text{T}} \Sigma_{\text{R}}^{-1/2}\right) \right\|_2 \,. \tag{6.3}$$

It is obvious that it reduces to the result in eq. (6.2) for pure Gaussian states. More interestingly, another advantage of this measure is that the unique geodesic between the

reference state and target state (*i.e.,* optimal circuit) is exactly solved by

$$\gamma_{\text{FR}}(s) \equiv \Sigma_{\text{R}}^{1/2}\left(\Sigma_{\text{R}}^{-1/2}\Sigma_{\text{T}}\Sigma_{\text{R}}^{-1/2}\right)^{s}\Sigma_{\text{R}}^{1/2}\,, \qquad 0 \leqslant s \leqslant 1\,, \tag{6.4}$$

which is also known as the s-geometric mean of matrices $\Sigma_{\text{T}}, \Sigma_{\text{R}}$. To close here, we remark that the Fisher-Rao distance is only well-defined for positive definite matrices like covariance matrices of Gaussian states. It is not clear how to generalize this distance measure to more general density matrices.

6.2 Mutual Complexity in QFT

In section 3.4.5, we considered beginning with the pure state $|\Psi_{\mathcal{AB}}\rangle$, and then constructed the two reduced density matrices, $\hat{\rho}_{\mathcal{A}}$ and $\hat{\rho}_{\mathcal{B}}$. Then in eq. (3.105), the mutual complexity was then defined as the combination [189],

$$\Delta\mathcal{C} = \mathcal{C}(\hat{\rho}_{\mathcal{A}}) + \mathcal{C}(\hat{\rho}_{\mathcal{B}}) - \mathcal{C}(|\Psi_{\mathcal{AB}}\rangle)\,, \tag{6.5}$$

which quantifies the additional correlations between the subsystems $\mathcal{A}$ and $\mathcal{B}$.

Our first application of this quantity was to compare the complexity of the TFD state with the purification complexity of the thermal mixed state produced by tracing out either the left or the right degrees of freedom, *e.g.,* see eq. (3.106). As a warm-up exercise, we evaluated the mutual complexity for a two-mode TFD state and as shown in eq. (3.109), we found $\Delta\mathcal{C}_1^{\text{diag}}(|\text{TFD}\rangle_{12}) > 0$. More generally, we might evaluate the mutual complexity for general two-mode pure Gaussian states $|\Psi\rangle_{12}$. That is, integrating out each of the degrees of freedom in term yields two distinct mixed states, $\hat{\rho}_1$ and $\hat{\rho}_2$, and so one might compare the purification complexity of these two mixed states with that of the parent pure state, with the analogous expression to that in eq. (6.5). In fact, using the results for the purification complexity of one-mode Gaussian states in eq. (3.36), it is straightforward to show that subadditivity always holds for any two-mode pure Gaussian state, *i.e.,*

$$\Delta\mathcal{C}_1^{\text{diag}}(|\Psi\rangle_{12}) = \mathcal{C}_1^{\text{diag}}(\hat{\rho}_1) + \mathcal{C}_1^{\text{diag}}(\hat{\rho}_2) - \mathcal{C}_1^{\text{diag}}(|\Psi\rangle_{12}) \geq 0\,. \tag{6.6}$$

However, this inequality does not extend to the purification complexity calculated in the physical basis, as in section 3.2.4. It would be interesting to investigate whether the above inequality can be made more restrictive, *e.g.,* where the mutual complexity is greater than some finite bound proportional to the entanglement entropy.

Since in section 3.4, the TFD state has a simple product structure for the free scalar field theory, the mutual complexity becomes simply a sum over the same quantity evaluated for each of the individual modes — see eqs. (3.110) and (3.124). Hence the positivity appearing in eq. (3.109) for the two-mode TFD states in the diagonal basis extends to the TFD state of the full scalar QFT. That is, $\Delta\mathcal{C}_1^{\text{diag}}(|\text{TFD}\rangle) > 0$ irrespective of the values of the temperature, reference frequency or the mass of the scalar.

This positivity is not replicated for the mutual complexity when it is evaluated using the physical basis, as shown in figure 3.10. There we showed that for a massless two-dimensional scalar, $\Delta\mathcal{C}_1^{\text{phys}}(|\text{TFD}\rangle)$ becomes negative when the reference frequency μ is much smaller or much larger than the temperature.

In section 3.4.5 we found that with $\mu \gg T$, the mutual complexity of the TFD state is proportional to entanglement entropy between the left and right copies of the field theory. However, in general, there would be an overall proportionality constant that contains a temperature dependence through the (dimensionless) ratio T/μ, as well as T/m for a massive scalar. This behaviour is easily seen analytically in the diagonal basis using eqs. (3.114) and (3.115), but similar results also apply in the physical basis, see comments at the end of section 3.4.5.2. In any event, the appearance of the entanglement entropy in the regime $\mu \gg T$ reinforces the intuition that the mutual complexity in eq. (6.5) quantifies the correlations between the subsystems to which the pure state is reduced.

Before turning to subregions, let us briefly comment again that $\Delta\mathcal{C}$ is UV finite for the TFD state. For the free scalar, we found that the leading UV divergence in the purification complexity of the thermal mixed state is the same for either the diagonal or physical basis, as determined in eqs. (3.88)-(3.90) or eq. (3.102), respectively. The precise form of this leading divergence can be found as

$$\mathcal{C}(\hat{\rho}_{\text{th}}(\beta)) \simeq \begin{cases} \frac{\Omega_{d-2}V_{d-1}}{2\,(2\pi)^{d-1}(d-1)}\,\Lambda^{d-1}\left(\ln\frac{\mu}{\Lambda}+\frac{1}{d-1}\right)\,, & \mu \geq \Lambda\,, \\ \frac{\Omega_{d-2}V_{d-1}}{2\,(2\pi)^{d-1}(d-1)}\,\Lambda^{d-1}\left(\ln\frac{\Lambda}{\mu}+\frac{2}{d-1}\left(\frac{\mu}{\Lambda}\right)^{d-1}-\frac{1}{d-1}\right)\,, & \mu \leq \Lambda\,. \end{cases} \tag{6.7}$$

Exactly, the same divergences also appear in the complexity of the vacuum state of the scalar field theory, *e.g.,* see appendix B of [69]. These divergences are also exactly one-half of those found for the TFD state, and hence the subtraction in eq. (3.106) yields $\Delta\mathcal{C}(|\text{TFD}\rangle)$ which is UV finite (in either basis). More precisely, all of the potentially divergent contributions cancel in the integrand of eq. (3.111) for the diagonal basis and of eq. (3.124) for the physical basis, and so all of the UV divergences cancel in the corresponding mutual complexities.

Of course, this UV finiteness is directly related to the fact that optimal purification of the thermal state $\hat{\rho}_{\text{th}}(\beta)$ is not the TFD state. Much of the preparation of the TFD

state involves introducing short-distance correlations in *both* copies of the field theory. Even though the optimal purification of $\hat{\rho}_{\rm th}(\beta)$ involves introducing a number of auxiliary degrees of freedom that is equivalent to introducing a second copy of the QFT, there is no need to prepare the purification with UV correlations amongst the ancillae since after they are integrated out, these will not affect the physical correlations of the thermal mixed state.[2] This is why the UV divergences in $\mathcal{C}(\hat{\rho}_{\rm th}(\beta))$ carry exactly a factor of one-half compared to $\mathcal{C}\left(|{\rm TFD}\rangle\right)$.[3]

In section 3.5, we considered the purification complexity of subregions of the vacuum. In this case, both the vacuum state and the mixed states produced by reducing to a subregion can again be written in a product form. However, the basis of states appearing in these products is not the same, *i.e.,* for the vacuum, we use momentum eigenstates (which are eigenstates of the Hamiltonian), while for the subregions, we use eigenstates of the corresponding modular Hamiltonian. Hence we can no longer apply eq. (6.6) to determine the sign of the mutual complexity of the vacuum divided into two complementary subregions, $\mathcal{A}$ and $\mathcal{B}$. However, we found that $\Delta\mathcal{C}_1^{\rm diag}$ is still positive in the diagonal basis, as illustrated in figure 3.13. In the physical basis, we gave two definitions of the mutual complexity in eq. (3.144), which differ by the basis in which the ground state complexity is evaluated. Our analysis indicates that $\Delta\mathcal{C}_1^{\rm phys}$ is generally negative, while $\Delta\tilde{\mathcal{C}}_1^{\rm phys}$ is positive, as illustrated in figure 3.17. The sign difference between these two definitions is due to the vacuum complexity being much larger in $\Delta\mathcal{C}_1^{\rm phys}$ than in $\Delta\tilde{\mathcal{C}}_1^{\rm phys}$. The cutoff dependence of $\Delta\mathcal{C}_1^{\rm phys}$ is related to the subleading divergences of the subregion complexities and the ground state complexity, which are all logarithmic. On the other hand, the cutoff dependence of $\Delta\tilde{\mathcal{C}}_1^{\rm phys}$ is dominated by the subleading divergence of $\mathcal{C}_1^{\mathcal{AB}}(|\Psi_0\rangle)$, which is linear in the cutoff. We turn to the comparison of the mutual complexity from our QFT and our holographic calculations in the next subsection.

Before closing here, let us note that for subregions of the vacuum, it is again the case that the original state, *i.e.,* the vacuum state, does not provide the optimal purification. If the vacuum were the optimal purification, then the subregion complexity would simply match the complexity of the ground state. As a result, the leading divergence of all of the subregion complexities would be $\mathcal{C} \sim V(\Sigma)/\delta^{d-1}$ (where $V(\Sigma)$ is the volume of the global time slice) and the corresponding mutual complexity would also exhibit a volume-

[2]Similar comments appear in [171] using the basis and spectrum language, *i.e.,* preparing the TFD state requires many gates which adjust the basis of the purifying system but which do not affect the mixed thermal state of the original system.

[3]Given the optimal purification of $\hat{\rho}_{\rm th}(\beta)$, it may be interesting to investigate the properties of $\rho_{\mathcal{A}^c}$, *i.e.,* the mixed state found after tracing out the physical degrees of freedom. For example, one should find that it is much less entangled at short distances.

	Thermal state	Subregions of the vacuum
QFT (diagonal basis)	$\Delta\mathcal{C} > 0$	$\Delta\mathcal{C} > 0$
QFT (physical basis)	$\Delta\mathcal{C} < 0$ for $\beta\mu \gg 1$ or $\beta\mu \ll 1$	$\Delta\mathcal{C} < 0$, $\Delta\tilde{\mathcal{C}} > 0$ [◇]
Holography (CV)	$\Delta\mathcal{C}_{\text{V}} \leq 0$ [§]	$\Delta\mathcal{C}_{\text{V}} \leq 0$ [§]
Holography (CA)	$\Delta\mathcal{C}_{\text{A}} < 0$ [†]	$\Delta\mathcal{C}_{\text{A}} < 0$ [‡]
Holography (CV2.0)	$\Delta\mathcal{C}_{\text{V2.0}} < 0$ [†]	$\Delta\mathcal{C}_{\text{V2.0}} < 0$ [‡]

Table 6.1: Comparison of the mutual complexity in field theory and in holography for the various cases studied in this paper. Above, μ is the characteristic frequency of the reference state while β is the inverse temperature.
[◇] there are two possible definitions for mutual complexity in the physical basis for subregions of the vacuum, see discussion around eq. (3.144) for more details; [§] the inequality is saturated (*i.e.,* $\Delta\mathcal{C}_{\text{V}} = 0$) when evaluated for $t_{\text{L}} = 0 = t_{\text{R}}$ for the TFD state and for $t = 0$ for the vacuum state, as was done in the preceding QFT calculations; [†] in both cases, $\Delta\mathcal{C}$ was proportional to the entropy of the thermal state; [‡] in both cases, the leading contribution to $\Delta\mathcal{C}$ had the same form as the leading divergence in the entanglement entropy of the subregions.

law divergence. Instead as shown in eqs. (3.135) and (3.142), the leading divergences are instead proportional to $V(\mathcal{A})$, the volume of the subregion, and as discussed above, the mutual complexity is then controlled by the subleading divergences appearing in the individual complexities. Again, this reflects the fact that in the optimal purification, there is no need to prepare UV correlations amongst the ancillae. Moreover, we might note that the ground state would not even be an essential purification (with the minimal number of ancilla) for subsystems whose size is less than half of that of the full system.

6.3 Holographic Complexity

Much of the motivation of our studies in chapter 4 was to compare the results for the purification complexity in the free scalar QFT to those for the mixed state complexity found in holography. Hence we now compare the QFT results of sections 3.4 and 3.5 for the purification complexity of thermal states and subregions in the vacuum state to the analogous results found with the subregion-CV (4.1), subregion-CA (4.2), and subregion-CV2.0 (4.4) prescriptions found in section 4.1. Recall that motivated by previous comparisons, we

focused our analysis of the complexity in the QFT on the F_1 cost function. For example, the structure of the UV divergences for the $\mathcal{C}_1$ complexity in QFT was found to be similar to that for holographic complexity [62, 69]. However, the basis dependence of this measure was found to play an important role in evaluating the complexity of TFD states [68], and so we also evaluated our QFT complexities in both the diagonal and physical bases here. One more observation, before turning to the results, is that the authors of [222] have argued that the relevant gates in holographic complexity should be non-local. Of course, the original analysis of the QFT complexity [62], which we adapt here in our analysis, also involves non-local gates. Hence this is a common point for the complexity in both frameworks.

The leading UV divergence in any of the holographic prescriptions for the complexity of the reduced state on a subregion has the same volume-law form as found for a pure state. That is, all three prescriptions yield an expression of the form $\mathcal{C} \simeq k_d\, V(\mathcal{A})/\delta^{d-1} + \cdots$ where $V(\mathcal{A})$ is the volume of the boundary subregion $\mathcal{A}$ on which the mixed state is defined, and k_d is some constant depending on the dimension, the central charge c_T and the prescription chosen. In the vacuum (or any pure state), the leading divergence is precisely the same except that $V(\mathcal{A})$ is replaced by $V(\Sigma)$, the volume of the entire Cauchy surface in the boundary theory. This volume-law behaviour is the same as found for the free scalar. For example, the leading divergence in the QFT complexity of the thermal state is shown in eq. (6.7). As noted there, this divergence is precisely the same as found for the vacuum state [69]. Similarly, for subregions in the vacuum state we found a leading divergence proportional to the volume of the subregion, *e.g.,* see eqs. (3.135) and (3.142).

When considering subregions of the vacuum, an interesting feature that distinguishes the subregion-CA and subregion-CV2.0 proposals from the subregion-CV prescription is that the former two generate subleading divergences that are associated with the geometry of the boundary of the subregion, *e.g.,* as shown in eq. (4.45). In contrast, no such contributions appear with the subregion-CV proposal, *e.g.,* see eq. (4.34).[4] Of course, as discussed in section 4.1, we could modify the subregion-CV prescription by adding a term proportional to the volume of the HRT surface, as in eq. (4.7). This modified prescription would yield boundary contributions similar to those found with the subregion-CA and subregion-CV2.0 proposals. As this modification of the subregion-CV prescription highlights, at least to leading order, the boundary contributions are proportional to the entanglement entropy of the reduced density matrix on the subregion.

We would like to explore further the relation between the subleading divergences in the

[4] While this equation does exhibit a subleading logarithmic divergence, there is no 'area-law' divergence proportional to R/δ.

complexity and entanglement entropy by returning to our results of AdS_3 in section 4.3. Recall that using global coordinates in the bulk of AdS_3 corresponds to the two-dimensional boundary CFT living on a circle with a finite circumference C. Further our results for the subregion complexity for the subregion-CA and subregion-CV2.0 proposals were presented in eqs. (4.36) and (4.41) with a finite term, which we could not determine analytically. However, in the limit of small subregions, *i.e.,* $\ell/C \ll 1$, we were able to predict the form of these finite functions $f(\ell/C)$ and $\tilde{f}(\ell/C)$ in eqs. (4.37) and (4.42), by comparing to the results coming from putting the boundary CFT on an infinite line. However, if we imagine that the boundary contributions to the subregion complexity are related to entanglement entropy, we should recall the formula for the entanglement entropy of an interval in CFT_2 on a finite circle: $S_{\rm EE} = \frac{c}{3}\ln\left(\frac{C}{\pi\delta}\sin\left(\frac{\pi\ell}{C}\right)\right)$ [223, 224]. This formula suggests that $f(\ell/C)$ and $\tilde{f}(\ell/C)$ should be given by the following expressions,

$$\begin{aligned} f(\ell/C) &= \frac{c}{3\pi^2}\left(-\ln\left(\frac{2\ell_{\rm ct}}{L}\right)\ln\left[\frac{1}{\pi}\sin\left(\frac{\pi\ell}{C}\right)\right] + \frac{\pi^2}{8}\right) , \\ \tilde{f}(\ell/C) &= -\frac{4\,c}{3}\left(\ln\left[\frac{1}{\pi}\sin\left(\frac{\pi\ell}{C}\right)\right] + \frac{\pi^2}{8}\right) . \end{aligned} \tag{6.8}$$

Of course, the expressions above reduce to those in eqs. (4.37) and (4.42) in the limit $\ell/C \to 0$. However, we note that eq. (6.8) is symmetric about $\ell/C = 1/2$, and so a similar logarithmic singularity appears in the limit $\ell/C \to 1$, *e.g.,* $\tilde{f}(\ell/C) \simeq -\frac{4\,c}{3}\ln[\frac{C-\ell}{C}]$ in this limit. This expression suggests a deep relation between the two quantities (at least for two-dimensional CFTs). See [204] for recent exploration on the relations between subregion complexity and entanglement entropy in AdS_3 and BTZ black hole.

With the subregion-CA or subregion-CV2.0 proposals, the boundary divergences discussed above dominate the mutual complexity of the vacuum state, *e.g.,* see eqs. (4.47) and (4.48). Hence, given a bipartition of the vacuum into subregions $\mathcal{A}$ and $\mathcal{B}$, the mutual complexity is UV divergent with the leading divergence taking the form $\Delta\mathcal{C} \sim V(\partial\mathcal{A})/\delta^{d-2}$, where we have implicitly used that $\partial\mathcal{A} = \partial\mathcal{B}$. Of course, this divergence has precisely the same form as the celebrated area-law term [225–227] found in the entanglement entropy between $\mathcal{A}$ and $\mathcal{B}$. This again supports the claim that the mutual complexity characterizes the correlations between the two subsystems appearing in eq. (6.5). Similar observations relating the mutual complexity and the entanglement entropy also appear in [198].

With a bipartition of the vacuum state on a fixed time slice, the mutual complexity precisely vanishes using the subregion-CV prescription. Of course, if we adopted the modified prescription for $\mathcal{C}'_V(\mathcal{A})$ in eq. (4.7), the resulting mutual complexity would, of course, be proportional to the entanglement entropy. Further, this construction emphasizes the observation below eq. (6.16) that it is more appropriate to think of these mutual complexities as

being proportional to the mutual information between the subregion and its complement. That is, applying eq. (4.7) to evaluate eq. (6.15) clearly yields $\Delta\mathcal{C}'_V = \eta\, I(\mathcal{A},\mathcal{B})$ where $I(\mathcal{A},\mathcal{B}) = S_{\rm EE}(\mathcal{A}) + S_{\rm EE}(\mathcal{B}) - S_{\rm EE}(\mathcal{A}\cup\mathcal{B})$ is precisely the mutual information of the two subregions.

The mutual complexity is, of course, an interesting quantity to compare between the holographic and QFT approaches. Our results for $\Delta\mathcal{C}$ are summarized in the table 6.1 for all three holographic prescriptions calculated in chapter 4, as well as those for the free scalar QFT calculated in chapter 3.

One feature common to holography and QFT complexities is that the UV divergences in the complexity of the thermal state $\hat{\rho}_{\rm th}(\beta)$ precisely match those found in the complexity of a single copy of the vacuum, or alternatively, they are precisely one-half of those found for the TFD state. As a consequence, the mutual complexity of the TFD state is UV finite in both holography and the free QFT. Further, we demonstrated that the mutual complexity for the TFD state calculated for the free scalar in the diagonal basis is proportional to the thermal entropy in (3.114), where we have taken $m = 0$ and also $\beta\mu \gg 1$. In the physical basis, we also expect that with the limit $\beta\mu \gg 1$ and $\beta m \ll 1$, the mutual complexity will be proportional to the entropy — see comments at the end of section 3.4.5.2. Again, this matches the behaviour found in eqs. (4.14) and (4.17) for the subregion-CA and subregion-CV2.0 approaches.

Unfortunately, the holographic complexity is superadditive, while in the diagonal basis, the QFT complexity is subadditive, *i.e.,* $\Delta\mathcal{C}(\text{TFD}) < 0$ for holography while $\Delta\mathcal{C}(\text{TFD}) > 0$ for the free QFT using the diagonal basis. However, the QFT mutual complexity in the physical basis was observed to be negative when the reference frequency $\beta\mu$ was either very small or very large, see the figure 3.10. Hence in these regimes, the physical basis results compare well with the holographic results, for the subregion-CA and subregion-CV2.0 proposals. Of course, for the $t_{\rm L} = 0 = t_{\rm R}$ time slice, the mutual complexity to the TFD state vanishes using the subregion-CV prescription. However, we could also apply the modified prescription in eq. (4.7), in which case we would find $\Delta\mathcal{C}'_{\rm V}(\text{TFD}) = 2\eta\, S$. In this case, the sign is determined entirely by the sign of the parameter η, and in particular, choosing $\eta > 0$ would yield a subadditive result as found using the diagonal basis in the free QFT.

For subregions in the vacuum state of a two-dimensional free scalar field theory, using numerical fits, we inferred the general divergence structure of the purification complexity in the diagonal basis in eq. (3.135) and in the physical basis in eq. (3.142). The leading divergence is a volume term $\frac{\ell}{2\delta}|\ln\frac{1}{\mu\delta}|$, where the coefficient precisely matches that found in the vacuum. In this respect, the QFT complexities show the same behaviour as found

with the three holographic subregion complexity proposals, in eq. (4.33) for subregion-CV, eq. (4.36) for subregion-CA and eq. (4.41) for subregion-CV2.0.[5] The numerical fits for the QFT complexities (see eqs. (3.135) and (3.142)) did reveal a subleading logarithmic divergence proportional to $\ln(C/\delta)$,[6] which was found in the holographic results for the subregion-CA and subregion-CV2.0 approaches (see eqs. (4.36) and (4.41)). However, our numerical results were not sensitive enough to resolve the precise form of the subleading contributions, *e.g.,* to find a form similar to that found for the corresponding holographic systems in eq. (6.8). It would be interesting to extend our QFT calculations to larger lattices, but also higher dimensional lattices where the subleading divergences become stronger.

Here, we might note that as discussed above, the subleading contributions in the subregion complexity are expected to dominate the corresponding mutual complexity. In this regard, the functional dependence of $\Delta\mathcal{C}$ on ℓ/C compares well between the QFT and the holographic results on general grounds. That is, we may compare the free scalar QFT results in figure 3.13 for the diagonal basis with the form (6.8) for the subleading contributions in the corresponding subregion-CA and subregion-CV2.0 results. The mutual complexity rises dramatically for small ℓ/C, has a broad maximum at $\ell/C = 1/2$ and is symmetric under $\ell/C \to (C-\ell)/C$. A preliminary examination of the QFT results for the diagonal basis showed the following gave a good fit to our numerical results[7]

$$\Delta\mathcal{C}_1^{\text{diag}} \approx \frac{200}{500+\mu C}\left[\ln\left(\frac{C}{\pi\delta}\sin\left(\frac{\pi\ell}{C}\right)\right) + 8.33 + 0.0214\,\mu C\right] . \tag{6.9}$$

Figure 6.1 compares this function to our numerical results in figure 3.13. It would be interesting to investigate these fits in more detail and in particular, to produce the analogous fitting function for the physical basis results as well.

Unfortunately, there was not a good match for the sign of these mutual complexities in comparing the holographic and free QFT results. In particular, for all three holographic approaches, the vacuum mutual complexity was generally superadditive, *i.e.,* $\Delta\mathcal{C} < 0$.[8] In contrast, using the diagonal basis in the free QFT produced a subadditive result for subregions of the vacuum. In the case of the physical basis, we actually proposed two

[5] Note that our QFT results of section 3.5 are valid for the circle and so should be compared to the holographic result in global coordinates, see footnote 29.

[6] Here we denote the total size of the system as $C(= L$ in section 3.5) to facilitate the comparison with the corresponding holographic results.

[7] Note that $L/\delta = 1000$ for all three curves.

[8] Of course, the modified subregion-CV approach (4.7) could yield either sign for the mutual complexity depending on the sign of the parameter η.

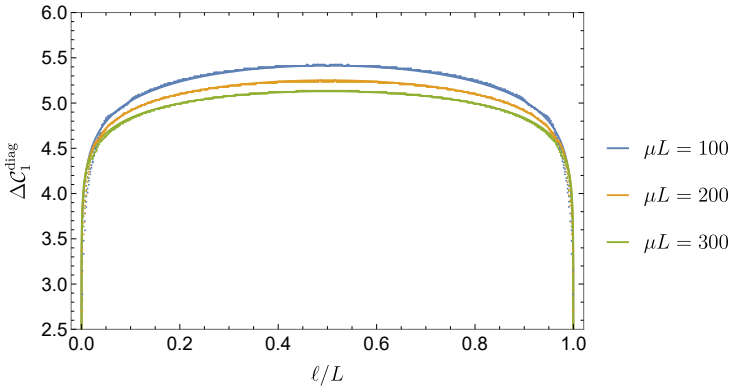

Figure 6.1: Fits (solid curves) and data (points) of the size dependence of the mutual complexity in the diagonal basis $\Delta\mathcal{C}_1^{\rm diag}$ for different reference frequencies $\mu L = 100$, 200 and 300. The cutoff was set to $\delta/L = 1/N = 1/1000$. The solid lines correspond to the fit in eq. (6.9).

definitions for the mutual complexity in eq. (3.144). With the first definition, where we introduce a partition of the vacuum degrees of freedom according to the arbitrary choice made for the subregions, $\Delta\mathcal{C}_1^{\rm phys} < 0$, which agrees with holography. However, the leading contribution in the QFT result appears to be linear, *i.e.,* proportional to ℓ/δ, whereas the leading term in the subregion-CA and subregion-CV2.0 results are proportional to $\ln(\ell/\delta)$ (see eq. (4.48)). With the second definition, where we subtract the standard vacuum complexity, $\Delta\tilde{\mathcal{C}}_1^{\rm phys} > 0$, which disagrees with the holographic results. However, in this case, the leading contribution in the QFT result appears to be logarithmic as shown in figure 3.17.

If we compare the leading divergences noted above in the purification complexity and the holographic complexity from subregion-CA, we are lead to identify[9]

$$\ln\left(\frac{\ell_{\rm ct}}{L}\right) \sim \big|\ln(\mu\delta)\big| = \begin{cases} \ln(\mu\delta)\,, & \text{for } \mu\delta > 1\,, \\ \ln\left(\frac{1}{\mu\delta}\right)\,, & \text{for } \mu\delta < 1\,. \end{cases} \tag{6.10}$$

We note that the definition of circuit complexity in the free scalar QFT introduces a new scale – the reference frequency μ, while the CA proposal for holographic complexity depends on the arbitrary length scale $\ell_{\rm ct}$, which is introduced by the null boundary counterterm [134]. The comparison of the divergences in these approaches motivates us to relate the

[9]Of course, the same identification comes from comparing leading divergences in the purification complexity of the thermal state, or even the complexity of vacuum state.

ratio $\mu\delta$ in the QFT complexity to ℓ_{ct}/L in the CA proposal with $\ell_{\rm ct}/L \sim \max(\mu\delta, 1/\mu\delta)$.[10] A similar identification was pointed out in [62, 69] and the discussion section of [112].

We observe that this identification has interesting implications for the subregion-CA results since the coefficient $\ln(\ell_{ct}/L)$ also appears in terms beyond the leading contribution to the complexity. For example, an extra factor of $|\ln(\mu\delta)|$ would appear in the leading term in the mutual complexity in eq. (4.47). If μ and δ are independent scales, this would mean that this leading term no longer matches the area-law divergence appearing in the entanglement entropy. However, this interpretation can be restored if the reference frequency scales with the UV cutoff, *e.g.,* $\mu\delta = e^{-\sigma}$ so that the logarithmic factor simply introduces a new numerical factor, *i.e.,* $|\ln(\mu\delta)| = |\sigma|$.

Let us summarize our comparison of the purification complexity for the free scalar QFT with the various subregion proposals in holography. Our results do show that various general features are common to the two frameworks. However, a detailed comparison does not lead to any definite conclusions. Based on comparisons of the mutual complexity for the TFD and vacuum states, it seems that details of the QFT results using the diagonal basis are quite different from the corresponding holographic results. Recall that previous calculations of the complexity of formation for the free scalar [68] already indicated that the diagonal basis did not produce results comparable to holography. The QFT results using the physical basis can be brought into closer alignment with the holographic results, at least in certain regimes, *e.g.,* $\beta\mu \gg 1$ or $\beta\mu \ll 1$ is required for the mutual complexity of the TFD state to be superadditive. These restrictions may be informing us about the microscopic model underlying holographic complexity. However, we are still left with apparent discrepancies for the mutual complexity of the vacuum state, as well as for the purification complexity of the thermal state, which may be warning us that these comparisons simply have limited applicability.

6.4 Open Questions and Future Directions

In closing here, we would like to discuss some potential new directions or open questions for future studies.

Path-integral Complexity of Mixed States

[10] We are implicitly assuming that $\ell_{\rm ct}/L > 1$ in order that the CA complexity is positive.

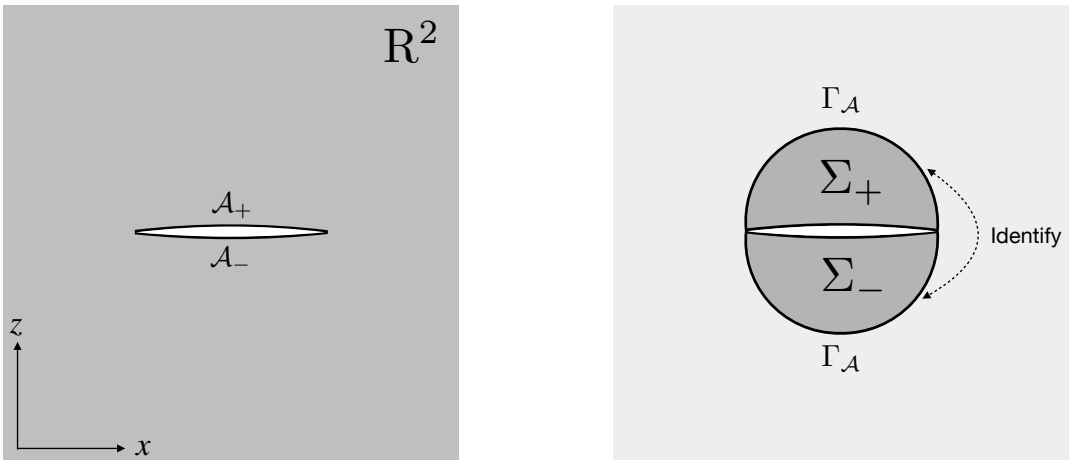

Figure 6.2: Left panel: the path-integral representation for a reduced density matrix $\hat{\rho}_{\mathcal{A}}$ in CFT_2. Right panel: The manifold after the optimization is given by two patches $\Sigma_\pm$ whose boundary is $\Sigma_\pm \cup \Gamma_{\mathcal{A}}$.

Roughly speaking, we consider two types of mixed-state complexity studied in chapters 3 and chapter 5 as the generalizations of Nielsen's geometric approach and Fubini-Study metric approach, respectively. In section 2.1.3, we also introduced an alternative method for evaluating the complexity of states in quantum field theory, *i.e.,* path-integral complexity introduced in [92,93]. Unlike Nielson's geometric method or complexity definitions based on the Fubini-Study metric, path-integral optimization considers the Euclidean path integral that prepares a given state in a two dimensional CFT and translates the problem of its optimal preparation to that of minimizing the Liouville action $S_{\text{L}}(\phi)$ obtained from Weyl rescaling the path-integral measure. Explicitly, the minimal Liouville action is identified as the path-integral complexity of the pure state $|\Psi\rangle$:

$$\mathcal{C}_{\text{L}}\left(\Psi\right) = \min_{\phi}\left[S_{\text{L}}(\phi)\right] , \tag{6.11}$$

where the minimization is done among arbitrary functions ϕ that describe the Weyl factor. The path-integral approach also allows one to handle mixed states as discussed in [93], where one need only include boundary contributions to the Liouville action. Choosing a subsystem $\mathcal{A}$ in 2D CFT to be an interval $-\Delta l \leq x \leq \Delta l$, its density matrix $\hat{\rho}_{\mathcal{A}}$ is defined from the CFT vacuum by tracing out the complement of $\mathcal{A}$. Then the path-integral optimization is done by minimizing the Liouville action with boundary contributions, *i.e.,*

$$S_{\text{Lb}} = \frac{c}{12\pi}\int_{\partial\Sigma_\pm} ds\left[K_0\phi + \mu_{\text{B}}e^{\phi}\right] , \tag{6.12}$$

where the optimized manifold is given by $\Sigma_+ \cup \Sigma_-$ with boundary $\partial\Sigma_\pm \equiv \Sigma_\pm \cup \Gamma_{\mathcal{A}}$ and K_0 is the trace of extrinsic curvature of the boundary $\partial\Sigma_\pm$. Refer to figure 6.2 for the illustration. It is natural to identify the Liouville action in the reduced subregion as the subregion complexity:

$$\mathcal{C}_{\text{L}}\left(\hat{\rho}_{\mathcal{A}}\right) = \min_{K_0,\phi}\left[S_{\text{L}}(\phi) + S_{\text{Lb}}\left(K_0,\phi\right)\right] , \tag{6.13}$$

where the minimization fixes the background metric via the value ϕ and also the boundary curve $\Gamma_{\mathcal{A}}$ to a geodesic. It is interesting to point out that path-integral optimization was recently used to shed light on entanglement of purification [228].

Alternatively, it is perhaps interesting to explore another definition for complexity of mixed states based on purification complexity using the path-integral complexity of pure states $\mathcal{C}_{\text{L}}\left(\Psi\right)$. In the same spirit of purification complexity (3.1), we can also define the path-integral complexity for mixed states as

$$\mathcal{P}_{\text{L}}\left(\hat{\rho}_{\mathcal{A}}\right) = \min_{\mathcal{A}^c}\left[\mathcal{C}_{\text{L}}\left(\Psi_{\mathcal{A}\mathcal{A}^c}\right)\right] , \tag{6.14}$$

where $|\Psi_{\mathcal{A}\mathcal{A}^c}\rangle$ denotes the purified state of our density matrix $\hat{\rho}_{\mathcal{A}}$ and the minimization is performed over all possible purifications. Although, the above definition looks natural for mixed states, this definition actually requires knowledge about the path-integral optimization of all purified states $|\Psi_{\mathcal{A}\mathcal{A}^c}\rangle$, which is absent by now. For simplicity, it is still interesting to consider the path-integral complexity of a subregion in the CFT by assuming the purified states exist in the same CFT and compare the results from our methods.

Generalizations of Mutual Complexity

Although so far we only considered the mutual complexity defined in eq. (6.5) for a pure state $|\Psi_{\mathcal{A}\mathcal{B}}\rangle$, let us note that there is no reason why in calculating the mutual complexity, that the initial state must be a pure state. That is, a simple generalization of the mutual complexity (6.5) would be

$$\Delta\mathcal{C} = \mathcal{C}(\hat{\rho}_{\mathcal{A}}) + \mathcal{C}(\hat{\rho}_{\mathcal{B}}) - \mathcal{C}(\hat{\rho}_{\mathcal{A}\cup\mathcal{B}}) , \tag{6.15}$$

where the combined system begins in a mixed state $\hat{\rho}_{\mathcal{A}\cup\mathcal{B}}$. We still expect that in this situation the mutual complexity (6.15) quantifies the additional correlations between the subsystems $\mathcal{A}$ and $\mathcal{B}$. Using our results, a simple example would be to consider two neighbouring (but not overlapping) subregions, $\mathcal{A}$ and $\mathcal{B}$, in the vacuum state. These combine to form the larger subregion $\mathcal{A}\cup\mathcal{B}$ (but note that we assume $\mathcal{A}\cap\mathcal{B} = 0$). Building

on eq. (4.47) in the holographic context, we would find that the leading contribution to the mutual complexity becomes

$$\begin{aligned}
\mathrm{AdS}_{d+1}, \mathrm{P}: \qquad \Delta\mathcal{C}_{\mathrm{A}} &= -\frac{L^{d-1}}{2\pi^2(d-2)G_N}\ln\left(\frac{2(d-1)\ell_{\mathrm{ct}}}{L}\right)\frac{V(\partial\mathcal{A}\cap\partial\mathcal{B})}{\delta^{d-2}}+\cdots\,, \\
\mathrm{AdS}_{d+1}, \mathrm{P}: \quad \Delta\mathcal{C}_{\mathrm{V2.0}} &= -\frac{4L^{d-1}}{d(d-1)(d-2)G_N}\frac{V(\partial\mathcal{A}\cap\partial\mathcal{B})}{\delta^{d-2}}+\cdots\,.
\end{aligned} \tag{6.16}$$

In this case, we observe that this leading divergence is comparable to that in the mutual information between the subregions $\mathcal{A}$ and $\mathcal{B}$. Of course, this suggests that in general one should think of the mutual complexity as being related to mutual information, rather than the entanglement entropy even when $\hat{\rho}_{\mathcal{AB}}$ is a pure state. It would be interesting to investigate this generalization (6.15) further in the case of disjoint (*i.e.,* non-neighbouring) subregions $\mathcal{A}$ and $\mathcal{B}$, where the mutual information is finite, and exhibits an interesting phase transition for holographic CFTs [229–231]. A similar setup studying purifications of two complementary subregions appears also in the context of the entanglement of purification [183–185, 232]. It would be interesting to investigate the relation between these two notions.

Further, we observe that the mutual complexity (6.15) for mixed states would generally be nonvanishing (but UV finite) using the subregion-CV approach (4.1), even if the subregions lie in a constant time slice on the boundary. Another interesting issue to investigate would be if inequalities similar to the Araki-Lieb inequality [45] can be used to bound the difference in complexity between two complementary subsystems when starting with a mixed state. Finally, let us comment on the case of partially overlapping subregions. In this case, one is naturally led to consider the following generalization of the mutual complexity

$$\Delta\mathcal{C} = \mathcal{C}(\hat{\rho}_{\mathcal{A}}) + \mathcal{C}(\hat{\rho}_{\mathcal{B}}) - \mathcal{C}(\hat{\rho}_{\mathcal{A}\cup\mathcal{B}}) - \mathcal{C}(\hat{\rho}_{\mathcal{A}\cap\mathcal{B}})\ . \tag{6.17}$$

With this difference of complexities, the leading divergences in the individual complexities cancel, and the sign of the result is nontrivial. It would be interesting to investigate the properties of these generalizations further in circuit complexity as well as holographic complexity.

To close here, we should also stress that the sign of the mutual complexity defined in eq. (6.15) and its generalization in eq. (6.17) determine the subadditivity and strong subadditivity of complexity. To compare with entanglement entropy, it is noted that entanglement entropy satisfies the subadditivity

$$S_{\mathrm{EE}}\left(\hat{\rho}_{\mathcal{A}}\right) + S_{\mathrm{EE}}\left(\hat{\rho}_{\mathcal{B}}\right) \geq S_{\mathrm{EE}}\left(\hat{\rho}_{\mathcal{AB}}\right)\ , \tag{6.18}$$

and also the strong subadditivity

$$\begin{aligned} S_{\text{EE}}\left(\hat{\rho}_{\mathcal{AB}}\right)+S_{\text{EE}}\left(\hat{\rho}_{\mathcal{BC}}\right) &\geq S_{\text{EE}}\left(\hat{\rho}_{\mathcal{A}}\right)+S_{\text{EE}}\left(\hat{\rho}_{\mathcal{C}}\right) \ , \\ S_{\text{EE}}\left(\hat{\rho}_{\mathcal{AB}}\right)+S_{\text{EE}}\left(\hat{\rho}_{\mathcal{BC}}\right) &\geq S_{\text{EE}}\left(\hat{\rho}_{\mathcal{ABC}}\right)+S_{\text{EE}}\left(\hat{\rho}_{\mathcal{B}}\right) \ . \end{aligned} \tag{6.19}$$

Taking the monotonicity of purification complexity $\mathcal{C}_{\text{IM}}$ under the partial trace (noting the similar monotonicity for von Neumann entropy $S_{\text{EE}}\left(\hat{\rho}_{\mathcal{AB}}\right) \geq S_{\text{EE}}\left(\hat{\rho}_{\mathcal{B}}\right)$ is not true.), it is straightforward to show the counterpart of the first strong subadditivity for the purification complexity $\mathcal{C}_{\text{IM}}$ is also satisfied for generic density matrices, *i.e.,*

$$\mathcal{C}_{\text{IM}}\left(\hat{\sigma}_{\mathcal{AB}},\hat{\rho}_{\mathcal{AB}}\right)+\mathcal{C}_{\text{IM}}\left(\hat{\sigma}_{\mathcal{BC}},\hat{\rho}_{\mathcal{BC}}\right) \geq \mathcal{C}_{\text{IM}}\left(\hat{\sigma}_{\mathcal{A}},\hat{\rho}_{\mathcal{A}}\right)+\mathcal{C}_{\text{IM}}\left(\hat{\sigma}_{\mathcal{C}},\hat{\rho}_{\mathcal{C}}\right) \ . \tag{6.20}$$

However, the subadditivity of complexity (*i.e.,* $\Delta\mathcal{C} \geq 0$) or its superadditivity (*i.e.,* $\Delta\mathcal{C} \leq 0$) is not proven in general for any mixed-state complexity studied in this thesis. Especially, if we believe the holographic complexity may require a specific (or a trivial) state as the universal reference state, it is still interesting to investigate whether 'holographic complexity' is always subadditive or superadditive.

Purification Complexity of Holographic States

As the first application of the mixed-state complexity $\mathcal{C}_{\text{IM}}$, we only examined an extremely simple Gaussian state $\hat{\rho}_1$ in section 5.3. However, we have made more efforts in chapter 3 on deriving the purification complexity of mixed Gaussian states in free scalar QFT, *e.g.,* a thermal state $\hat{\rho}_{\text{th}}(\beta)$ defined in (3.84) and the mixed states $\hat{\rho}_{\mathcal{A}}$ on finite subregions of the vacuum state. Considering the purification complexity $\mathcal{C}_{\text{IM}}$ has gotten rid of the challenges in finding the optimal purification, it is interesting to apply the definition of complexity $\mathcal{C}_{\text{IM}}$ to quantum states in QFT. Although it is not easy to calculate the quantum fidelity (5.6) or quantum Fisher information metric for arbitrary QFT states due to the appearance of the square root of the density operators, it is not so hard for a free quantum field theory. With some effort, the quantum fidelity and Bures metric for arbitrary two Gaussian (bosonic or fermionic) states have been derived in *e.g.,* [233–236]. With the knowledge of the QFIM for any Gaussian states, it would be interesting to consider the same Gaussian states $\hat{\rho}_{\text{th}}(\beta), \hat{\rho}_{\mathcal{A}}$ in free scalar theory and compare the results with that derived in chapter 3. As a natural generalization, one may also ask what is the purification complexity in free fermionic field theory. We note that the latter with the F_2 cost function has been explored in [237].

As we discussed before, the results between holographic subregion complexity and purification complexity from free theory still have distinctions. At present, we do not have a first principle approach to show whether purification complexity is holographic or not.

As a first step toward this open question, the results from the purification complexity of holographic state rather than free theories should shed light on that. For example, one can consider the thermal density matrix of CFT, *i.e.,* the density operator $\hat{\rho}_{\text{th}}$ defined in eq. (1.24). The potential holographic duals of its complexity have been discussed in section 4.2. Furthermore, we have learned the holographic density operator for a subregion $\mathcal{A}$ is constrained by the modular Hamiltonian $\hat{K}_{\mathcal{A}}$ in the form like [194]

$$-\log\hat{\rho}_{\mathcal{A}}\equiv\hat{K}_{\mathcal{A}}=\frac{\hat{A}_{\text{ext}}\left(\mathcal{E}_{\mathcal{A}}\right)}{4G_{\text{N}}}+\hat{K}_{\text{bulk}}+\cdots+\mathcal{O}(G_{\text{N}})\,, \tag{6.21}$$

where the $\hat{A}_{\text{ext}}$ denotes the area operator associated with the extremal surface $\mathcal{E}_{\mathcal{A}}$ and $\hat{K}_{\text{bulk}}$ is the bulk modular Hamiltonian of the bulk region enclosed by $\mathcal{E}_{\text{A}}$. It is definitely interesting to investigate what would be the purification complexity for these holographic states $\hat{\rho}_{\mathcal{A}}$.

Optimal Purification in Holographic Spacetime

In the end, let's simply assume that the purification complexity is a holographic quantity. By definition, we can find a optimal purified state for a given holographic state $\hat{\rho}_{\mathcal{A}}$. As shown in chapter 3, we found that TFD state is not the optimal purification of thermal state $\hat{\rho}_{\text{th}}(\beta)$ and the vacuum state is neither the optimal state for its subregion $\hat{\rho}_{\mathcal{A}}$. For simplicity, it is interesting to further assume that the optimal purified state is also dual to a holographic spacetime. And then a natural question is what kind of spacetime is dual to the optimal purification.

Although the answer should depend on the details of the holographic dual of purification complexity, we can find that the non-increasing property of purification complexity $\mathcal{C}_{\text{IM}}$, *i.e.,* eq. (5.32) would help to impose strong constraints on the optimal purification. Assuming the target state $\hat{\rho}_{\mathcal{A}}$ as a boundary subregion $\mathcal{A}$ as shown in the figure 6.3, it is obvious that the full boundary is also a purification of the subregion $\mathcal{A}$. However, this purified state denoted by $|\Psi_{\mathcal{A}\mathcal{A}^c}\rangle$ generally is not the optimal purification because of the extra degrees of freedom in its Hilbert space. In order to find other purifications, we can then perform a unitary transformation and then trace out part of the auxiliary degrees of freedom in the bulk geometry. As a result of an iterative procedures, it can push the boundary region $\mathcal{A}^c$ into the bulk spacetime, *i.e.,* cutting part of the portion inside the subregion enclosed by RT surface, *e.g.,* the white region in figure 6.3. And all these truncated spacetimes are dual to the purification of $\hat{\rho}_{\mathcal{A}}$. The non-increasing property of the purification complexity implies that this procedure (unitary transformation, tracing out some degrees of freedom) would

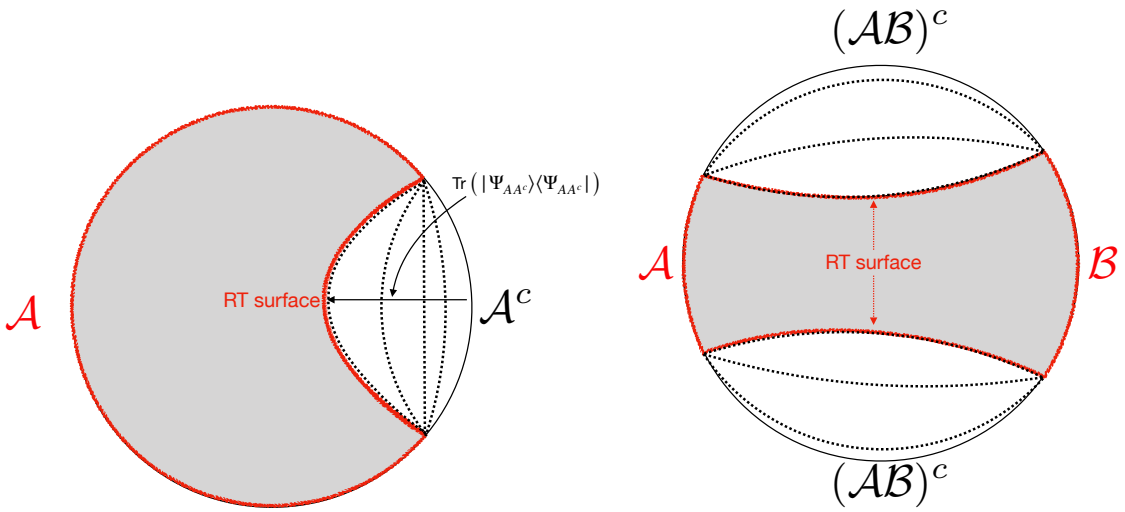

Figure 6.3: The optimal purified state with the smallest complexity corresponds to the holographic spacetime geometry shown in the shadowed region whose boundary is taken as the boundary subregion and its RT surface as shown by the red curves. The dashed black lines represent various cut-off surfaces and correspondingly define different purified states for a fixed boundary subregion. Left: A generic mixed state $\hat{\rho}_{\mathcal{A}}$ corresponding to a boundary subregion $\mathcal{A}$. Right: A bipartite mixed state $\hat{\rho}_{\mathcal{AB}}$.

decrease (or least not change) the complexity of the purified state. Finally, we can approach the optimal purification by pushing the cut-off surface to the RT surface of the boundary subregion $\mathcal{A}$. As a naive idea, this picture about optimal purification is also consistent with the CV conjecture and subregion-CV. If we adopt the holographic complexity of a pure state as the maximum volume, the holographic complexity of the optimal purification (*i.e.,* holographic purification complexity) then is given by the maximum volume of subregion $\mathcal{R}_{\mathcal{A}}$ which is bounded by the boundary subregion $\mathcal{A}$ and its HRT surface $\mathcal{E}_{\mathcal{A}}$, *i.e.,*

$$\mathcal{C}_{\mathrm{V}}(\mathcal{A}) \equiv \min_{\mathcal{A}^c}\left[\mathcal{C}_{\mathrm{V}}\left(\mathcal{A}\mathcal{A}^c\right)\right] = \max_{\partial\mathcal{R}_{\mathcal{A}}=\mathcal{A}\cup\mathcal{E}_{\mathcal{A}}}\left[\frac{\mathcal{V}(\mathcal{R}_{\mathcal{A}})}{G_N\,\ell_{\mathrm{bulk}}}\right]. \tag{6.22}$$

Of course, this is nothing but the subregion-CV conjecture defined in eq. (4.1). It would be interesting to explore this idea in more detail, *e.g.,* considering a black hole geometry.

On the other hand, if we are interested in a bipartite target state $\hat{\rho}_{\mathcal{AB}}$ corresponding to a disjoint subregions $\mathcal{A}\cup\mathcal{B}$ on the boundary, the optimal purification in holography is the same as the one from the viewpoint of entanglement of purification. See the figure 6.3 and references *e.g.,* [190, 238, 239] for more illustrations. Besides, the area of the entanglement

wedge cross-section is proposed to be dual to the reflected entropy of a bipartite state $\hat{\rho}_{\mathcal{AB}}$ in the reference [240] where the canonical purification plays a crucial role. Similar to the above argument, the canonical purification also includes too many extra degrees of freedom and should have a larger complexity than the optimal one. It would also be interesting and natural to explore what is the role of canonical purification from the viewpoint of purification complexity.

References

[1] M. Guo, J. Hernandez, R. C. Myers and S.-M. Ruan, *Circuit Complexity for Coherent States*, *JHEP* **10** (2018) 011 [1807.07677]. iv, 27, 30, 33, 34, 36, 39, 53, 56, 125, 152

[2] E. Caceres, S. Chapman, J. D. Couch, J. P. Hernandez, R. C. Myers and S.-M. Ruan, *Complexity of Mixed States in QFT and Holography*, *JHEP* **03** (2020) 012 [1909.10557]. iv, 27, 51, 74, 108, 119, 121, 124, 130, 139, 143, 145, 148

[3] S.-M. Ruan, *Purification Complexity without Purifications*, *JHEP* **01** (2021) 092 [2006.01088]. iv, 125, 154

[4] A. Bernamonti, F. Galli, J. Hernandez, R. C. Myers, S.-M. Ruan and J. Simon, *First Law of Holographic Complexity*, *Phys. Rev. Lett.* **123** (2019) 081601 [1903.04511]. iv, 34, 140, 141

[5] H. Z. Chen, Z. Fisher, J. Hernandez, R. C. Myers and S.-M. Ruan, *Information Flow in Black Hole Evaporation*, *JHEP* **03** (2020) 152 [1911.03402]. iv

[6] A. Bernamonti, F. Galli, J. Hernandez, R. C. Myers, S.-M. Ruan and J. Simon, *Aspects of the first law of complexity*, *J. Phys. A: Math.Theor.* **53** (2020) 294002 [2002.05779]. v, 34, 47, 141

[7] H. Z. Chen, Z. Fisher, J. Hernandez, R. C. Myers and S.-M. Ruan, *Evaporating Black Holes Coupled to a Thermal Bath*, *JHEP* **01** (2021) 065 [2007.11658]. v

[8] J. Hernandez, R. C. Myers and S.-M. Ruan, *Quantum extremal islands made easy. Part III. Complexity on the brane*, *JHEP* **02** (2021) 173 [2010.16398]. v

[9] J. M. Maldacena, *The Large N limit of superconformal field theories and supergravity*, *Adv. Theor. Math. Phys.* **2** (1998) 231 [hep-th/9711200]. 2, 3, 4, 6

[10] G. 't Hooft, *Dimensional reduction in quantum gravity*, *Conf. Proc. C* **930308** (1993) 284 [gr-qc/9310026]. 2

[11] L. Susskind, *The World as a hologram*, *J. Math. Phys.* **36** (1995) 6377 [hep-th/9409089]. 2

[12] J. Casalderrey-Solana, H. Liu, D. Mateos, K. Rajagopal and U. A. Wiedemann, *Gauge/String Duality, Hot QCD and Heavy Ion Collisions*. Cambridge University Press, 2014, 10.1017/CBO9781139136747, [1101.0618]. 2, 7

[13] M. Natsuume, *AdS/CFT Duality User Guide*, vol. 903. 2015, 10.1007/978-4-431-55441-7, [1409.3575]. 2

[14] M. Ammon and J. Erdmenger, *Gauge/gravity duality: Foundations and applications*. Cambridge University Press, Cambridge, 4, 2015. 2, 4, 7

[15] J. Zaanen, Y.-W. Sun, Y. Liu and K. Schalm, *Holographic Duality in Condensed Matter Physics*. Cambridge Univ. Press, 2015. 2, 4, 7

[16] H. Nastase, *Introduction to the ADS/CFT Correspondence*. Cambridge University Press, 9, 2015. 2, 7

[17] D. Harlow, *Jerusalem Lectures on Black Holes and Quantum Information*, *Rev. Mod. Phys.* **88** (2016) 015002 [1409.1231]. 2, 16

[18] M. Van Raamsdonk, *Lectures on Gravity and Entanglement*, in *Theoretical Advanced Study Institute in Elementary Particle Physics: New Frontiers in Fields and Strings*, 8, 2016, DOI [1609.00026]. 2, 16

[19] S. A. Hartnoll, A. Lucas and S. Sachdev, *Holographic quantum matter*, 1612.07324. 2, 4, 7

[20] O. Aharony, S. S. Gubser, J. M. Maldacena, H. Ooguri and Y. Oz, *Large N field theories, string theory and gravity*, *Phys. Rept.* **323** (2000) 183 [hep-th/9905111]. 7

[21] S. S. Gubser, I. R. Klebanov and A. M. Polyakov, *Gauge theory correlators from noncritical string theory*, *Phys. Lett. B* **428** (1998) 105 [hep-th/9802109]. 9, 10, 12

[22] E. Witten, *Anti-de Sitter space and holography*, *Adv. Theor. Math. Phys.* **2** (1998) 253 [hep-th/9802150]. 9, 10, 12

[23] I. Heemskerk, J. Penedones, J. Polchinski and J. Sully, *Holography from Conformal Field Theory*, *JHEP* **10** (2009) 079 [0907.0151]. 13

[24] T. Hartman, C. A. Keller and B. Stoica, *Universal Spectrum of 2d Conformal Field Theory in the Large c Limit*, *JHEP* **09** (2014) 118 [1405.5137]. 13

[25] A. Belin, J. de Boer, J. Kruthoff, B. Michel, E. Shaghoulian and M. Shyani, *Universality of sparse $d > 2$ conformal field theory at large N*, *JHEP* **03** (2017) 067 [1610.06186]. 13

[26] S. Ryu and T. Takayanagi, *Holographic derivation of entanglement entropy from AdS/CFT*, *Phys. Rev. Lett.* **96** (2006) 181602 [hep-th/0603001]. 16, 17, 108

[27] S. Ryu and T. Takayanagi, *Aspects of Holographic Entanglement Entropy*, *JHEP* **08** (2006) 045 [hep-th/0605073]. 16, 108

[28] V. E. Hubeny, M. Rangamani and T. Takayanagi, *A Covariant holographic entanglement entropy proposal*, *JHEP* **07** (2007) 062 [0705.0016]. 16, 24, 108

[29] M. Rangamani and T. Takayanagi, *Holographic Entanglement Entropy*, vol. 931. Springer, 2017, 10.1007/978-3-319-52573-0, [1609.01287]. 16

[30] B. Swingle, *Entanglement Renormalization and Holography*, *Phys. Rev. D* **86** (2012) 065007 [0905.1317]. 16, 40

[31] R. C. Myers and A. Sinha, *Holographic c-theorems in arbitrary dimensions*, *JHEP* **01** (2011) 125 [1011.5819]. 16

[32] D. D. Blanco, H. Casini, L.-Y. Hung and R. C. Myers, *Relative Entropy and Holography*, *JHEP* **08** (2013) 060 [1305.3182]. 16

[33] X. Dong, *Holographic Entanglement Entropy for General Higher Derivative Gravity*, *JHEP* **01** (2014) 044 [1310.5713]. 16

[34] T. Faulkner, M. Guica, T. Hartman, R. C. Myers and M. Van Raamsdonk, *Gravitation from Entanglement in Holographic CFTs*, *JHEP* **03** (2014) 051 [1312.7856]. 16, 116

[35] A. Almheiri, X. Dong and D. Harlow, *Bulk Locality and Quantum Error Correction in AdS/CFT*, *JHEP* **04** (2015) 163 [1411.7041]. 16

[36] F. Pastawski, B. Yoshida, D. Harlow and J. Preskill, *Holographic quantum error-correcting codes: Toy models for the bulk/boundary correspondence*, *JHEP* **06** (2015) 149 [1503.06237]. 16

[37] J. Cotler, P. Hayden, G. Penington, G. Salton, B. Swingle and M. Walter, *Entanglement Wedge Reconstruction via Universal Recovery Channels*, *Phys. Rev. X* **9** (2019) 031011 [1704.05839]. 16

[38] C.-F. Chen, G. Penington and G. Salton, *Entanglement Wedge Reconstruction using the Petz Map*, *JHEP* **01** (2020) 168 [1902.02844]. 16

[39] T. Nishioka, *Entanglement entropy: holography and renormalization group*, *Rev. Mod. Phys.* **90** (2018) 035007 [1801.10352]. 16

[40] D. Harlow, *TASI Lectures on the Emergence of Bulk Physics in AdS/CFT*, *PoS* **TASI2017** (2018) 002 [1802.01040]. 16, 51

[41] A. Strominger and C. Vafa, *Microscopic origin of the Bekenstein-Hawking entropy*, *Phys. Lett. B* **379** (1996) 99 [hep-th/9601029]. 17

[42] M. A. Nielsen and I. L. Chuang, *Quantum Computation and Quantum Information*. Cambridge University Press, Cambridge, 2000. 17, 35, 52, 124, 125, 126, 127, 128, 202

[43] M. M. Wilde, *Quantum information theory*. Cambridge University Press, 2013. 17, 127, 202

[44] J. Watrous, *Theory of Quantum Information*. Cambridge University Press, 2018. 17, 29, 127

[45] H. Araki and E. H. Lieb, *Entropy inequalities*, *Commun. Math. Phys.* **18** (1970) 160. 20, 167

[46] C. Weedbrook, S. Pirandola, R. García-Patrón, N. J. Cerf, T. C. Ralph, J. H. Shapiro et al., *Gaussian quantum information*, *Rev. Mod. Phys.* **84** (2012) 621. 21, 56, 200, 201

[47] A. Ferraro, S. Olivares and M. G. Paris, *Gaussian states in continuous variable quantum information*, quant-ph/0503237. 21, 56, 200, 201

[48] A. Serafini, *Quantum Continuous Variables: A Primer of Theoretical Methods*. CRC Press, 2017. 21, 56, 200, 201, 203

[49] J. M. Maldacena, *Eternal black holes in anti-de Sitter*, *JHEP* **04** (2003) 021 [hep-th/0106112]. 23

[50] H. Casini, M. Huerta and R. C. Myers, *Towards a derivation of holographic entanglement entropy*, *JHEP* **05** (2011) 036 [1102.0440]. 25, 116

[51] X. Dong, A. Lewkowycz and M. Rangamani, *Deriving covariant holographic entanglement*, *JHEP* **11** (2016) 028 [1607.07506]. 25, 108

[52] M. Van Raamsdonk, *Comments on quantum gravity and entanglement*, 0907.2939. 25

[53] M. Van Raamsdonk, *Building up spacetime with quantum entanglement*, *Gen. Rel. Grav.* **42** (2010) 2323 [1005.3035]. 25

[54] L. Susskind, *Entanglement is not enough*, *Fortsch. Phys.* **64** (2016) 49 [1411.0690]. 25, 44, 51

[55] L. Susskind, *Computational Complexity and Black Hole Horizons; Addendum to Computational Complexity and Black Hole Horizons*, *Fortsch. Phys.* **64** (2016) 24 [arXiv:1402.5674,1403.5695]. 25, 44, 51, 107

[56] D. Stanford and L. Susskind, *Complexity and Shock Wave Geometries*, *Phys. Rev.* **D90** (2014) 126007 [1406.2678]. 25, 35, 44, 47, 51, 107

[57] A. R. Brown, D. A. Roberts, L. Susskind, B. Swingle and Y. Zhao, *Complexity, action, and black holes*, *Phys. Rev.* **D93** (2016) 086006 [1512.04993]. 25, 44, 47, 48, 50, 51, 107

[58] A. R. Brown, D. A. Roberts, L. Susskind, B. Swingle and Y. Zhao, *Holographic Complexity Equals Bulk Action?*, *Phys. Rev. Lett.* **116** (2016) 191301 [1509.07876]. 25, 44, 47, 48, 50, 51, 107

[59] M. A. Nielsen, M. R. Dowling, M. Gu and A. C. Doherty, *Quantum computation as geometry*, *Science* **311** (2006) 1133. 27, 28, 38, 123

[60] M. R. Dowling and M. A. Nielsen, *The geometry of quantum computation*, *Quantum Info. Comput.* **8** (2008) 861. 27, 28, 38, 123

[61] M. A. Nielsen, *A geometric approach to quantum circuit lower bounds*, *Quantum Info. Comput.* **6** (2006) 213. 27, 28, 29, 38, 123

[62] R. Jefferson and R. C. Myers, *Circuit complexity in quantum field theory*, *JHEP* **10** (2017) 107 [1707.08570]. 27, 28, 29, 30, 32, 33, 34, 36, 38, 39, 50, 51, 53, 59, 77, 81, 99, 123, 138, 144, 145, 159, 164, 192

[63] A. R. Brown, L. Susskind and Y. Zhao, *Quantum Complexity and Negative Curvature*, *Phys. Rev.* **D95** (2017) 045010 [1608.02612]. 29

[64] A. R. Brown and L. Susskind, *Second law of quantum complexity*, *Phys. Rev.* **D97** (2018) 086015 [1701.01107]. 29, 50

[65] L. Hackl and R. C. Myers, *Circuit complexity for free fermions*, *JHEP* **07** (2018) 139 [1803.10638]. 29, 30, 34, 154

[66] R. Bhatia, *Matrix analysis*, vol. 169. Springer Science & Business Media, 2013. 29

[67] M. I. Gil, *Operator functions and localization of spectra*. Springer, 2003. 29

[68] S. Chapman, J. Eisert, L. Hackl, M. P. Heller, R. Jefferson, H. Marrochio et al., *Complexity and entanglement for thermofield double states*, *SciPost Phys.* **6** (2019) 034 [1810.05151]. 30, 33, 34, 53, 57, 59, 81, 87, 91, 154, 159, 164, 193, 195

[69] S. Chapman, M. P. Heller, H. Marrochio and F. Pastawski, *Toward a Definition of Complexity for Quantum Field Theory States*, *Phys. Rev. Lett.* **120** (2018) 121602 [1707.08582]. 32, 33, 34, 35, 36, 38, 39, 50, 51, 53, 59, 99, 123, 125, 126, 144, 156, 159, 164

[70] L. Hackl and R. C. Myers, *Circuit complexity for free fermions*, *JHEP* **07** (2018) 139 [1803.10638]. 33, 51, 53

[71] S. Chapman, H. Marrochio and R. C. Myers, *Complexity of Formation in Holography*, *JHEP* **01** (2017) 062 [1610.08063]. 33, 50

[72] M. Guo, Z.-Y. Fan, J. Jiang, X. Liu and B. Chen, *Circuit complexity for generalized coherent states in thermal field dynamics*, *Phys. Rev. D* **101** (2020) 126007 [2004.00344]. 34

[73] A. Bhattacharyya, A. Shekar and A. Sinha, *Circuit complexity in interacting QFTs and RG flows*, *JHEP* **10** (2018) 140 [1808.03105]. 34

[74] T. Ali, A. Bhattacharyya, S. Shajidul Haque, E. H. Kim and N. Moynihan, *Time Evolution of Complexity: A Critique of Three Methods*, *JHEP* **04** (2019) 087 [1810.02734]. 34

[75] J. Jiang and X. Liu, *Circuit Complexity for Fermionic Thermofield Double states*, *Phys. Rev.* **D99** (2019) 026011 [1812.00193]. 34

[76] M. Sinamuli and R. B. Mann, *Holographic Complexity and Charged Scalar Fields*, *Phys. Rev. D* **99** (2019) 106013 [1902.01912]. 34

[77] M. Doroudiani, A. Naseh and R. Pirmoradian, *Complexity for Charged Thermofield Double States*, *JHEP* **01** (2020) 120 [1910.08806]. 34

[78] S. Chapman and H. Z. Chen, *Charged Complexity and the Thermofield Double State*, *JHEP* **02** (2021) 187 [1910.07508]. 34

[79] A. R. Brown and L. Susskind, *Complexity geometry of a single qubit*, *Phys. Rev. D* **100** (2019) 046020 [1903.12621]. 34

[80] I. Bengtsson and K. Życzkowski, *Geometry of quantum states: an introduction to quantum entanglement*. Cambridge University Press, 2017. 35

[81] M. Miyaji, T. Numasawa, N. Shiba, T. Takayanagi and K. Watanabe, *Distance between Quantum States and Gauge-Gravity Duality*, *Phys. Rev. Lett.* **115** (2015) 261602 [1507.07555]. 35

[82] L. Susskind, *Computational Complexity and Black Hole Horizons*, *Fortsch. Phys.* **64** (2016) 44 [1403.5695]. 35

[83] N. Lashkari and M. Van Raamsdonk, *Canonical Energy is Quantum Fisher Information*, *JHEP* **04** (2016) 153 [1508.00897]. 35

[84] S. Banerjee, J. Erdmenger and D. Sarkar, *Connecting Fisher information to bulk entanglement in holography*, 1701.02319. 35

[85] M. Alishahiha and A. Faraji Astaneh, *Holographic Fidelity Susceptibility*, *Phys. Rev.* **D96** (2017) 086004 [1705.01834]. 35

[86] A. Belin, A. Lewkowycz and G. Sárosi, *The boundary dual of the bulk symplectic form*, *Phys. Lett. B* **789** (2019) 71 [1806.10144]. 35

[87] P. Caputa and J. M. Magan, *Quantum Computation as Gravity*, *Phys. Rev. Lett.* **122** (2019) 231302 [1807.04422]. 39

[88] J. Erdmenger, M. Gerbershagen and A.-L. Weigel, *Complexity measures from geometric actions on Virasoro and Kac-Moody orbits*, 2004.03619. 39

[89] M. Flory and M. P. Heller, *Conformal field theory complexity from Euler-Arnold equations*, *JHEP* **12** (2020) 091 [2007.11555]. 39

[90] M. Flory and M. P. Heller, *Geometry of Complexity in Conformal Field Theory*, *Phys. Rev. Res.* **2** (2020) 043438 [2005.02415]. 39

[91] N. Chagnet, S. Chapman, J. de Boer and C. Zukowski, *Complexity for Conformal Field Theories in General Dimensions*, 2103.06920. 39

[92] P. Caputa, N. Kundu, M. Miyaji, T. Takayanagi and K. Watanabe, *Anti-de Sitter Space from Optimization of Path Integrals in Conformal Field Theories*, *Phys. Rev. Lett.* **119** (2017) 071602 [1703.00456]. 39, 40, 41, 42, 123, 165

[93] P. Caputa, N. Kundu, M. Miyaji, T. Takayanagi and K. Watanabe, *Liouville Action as Path-Integral Complexity: From Continuous Tensor Networks to AdS/CFT*, *JHEP* **11** (2017) 097 [1706.07056]. 39, 40, 41, 42, 43, 123, 165

[94] G. Evenbly and G. Vidal, *Tensor network renormalization*, *Physical review letters* **115** (2015) 180405. 40

[95] G. Evenbly and G. Vidal, *Tensor network renormalization yields the multiscale entanglement renormalization ansatz*, *Physical review letters* **115** (2015) 200401. 40

[96] J. Haegeman, T. J. Osborne, H. Verschelde and F. Verstraete, *Entanglement Renormalization for Quantum Fields in Real Space*, *Phys. Rev. Lett.* **110** (2013) 100402 [1102.5524]. 40

[97] P. H. Ginsparg and G. W. Moore, *Lectures on 2-D gravity and 2-D string theory*, in *Theoretical Advanced Study Institute (TASI 92): From Black Holes and Strings to Particles*, 10, 1993, hep-th/9304011. 42

[98] B. Czech, *Einstein Equations from Varying Complexity*, *Phys. Rev. Lett.* **120** (2018) 031601 [1706.00965]. 42

[99] A. Bhattacharyya, P. Caputa, S. R. Das, N. Kundu, M. Miyaji and T. Takayanagi, *Path-Integral Complexity for Perturbed CFTs*, *JHEP* **07** (2018) 086 [1804.01999]. 43

[100] H. A. Camargo, M. P. Heller, R. Jefferson and J. Knaute, *Path integral optimization as circuit complexity*, *Phys. Rev. Lett.* **123** (2019) 011601 [1904.02713]. 43

[101] J. Boruch, P. Caputa and T. Takayanagi, *Path-Integral Optimization from Hartle-Hawking Wave Function*, *Phys. Rev. D* **103** (2021) 046017 [2011.08188]. 43

[102] P. Caputa and I. MacCormack, *Geometry and Complexity of Path Integrals in Inhomogeneous CFTs*, *JHEP* **01** (2021) 027 [2004.04698]. 43

[103] J. Boruch, P. Caputa, D. Ge and T. Takayanagi, *Holographic Path-Integral Optimization*, 2104.00010. 43

[104] G. Jafari, A. Naseh and H. Zolfi, *Path Integral Optimization for $T\bar{T}$ Deformation*, *Phys. Rev. D* **101** (2020) 026007 [1909.02357]. 43

[105] M. Ghodrati, *Complexity and emergence of warped AdS_3 space-time from chiral Liouville action*, *JHEP* **02** (2020) 052 [1911.03819]. 43

[106] J. Molina-Vilaplana and A. Del Campo, *Complexity Functionals and Complexity Growth Limits in Continuous MERA Circuits*, *JHEP* **08** (2018) 012 [1803.02356]. 43

[107] T. Takayanagi, *Holographic Spacetimes as Quantum Circuits of Path-Integrations*, *JHEP* **12** (2018) 048 [1808.09072]. 43

[108] I. Akal, *Reflections on Virasoro circuit complexity and Berry phase*, 1908.08514. 43

[109] J. Couch, S. Eccles, T. Jacobson and P. Nguyen, *Holographic Complexity and Volume*, *JHEP* **11** (2018) 044 [1807.02186]. 44, 47, 108, 109

[110] D. Carmi, S. Chapman, H. Marrochio, R. C. Myers and S. Sugishita, *On the Time Dependence of Holographic Complexity*, *JHEP* **11** (2017) 188 [1709.10184]. 46, 47, 48, 50, 113, 198, 199

[111] S. Chapman, H. Marrochio and R. C. Myers, *Holographic complexity in Vaidya spacetimes. Part I*, *JHEP* **06** (2018) 046 [1804.07410]. 46, 47, 50, 114

[112] S. Chapman, H. Marrochio and R. C. Myers, *Holographic complexity in Vaidya spacetimes. Part II*, *JHEP* **06** (2018) 114 [1805.07262]. 46, 47, 50, 114, 164

[113] D. A. Roberts, D. Stanford and L. Susskind, *Localized shocks*, *JHEP* **03** (2015) 051 [1409.8180]. 47, 50

[114] D. Carmi, R. C. Myers and P. Rath, *Comments on Holographic Complexity*, *JHEP* **03** (2017) 118 [1612.00433]. 47, 49, 50, 52, 107, 108, 110, 114, 118, 122

[115] J. Couch, W. Fischler and P. H. Nguyen, *Noether charge, black hole volume, and complexity*, *JHEP* **03** (2017) 119 [1610.02038]. 47, 51, 107, 109

[116] A. Reynolds and S. F. Ross, *Complexity in de Sitter Space*, *Class. Quant. Grav.* **34** (2017) 175013 [1706.03788]. 47

[117] B. Swingle and Y. Wang, *Holographic Complexity of Einstein-Maxwell-Dilaton Gravity*, *JHEP* **09** (2018) 106 [1712.09826]. 47, 50

[118] Z. Fu, A. Maloney, D. Marolf, H. Maxfield and Z. Wang, *Holographic complexity is nonlocal*, *JHEP* **02** (2018) 072 [1801.01137]. 47, 50

[119] M. Flory and N. Miekley, *Complexity change under conformal transformations in AdS_3/CFT_2*, *JHEP* **05** (2019) 003 [1806.08376]. 47, 50

[120] B. Chen, B. Czech and Z.-z. Wang, *Query complexity and cutoff dependence of the CFT2 ground state*, *Phys. Rev. D* **103** (2021) 026015 [2004.11377]. 47

[121] D. Sarkar and M. Visser, *The first law of differential entropy and holographic complexity*, 2008.12673. 47

[122] Y.-S. An, R.-G. Cai, L. Li and Y. Peng, *Holographic complexity growth in an FLRW universe*, *Phys. Rev. D* **101** (2020) 046006 [1909.12172]. 47

[123] A. Al Balushi, R. A. Hennigar, H. K. Kunduri and R. B. Mann, *Holographic complexity of rotating black holes*, 2010.11203. 47, 50

[124] R.-G. Cai, S. He, S.-J. Wang and Y.-X. Zhang, *Revisit on holographic complexity in two-dimensional gravity*, *JHEP* **08** (2020) 102 [2001.11626]. 47

[125] S.-K. Jian, B. Swingle and Z.-Y. Xian, *Complexity growth of operators in the SYK model and in JT gravity*, 2008.12274. 47

[126] Z.-Y. Fan and M. Guo, *On the Noether charge and the gravity duals of quantum complexity*, *JHEP* **08** (2018) 031 [1805.03796]. 47, 109

[127] A. Belin, A. Lewkowycz and G. Sárosi, *The boundary dual of the bulk symplectic form*, *Phys. Lett. B* **789** (2019) 71 [1806.10144]. 47

[128] A. Belin, A. Lewkowycz and G. Sárosi, *Complexity and the bulk volume, a new York time story*, *JHEP* **03** (2019) 044 [1811.03097]. 47

[129] A. Al Balushi, R. A. Hennigar, H. K. Kunduri and R. B. Mann, *Holographic Complexity and Thermodynamic Volume*, *Phys. Rev. Lett.* **126** (2021) 101601 [2008.09138]. 47, 50

[130] S. Lloyd, *Ultimate physical limits to computation*, *Nature* **406** (2000) 1047. 48

[131] R.-G. Cai, S.-M. Ruan, S.-J. Wang, R.-Q. Yang and R.-H. Peng, *Action growth for AdS black holes*, *JHEP* **09** (2016) 161 [1606.08307]. 48, 50

[132] J. W. York, *Role of conformal three-geometry in the dynamics of gravitation*, *Phys. Rev. Lett.* **28** (1972) 1082. 48, 49

[133] G. W. Gibbons and S. W. Hawking, *Action integrals and partition functions in quantum gravity*, *Phys. Rev. D* **15** (1977) 2752. 48, 49

[134] L. Lehner, R. C. Myers, E. Poisson and R. D. Sorkin, *Gravitational action with null boundaries*, *Phys. Rev. D* **94** (2016) 084046 [1609.00207]. 48, 49, 50, 109, 115, 116, 117, 163

[135] K. Parattu, S. Chakraborty, B. R. Majhi and T. Padmanabhan, *A Boundary Term for the Gravitational Action with Null Boundaries*, *Gen. Rel. Grav.* **48** (2016) 94 [1501.01053]. 48

[136] G. Hayward, *Gravitational action for spacetimes with nonsmooth boundaries*, *Phys. Rev. D* **47** (1993) 3275. 48

[137] D. Brill and G. Hayward, *Is the gravitational action additive?*, *Phys. Rev.* **D50** (1994) 4914 [gr-qc/9403018]. 48

[138] J. L. F. Barbon and E. Rabinovici, *Holographic complexity and spacetime singularities*, *JHEP* **01** (2016) 084 [1509.09291]. 50

[139] J. L. F. Barbon and J. Martin-Garcia, *Holographic Complexity Of Cold Hyperbolic Black Holes*, *JHEP* **11** (2015) 181 [1510.00349]. 50

[140] A. Reynolds and S. F. Ross, *Divergences in Holographic Complexity*, *Class. Quant. Grav.* **34** (2017) 105004 [1612.05439]. 50

[141] M. Moosa, *Evolution of Complexity Following a Global Quench*, *JHEP* **03** (2018) 031 [1711.02668]. 50

[142] J. Couch, S. Eccles, W. Fischler and M.-L. Xiao, *Holographic complexity and noncommutative gauge theory*, *JHEP* **03** (2018) 108 [1710.07833]. 50

[143] R.-G. Cai, M. Sasaki and S.-J. Wang, *Action growth of charged black holes with a single horizon*, *Phys. Rev.* **D95** (2017) 124002 [1702.06766]. 50

[144] M. Flory, *A complexity/fidelity susceptibility g-theorem for $AdS_3/BCFT_2$*, *JHEP* **06** (2017) 131 [1702.06386]. 50

[145] Y. Zhao, *Uncomplexity and Black Hole Geometry*, *Phys. Rev. D* **97** (2018) 126007 [1711.03125]. 50

[146] A. P. Reynolds and S. F. Ross, *Complexity of the AdS Soliton*, *Class. Quant. Grav.* **35** (2018) 095006 [1712.03732]. 50

[147] R. Abt, J. Erdmenger, H. Hinrichsen, C. M. Melby-Thompson, R. Meyer, C. Northe et al., *Topological Complexity in AdS_3/CFT_2*, *Fortsch. Phys.* **66** (2018) 1800034 [1710.01327]. 50, 108, 118, 120

[148] M. Alishahiha, A. Faraji Astaneh, M. R. Mohammadi Mozaffar and A. Mollabashi, *Complexity Growth with Lifshitz Scaling and Hyperscaling Violation*, *JHEP* **07** (2018) 042 [1802.06740]. 50

[149] Y.-S. An and R.-H. Peng, *Effect of the dilaton on holographic complexity growth*, *Phys. Rev. D* **97** (2018) 066022 [1801.03638]. 50

[150] P. A. Cano, *Lovelock action with nonsmooth boundaries*, *Phys. Rev. D* **97** (2018) 104048 [1803.00172]. 50

[151] S. Mahapatra and P. Roy, *On the time dependence of holographic complexity in a dynamical Einstein-dilaton model*, *JHEP* **11** (2018) 138 [1808.09917]. 50

[152] P. A. Cano, R. A. Hennigar and H. Marrochio, *Complexity Growth Rate in Lovelock Gravity*, *Phys. Rev. Lett.* **121** (2018) 121602 [1803.02795]. 50

[153] J. L. F. Barbon and J. Martin-Garcia, *Terminal Holographic Complexity*, *JHEP* **06** (2018) 132 [1805.05291]. 50

[154] L. Susskind, *Black Holes and Complexity Classes*, 1802.02175. 50

[155] L. Susskind, *Why do Things Fall?*, 1802.01198. 50

[156] S. Cooper, M. Rozali, B. Swingle, M. Van Raamsdonk, C. Waddell and D. Wakeham, *Black Hole Microstate Cosmology*, *JHEP* **07** (2019) 065 [1810.10601]. 50, 108

[157] J. Jiang and H. Zhang, *Surface term, corner term, and action growth in $F(R_{abcd})$ gravity theory*, *Phys. Rev. D* **99** (2019) 086005 [112]. 50

[158] T. Numasawa, *Holographic Complexity for disentangled states*, *PTEP* **2020** (2020) 033B02 [1811.03597]. 50

[159] A. R. Brown, H. Gharibyan, A. Streicher, L. Susskind, L. Thorlacius and Y. Zhao, *Falling Toward Charged Black Holes*, *Phys. Rev. D* **98** (2018) 126016 [1804.04156]. 50

[160] K. Goto, H. Marrochio, R. C. Myers, L. Queimada and B. Yoshida, *Holographic Complexity Equals Which Action?*, *JHEP* **02** (2019) 160 [1901.00014]. 50

[161] C. A. Agón, M. Headrick and B. Swingle, *Subsystem Complexity and Holography*, *JHEP* **02** (2019) 145 [1804.01561]. 50, 108, 130, 139

[162] S. Chapman, D. Ge and G. Policastro, *Holographic Complexity for Defects Distinguishes Action from Volume*, *JHEP* **05** (2019) 049 [1811.12549]. 50, 108, 119, 120

[163] M. Flory, *WdW-patches in AdS_3 and complexity change under conformal transformations II*, *JHEP* **05** (2019) 086 [1902.06499]. 50

[164] P. Braccia, A. L. Cotrone and E. Tonni, *Complexity in the presence of a boundary*, *JHEP* **02** (2020) 051 [1910.03489]. 50, 108

[165] Y. Sato and K. Watanabe, *Does Boundary Distinguish Complexities?*, *JHEP* **11** (2019) 132 [1908.11094]. 50, 108

[166] R. Auzzi, S. Baiguera, M. Grassi, G. Nardelli and N. Zenoni, *Complexity and action for warped AdS black holes*, *JHEP* **09** (2018) 013 [1806.06216]. 50

[167] R. Auzzi, S. Baiguera and G. Nardelli, *Volume and complexity for warped AdS black holes*, *JHEP* **06** (2018) 063 [1804.07521]. 50

[168] S. F. Ross, *Complexity and typical microstates*, *Phys. Rev. D* **100** (2019) 066014 [1905.06211]. 50

[169] A. Bhattacharya, K. T. Grosvenor and S. Roy, *Entanglement Entropy and Subregion Complexity in Thermal Perturbations around Pure-AdS Spacetime*, *Phys. Rev. D* **100** (2019) 126004 [1905.02220]. 50, 108

[170] A. Ghosh and R. Mishra, *Inhomogeneous Jacobi equation and Holographic subregion complexity*, 1907.11757. 50

[171] C. A. Agón, M. Headrick and B. Swingle, *Subsystem Complexity and Holography*, *JHEP* **02** (2019) 145 [1804.01561]. 51, 52, 59, 86, 108, 109, 110, 111, 112, 113, 152, 153, 154, 157

[172] O. Aharony, S. S. Gubser, J. M. Maldacena, H. Ooguri and Y. Oz, *Large N field theories, string theory and gravity*, *Phys. Rept.* **323** (2000) 183 [hep-th/9905111]. 51

[173] T. Nishioka, S. Ryu and T. Takayanagi, *Holographic Entanglement Entropy: An Overview*, *J. Phys.* **A42** (2009) 504008 [0905.0932]. 51

[174] A. Almheiri, X. Dong and D. Harlow, *Bulk Locality and Quantum Error Correction in AdS/CFT*, *JHEP* **04** (2015) 163 [1411.7041]. 51

[175] B. Swingle, *Entanglement Renormalization and Holography*, *Phys. Rev.* **D86** (2012) 065007 [0905.1317]. 51

[176] J. Watrous, *Quantum computational complexity*, in *Encyclopedia of Complexity and Systems Science, ed., R. A. Meyers* (2009) 7174 [0804.3401]. 51, 52, 152, 153

[177] S. Aaronson, *The Complexity of Quantum States and Transformations: From Quantum Money to Black Holes*, 2016, 1607.05256. 51

[178] R. Khan, C. Krishnan and S. Sharma, *Circuit Complexity in Fermionic Field Theory*, *Phys. Rev.* **D98** (2018) 126001 [1801.07620]. 51

[179] A. Bhattacharyya, A. Shekar and A. Sinha, *Circuit complexity in interacting QFTs and RG flows*, *JHEP* **10** (2018) 140 [1808.03105]. 51

[180] M. Alishahiha, *Holographic Complexity*, *Phys. Rev.* **D92** (2015) 126009 [1509.06614]. 52, 107, 108, 114, 118

[181] W. F. Stinespring, *Positive functions on c*-algebras*, *Proceedings of the American Mathematical Society* **6** (1955) 211. 52, 153

[182] D. Aharonov, A. Kitaev and N. Nisan, *Quantum circuits with mixed states*, in *Proceedings of the Thirtieth Annual ACM Symposium on Theory of Computing* (1998) 20 [quant-ph/9806029]. 52, 152

[183] A. Bhattacharyya, T. Takayanagi and K. Umemoto, *Entanglement of Purification in Free Scalar Field Theories*, *JHEP* **04** (2018) 132 [1802.09545]. 53, 71, 167

[184] K. Umemoto and T. Takayanagi, *Entanglement of purification through holographic duality*, *Nature Phys.* **14** (2018) 573 [1708.09393]. 53, 167

[185] P. Nguyen, T. Devakul, M. G. Halbasch, M. P. Zaletel and B. Swingle, *Entanglement of purification: from spin chains to holography*, *JHEP* **01** (2018) 098 [1709.07424]. 53, 167

[186] A. Mann and M. Revzen, *Gaussian density matrices: quantum analogs of classical states*, *Fortschritte der Physik/Progress of Physics* **41** (1993) 431. 54

[187] A. Erdélyi, W. Magnus, F. Oberhettinger and F. G. Tricomi, *Higher transcendental functions, Vol. 2*, Calif. Inst. Technol. Bateman Manuscr. Project. McGraw-Hill, New York, NY, 1953. 56

[188] H. A. Camargo, L. Hackl, M. P. Heller, A. Jahn, T. Takayanagi and B. Windt, *Entanglement and complexity of purification in (1+1)-dimensional free conformal field theories*, *Phys. Rev. Res.* **3** (2021) 013248 [2009.11881]. 70, 124

[189] M. Alishahiha, K. Babaei Velni and M. R. Mohammadi Mozaffar, *Subregion Action and Complexity*, 1809.06031. 84, 85, 155

[190] E. Caceres, J. Couch, S. Eccles and W. Fischler, *Holographic Purification Complexity*, 1811.10650. 86, 108, 110, 170

[191] B. Czech, J. L. Karczmarek, F. Nogueira and M. Van Raamsdonk, *The Gravity Dual of a Density Matrix*, *Class. Quant. Grav.* **29** (2012) 155009 [1204.1330]. 107, 108

[192] M. Headrick, V. E. Hubeny, A. Lawrence and M. Rangamani, *Causality & holographic entanglement entropy*, *JHEP* **12** (2014) 162 [1408.6300]. 107, 108

[193] A. C. Wall, *Maximin Surfaces, and the Strong Subadditivity of the Covariant Holographic Entanglement Entropy*, *Class. Quant. Grav.* **31** (2014) 225007 [1211.3494]. 107, 108

[194] D. L. Jafferis, A. Lewkowycz, J. Maldacena and S. J. Suh, *Relative entropy equals bulk relative entropy*, *JHEP* **06** (2016) 004 [1512.06431]. 107, 169

[195] X. Dong, D. Harlow and A. C. Wall, *Reconstruction of Bulk Operators within the Entanglement Wedge in Gauge-Gravity Duality*, *Phys. Rev. Lett.* **117** (2016) 021601 [1601.05416]. 107

[196] E. Bakhshaei, A. Mollabashi and A. Shirzad, *Holographic Subregion Complexity for Singular Surfaces*, *Eur. Phys. J.* **C77** (2017) 665 [1703.03469]. 108

[197] R. Abt, J. Erdmenger, M. Gerbershagen, C. M. Melby-Thompson and C. Northe, *Holographic Subregion Complexity from Kinematic Space*, *JHEP* **01** (2019) 012 [1805.10298]. 108, 120

[198] E. Caceres and M.-L. Xiao, *Complexity-action of subregions with corners*, *JHEP* **03** (2019) 062 [1809.09356]. 108, 119, 120, 160

[199] B. Chen, W.-M. Li, R.-Q. Yang, C.-Y. Zhang and S.-J. Zhang, *Holographic subregion complexity under a thermal quench*, *JHEP* **07** (2018) 034 [1803.06680]. 108

[200] R. Auzzi, S. Baiguera, A. Mitra, G. Nardelli and N. Zenoni, *Subsystem complexity in warped AdS*, *JHEP* **09** (2019) 114 [1906.09345]. 108

[201] R. Auzzi, G. Nardelli, F. I. Schaposnik Massolo, G. Tallarita and N. Zenoni, *On volume subregion complexity in Vaidya spacetime*, *JHEP* **11** (2019) 098 [1908.10832]. 108

[202] Y. Ling, Y. Liu, C. Niu, Y. Xiao and C.-Y. Zhang, *Holographic Subregion Complexity in General Vaidya Geometry*, *JHEP* **11** (2019) 039 [1908.06432]. 108

[203] O. Ben-Ami and D. Carmi, *On Volumes of Subregions in Holography and Complexity*, *JHEP* **11** (2016) 129 [1609.02514]. 108

[204] R. Auzzi, S. Baiguera, A. Legramandi, G. Nardelli, P. Roy and N. Zenoni, *On subregion action complexity in AdS_3 and in the BTZ black hole*, *JHEP* **01** (2020) 066 [1910.00526]. 108, 160

[205] D. Kastor, S. Ray and J. Traschen, *Enthalpy and the Mechanics of AdS Black Holes*, *Class. Quant. Grav.* **26** (2009) 195011 [0904.2765]. 109

[206] J. D. Brown and M. Henneaux, *Central Charges in the Canonical Realization of Asymptotic Symmetries: An Example from Three-Dimensional Gravity*, *Commun. Math. Phys.* **104** (1986) 207. 118

[207] A. Buchel, J. Escobedo, R. C. Myers, M. F. Paulos, A. Sinha and M. Smolkin, *Holographic GB gravity in arbitrary dimensions*, *JHEP* **03** (2010) 111 [0911.4257]. 118

[208] R. Emparan, C. V. Johnson and R. C. Myers, *Surface terms as counterterms in the AdS / CFT correspondence*, *Phys. Rev.* **D60** (1999) 104001 [hep-th/9903238]. 119

[209] C. Agón, E. Cáceres and M. L. Xiao *work in progress* . 120

[210] I. Bengtsson and K. Życzkowski, *Geometry of quantum states: an introduction to quantum entanglement*. Cambridge university press, 2017. 124, 130, 205

[211] D. Chruscinski and A. Jamiolkowski, *Geometric phases in classical and quantum mechanics*, vol. 36. Springer Science & Business Media, 2012. 124, 130, 205

[212] A. Uhlmann, *The transition probability in the state space of c-algebra*, *Reports on Mathematical Physics* **9** (1976) 273. 125

[213] S.-J. GU, *Fidelity approach to quantum phase transitions*, *International Journal of Modern Physics B* **24** (2010) 4371 [0811.3127]. 125

[214] R. Jozsa, *Fidelity for mixed quantum states*, *Journal of modern optics* **41** (1994) 2315. 127, 130

[215] H. Barnum, C. M. Caves, C. A. Fuchs, R. Jozsa and B. Schumacher, *Noncommuting mixed states cannot be broadcast*, *Phys. Rev. Lett.* **76** (1996) 2818. 127, 128

[216] M. A. Nielsen, *The Entanglement fidelity and quantum error correction*, quant-ph/9606012. 127

[217] D. Bures, *An extension of kakutani's theorem on infinite product measures to the tensor product of semifinite w*-algebras*, *Transactions of the American Mathematical Society* **135** (1969) 199. 130, 205

[218] J. Liu, H. Yuan, X.-M. Lu and X. Wang, *Quantum Fisher information matrix and multiparameter estimation*, *J. Phys. A* **53** (2020) 023001 [1907.08037]. 130, 205, 209, 210

[219] J. Twamley, *Bures and statistical distance for squeezed thermal states*, *Journal of Physics A: Mathematical and General* **29** (1996) 3723. 142

[220] G. Di Giulio and E. Tonni, *Complexity of mixed Gaussian states from Fisher information geometry*, *JHEP* **12** (2020) 101 [2006.00921]. 154, 206

[221] G. Di Giulio and E. Tonni, *Subsystem complexity after a global quantum quench*, 2102.02764. 154, 206

[222] Z. Fu, A. Maloney, D. Marolf, H. Maxfield and Z. Wang, *Holographic complexity is nonlocal*, *JHEP* **02** (2018) 072 [1801.01137]. 159

[223] P. Calabrese and J. L. Cardy, *Entanglement entropy and quantum field theory*, *J. Stat. Mech.* **0406** (2004) P06002 [hep-th/0405152]. 160

[224] P. Calabrese and J. L. Cardy, *Entanglement entropy and quantum field theory: A Non-technical introduction*, *Int. J. Quant. Inf.* **4** (2006) 429 [quant-ph/0505193]. 160

[225] R. D. Sorkin, *On the Entropy of the vacuum outside a horizon*, arXiv:1402.3589. 160

[226] L. Bombelli, R. K. Koul, J. Lee and R. D. Sorkin, *Quantum source of entropy for black holes*, *Phys. Rev. D* **34** (1986) 373. 160

[227] M. Srednicki, *Entropy and area*, *Phys. Rev. Lett.* **71** (1993) 666 [arXiv:hep-th/9303048]. 160

[228] P. Caputa, M. Miyaji, T. Takayanagi and K. Umemoto, *Holographic Entanglement of Purification from Conformal Field Theories*, *Phys. Rev. Lett.* **122** (2019) 111601 [1812.05268]. 166

[229] M. Headrick, *Entanglement Renyi entropies in holographic theories*, *Phys. Rev.* **D82** (2010) 126010 [1006.0047]. 167

[230] T. Hartman, *Entanglement Entropy at Large Central Charge*, 1303.6955. 167

[231] T. Faulkner, *The Entanglement Renyi Entropies of Disjoint Intervals in AdS/CFT*, 1303.7221. 167

[232] B. M. Terhal, M. Horodecki, D. W. Leung and D. P. DiVincenzo, *The entanglement of purification*, *Journal of Mathematical Physics* **43** (2002) 4286. 167

[233] L. Banchi, P. Giorda and P. Zanardi, *Quantum information-geometry of dissipative quantum phase transitions*, *Phys. Rev. E* **89** (2014) 022102. 168

[234] L. Banchi, S. L. Braunstein and S. Pirandola, *Quantum fidelity for arbitrary gaussian states*, *Phys. Rev. Lett.* **115** (2015) 260501. 168

[235] A. Carollo, B. Spagnolo and D. Valenti, *Uhlmann curvature in dissipative phase transitions*, *Scientific reports* **8** (2018) 9852. 168

[236] H. Nha and H. J. Carmichael, *Distinguishing two single-mode gaussian states by homodyne detection: An information-theoretic approach*, *Phys. Rev. A* **71** (2005) 032336. 168

[237] H. A. Camargo, P. Caputa, D. Das, M. P. Heller and R. Jefferson, *Complexity as a novel probe of quantum quenches: universal scalings and purifications*, *Phys. Rev. Lett.* **122** (2019) 081601 [1807.07075]. 168

[238] T. Takayanagi and K. Umemoto, *Entanglement of purification through holographic duality*, *Nature Phys.* **14** (2018) 573 [1708.09393]. 170

[239] H. Hirai, K. Tamaoka and T. Yokoya, *Towards Entanglement of Purification for Conformal Field Theories*, *PTEP* **2018** (2018) 063B03 [1803.10539]. 170

[240] S. Dutta and T. Faulkner, *A canonical purification for the entanglement wedge cross-section*, 1905.00577. 171

[241] M. G. Paris, *Quantum estimation for quantum technology*, *International Journal of Quantum Information* **7** (2009) 125. 205, 208, 209, 210

[242] M. Hübner, *Explicit computation of the bures distance for density matrices*, *Physics Letters A* **163** (1992) 239 . 207, 210

APPENDICES

Appendix A

Complexity Basis Dependence

In this paper, we refer to two different bases for the definition of the $\mathcal{C}_1$ complexity: the *diagonal basis* and the *physical(-ancilla) basis*. In addition, for coupled harmonic oscillators representing a lattice quantum field theory, a natural basis to consider is the original *position basis*, where each harmonic oscillator represents a position in the lattice. To help clarify the difference and relations between these bases, in this appendix we explicitly construct a example of a discretized free scalar field theory on a lattice and write down the wavefunction matrix of the ground state in each of these three bases. By looking at the example of four coupled harmonic oscillators, we explicitly find the parameter matrices in the three bases. The position basis and the physical basis are different in this case, and we show that the ground state can be understood as the thermofield double of a two harmonic oscillator modular Hamiltonian, which we explicitly write. The physical basis modes are the eigenmodes of the modular Hamiltonians of each subregion.

Before going into the specific example, we explicitly rewrite some of the formulas in section 3.4 for the one dimensional case to describe the one-dimensional chain of N harmonic oscillators. We begin with the lattice of harmonic oscillators (3.79) realizing a regularization of a free quantum field theory (3.78) on a one-dimensional circle of length L corresponding to the Hamiltonian[1]

$$H = \frac{1}{2M}\sum_{a=1}^{N}[\bar{p}_a^2 + M^2\bar{\omega}^2\bar{x}_a^2 + M^2\Omega^2(\bar{x}_a - \bar{x}_{a+1})^2]\,, \tag{A.1}$$

where we have defined $\bar{x}_n \equiv \delta\phi(n)$, $\bar{p}_n \equiv \pi(n)$, $\bar{\omega} \equiv m$ and $\Omega = M \equiv 1/\delta$, see, *e.g.,* [62], and assumed periodic boundary conditions $\bar{x}_{N+1} := \bar{x}_1$. The lattice spacing δ is related to the

[1]The following are the one dimensional versions of eqs. (3.79), (3.80) and (3.81).

size of the system and the number of harmonic oscillators by $\delta = L/N$. The Hamiltonian can be written in terms of normal modes as in eq. (3.80)

$$x_k \equiv \frac{1}{\sqrt{N}} \sum_{a=1}^{N} \exp\left(\frac{2\pi i k}{N} a\right) \bar{x}_a, \quad \omega_k^2 = \bar{\omega}^2 + 4\Omega^2 \sin^2 \frac{\pi k}{N}\,, \tag{A.2}$$

where $k \in 1, \ldots N$ (see, e.g., section 5.1 of [68]). Using these degrees of freedom, the Hamiltonian reads (3.81)

$$H = \frac{1}{2M} \sum_{k=1}^{N} \left(|p_k|^2 + M^2 \omega_k^2 |x_k|^2\right), \tag{A.3}$$

where we have used that $x_k^\dagger = x_{N-k}$. The ground state wavefunction of this system of harmonic oscillators is straightforward to find in normal mode basis and is given by eq. (3.125). This can be explicitly written in the physical basis using the transformation (3.80) and is given by eqs. (3.126)-(3.127).

A.1 Example: Four Coupled Harmonic Oscillators

We restrict to the example of a lattice of four harmonic oscillators with the goal of explicitly providing an example of the ground state in the normal mode basis, in position basis and in the physical(-ancilla) basis. We will express these in terms of the parameter matrix M used throughout the main body of the paper. That is, we use M_{basis} to represent the state[2]

$$\Psi_0(x_{\text{basis}}) = \left(\det\left(\frac{M_{\text{basis}}}{\pi}\right)\right)^{1/4} \exp\left[-\frac{1}{2} x_{\text{basis}}^\dagger M_{\text{basis}} x_{\text{basis}}\right]. \tag{A.4}$$

The state we are interested in is the ground state of the free QFT lattice Hamiltonian consisting of four coupled harmonic oscillators, *i.e.*, the $N = 4$ case of (A.1). This state was already written in normal mode basis in eq. (3.125). For a lattice of four harmonic oscillators, the normal modes $x_k \equiv (x_1, x_2, x_3, x_4)^T$ are related to the original physical basis modes $\bar{x}_a \equiv (\bar{x}_1, \bar{x}_2, \bar{x}_3, \bar{x}_4)^T$ by eq. (A.2), namely

$$x = R\bar{x}\,, \quad \text{where} \quad R = \frac{1}{2}\begin{pmatrix} i & -1 & -i & 1 \\ -1 & 1 & -1 & 1 \\ -i & -1 & i & 1 \\ 1 & 1 & 1 & 1 \end{pmatrix}, \tag{A.5}$$

[2]We use the generalization of eq. (2.9) for a complex basis. This will be necessary since the Fourier transformation in eq. (A.2) yields complex normal modes.

or, explicitly

$$\begin{aligned} x_1 &= \frac{1}{2}\left(i\bar{x}_1 - \bar{x}_2 - i\bar{x}_3 + \bar{x}_4\right) , & x_2 &= \frac{1}{2}\left(-\bar{x}_1 + \bar{x}_2 - \bar{x}_3 + \bar{x}_4\right) , \\ x_3 &= \frac{1}{2}\left(-i\bar{x}_1 - \bar{x}_2 + i\bar{x}_3 + \bar{x}_4\right) , & x_4 &= \frac{1}{2}\left(\bar{x}_1 + \bar{x}_2 + \bar{x}_3 + \bar{x}_4\right) . \end{aligned} \tag{A.6}$$

Notice that, while the position basis degrees of freedom are real valued, this is not the case for the normal mode degrees of freedom where, in particular $x_1^* = x_3$ so that $x^\dagger_{\text{normal}} = (x_3, x_2, x_1, x_4)$.[3] The parameter matrix in normal mode basis can easily be read off eqs. (3.125) and (A.2)

$$M_{\text{normal}} = \begin{pmatrix} \bar{\omega}_1 & 0 & 0 & 0 \\ 0 & \bar{\omega}_2 & 0 & 0 \\ 0 & 0 & \bar{\omega}_3 & 0 \\ 0 & 0 & 0 & \bar{\omega}_4 \end{pmatrix} , \tag{A.7}$$

where

$$\bar{\omega}_1 = \bar{\omega}_3 = \sqrt{\bar{\omega}^2 + 2\sqrt{2}\Omega^2} , \quad \bar{\omega}_2 = \sqrt{\bar{\omega}^2 + 4\Omega^2} , \quad \bar{\omega}_4 = \bar{\omega} . \tag{A.8}$$

The fact that the parameter matrix in normal mode basis is diagonal reflects the fact that there is no entanglement between normal mode degrees of freedom.[4]

The physical basis parameter matrix can be found by applying the transformation (A.5) to the normal mode basis parameter matrix (A.7)

$$M_{\text{pos}} = R^\dagger M_{\text{normal}} R \tag{A.9}$$

or simply be read off eq. (3.127). Either way, for our four harmonic oscillator example it takes the form

$$M_{\text{pos}} = \frac{1}{4}\begin{pmatrix} \bar{\omega} + \bar{\omega}_2 + 2\bar{\omega}_1 & \bar{\omega} - \bar{\omega}_2 & \bar{\omega} + \bar{\omega}_2 - 2\bar{\omega}_1 & \bar{\omega} - \bar{\omega}_2 \\ \bar{\omega} - \bar{\omega}_2 & \bar{\omega} + \bar{\omega}_2 + 2\bar{\omega}_1 & \bar{\omega} - \bar{\omega}_2 & \bar{\omega} + \bar{\omega}_2 - 2\bar{\omega}_1 \\ \bar{\omega} + \bar{\omega}_2 - 2\bar{\omega}_1 & \bar{\omega} - \bar{\omega}_2 & \bar{\omega} + \bar{\omega}_2 + 2\bar{\omega}_1 & \bar{\omega} - \bar{\omega}_2 \\ \bar{\omega} - \bar{\omega}_2 & \bar{\omega} + \bar{\omega}_2 - 2\bar{\omega}_1 & \bar{\omega} - \bar{\omega}_2 & \bar{\omega} + \bar{\omega}_2 + 2\bar{\omega}_1 \end{pmatrix} . \tag{A.10}$$

[3] Recall that the Fourier transform obeys the identity $x_k^\dagger = x_{N-k}$, see comment below eq. (A.3).

[4] Note that substituting the parameter matrix (A.7) into the bi-linear form in eq. (A.4) yields a wave-function whose dependence on the x_1 and x_3 coordinates is of the form $\Psi_0 \propto \exp\left[-\alpha(|x_1|^2 + |x_3|^2)\right] = \exp\left[-2\alpha x_1 x_3\right]$, where $\alpha = \frac{1}{2}\bar{\omega}^2 + \sqrt{2}\Omega^2$. So although the form seems orthogonal in complex coordinates, it does not look orthogonal when reexpressing the conjugate coordinates in terms of the original ones. This is due to the fact that the normal mode basis given by eq. (A.2) is not Hermitian. This awkward dependence on the product of seemingly different degrees of freedom can be removed by using a real Fourier transformation involving $\sin(\cdots)$ and $\cos(\cdots)$ instead of the complex exponentials in eq. (A.2). An equivalent way of getting rid of this dependence is to make a second transformation $x_k^{\text{real}} = \frac{1}{2}\left(x_k + x_k^*\right)$ and $x_{N-k}^{\text{real}} = \frac{1}{2i}\left(x_k - x_k^*\right)$ for those values of k for which x_k are not real.

The form of the parameter matrix makes evident that the position basis degrees of freedom are entangled with each other. Furthermore, the entanglement decays for longer distances since $\bar{\omega} < \bar{\omega}_1 < \bar{\omega}_2$ implies $|\bar{\omega}-\bar{\omega}_2| > |\bar{\omega}+\bar{\omega}_2-2\bar{\omega}_1|$. This is to be expected for entanglement being spread by nearest neighbor interactions coming from the discretized kinetic term (the last term in (A.1)).

The position and normal mode basis should be familiar to most readers; they are the lattice equivalents of the position and momentum bases in quantum field theory. The physical-ancilla basis is less familiar. In [68], it appears under the name *left/right* basis since it was used in the context of the TFD state, which is considered a natural purification of the thermal state where the left/right division corresponds to the physical degrees of freedom of the thermal system and the ancilla degrees of freedom introduced in order to purify it.

To define the physical-ancilla basis, we must partition the system into a physical subsystem and an ancilla subsystem. In other words, we consider the four harmonic oscillator ground state (A.4) as a purification of a mixed state of a subset of the oscillators. This is an important property of the physical-ancilla basis: it depends on a specific partition of the full system. In our example, we will choose to partition the system in two: the $\bar{x}_1$ and $\bar{x}_2$ oscillators as one subsystem and the $\bar{x}_3$ and $\bar{x}_4$ oscillators as the other subsystem. Which subsystem we call physical and which one ancilla depends on which degrees of freedom are traced out in order to construct the given two-mode mixed state.

With this partition in mind, we can decompose the physical basis parameter matrix (A.10), as in eq. (3.60), into[5]

$$M_{\text{pos}} = \begin{pmatrix} \Gamma & K \\ K^T & \Sigma \end{pmatrix} \tag{A.12}$$

where

$$\begin{aligned} \Gamma = \Sigma &= \frac{1}{4}\begin{pmatrix} \bar{\omega}+\bar{\omega}_2+2\bar{\omega}_1 & \bar{\omega}-\bar{\omega}_2 \\ \bar{\omega}-\bar{\omega}_2 & \bar{\omega}+\bar{\omega}_2+2\bar{\omega}_1 \end{pmatrix}, \\ K &= \frac{1}{4}\begin{pmatrix} \bar{\omega}+\bar{\omega}_2-2\bar{\omega}_1 & \bar{\omega}-\bar{\omega}_2 \\ \bar{\omega}-\bar{\omega}_2 & \bar{\omega}+\bar{\omega}_2-2\bar{\omega}_1 \end{pmatrix}. \end{aligned} \tag{A.13}$$

[5] In section 3.3.1 we introduced the decomposition (3.60)

$$M_{\text{pos}} = \begin{pmatrix} \Gamma & K \\ K^T & \Omega \end{pmatrix}, \tag{A.11}$$

which has the unfortunate notation Ω for the lower right sub-matrix. In the following, we use instead the letter Σ to denote this sub-matrix in order to avoid confusion with the oscillator coupling Ω in eq. (A.1).

The physical-ancilla basis is defined as the basis which diagonalizes the sub-matrices Γ and Σ without mixing the two subsystems. More precisely, we look for transformations of the form

$$R_{\text{phys-anc}} = \begin{pmatrix} R_{\text{phys}} & 0 \\ 0 & R_{\text{anc}} \end{pmatrix} \tag{A.14}$$

that diagonalize both Γ and Σ. In our example, this transformation is given by

$$R_{\text{phys}} = \frac{1}{\sqrt{2}} \begin{pmatrix} 1 & 1 \\ -1 & 1 \end{pmatrix} , \quad R_{\text{anc}} = \frac{1}{\sqrt{2}} \begin{pmatrix} 1 & 1 \\ 1 & -1 \end{pmatrix} , \tag{A.15}$$

or, explicitly

$$\begin{aligned} x_1^{\text{phys}} &= \frac{1}{\sqrt{2}}(\bar{x}_1 + \bar{x}_2) , & x_2^{\text{phys}} &= \frac{1}{\sqrt{2}}(\bar{x}_2 - \bar{x}_1) , \\ x_3^{\text{phys}} &= \frac{1}{\sqrt{2}}(\bar{x}_3 + \bar{x}_4) , & x_4^{\text{phys}} &= \frac{1}{\sqrt{2}}(\bar{x}_3 - \bar{x}_4) . \end{aligned} \tag{A.16}$$

The physical-ancilla basis parameter matrix can be found by applying the transformation (A.14) to the position basis parameter matrix (A.10)

$$M_{\text{phys}} = \frac{1}{2} \begin{pmatrix} \bar{\omega} + \bar{\omega}_1 & 0 & \bar{\omega} - \bar{\omega}_1 & 0 \\ 0 & \bar{\omega}_2 + \bar{\omega}_1 & 0 & \bar{\omega}_1 - \bar{\omega}_2 \\ \bar{\omega} - \bar{\omega}_1 & 0 & \bar{\omega} + \bar{\omega}_1 & 0 \\ 0 & \bar{\omega}_1 - \bar{\omega}_2 & 0 & \bar{\omega}_2 + \bar{\omega}_1 \end{pmatrix} . \tag{A.17}$$

In this basis, there is no entanglement between the modes in each subsystem (x_1^{phys} is not entangled with x_2^{phys} and similarly for x_3^{phys} and x_4^{phys}). However, the entanglement between the two subregions cannot be removed by transformations of the form (A.14). Consequently, the modes between regions remain entangled. In our case, the state factorizes to a product state form where x_1^{phys} is entangled with x_3^{phys} and x_2^{phys} with x_4^{phys}. Bellow we will also see that the ground state is the TFD for a 2 harmonic oscillator modular Hamiltonian.

To see this, we compare the physical basis parameter matrix to the thermal parameters by using eqs. (3.26) and (3.25) for each factor of the factorized state (A.17). First, focusing on the x_1^{phys} and x_3^{phys} modes, we see that they are in a TFD state with inverse temperature β_{13} and frequency ω_{13} given by

$$\beta_{13}\omega_{13} = 2\,\text{arcosh}\left(\frac{\bar{\omega} + \bar{\omega}_1}{\bar{\omega}_1 - \bar{\omega}}\right) , \quad \omega_{13} e^{2r_{13}} = \sqrt{\bar{\omega}\,\bar{\omega}_1} , \tag{A.18}$$

and the x_2^{phys} and x_4^{phys} modes are in a TFD state with inverse temperature β_{24} and frequency ω_{24} given by

$$\beta_{24}\omega_{24} = 2\,\text{arcosh}\left(\frac{\bar{\omega}_1+\bar{\omega}_2}{\bar{\omega}_2-\bar{\omega}_1}\right), \quad \omega_{24}e^{2r_{24}} = \sqrt{\bar{\omega}_1\,\bar{\omega}_2}\,. \tag{A.19}$$

For these to have the same inverse temperature β_0 we must fix[6]

$$e^{-2r_{13}} = \frac{2}{\beta_0\sqrt{\bar{\omega}\,\bar{\omega}_1}}\,\text{arcosh}\left(\frac{\bar{\omega}+\bar{\omega}_1}{\bar{\omega}_1-\bar{\omega}}\right), \quad e^{-2r_{24}} = \frac{2}{\beta_0\sqrt{\bar{\omega}_1\,\bar{\omega}_2}}\,\text{arcosh}\left(\frac{\bar{\omega}_1+\bar{\omega}_2}{\bar{\omega}_2-\bar{\omega}_1}\right), \tag{A.20}$$

which leads to the following frequencies of the Rindler modes

$$\omega_{13} = \frac{2}{\beta_0}\,\text{arcosh}\left(\frac{\bar{\omega}+\bar{\omega}_1}{\bar{\omega}_1-\bar{\omega}}\right), \quad \omega_{24} = \frac{2}{\beta_0}\,\text{arcosh}\left(\frac{\bar{\omega}_1+\bar{\omega}_2}{\bar{\omega}_2-\bar{\omega}_1}\right). \tag{A.21}$$

Lastly, we can explicitly write the modular Hamiltonian of the x_1^{phys} and x_2^{phys} system from the expression of their frequencies (A.21)

$$\begin{aligned} H_{\text{mod}} =& \frac{1}{2M_0}\left(p_1^{\text{phys}}\right)^2 + \frac{2\,M_0}{\beta_0^2}\,\text{arcosh}^2\left(\frac{\bar{\omega}+\bar{\omega}_1}{\bar{\omega}_1-\bar{\omega}}\right)\left(x_1^{\text{phys}}\right)^2 \\ &+ \frac{1}{2M_0}\left(p_2^{\text{phys}}\right)^2 + \frac{2\,M_0}{\beta_0^2}\,\text{arcosh}^2\left(\frac{\bar{\omega}_1+\bar{\omega}_2}{\bar{\omega}_2-\bar{\omega}_1}\right)\left(x_2^{\text{phys}}\right)^2. \end{aligned} \tag{A.22}$$

[6]The temperature is a free parameter because the modular Hamiltonian can always be rescaled to change the value of β_0. However, the dimensionless products $\omega\beta_0$ will remain fixed.

Appendix B

Superadditivity of $\mathcal{C}_A(|\mathbf{TFD}\rangle)$ at general times

Using the results of [110] we can demonstrate that the mutual complexity of the time evolved TFD state using the subregion-CA proposal is in general negative. As mentioned in the main text $\mathcal{C}_{\text{A}}(\mathcal{L})$ and $\mathcal{C}_{\text{A}}(\mathcal{R})$ are invariant under time evolution and we therefore have

$$\Delta\mathcal{C}_{\text{A}}(t) \equiv \mathcal{C}_A(\mathcal{L}) + \mathcal{C}_A(\mathcal{R}) - \mathcal{C}_A(\mathcal{L}\cup\mathcal{R})(t) = \Delta\mathcal{C}_{\text{A}}(t=0) - \delta\mathcal{C}_{\text{A}}\,, \tag{B.1}$$

where $\Delta\mathcal{C}_{\text{A}}(t=0)$ can be found in eq. (4.14)

$$\Delta\mathcal{C}_{\text{A}}(t=0) = -\frac{2S}{\pi^2}\ln\left(\frac{\ell_{ct}(d-1)}{L}\right) + \text{negative}, \tag{B.2}$$

and we have defined

$$\delta\mathcal{C}_{\text{A}} = \mathcal{C}_A(\mathcal{L}\cup\mathcal{R})(t) - \mathcal{C}_A(\mathcal{L}\cup\mathcal{R})(0)\,. \tag{B.3}$$

The most negative value obtained by $\delta\mathcal{C}_{\text{A}}$ can be bounded using the results of [110] for the rate of change of the complexity of the TFD state. There the authors found that the rate of change of the complexity was vanishing for $t = t_{\mathcal{L}} + t_{\mathcal{R}} < t_c$ where $t_c = 2(r^*_\infty - r^*(0))$ is the critical time where the WDW patch leaves the past singularity,[1] and after this time, the rate of change became negative for a brief amount of time and later on approached

[1] For the definition of the critical time we have used the tortoise coordinate $r^*(r) = \int dr/f(r)$ as well as the blackening factor $f(r) = \frac{r^2}{L^2} + k - \frac{\omega^{d-2}}{r^{d-2}}$ and the mass parameter $\omega^{d-2} = r_h^{d-2}\left(\frac{r_h^2}{L^2}+k\right)$, where $k = 0, \pm 1$ correspond to the various possible horizon geometries.

a positive constant proportional to the mass of the black hole. The explicit expression is give in eq. (E.9) of [110] and reads

$$\left.\frac{d\mathcal{C}_{\rm A}}{dt}\right|_{t>t_c}=\frac{\Omega_{k,d-1}(d-1)f\left(r_m\right)}{16\pi^2G_N}\left[\frac{2\omega^{d-2}}{f\left(r_m\right)}-r_m^{d-2}\left[\ln\frac{r_m^2}{L^2|f(r_m)|}-2\ln\frac{(d-1)\ell_{\rm ct}}{L}\right]\right], \tag{B.4}$$

where r_m is the place where the null boundaries of the WDW patch meet behind the past horizon and is fixed according to the equation $\frac{t-t_c}{2}+r^*(r_m)-r^*(0)=0$. This rate of change is negative for times $t\in(t_c,t_{c,2})$ corresponding to the region $r_m\in(0,r_{c,2})$. Here, the second critical time, or the critical radius $r_{c,2}$, are found by solving the equation $\frac{dC_A}{dt}\big|_{t_{c,2}}=0$ and correspond to the time in which the rate of change in complexity becomes positive and the complexity starts increasing again. Of course, we have $r_{c,2}<r_h$. In order to check that the time-evolved TFD state is always superadditive, we need to consider the minimal value of the complexity for the TFD state which is decided by

$$\begin{aligned}\delta\mathcal{C}_{\rm A}^{\rm min}&=\int_{t_c}^{t_{c,2}}\frac{d\mathcal{C}_{\rm A}}{dt}\,dt=\frac{\Omega_{k,d-1}(d-1)}{8\pi^2G_N}\\&\quad\times\int_0^{r_{c,2}}\left[-\frac{2\omega^{d-2}}{f(r_m)}+r_m^{d-2}\left(\ln\left(\frac{r_m^2}{L^2|f(r_m)|}\right)-2\ln\left(\frac{(d-1)\ell_{\rm ct}}{L}\right)\right)\right]dr_m\\&=-\frac{\Omega_{k,d-1}r_{c,2}^{d-1}}{4\pi^2G_N}\ln\left(\frac{(d-1)\ell_{\rm ct}}{L}\right)+\frac{\Omega_{k,d-1}(d-1)}{8\pi^2G_N}\times\text{positive}\\&>-\frac{S}{\pi^2}\ln\left(\frac{(d-1)\ell_{\rm ct}}{L}\right),\end{aligned} \tag{B.5}$$

where in the first equality we have used the relation $dt=-2\frac{dr_m}{f(r_m)}$ to change the variable of integration to r_m and where the last inequality follows from $r_{c,2}<r_h$. The extra piece in the third line of eq. (B.5) is always positive. This can be demonstrated by using the explicit form of the blackening factor and the mass parameter as well as the relation $r_m\leq r_{c,2}<r_h$. Combining eqs. (B.1), (B.2) and (B.5), we arrive at the conclusion that the mutual complexity of the time-evolved TFD state is negative as advertised, *i.e.*,

$$\Delta\mathcal{C}_{\rm A}(t)=\Delta\mathcal{C}_{\rm A}(t=0)-\delta\mathcal{C}_{\rm A}<\Delta\mathcal{C}_{\rm A}(t=0)-\delta\mathcal{C}_{\rm A}^{\rm min}<0\,. \tag{B.6}$$

Appendix C

Background Materials on Quantum Information

In this appendix, we provide a minimal introduction to some notations and terminologies in quantum information, which are used in the main content.

C.1 Gaussian State and Covariance Matrix

It is known that the any Gaussian states $\hat{\rho}_{\mathrm{G}}$ can be equivalently described by its covariance matrix Σ_{G}. See [46–48] for more details about Gaussian states. Considering any Gaussian state with N modes, we can find N pairs of the standard self-adjoint canonical operators $\hat{x}_i, \hat{p}_i$ with the canonical commutation relations

$$[\hat{x}_i,\, \hat{p}_j] = i\delta_{ij}\hbar\,, \qquad \hbar = 1\,, \quad \hat{a}_i = \frac{\hat{x}_i + i\hat{p}_i}{\sqrt{2}}\,, \tag{C.1}$$

whose vector form is defined to be

$$[\hat{\mathbf{R}},\, \hat{\mathbf{R}}^{\intercal}] = i\Omega \equiv i\bigoplus_{k=1}^{n}\Omega_k\,, \quad \Omega_k = \begin{pmatrix} 0 & 1 \\ -1 & 0 \end{pmatrix}\,, \quad \hat{\mathbf{R}} = (\hat{x}_1, \hat{p}_1, \hat{x}_2, \hat{p}_2, \cdots \hat{x}_n, \hat{p}_n)^{\intercal}\,, \tag{C.2}$$

where Ω is the symplectic form satisfying $\Omega^{\intercal}\Omega = -\Omega^2 = \mathbb{I}_{2n}$. The *covariance matrix* (CM) Σ_{G} of any Gaussian state $\hat{\rho}_{\mathrm{G}}$ is defines as

$$(\Sigma_{\mathrm{G}})_{ij} \equiv \mathrm{Tr}\left(\hat{\rho}_{\mathrm{G}}\left\{\left(\hat{\mathbf{R}} - \langle\hat{\mathbf{R}}\rangle\right), \left(\hat{\mathbf{R}} - \langle\hat{\mathbf{R}}\rangle\right)^{\intercal}\right\}\right) = \left\langle \hat{\mathbf{R}}_i\hat{\mathbf{R}}_j + \hat{\mathbf{R}}_j\hat{\mathbf{R}}_i\right\rangle - 2\langle\hat{\mathbf{R}}_i\rangle\langle\hat{\mathbf{R}}_j\rangle\,. \tag{C.3}$$

For example, the covariance matrix Σ_1 for a single mode reads

$$\Sigma_1 = 2\begin{pmatrix} \langle\hat{x}^2\rangle - \langle\hat{x}\rangle^2 & \langle\{\hat{x},\hat{p}\}\rangle - \langle\hat{p}\rangle\langle\hat{x}\rangle \\ \langle\{\hat{x},\hat{p}\}\rangle - \langle\hat{p}\rangle\langle\hat{x}\rangle & \langle\hat{p}^2\rangle - \langle\hat{p}\rangle^2 \end{pmatrix}. \tag{C.4}$$

The physical Gaussian state $\hat{\rho}_{\rm G}$ with covariance matrix $\Sigma_{\rm G}$ should also satisfy the uncertainty principle

$$\Sigma_{\rm G} + i\Omega \geq 0\,, \tag{C.5}$$

which is invariant under the symplectic transformations. For a single-mode quantum state, the physical constrains are reduced to

$$\det\Sigma_1 \geq 1\,, \qquad \Sigma_1 \geq 0\,. \tag{C.6}$$

As a consequence of Williamson theorem, the covariance matrix $\Sigma_{\rm G}$ of the most general Gaussian state $\hat{\rho}_{\rm G}$ can be decomposed as

$$\Sigma_{\rm G}\left(\hat{\rho}_{\rm G}\right) = S\bigoplus_{k=1}^{n}\begin{pmatrix} \nu_k & 0 \\ 0 & \nu_k \end{pmatrix} S^{\intercal}\,, \qquad S \in {\rm Sp}(2n,\mathbb{R})\,, \qquad \nu_k \geq 1\,. \tag{C.7}$$

where ν_k are the symplectic eigenvalues of CM. Correspondingly, we can also obtain the decomposition of generic Gaussian state [46–48]

$$\hat{\rho}_{\rm G} = \hat{D}^{\dagger}\hat{S}^{\dagger}\left(\bigotimes_{k}^{n}\hat{\upsilon}_{\rm th}(\beta_k,\omega_k)\right)\hat{D}\hat{S}\,, \tag{C.8}$$

where $\hat{D},\hat{S}$ denote the displacement operator and squeezing operator, respectively, and $\hat{\upsilon}_{\rm th}$ is the thermal density matrix defined in (3.15) with the inverse temperature $\beta_k\omega_k$ associated with symplectic values of the covariance matrix by $\nu_k = \coth\left(\frac{\beta_k\omega_k}{2}\right) = \cosh 2\alpha_k$. From the covariance matrix, we can easily distinguish pure Gaussian states and mixed Gaussian states by considering its determinant, *i.e.,*

$$\det\left(\Sigma\right) = \begin{cases} +1\,, \text{pure}, \\ > 1\,, \text{mixed}\,. \end{cases} \qquad \text{with} \qquad {\rm Tr}\left(\hat{\rho}_{\rm G}^2\right) = \prod_{k=1}^{n}\frac{1}{\nu_k} = \frac{1}{\sqrt{\det\Sigma_{\rm G}}}\,. \tag{C.9}$$

For later use, one can also find

$$\mathrm{Tr}\left(\hat{\rho}_{\rm G}\hat{\rho}'_{\rm G}\right) = \frac{1}{\sqrt{\det\frac{1}{2}\left(\Sigma_{\rm G}+\Sigma'_{\rm G}\right)}}\,. \tag{C.10}$$

In this paper, we also discuss the partial trace with discarding some modes in the full system. In the representation of Gaussian states with the vector $\hat{\mathbf{R}}$ and covariance matrix, it is easy to see the action for tracing out a subsystem. Diving the N-mode system $\hat{\rho}_{\mathcal{AB}}$ into two parts with a n-mode system $\mathcal{A}$ and a m-mode system $\mathcal{B}$, we can decompose the covariance matrix in the way like

$$\Sigma_{\mathcal{AB}} = \begin{pmatrix} \Sigma_{nn} & \Sigma_{nm} \\ \Sigma_{mn} & \Sigma_{mm} \end{pmatrix} , \qquad \hat{\mathbf{R}}_{\mathcal{AB}} = \begin{pmatrix} \hat{\mathbf{R}}_n \\ \hat{\mathbf{R}}_m \end{pmatrix} , \tag{C.11}$$

where the Σ_{nm} denotes a $2n$-by-$2m$ matrix. Then the reduced density matrix $\hat{\rho}_{\mathcal{A}} = \mathrm{Tr}_{\mathcal{B}}\left(\hat{\rho}_{\mathcal{AB}}\right)$ for the subsystem $\mathcal{A}$ is easily obtained by

$$\Sigma_{\mathcal{A}} = \Sigma_{nn} , \qquad \text{with} \quad \hat{\mathbf{R}}_{\mathcal{A}} = \hat{\mathbf{R}}_n . \tag{C.12}$$

C.2 Quantum Operation (Quantum Channel)

It is obvious that we can use unitary operations to realize the transformations from a pure state to another one. For a generic quantum state $\hat{\rho}_{\mathcal{A}}$ in a principle system $\mathcal{A}$, we need to introduce a more general transformation beyond unitraies as

$$\hat{\rho}'_{\mathcal{A}} = \mathcal{E}\left(\hat{\rho}_{\mathcal{A}}\right) , \tag{C.13}$$

where the map $\mathcal{E}$ is called a quantum operation. In the literatures of quantum computation, a quantum operation is also called a *quantum channel* [1]. With one more terminology used in the main content, we only focus on the quantum operation defined as the *completely positive trace-preserving map* (CPTP map)

$$\mathcal{E} : \hat{\rho}_{\mathcal{A}} \longrightarrow \mathcal{E}\left(\hat{\rho}_{\mathcal{A}}\right) , \tag{C.14}$$

with $\mathrm{Tr}\left(\hat{\rho}_{\mathcal{A}}\right) = \mathrm{Tr}\left(\mathcal{E}\left(\hat{\rho}_{\mathcal{A}}\right)\right)$. As it is known, *e.g.,* [42, 43], the *quantum operation* formalism (C.13) can be represented in different but equivalent ways. For example, we can consider the quantum operation $\mathcal{E}\left(\hat{\rho}_{\mathcal{A}}\right)$ on density operators $\hat{\rho}_{\mathcal{A}}$ as the unitary transformation with ancillae (or environment) in the extended Hilbert space $\mathcal{H}_{\mathcal{A}} \otimes \mathcal{H}_{\mathcal{A}^c}$, *i.e.,*

$$\mathcal{E}\left(\hat{\rho}_{\mathcal{A}}\right) = \mathrm{Tr}_{\mathcal{A}^c}\left(U_{\mathcal{A}\mathcal{A}^c}\left(\hat{\rho}_{\mathcal{A}} \otimes \hat{\rho}_{\mathcal{A}^c}\right) U^{\dagger}_{\mathcal{A}\mathcal{A}^c}\right) , \tag{C.15}$$

[1] In some literature, the term "quantum operation" specifically denotes completely positive (CP) and non-trace-increasing maps on the space of density matrices. Instead, the term "quantum channel" refers to CPTP. In this paper, we only consider CPTP and it is referred to as "quantum operation".

where the density operator $\hat{\rho}_{\mathcal{A}^c}$ denotes an initial state for the auxiliary system and $\mathrm{Tr}_{\mathcal{A}^c}$ traces out the ancilla part. Taking the initial state as any pure state $|\psi_0\rangle$ in its orthogonal basis, it is easy to find that the reduced density operator after tracing out $\mathbb{H}_{\mathcal{A}^c}$ reads

$$\mathcal{E}\left(\hat{\rho}_{\mathcal{A}}\right) = \mathrm{Tr}_{\mathcal{A}^c}\left(U_{\mathcal{A}\mathcal{A}^c}\left(\hat{\rho}_{\mathcal{A}} \otimes |\psi_0\rangle\langle\psi_0|\right) U_{\mathcal{A}\mathcal{A}^c}^{\dagger}\right) \equiv \sum_k \hat{M}_k \hat{\rho}_{\mathcal{A}} \hat{M}_k^{\dagger}\,, \tag{C.16}$$

with $\hat{M}_k \equiv \langle\psi_k| U_{\mathcal{A}\mathcal{A}^c} |\psi_0\rangle$ defined as the operation elements for this quantum operation $\mathcal{E}$. This representation (C.16) is known as the *operator-sum representation* describing the dynamics of the principal system $\mathcal{A}$ without having to explicitly consider any properties of the auxiliary system $\mathcal{A}^c$. More importantly, this special representation benefits us from avoiding purifying the system $\mathcal{A}$ and making our interpretation to the purification complexity $\mathcal{C}_{\text{IM}}$ not require any explicit purifications. Furthermore, we can also consider the measurements on the principle system by taking the outcome as $\hat{\rho}_k$ with probability $p(k)$ after measurement. Obviously, the redefinitions

$$\hat{\rho}_k = \frac{\hat{M}_k \hat{\rho}_{\mathcal{A}} \hat{M}_k^{\dagger}}{\mathrm{Tr}\left(\hat{M}_k \hat{\rho}_{\mathcal{A}} \hat{M}_k^{\dagger}\right)}\,, \qquad p(k) = \mathrm{Tr}\left(\hat{M}_k \hat{\rho}_{\mathcal{A}} \hat{M}_k^{\dagger}\right), \tag{C.17}$$

relate the quantum operation $\mathcal{E}$ to measurements without reporting outcomes by rewriting the quantum operation as

$$\mathcal{E}\left(\hat{\rho}_{\mathcal{A}}\right) = \sum_k p(k)\hat{\rho}_k\,. \tag{C.18}$$

In order to describe the transformation from a physical and normalized state to another one, the trace-preserving quantum operations are restricted by the normalization condition

$$\sum_k \hat{M}_k^{\dagger}\hat{M}_k = \mathbb{I}\,. \tag{C.19}$$

In the following, we use Gaussian states as an example to illustrate the quantum operations acting on quantum states can be understood as the unitary operations acting on purified states in the extended Hilbert space. For any N-mode Gaussian state $\hat{\rho}_{\text{G}}$, the CPTP map $\mathcal{E}\left(\hat{\rho}_{\text{G}}\right)$ (also called bosonic Gaussian channel) is completely characterized by two real $2N$-by-$2N$ matrices $\mathbf{T}, \mathbf{N}$ acting on its vector and covariance matrix in the following way [48]

$$\begin{aligned} \hat{\mathbf{R}}_{\text{G}} &\longrightarrow \mathbf{T}\hat{\mathbf{R}}_{\text{G}}\,, \\ \Sigma_{\text{G}} &\longrightarrow \mathbf{T}\,\Sigma_{\text{G}}\,\mathbf{T}^{\intercal} + \mathbf{N}\,, \end{aligned} \tag{C.20}$$

where the real matrices $\mathbf{T}, \mathbf{N}$ are constrained by the complete positivity condition

$$\mathbf{N} + i\Omega \geq i\mathbf{T}\Omega\mathbf{T}^{\intercal} \,. \tag{C.21}$$

As we have shown in (C.16), the action of a CP map on any Gaussian state $\hat{\rho}_{\mathcal{A}}$ with n modes can be obtained by tracing out the ancillae (with m modes) after the unitary operation on the global system $\mathcal{A}\mathcal{A}^c$ where the evolution in the full system is parametrized by the $2(n+m)$-by-$2(n+m)$ symplectic matrix $S_{\mathcal{A}\mathcal{A}^c}$ acting on the extended covariance matrix, *i.e.,* $S_{\mathcal{A}\mathcal{A}^c}\left(\Sigma_{\mathcal{A}} \otimes \Sigma_{\mathcal{A}^c}\right) S^{\dagger}_{\mathcal{A}\mathcal{A}^c}$. Considering the bipartition of the extended system $\mathcal{A}\mathcal{A}^c$, we can divide the full symplectic matrix into four sub-matrices

$$S_{\mathcal{A}\mathcal{A}^c} = \begin{pmatrix} S_{\mathcal{A}} & S_{\mathcal{A}\mathcal{A}^c} \\ S_{\mathcal{A}^c\mathcal{A}} & S_{\mathcal{A}^c} \end{pmatrix} , \tag{C.22}$$

corresponding to the bipartite covariance matrix shown in (C.11). Applying the symplectic condition for $S_{\mathcal{A}\mathcal{A}^c}$ on the purified Gaussian states $\hat{\rho}_{\mathcal{A}\mathcal{A}^c}$, we can find the following constrains

$$S_{\mathcal{A}\mathcal{A}^c}\,\Omega\,S^{\intercal}_{\mathcal{A}\mathcal{A}^c} = \begin{pmatrix} S_{\mathcal{A}}\Omega_n S^{\intercal}_{\mathcal{A}} + S_{\mathcal{A}\mathcal{A}^c}\Omega_m S^{\intercal}_{\mathcal{A}\mathcal{A}^c} & S_{\mathcal{A}}\Omega_n S^{\intercal}_{\mathcal{A}^c\mathcal{A}} + S_{\mathcal{A}\mathcal{A}^c}\Omega_m S^{\intercal}_{\mathcal{A}^c} \\ S_{\mathcal{A}^c\mathcal{A}}\Omega_n S^{\intercal}_{\mathcal{A}} + S_{\mathcal{A}^c}\Omega_m S^{\intercal}_{\mathcal{A}\mathcal{A}^c} & S_{\mathcal{A}^c\mathcal{A}}\Omega_n S^{\intercal}_{\mathcal{A}^c\mathcal{A}} + S_{\mathcal{A}^c}\Omega_m S^{\intercal}_{\mathcal{A}^c} \end{pmatrix} = \begin{pmatrix} \Omega_n & 0 \\ 0 & \Omega_m \end{pmatrix} . \tag{C.23}$$

From the above equation, it is easy to find that the $S_{\mathcal{A}}$ has to be symplectic if $S_{\mathcal{A}\mathcal{A}^c} = 0$. More generally, after tracing out the auxiliary system $\mathcal{A}^c$ with m modes, *i.e.,*

$$\mathcal{E}\left(\Sigma_{\mathcal{A}}\right) = \mathrm{Tr}_{\mathcal{A}^c}\left(S_{\mathcal{A}\mathcal{A}^c}\left(\Sigma_{\mathcal{A}} \otimes \Sigma_{\mathcal{A}^c}\right) S^{\dagger}_{\mathcal{A}\mathcal{A}^c}\right) , \tag{C.24}$$

we can find that the generic Gaussian CP map (C.20) acting on the reduced density matrix $\hat{\rho}_{\mathcal{A}}$ is obtained by

$$\mathbf{T} = S_{\mathcal{A}} \,, \quad \mathbf{N} = S_{\mathcal{A}\mathcal{A}^c}\Sigma_{\mathcal{A}^c}S^{\intercal}_{\mathcal{A}\mathcal{A}^c} \,. \tag{C.25}$$

which illustrates the connections between the quantum operations (Gaussian channels) and unitary operations with ancillae. Specifically, we can find that the $\mathbf{T}$-part provides the full information of the operations acting only on the principle system $\mathcal{A}$ while the crossing $\mathbf{N}$-part encodes the information of entangled gates. From the above identifications, it is also obvious that the unitary operation in the full system $\mathcal{A}\mathcal{A}^c$ is not unique because the quantum operations on $\hat{\rho}_{\mathcal{A}}$ are only sensitive to the sub-matrix $S_{\mathcal{A}}$ and $S_{\mathcal{A}\mathcal{A}^c}$, reflecting the freedom in purifications.

C.3 Bures Metric and Quantum Fisher Information Metric

In the literatures of quantum information or quantum estimation (*e.g.,* [218, 241]), the quantum Fisher information metric (QFIM) is defined in various ways and also different from Bures metric. In this section, we show they are equivalent up to a irrelevant constant factor and also introduce some equivalent expressions for the QFIM.

C.3.1 Bures Distance and Bures Metric

In the main content, we introduce Bures metric or QFIM by considering Uhlmann's fidelity susceptibility. However, it can be also derived from a finite distance between two respective quantum states, *i.e.,* Bures distance, which is defined by [210, 211, 217]

$$D_{\mathrm{B}}\left(\hat{\rho},\hat{\sigma}\right)=\sqrt{\mathrm{Tr}(\hat{\rho})+\mathrm{Tr}(\hat{\sigma})-2F\left(\hat{\rho},\hat{\sigma}\right)}=\sqrt{2\left(1-F(\hat{\rho},\hat{\sigma})\right)}\,, \tag{C.26}$$

where we only consider normalized density matrices with $\mathrm{Tr}\left(\hat{\rho}\right)=1$ and the quantum fidelity $F\left(\hat{\rho},\hat{\sigma}\right)$ is given by (5.6). As before, it also reduces to the Fubini-Study distance for two pure states. From another definition of Bures distance [211], *i.e.,*

$$D_{\mathrm{B}}^{2}\left(\hat{\rho},\hat{\sigma}\right)=\min_{W_i}\,||W_1-W_2||_{\mathrm{HS}}^{2}=\min_{W_i}\,\left(\mathrm{Tr}\left((W_1-W_2)^{\dagger}(W_1-W_2)\right)\right)\,, \tag{C.27}$$

where the minimization is taken over all Hilbert-Schmidt operator with $W_1^{\dagger}W_1=\hat{\rho},W_2^{\dagger}W_2=\hat{\sigma}$, it is clear that the Bures distance is the perfect analogue of Fubini-Study distance. Here we sketch the proof to show the above minimization results in the Uhlmann's fidelity, which also illustrates our motivation to choose the Uhlmann's fidelity. For arbitrary positive density matrix $\hat{\rho}$, we can define a matrix W such that

$$W^{\dagger}W=\hat{\rho}\,. \tag{C.28}$$

The matrix W plays the role of the purification of $\hat{\rho}$ and can be considered as a vector in Hilbert-Schmidt space. The freedom in purification is equivalent to the gauge symmetry $\hat{\rho}=(UW)^{\dagger}(UW)$ with $U\in\mathrm{U}(n)$. A natural Euclidean distance between two vectors are defined by the root of

$$||W_1-W_2||_{\mathrm{HS}}^{2}=\mathrm{Tr}(\hat{\rho})+\mathrm{Tr}(\hat{\sigma})-\left(W_1^{\dagger}W_2+W_1W_2^{\dagger}\right)\,, \tag{C.29}$$

with $W_1^\dagger W_1 = \hat{\rho}\,, W_2^\dagger W_2 = \hat{\sigma}$. The minimization for Bures metric between $\hat{\rho}$ and $\hat{\sigma}$ is reduced to the maximization

$$\max_{W_i}\left(\frac{1}{2}\mathrm{Tr}\left(W_1^\dagger W_2 + W_1 W_2^\dagger\right)\right) = \max_{W_i}\left|\mathrm{Tr}\left(W_1 W_2^\dagger\right)\right| = F\left(\hat{\rho},\hat{\sigma}\right)\,, \tag{C.30}$$

which will be shown below to be the Uhlmann's fidelity. Applying the polar decomposition [2], *i.e.,* $W_i = \sqrt{\hat{\rho}_i}U_i$, one can get

$$\mathrm{Tr}\left(W_1 W_2^\dagger\right) = \mathrm{Tr}\left(\sqrt{\hat{\sigma}}\sqrt{\hat{\rho}}U_1 U_2^\dagger\right)\,. \tag{C.31}$$

Noting the existence of another polar decomposition $\sqrt{\hat{\sigma}}\sqrt{\hat{\rho}} = \sqrt{\sqrt{\hat{\sigma}}\hat{\rho}\sqrt{\hat{\sigma}}}U_{12}$, it is not hard to find that the special choice $U_{12}U_1U_2^\dagger = \mathbb{I}$ realizes the maximization with

$$F\left(\hat{\rho},\hat{\sigma}\right) = \mathrm{Tr}\left(\sqrt{\sqrt{\hat{\sigma}}\hat{\rho}\sqrt{\hat{\sigma}}}\right)\,, \tag{C.32}$$

which is nothing but Uhlmann's fidelity (5.6). We also note the maximization condition also implies the two purifications are connected by the *geometric mean* (see [220, 221] for more discussion about its application to the complexity of Gaussian states), *i.e.,*

$$\begin{aligned}\sqrt{\hat{\sigma}}W_1 &= \sqrt{\sqrt{\hat{\sigma}}\hat{\rho}\sqrt{\hat{\sigma}}}\,U_2\,,\\ W_1 &= \left(\hat{\sigma}^{-\frac{1}{2}}\sqrt{\sqrt{\hat{\sigma}}\hat{\rho}\sqrt{\hat{\sigma}}}\,\hat{\sigma}^{-\frac{1}{2}}\right)W_2\,.\end{aligned} \tag{C.33}$$

where we have assumed the density matrices are positive definite to derive the second line. Instead of the finite Bures distance between two density matrices, we prefer the geodesic distances on Riemannian geometry where geodesics can simulate the properties of optimal circuits. Then we focus on the infinitesimal metric from Bures distance, *i.e.,* Bures metric

$$ds_{\mathrm{B}}^2 =_2 D_{\mathrm{B}}^2\left(\hat{\rho},\hat{\rho}+\delta\hat{\rho}\right) = 2\left(1-\mathrm{Tr}(\sqrt{\sqrt{\hat{\rho}}(\hat{\rho}+\delta\hat{\rho})\sqrt{\hat{\rho}}})\right)\,, \tag{C.34}$$

which can also be explained as the fidelity susceptibility of mixed states. Due to the appearance of two square roots of positive operators in the definition of quantum fidelity,

[2] Polar decomposition means that an arbitrary linear operator W can be decomposed into product of unitary operator U and positive operators such that $W = U\sqrt{W^\dagger W} = \sqrt{WW^\dagger}U$

the Bures metric is not easy to be written as a simple form of $\delta\hat{\rho}$ like Schatten norms. In order to obtain some explicit forms of Bures metric, we can start from the series expansion

$$\sqrt{\sqrt{\hat{\rho}}(\hat{\rho}+\delta\hat{\rho})\sqrt{\hat{\rho}}} \approx \hat{\rho} + \hat{X} + \hat{Y} + \mathcal{O}(\delta\hat{\rho}^3)\,, \tag{C.35}$$

where we keep the first two orders, *i.e.,* $\hat{X} \sim \delta\hat{\rho}$, $\hat{Y} \sim \delta\hat{\rho}\delta\hat{\rho}$. And we note that there are simple constrains $\mathrm{Tr}d\hat{\rho} = 0 = \mathrm{Tr}\hat{X}$ due to the normalization condition $\mathrm{Tr}\hat{\rho} = 1 = \mathrm{Tr}\,(\hat{\rho} + d\hat{\rho})$. Taking the square of the above series expansion, one can simply find

$$\begin{aligned} \sqrt{\hat{\rho}}\, d\hat{\rho}\, \sqrt{\hat{\rho}} &= \hat{\rho}\hat{X} + \hat{X}\hat{\rho}\,, \\ \hat{X}^2 + \hat{\rho}\hat{Y} + \hat{Y}\hat{\rho} &= 0\,. \end{aligned} \tag{C.36}$$

Choosing the basis of the density matrix $\hat{\rho}$ by $\hat{\rho} = p_i \left|\psi_i\right\rangle \left\langle\psi_i\right|$, we can obtain the basis-dependent results

$$\begin{aligned} \left\langle\psi_i\right| \hat{X} \left|\psi_j\right\rangle &= \frac{\sqrt{p_i}\sqrt{p_j}}{p_i + p_j} \left\langle\psi_i\right| d\hat{\rho} \left|\psi_j\right\rangle\,, \\ \left\langle\psi_i\right| \hat{Y} \left|\psi_j\right\rangle &= -\frac{\left\langle\psi_i\right| \hat{X}\hat{X} \left|\psi_j\right\rangle}{p_i + p_j}\,, \end{aligned} \tag{C.37}$$

which simply result in

$$\mathrm{Tr}\,\hat{Y} = -\sum_{i,j} \frac{1}{2p_i} \left\langle\psi_i\right| \hat{X} \left|\psi_j\right\rangle \left\langle\psi_j\right| \hat{X} \left|\psi_i\right\rangle = -\frac{1}{4}\sum_{i,j} \frac{\left|\left\langle\psi_i\right| d\hat{\rho} \left|\psi_j\right\rangle\right|^2}{p_i + p_j}\,. \tag{C.38}$$

Correspondingly, the Bures metric defined in (C.34) reads [242]

$$\begin{aligned} ds_{\mathrm{B}}^2 &= 2\left(1 - \mathrm{Tr}(\hat{\rho} + \hat{X} + \hat{Y})\right) \\ &= -2\mathrm{Tr}\,\hat{Y} = \frac{1}{2}\sum_{i,j} \frac{\left|\left\langle\psi_i\right| d\hat{\rho} \left|\psi_j\right\rangle\right|^2}{p_i + p_j}\,. \end{aligned} \tag{C.39}$$

C.3.2 Quantum Fisher Information Metric

Different from the original definition of Bures metric as eq. (C.34), quantum Fisher information metric is defined by

$$ds_{\mathrm{IM}}^2 = \mathrm{Tr}(G\hat{\rho}G) = \frac{1}{2}\mathrm{Tr}\,(Gd\hat{\rho})\,, \tag{C.40}$$

where the hermitian operator G known as *symmetric logarithmic derivative* is uniquely determined by the Laypunov equation, namely

$$d\hat{\rho} = G\hat{\rho} + \hat{\rho}G\,. \tag{C.41}$$

In our coordinate system with $\hat{\rho}(\lambda^\mu)$, the metric components read

$$g^{\rm IM}_{\mu\nu} = \frac{1}{2}{\rm Tr}\big(\hat{\rho}\left(G_\mu G_\nu + G_\nu G_\mu\right)\big)\,, \qquad d\hat{\rho} = \partial_\mu\hat{\rho}(\lambda)d\lambda^\mu\,, \quad G = G_\mu d\lambda^\mu\,, \tag{C.42}$$

which is generally called *quantum Fisher information metric (matrix)* [241]. If we are restricted on pure states with $\hat{\rho} = \hat{\rho}^2, {\rm Tr}\hat{\rho} = {\rm Tr}\left(\hat{\rho}^2\right) = 1$, we can find

$$\begin{aligned} d\hat{\rho} &= \hat{\rho}d\hat{\rho} + d\hat{\rho}\hat{\rho}\,,\,, \\ {\rm Tr}\left(d\hat{\rho}\right) = 0 &= {\rm Tr}\left(\hat{\rho}d\hat{\rho}\right)\,, \end{aligned} \tag{C.43}$$

and obtain the symmetric logarithmic derivative as

$$G = d\hat{\rho} = |d\psi\rangle\langle\psi| + |\psi\rangle\langle d\psi|\,. \tag{C.44}$$

Correspondingly, the quantum Fisher information metric for pure states is simplified to be

$$\begin{aligned} ds^2_{\rm IM} &= {\rm Tr}(G\hat{\rho}G) = {\rm Tr}\left(\hat{\rho}(d\hat{\rho})^2\right) = \frac{1}{2}{\rm Tr}\left(d\hat{\rho}d\hat{\rho}\right) \\ &= \langle d\psi|d\psi\rangle - \langle\psi|d\psi\rangle\langle d\psi|\psi\rangle\,. \end{aligned} \tag{C.45}$$

which is nothing but the Fubini-Study metric as advertised in the introduction. The challenge in calculations for quantum fidelity or Bures metric originates from the square root and also the non-commutation between $\hat{\rho}$ and $\delta\hat{\rho}$. If we focus on the special case where $\hat{\rho}$, $\delta\hat{\rho}$ commute, we can derive the explicit form for the QFIM by

$$ds^2_{\rm IM} = {\rm Tr}\left(\left(d\sqrt{\hat{\rho}}\right)^2\right) = \frac{1}{4}{\rm Tr}\left(\hat{\rho}^{-1}d\hat{\rho}d\hat{\rho}\right)\,, \tag{C.46}$$

with

$$[\delta\hat{\rho}, \hat{\rho}] = 0\,, \qquad G = \frac{1}{2}\hat{\rho}^{-1}d\hat{\rho}\,. \tag{C.47}$$

As expected, the QFIM in the above case actually reduces to the **classical** Fisher information matrix defined by

$$g_{\mu\nu}\left(\lambda\right) = \int dx\, P\left(\lambda; x\right)\frac{\partial^2\ln P(\lambda;x)}{\partial\lambda^\mu\partial\lambda^\nu} = \int dx\, P\left(\lambda; x\right)\frac{\partial\ln P(\lambda;x)}{\partial\lambda^\mu}\frac{\partial\ln P(\lambda;x)}{\partial\lambda^\nu}\,, \tag{C.48}$$

for any distribution $P(\lambda; x)$ on the parameter space λ^μ.

Following the popular conventions in quantum information or quantum estimation (see *e.g.,* [218, 241]), Bures metric is related to the **quantum** Fisher information metric ($H_{\mu\nu}$) in the way of

$$g_{\mu\nu} = \frac{1}{4} H_{\mu\nu} \,. \tag{C.49}$$

In the main content, we don't distinguish the Bures metric and QFIM by simply taking $ds^2_{\text{IM}} = ds^2_{\text{B}}$ because we need to normalize various metrics before taking them as the complexity measure in eq. (5.19).

In order to show the equivalence between Bures metric and QFIM in a basis-independent expression, we can relate the symmetric logarithmic derivative to the first order variation $\hat{X}$ by

$$\hat{G} = \hat{\rho}^{-\frac{1}{2}} \hat{X} \hat{\rho}^{-\frac{1}{2}} \,. \tag{C.50}$$

Obviously, one can get the following constrain equations

$$\begin{aligned} d\hat{\rho} &= G\hat{\rho} + \hat{\rho} G \\ 0 &= \hat{\rho}^{-1}\hat{X}^2 + \hat{Y} + \hat{\rho}^{-1}\hat{Y}\hat{\rho} \longrightarrow -2\text{Tr}\hat{Y} = \text{Tr}\left(\hat{\rho}^{-1}\hat{X}^2\right) \,. \end{aligned} \tag{C.51}$$

As a result, we can rewrite the Bures metric derived in eq. (C.39) into the new form

$$\begin{aligned} ds^2_{\text{B}} &= -2\text{Tr}\hat{Y} = \text{Tr}\left(\hat{\rho}^{-\frac{1}{2}}\hat{X}\hat{X}\hat{\rho}^{-\frac{1}{2}}\right) = \text{Tr}\left(\hat{\rho}^{-\frac{1}{2}}\hat{X}\hat{\rho}^{-\frac{1}{2}}\hat{\rho}\hat{\rho}^{-\frac{1}{2}}\hat{X}\hat{\rho}^{-\frac{1}{2}}\right) \\ &= \text{Tr}(G\hat{\rho}G) = \frac{1}{2}\text{Tr}\left(Gd\hat{\rho}\right) \,. \end{aligned} \tag{C.52}$$

which is nothing but the quantum fisher information defined in eq. (C.40). With the help of the unique solution of Lyapunov equation, *i.e.,*

$$d\hat{\rho} = G\hat{\rho} + \hat{\rho}G \,, \qquad G = \int_0^\infty \left(e^{-t\hat{\rho}} d\hat{\rho} e^{-t\hat{\rho}}\right) dt \,, \tag{C.53}$$

we can further calculate the Bures metric by the integral

$$ds^2_{\text{IM}} = ds^2_{\text{B}} = \frac{1}{2}\int_0^\infty \text{Tr}\left(e^{-\hat{\rho}t} d\hat{\rho} e^{-\hat{\rho}t} d\hat{\rho}\right) dt \,, \tag{C.54}$$

which is obviously basis-independent.

Taking the density matrix $\hat{\rho}$ into the diagonal basis with $\hat{\rho} = \sum_k p_k \left|\psi_k\right\rangle \left\langle\psi_k\right|$, a simple forms for the quantum Fisher information metric is given by [218, 241, 242]

$$g^{\text{IM}}_{\mu\nu} = \frac{1}{2} \sum_{k,l} \Re \left(\frac{\left\langle\psi_k\right| \partial_\mu \hat{\rho} \left|\psi_l\right\rangle \left\langle\psi_l\right| \partial_\nu \hat{\rho} \left|\psi_k\right\rangle}{p_k + p_l} \right) , \tag{C.55}$$

which has been shown in (C.39). Furthermore, we can also expand the variation $d\hat{\rho} = \partial_\mu \hat{\rho}\, d\lambda^\mu$ in a specific basis. Noting the basis for $\hat{\rho}(\lambda) = p_i(\lambda) \left|\psi_i(\lambda)\right\rangle \left\langle\psi_i(\lambda)\right|$ also depend on the parameters λ^μ like the spectrum of $\hat{\rho}$, *i.e.*, $p_i(\lambda^\mu)$, one can find

$$\partial_\mu \hat{\rho}(\lambda) = \sum_j \left(\partial_\mu p_j \left|\psi_i\right\rangle \left\langle\partial_\mu \psi_i\right| + p_j \left|\psi_i\right\rangle \left\langle\psi_i\right| + p_j \left|\psi_i\right\rangle \left\langle\partial_\mu \psi_i\right| \right) . \tag{C.56}$$

Then the Bures metric is rewritten as [218]

$$g^{\text{IM}}_{\mu\nu} = \sum_i \frac{\partial_\mu p_i \partial_\nu p_i}{p_i} + \sum_{i \neq j} \frac{(p_i - p_j)^2}{p_i + p_j} \left(\left\langle\psi_i\right|\left.\partial_\mu \psi_j\right\rangle \left\langle\partial_\nu \psi_j\right|\left.\psi_i\right\rangle + \left\langle\psi_i\right|\left.\partial_\nu \psi_j\right\rangle \left\langle\partial_\mu \psi_j\right|\left.\psi_i\right\rangle \right) , \tag{C.57}$$

where the first term is the same as the **classical** Fisher information metric defined in (C.48) and the second terms count the quantum contributions.